The Alpha Foundation for the Improvement of Mine Safety and Health, Inc

Final Technical Report

1.0 Cover Page

AFC719-68: Methane Watchdog System – A Cost Effective Approach to Longwall Methane Monitoring and Control

Organization: West Virginia University Research Corporation

Principal Investigator: Derek Johnson, PhD, PE
Office: 304-293-5725, **Cell:** 304-216-6592, **Fax:** 304-293-6689
Email: derek.johnson@mail.wvu.edu
Co-Principal Investigator: Nigel Clark, PhD

Period of Performance: July 1st, 2018 – December 31st, 2019

Acknowledgement/Disclaimer
"This Study was sponsored by the Alpha Foundation for the Improvement of Mine Safety and Health, Inc. (ALPHA FOUNDATION). The views, opinions and recommendations expressed herein are solely those of the authors and do not imply any endorsement by the ALPHA FOUNDATION, its Directors and staff."

Contents

2.0 Executive Summary

Although coal mine explosions are rare, the consequences are devastating. High fidelity detection of high methane concentration zones is essential to eliminate a major source of possible ignitions and explosions. Our research team at West Virginia University (WVU) has completed component design and assembled a first-generation version of the Methane Watchdog System (MWS). The ultimate goal of the research is the development of a cost-effective, multi-nodal network of methane sensors that can be deployed across an entire longwall system and that supports intelligent detection of localized zones of high methane concentration. Such an advanced measurement method will improve mine safety and enable extensive data collection that could beneficially impact future mine designs. Currently, industry uses a single, shearer-mounted methane sensor for continuous monitoring; however, the MWS enables the monitoring of methane at additional regions of focus. Literature has shown that methane concentrations tend to be highest near the gob and the front tip of the mine shield. As such, we have developed a system where multiple shields will serve as hosts for measurement nodes across the entire face – from headgate (HG) to tailgate (TG). The first-generation prototype system included ten measurement nodes capable of sampling from up to 20 locations. However, the central processing hub (CPH) and its communication protocols can accommodate a far higher count of nodes for higher resolution and increased longwall shearer travel.

Our MWS approach will enable *proactive* instead of *reactive* safety measures. The MWS includes a CPH which communicates to each node. Located at each node is a sampling box that includes a full suite of sensors to monitor methane and other relevant parameters. The sampling box includes a tubing system that enables periodic sampling from both the gob and front shield tip locations of the nodes. We conducted research on sampling methods that would be inherently explosion proof and robust, preferring not to employ any electrically powered pumps, fans, or compressors. The result is a custom water ejector that can use compressed water to induce the sample flow rate. Water at suitable pressure already is available for longwall operations. This enables the sampling box to be mounted at a convenient location on the shield, while still sampling from locations that are difficult to access. Due to the dust conditions in a mine, we also assessed commercially available filters that can be installed at each sampling location to prevent clogging of the sample lines and ejectors. The nodes are physically operated in a series/parallel configuration so that each node can communicate with the CPH. The system is readily integrated with current commercial shield designs that use low-voltage direct current power.

Current regulations require different safety shut-down procedures at 1, 1.5, and 2% methane by volume. These regulations apply to current sensors such as those mounted on the shearer and that are based on catalytic oxidation. These sensors deploy passive sampling and are anecdotally prone to issues with fouling from coal and other dust, especially when mounted on the shearer. Recent literature has suggested that alternative sensors may provide better response and accuracy. Therefore, we focused on alternative infrared and metal-oxide sensors combined with an active sampling approach. This approach needs to detect these levels reliably, but also needs to detect lower methane concentrations to enable inference of developing methane clouds and support intelligent modeling to maximize safety and minimize false alarms (i.e. downtime/lost production). Our design satisfies these requirements, while remaining cost sensitive. We examined two inexpensive methane sensor technologies, metal oxide sensors (MOS) and infrared sensors (IRS). The MOS has very low cost but current designs are limited to measurement ranges of around 1%. We have shown that the MOS is capable of accurately measuring above this level, but excessive

methane exposure may yield significant sensor drift. Additionally, the MOS enables sensitive detection of low methane concentrations, <0.1% but its accuracy is significantly impacted by other variables such as humidity. The IRS have higher (but acceptable) cost and are capable of accurately measuring methane concentrations up to 5% and they are less sensitive to other variables such as humidity. However, the IRS do not provide low concentration sensitivity as the MOS.

The current MWS utilizes paired MOS and IRS for optimized performance, sensor fault inference, and measurement redundancy. Each sample box monitors temperature, relative humidity, absolute pressure, and sample flow rate to improve accuracy and expand capabilities of the MWS to include model-based detection. We have demonstrated the prototype in a full-scale wind tunnel (over 30.48 m (100 ft)) representative of a short horizontal mine. Alarm and relay control were demonstrated, and the system operated unmanned for several days.

The system is able to operate in open loop, but we have also initiated an approach that uses modeling of the sampling system, modeling of gas cloud evolution and dispersion, and machine learning to predict an alarm situation rapidly and reliably. With these data, we have created 1-D, 2-D, and 3-D models to assess the initial response time of the system with respect to realistic methane concentrations, shearer and ventilation velocities. We have shown there are multiple scenarios where the MWS would alert mine operators of methane plumes far from the shearer. Further, the MWS can enable pre-emptive control to avoid 1% methane and avoid a shutdown. Pre-emptive control may include real time management of shearer speeds to maintain a safe operating margin of localized concentration. With intelligent processing of the multiple concentration signals, an experiential algorithm can infer a future high concentration event well in advance using time-varying information. Essentially, the MWS can act as an expert system, while also archiving data, managing audible alarms and shutdowns, and performing system control.

Based on these insights we have identified key research and development targets to realize the full potential of the MWS. These include full development of the sophisticated algorithms that will place the MWS above a simple concentration measurement device to enhance longwall operation economics while increasing safety. Also, we propose to optimize the physical design by identifying sampling tube dimensions that reduce response time and ejector designs that improve flow velocities and efficiency. We seek future funding to enable this added optimization and design sophistication.

During our literature review we determined that there is a dearth of continuous methane data available and little quantitative research relating to localized methane clouds. We have also found no substantive intellectual property in this space. Therefore, we limited public disclosures of the MWS design and submitted an invention disclosure to the WVU Office of Technology Transfer (OTT). TreMonti Consulting has completed an external review for WVU OTT and determined that the MWS likely has commercial potential and that the MWS represents intellectual property that should be protected. We are therefore working toward a provisional patent. Under nondisclosure protection, we have also engaged with a major emissions systems and sensor manufacturer to determine commercialization potential and improvements to the methane sensing approach, which would benefit from future work.

3.0 Problem Statement and Objective

3.1 Problem Statement

Longwall mining in underground coal mines is considered the safest and most productive mining method. However, due to its high productivity, the methane emissions from the large newly exposed coal face and from the gob area are often excessively high. As the longwall panels become wider (with the widest currently being 487.7 m (1,600 ft)) and longer, the total amount of methane emitted from the longwall panel tends to increase proportionally with the area of the panel. As a result, most of the longwall coal mines in the U.S. must rely on multiple degasification methods to lower the methane content before longwall mining operations can be safely conducted in the coal seams.

Along the longwall face, a methane liberation rate of up to 0.001 m^3/s per m^2 (2 to 4 cubic feet per minute (cfm)) per (ft^2)) is expected from the freshly exposed coal surface as the coal is cut by the shearer and the methane concentration gradually diminishes as the shearer moves away. Because of methane's lower density and more complex flows of ventilation air near the shearer, it is possible to form pockets of explosive methane concentration near the front corner of the roofline and coal face, especially when caved pockets form at the upper corner due to severe face spalling. If the shearer cuts into unexpected hard rock roof, sparks could ignite methane and small-scale explosions can occur.

In a longwall panel, high methane concentrations of 90% or more could form in the central part of the gob area. Such high concentrations are above the UEL of 15% and are acceptable so long as they do not migrate towards the rear of the panels. However, the methane concentration along the gob edges immediately behind the longwall face and beside the panel HG and TG are normally controlled by ventilation to under 1.0%. Therefore, there must be a transition zone where methane concentration varies between the methane's lower explosive limit of 5% and its upper explosive limit of 15% in the gob area some distance inside the gob edges. In a typical longwall gob, this explosive zone is closest to the longwall face near the TG and face corner. If not properly controlled, this explosive zone could even penetrate the longwall face causing hazardous conditions as in the case of the mine explosion at the Upper Big Branch mine. The current bleeder ventilation system employed in majority of the U.S. longwall mines is to keep the 5% methane concentration sufficiently distant from the longwall face while not over-ventilating the gob area.

Fires and explosions are still the most feared hazards in underground coal mines. Thirteen of 15 coal mine disasters (i.e., accidents with 5 or more fatalities) since 1980 have resulted from fires and explosions [1]. The most recent coal mine disaster in the U.S. occurred at Upper Big Branch Mine where 29 miners lost their lives nearly instantly because of an explosion initiated by methane ignition near the TG of the longwall face that intensified with the participation of coal dust. Table 3.1.1 includes all major worldwide mining disasters since 2000 that were due to explosions [2].

Table 3.1.1: Major underground coal mine explosions after 2000, reproduced from [2].

Country	Date	Coal Mine	Fatalities
China	February 14, 2005	Sunjiawan, Haizhou Shaft, Fuxin	214
USA	June 2, 2006	Sago, West Virginia	12
Poland	November 21, 2006	KWK Halemba, Ruda Slaska	19
Kazakhstan	September 20, 2006	Lenina, Karaganda	43
Russia	March 19, 2007	Ulyanovskaya, Kemerovo	108
Ukraine	November 19, 2007	Zasyadko, Donetzk	80
Poland	September 18, 2009	KWK Wujek, Ruda Slaska	20
USA	April 5, 2010	Upper Big Branch, West Virginia	29
Russia	May 8, 2010	Raspadskaya, Kemerovo Oblast	66
Turkey	May 17, 2010	Karadon, Zonguldak	30
New Zealand	November 19, 2010	Pike River Mine	29
Turkey	May 13, 2014	Soma, Turkey	301
Ukraine	March 4, 2015	Zasyadko, Donetzk	33
China	October 30, 2016	Jinshangou, Chongqing	33

Therefore, methane still presents hazardous conditions in the longwall faces where the coal is cut, loaded, and transported in much higher production rates than other mining methods used in the coal industry. Currently methane concentrations are detected with stationary or portable handheld instruments that typically work on the principle of catalytic oxidation. The current federal standard mandates that methane concentrations be controlled under 1.0% in any active part of underground mine other than the bleeder system where up to 2% is allowed. In all working faces, powered equipment should be de-energized when 1.0% methane is detected while electric power shall be disconnected when 1.5% methane is present. Details on mine air requirements are set forth in the Code of Federal Regulations (CFR) Part 30 Section 75 [3]. Longwall mines often adopt their own standard to control the methane concentration from 0.7 to 0.8%, so that mining operation is not frequently interrupted because of highly variable methane emissions at the working face.

Currently, MSHA regulations require that only one methane monitor be mounted on the longwall shearer in a longwall face. Methane is generally measured in one or two locations – at the shearer and TG. Early research focused on optimal sampling locations near the shearer but found that sensors typically failed or fowled nearer the shearer edge where concentrations were highest and subsequently suggested a location nearer the back of the shearer [4]. Therefore, a single gas monitor is unable to detect the zones of higher methane concentrations, possibly explosive, either at the front upper (top) corner of the longwall face and along the front longwall gob edge immediately behind the shields. In addition, the response time of current sensors may be ten or

more seconds – which reduces its spatial reliability. For example, if the gas monitor on the shearer detects an explosive methane condition, the cutting drums (potential ignition source) may have already penetrated the explosive gas zone due to the delayed response from a single point measurement. Therefore, to improve further the safety at the longwall mining operations, a more responsive, multi-nodal gas monitoring system must be developed and deployed to control ventilation at the longwall faces and serve to proactively control shearer power to avoid explosive conditions and reduce equipment downtime.

3.2 Project Objectives

Our main objective was to develop the Methane Watchdog System (MWS) based on sound engineering research, reviews of literature, robust experimental validation, and interaction with industry; in order to improve the understanding of methane concentrations along a longwall face to increase the safety and health of mineworkers and equipment.

The MWS was comprised of the following key elements 1.) Sensor block encompassing at least one methane sensor and other sensors necessary to improve methane measurement accuracy, 2.) valving, tubing, and filter components necessary to sample from harsh, hard-to-reach environments, 3.) Communications and electrical network that could easily be integrated into current shield systems, and 4.) Central processing hub (CPH) that served to alarm or control external equipment, store data and provide a user interface. For research purposes, we demonstrated a system capable of measuring methane at ten discrete nodes. Each node included a sampling box, where sensors and electronics were safely installed. Each sampling box was capable of sampling from two locations – near the gob and near the front shield tip. A robust and explosion proof sampling method was of the utmost concern. Originally, research focused on either passive or active air powered samplers, but our efforts refocused on the design and demonstration of a water powered ejector.

Each of the locations included filters that ensured particulates such as coal dust and water droplets did not impinge the sampler circuit leading to premature failure or false positive readings. Each sampling location would have a quick disconnect system for easy installation and replacement of the sensor and filter if applicable. The connection network included shielded low voltage DC power and signal wires. Each sampling node was connected to the CPH. The CPH recorded methane data from each node and had analog or digital output capabilities for communications with other systems and for shearer power control. Along with a CPH, the system included a visual interface that allowed operators to view methane concentrations in nearly real time.

Our research objective was to overcome current methane monitoring limitations by developing a robust and cost-effective methane-monitoring network that can be used to predict and detect high concentrations, de-energize the shearer, and interface with automated ventilation control units. Our primary aim focused on the aspect of low capital costs. Additional aims focused on durability of the sampling system and maintenance requirements of the proposed system. By targeting these three aims, not only will safety be improved but operational efficiency will be improved through a reduction in shearer downtime.

To achieve our objectives, we completed the following research tasks.

Research tasks:

1.) Reviewed literature and worked with industry to identify representative conditions necessary to design robust system components to improve accuracy and response time.
2.) Selected low-cost methane sensors while designing and testing active and passive sampling and filtration systems.
3.) Procured a data acquisition system necessary to integrate and communicate with up to ten nodes but includes modular expansion capabilities.
4.) Developed a testing chamber and mock longwall laboratory in order to conduct durability tests of low-cost sensors and samplers and develop the integrated system.
5.) Reviewed the communications and electrical requirements necessary to develop a robust electrical and communications system that could be easily installed and interface with current longwall mine systems.
6.) Integrated system and electrical components from two and three and developed a data logging and management interface used to record, analyze, visualize methane concentrations, and control output variables.
7.) Demonstrated a fully functioning Methane Watchdog System with ten nodes – including the capabilities of controlling virtual shearers and ventilation systems.

4.0 Research Approach

4.1 Literature Review

Mining Conditions

Temperature and Humidity

The air supplied to the mine is brought in from the air above ground by means of large intake or exhaust fans. This meant that temperatures expected underground were mainly dependent on outside conditions. Air is heated and cooled due to location of operations and from working processes and vary on region/country of the longwall coal mine [5]. Data included in the Proceedings of the 22nd MPES Conference showed the ventilation exhaust temperatures ranged from around 16.1 to 23.9 °C (61 to 75 °F) [5]. Large ventilation rates also meant that humidity would likely vary regionally and diurnally. However, water is supplied to the working face via sprayers that are integrated into both the shields and shearer; this is a method used to control dust and help prevent explosions caused by coal dust ignition. Because of the abundance of water sprays, humidity and moisture levels can be expected to reach near 100 % relative humidity (RH) around the shearer due to continuous spraying.

Particle Matter

As a result of fracturing and crushing coal within a confined space, respirable dust was not only a major concern for the miner's health but also for the functionality of a deployed methane detection system. Today, advanced dust control techniques are in place to help limit the number of respirable particles from entering the main ventilation air by means of sprayers and ventilation checks. In industry, dust samples are collected to ensure that operations did not exceed air quality standards. The most common type of dust sampler used for these checks is a gravimetric sampler that quantified a volumetric flow for the prescribed sampling time and its collected weight of particles [6]. Federal regulations (30 CFR part 70.100) state that respirable dust must be continuously maintained to at or below 1.5 mg/m^3 (9.4x10^{-8} lb/ft^3) in active workings and 0.5 mg/m^3 (3.1x10^{-8} lb/ft^3) within 61.0 m (200 ft) out by the working face of each section's intake airways. Peng et al examined respirable control and presented data on sources and size distribution [7]. NIOSH reported on the coal dust sizes from 47 coal mines and presented results for mesh size and median diameter [8]. They also examined the breakdown of samples with a focus on rock dust, which was required for bituminous mining [9].

Based on reviews of literature, mining standards, and discussions with industry, see Table 4.1.1.

Table 4.1.1: Selected conditions for design and testing.

Mine Conditions			
	Average	**Minimum**	**Maximum**
Air Temperature (°F)	55-71	30	100
Absolute Humidity (lb/lb)	0.0092-0.0164	0.0035	0.0431
Relative Humidity (%)	50-90	20	100
Dust Loading (mg/m^3)	1.5	<1.5	<2.0
Dust Diameter (µm)	116-169	98	197
Dust by Size (70 Mesh) (%)	59-77	53	83
Dust by Size (200 Mesh) (%)	28-39	25	43

Longwall Mine Dimensions/Scale

Characteristic dimensions of working longwalls vary from region to region due to geological limitations, therefore an average length and effective cross-sectional area were derived from relevant data. A study completed in 2006 aimed to predict longwall methane emissions that resulted from increasing longwall face length in a Pittsburgh coalbed [10]. The actual working face in their study was 315 m (1032 ft), and projections for methane emission rates were made up to 488 m (1600 ft). The coal thickness or height (h) was 2.0 to 2.4 m (6.5 - 8.0 ft) and the width was unknown. Based on the time period and region of mining, it was more than likely a typical shield had a canopy length of 4.9 – 6.1 m (16 – 20 ft). From this, an assumed effective width of the longwall was 4.9 m (16 ft). Another study conducted a similar set of experiments that evaluated differences in two adjacent longwalls in Pocahontas No. 3 Coalbed (VP-1 Mine and VP-3 Mine). [11] The VP-1 Mine had a working longwall face of 228.6 m (750 ft) whereas the VP-3 Mine was 304.8 m (1000 ft). Coal thickness ranged from 1.5 to 1.9 m (5.0 to 6.3 ft) at the VP-1 site and 1.7 to 2.0 m (5.5 to 6.5 ft) at the VP-3 site. Once again, an effective width was assumed to be 4.8 m (16 ft). A later study was conducted in a longwall section of a Lower Kittanning mine in central Pennsylvania where continuous monitoring of both ventilation air flow and methane emissions were recorded in the return airways [12]. The longwall face in the study was 178.3 m (585 ft) long and had an average thickness of 1.37 m (4.5 ft). The type of shield used during these operations was unknown, though they were reported to have four 42-ton-capacity hydraulic props. We assumed that the effective width was less than that of the more recent studies due to smaller operations and age of equipment. Table 4.1.2 shows a summary of these data which were used as the basis of models in our study.

Table 4.1.2: Average working longwall coal mine dimensions.

Mine	Length	Width	Height
	m (ft)	m (ft)	m (ft)
Pittsburgh Coalbed (2006)	315 (1032)	4.9 (16)	2.0 - 2.4 (6.5 – 8.0)
Pocahontas No.3 VP-1 (1999)	229 (750)	4.9 (16)	1.5 - 1.9 (5.0 - 6.3)
Pocahontas No.3 VP-3 (1999)	305 (1000)	4.9 (16)	1.7 – 2.0 (5.5 - 6.5)
Lower Kittanning (1969)	178 (585)	< 4.9 (16)	1.4 (4.5)
Average	**257 (843)**	**4.9 (16)**	**1.8 (5.9)**

Methane and Its Control

Some of the most predominant dangers in coal mining operations are methane related explosions. Methane is a colorless and odorless gas that is one of the emissions of coal and it is flammable within its explosive range. The explosive range of methane is 5 to 15% methane by volume (in mixture with air) in which an ignition could occur; therefore, permitted methane concentrations in coal mines are federally regulated and why methane monitoring and mitigation is crucial. The amount of methane emitted from mines has increased, while the number of coal mines in operation have decreased of the last 50 or so years [13]. This is due in part to increased production from technologies such as longwall mining. Longwall mining originates back to the 18th century and grew to contribute 50% of overall underground coal yield as of 2007 [14].

Since efficiency in longwall coal mining operations is of high importance, it was ideal to maximize production rate while keeping methane concentrations below regulation limits. Thus, various

methods to help control methane emissions and allow for increased production rates have been a major focus over the past decades. A variety of methods now exist to abate methane related safety concerns, such as methane drainage systems and improved ventilation plans. Some methane drainage systems that have been beneficial to longwall mining include the use of boreholes and integration of bleeder systems into the ventilation plans [15]. Another methane control strategy is the addition of inert gases, such as carbon dioxide and nitrogen, to methane-air mixtures in order to make a less reactive mixture [16]. It is more advantageous, in cost and mining efficiency, to include the drainage and control systems in the original design than to implement them after the construction of the mine has taken place. These drainage systems and other methane control strategies aid in the ability to increase production rates while maintaining statutory limits of methane in the longwall.

Methane can be ignited as a resultant of the friction of cutting coal, which is one of the most common ignition sources. Temperatures that can ignite methane range from 630 to 1220 °C (1166 to 2228 °F). Methane can also be ignited by more readily in the presence of flammable particles such as coal dust. Therefore, to improve mine safety the Mine Safety and Health Administration (MSHA) sets regulations on permissible methane concentration, dust concentrations, and the required ventilation rates necessary to ensure safety during operation. Key regulations are Code of Federal Regulations (CFR) Part 30 Section and are summarized below [3].

- 75.342 – Methane Monitors
    - Require sensor on cutting machines and face equipment, placed as near the face as possible
    - Provide a warning signal at 1% to enable a person to deenergize equipment
    - Automatically deenergize at 2%
    - Monthly calibrations (31 days)
- 75.323 – Excessive Methane
    - Changes to ventilation or work at 1%
    - Removal of non-key personnel at 1.5%
    - Limit bleeders to 2.0%
- 75.325 – Air Quantity
    - In longwalls – at least 30,000 cfm at the face
    - Velocity reporting at least 15.2 m (50 ft) but no more than 30.5 m (100 ft) from HG and TG, respectively
- Part 22-Portable Methane Detectors
    - Minimum indication range from 0.25 to 4.0%
    - Other standards for permissibility

Ventilation Plans

Adequate ventilation along the longwall face is crucial for control of methane emissions that are a product of mined and fractured coal. Methane ventilation plans are required for all longwall mines. Such plans must meet minimum flow rates, which are federally regulated, but the actual flow rates vary by mine. Mines that experience increased levels of methane due to high ranking coal of the region may require additional ventilation strategies such as bore hole degasification techniques or slower production rates. In addition, seam height and cross-sectional flow area vary, thus leading to variable flow velocities in mines. Ventilation goals aim to direct the majority of air across the face however some air flow is lost past curtains and into areas such as the gob. Complexities of

controlled pathways along the entry and returns of a longwall mining operation can limit the amount of available fresh air to send down the face. Because of these limitations, production may be stopped due to rising methane levels. Early studies showed dilution flow rates of 47.2 m^3/s (100,000 cfm) with velocities over 5.1 m/s (1000 feet per minute (fpm)). Krog et al used sulfur hexafluoride (SF6) releases to study air flow pattern along longwall faces and through ventilation systems. Velocities varied throughout the mine and along the face, but they reported velocities as high as 3.6 to 6.1 m/s (700 to 1200 fpm) [17]. Schatzel et al also reported average face velocities from 2.2 to 3.0 m/s (433 to 596 fpm) in another study [18]. Recently, modeling efforts presented average face velocities from around 1.5 to 4.6 m/s (300 to 900 fpm) [2].

Methane emissions and airflow patterns in a bleederless longwall operation were studied by the Pittsburgh Mining Research Division (PMRD) and the U.S. National Institute for Occupational Safety and health (NIOSH) [17]. This study was conducted in a western longwall coal mine with a working face of 300 m (984 ft) where the average face air velocities were reported to be 3.03 m/s (596 fpm) at shield 57 and 2.20 m/s (433 fpm) at shield 165. The longwall used 176 shields to support the roof which had a mining height of 3.4 m (11 ft). From the Lower Kittanning study of 1969, air velocities were measured in the return airway of two different mining sections. [12] An average was taken from a set of measurements along the cross-section in a grid fashion with a hand-held vane type anemometer. The average velocity for the first section was 2.5 m/s (495 fpm) at a cross-sectional area of 6.1 m^2 (66 ft^2) and 2.3 m/s (454 fpm) at 7.7 m^2 (83 ft^2) for the second section. The respective volumetric flow rates would be 15.4 m^3/s (32,670 cfm) and 17.8 m^3/s (37,683 cfm). Values were also estimated by industry from a Pennsylvania mining operation to be 23.6 m^3/s (50,000 cfm) of air along the face, where a velocity of 2.54 m/s (500 fpm) at shield 20 and 2.03 m/s (400 fpm) at shield 270 must be maintained. Table 4.1.3 shows the summary of ventilation data reviewed.

Table 4.1.3: Average ventilation velocity along the longwall face.

Mine	Velocity HG and TG	Volumetric Flow
	m/s (fpm)	**cfm**
Western longwall	3.03 (596) and 2.20 (433)	105,000
Lowe Kittanning	2.50 (495) and 2.31 (454)	32,670 and 37,683
Pennsylvania mine	2.54 (500) and 2.03 (400)	50,000
Average	**2.69 (530) and 2.18 (429)**	**-**

Note: HG = Headgate, TG = Tailgate

Production Rates

Bituminous coal contains a considerable amount of methane that is released or desorbed as a result of fracturing and shearing the coal. Therefore, the rate at which the coal is cut or produced can directly affect the methane concentrations downwind near the TG where the air exits the face. These emissions can be immediate contributors, whereas fallen coal in the gob is constantly releasing and accumulating methane as its desorbed. The production data found were compiled from a study in a central Pennsylvania coal mine and can be seen in the Table 4.1.4. We note that this study was older but does provide useful data regarding the amount of coal produced versus the methane emissions.

Table 4.1.4: Coal production analysis from previous work [12].

Production data from 1969 Study				
Working	**Idle**	**Coal Produced**	**Production Rate**	**Idle Percentage**
min	**min**	**tons**	**tons/min**	**%**
140	340	180	1.286	71
30	450	40	1.333	94
10	470	1	0.100	98
120	360	154	1.283	75
45	435	58	1.289	91
0	480	0	0.000	100
110	370	131	1.191	77
180	300	231	1.283	63
100	380	129	1.290	79
0	1400	0	0.000	292
0	1440	0	0.000	300
120	360	154	1.283	75
0	480	0	0.000	100
152	328	185	1.217	68
155	325	199	1.284	68
120	360	154	1.283	75
45	435	59	1.311	91
130	350	167	1.285	73

Note: Approximately 200 tons of coal were produced during a single pass.
Average Production Rate = 0.9288 tons/min (volumetric equivalent = 22.1 cfm)

Production rates directly correlated to the shearer velocities. Shearer velocities were much slower than the wind speeds. Mitchell examined various shearer and cutting methods and peak shearer velocities ranged from 0.16 to 0.25 m/s (32 to 50 fpm) [19]. Similar values of 0.17 to 0.25 m/s (33 to 50 fpm) were also referenced in Guidelines for the Prediction and Control of Methane Emissions in Longwalls [20]. Krog et al later referenced average shearer velocities as 0.23 m/s (46 fpm) with an average longwall face ventilation velocity of 2.5 m/s (500 fpm) [21]. Shearer rate data were also compiled from a 1999 NIOSH study and can be seen in Tables 4.1.5 and 4.1.6.

Table 4.1.5: Average cutting (production) rate for a single 750 ft pass [11].

Avg. single pass data (750ft long face) 1999			
Working	**Idle**	**Total Time**	**Shearer Rate**
min	***min***	***min***	***fpm***
45.8	6	51.8	14.5
42.1	2.6	44.7	16.8
39.9	1	40.9	18.3
Average	**-**	**-**	**16.5**

Table 4.1.6: Average cutting (production) rate for a single 1000 ft pass [11].

Avg. single pass data (1000 ft long face) 1999			
Working	**Idle**	**Total Time**	**Shearer Rate**
min	***min***	***min***	***fpm***
65.9	27.7	93.6	10.7
49.6	11.5	61.1	16.4
Average	**-**	**-**	**13.5**

Yearly production reports are readily available for most mines in the country and can be dated back nearly 100 years. Unfortunately, the industry only reports coal production on a tons per year basis and a total number of hours worked by underground employment. Sometimes a production or efficiency rate can be found that divides the produced tons by the total number of hours worked to get a 'tons per miner hour'. These values provide little insight into deriving an equivalent emission rate based on a time varying volumetric removal.

Methane Emissions Studies

When predicting methane emissions along the face and determining its correlation to production, a few considerations must be examined. Standard practice in longwall coal mining required fresh ventilated air to always flow from HG to TG of the face. The shearer on the other hand, will cut coal in both the HG to TG and TG to HG directions. This meant that coal is mined both with and against the direction of ventilated air with each pass. Because of this, the question may arise whether methane emissions are greater at the TG (downstream of ventilation) for one of these scenarios. It was reported that methane emissions were slightly higher in HG to TG passes than those of TG to HG. [11] From a production analysis conducted in their study, it was reasoned that elevated emissions may have been the cause of longer production times required to cut in the HG to TG direction, allowing more time for methane to bleed off from the recently fractured coal. The production analysis categorized data into three bins that were defined by the percentage of delay time: All Data, <50% delay, and <25% delay. With <25% data being the most stringent case where delay time during segment passes was minimal, data collected within this scenario were minimal and showed how significant delay time was throughout production due to elevated methane levels. No ventilation flow rates were reported, only flow rates of methane, therefore an actual percentage profile of methane experienced during the study was unknown.

In 2006, a case study was conducted that aimed to predict longwall methane emissions as a consequence of increasing longwall face lengths [10]. Their findings were more complete and provided insight to methane emission profiles along the face for uninterrupted production. Implementing three continuously methane monitoring stations at shields 20, 80, and 145, multiple passes were recorded in both the HG to TG and TG to HG directions. From these data, an analysis was performed on both a single pass and daily operational basis. The difference in concentrations measured between the consecutive sensors (shield locations) was plotted and fitted to form a linear relation, shown by Eq. 4.1.1. This equation was used to solve for expected methane concentrations for extended longwall faces of 426 m (1400 ft) and 488 m (1600 ft). From Eq. 4.1.1, a relationship was made from this trend and the amount of coal produced from the single pass. Note, methane

was considered negligible at the entry and therefore no data were provided before the first sensor at shield 20.

$$y = 0.0002329x - 0.00783; \quad R^2 = 0.993 \qquad \textbf{Eq. 4.1.1}$$

Methane Sensors and Analyzers

Multiple forms of methane sensors are currently available on the market for a variety of applications. Some operational principles of methane sensors include metal oxide and catalytic bead sensors, infrared (IR) sensors, and advanced laser spectroscopy methods. For decades, industry relied on the standard catalytic or LEL type sensors for their fast response times and low cost [22]. With more recent developments of gas detection technology in other industries, there are a variety of sensors and methods to quantify and monitor atmospheric gases which could potentially be implemented in the longwall mining industry.

Metal Oxide Semiconductor (MOS) Sensors

MOS gas detection sensors operate on the principle of absorption and release of oxygen from the semiconducting metal oxides (SMOX) in the presence of a target gas. In other words, the surface containing the metal oxides, in most cases tin dioxide, absorbs oxygen at temperatures between 150 and 400 °C (302 and 752 °F)from the surrounding air and reacts with the combustible, reducing, or oxidizing species [23]. When this reaction occurs, it effectively changes the resistance across the sensor element as the donor electrons release the absorbed oxygen. The resulting change in resistance is correlated to the change in gas concentration using data acquisition and signal processing. These types of sensors are highly sensitive to fluctuations in concentration, and therefore possess desirable response times [24]. Due to the chemical reactive principle of these sensors however, most species containing the hydrocarbon bond in combustible gasses will react with the sensing element and may alter the measurement of a targeted gas. Calibration techniques and specific element doping of the semiconductors have been used to combat these issues and filter out target gas responses. The MOS sensors have been widely used in industry for a cost effective and robust approach to measuring dangerous gasses [25].

Catalytic (CAT) LEL Sensors

Catalytic-type sensors, or catalytic combustion sensors, reduce the ignition temperature of combustible gasses as they interact with the catalytic material of the sensor element. As a result, oxidation of the gas molecule will occur and cause the temperature of the catalytic element to increase. The conductive properties of the signal wire, which contain the catalytic bead, will change with temperature. The resulting temperature changes from the reaction of the target gas will vary the voltage output and therefore be correlated to the concentration of gas present. The CAT sensors also make use of a Wheatstone Bridge electrical circuit to reference an inactive catalytic bead. The reference bead does not react to the gas present and therefore allowed for a perfectly balanced and compensated circuit. This pair of catalytic beads and coiled wire integrated into the circuit create a stable and rugged construction that produce a linear output as a function of gas concentration. The rate of reaction is directly proportional to the sensors response and therefore creates accurate measurements and fast response times [26].

Infrared (IR) Sensors

Unlike the electrochemical properties of the LEL sensors commonly used, the infrared sensor quantifies a concentration based on the absorption of IR radiation. Known wavelengths of radiation will pass through the volume of the analyzer; when a gas is present in the volume, the absorption

of radiation will be affected, and the resulting signal corresponds to a concentration of gas. These analyzers can be precisely tuned to operate within a specific range of gas concentration and for a specific species of gas. The IR analyzers can also be classified as both point and open path detectors that may be used depending on the measuring application. Point detectors are single compact units that contain a fixed absorption path length whereas open path detectors have both a source and receive component that can be placed across an area of interest of up to 130 meters. A key component to the IR sensing technology over the LEL sensors is their sophisticated on-board diagnostics. The IR sensing unit can communicate its current status and faults to the user in the event the sensors operational behavior changes. The IR detectors are also impervious to poisoning as a result of exposure to highly concentrated gas or repeated use [27].

Advanced Methods

Other more advanced forms of quantifying target gas and emissions exist but are usually costly and limited in application. These analyzers are usually used among research and require additional resources to analyze data. The Los Gatos Research (LGR) group manufactures several analyzers for detecting greenhouse gasses that operate on the principle of off-axis integrated cavity output spectroscopy (OA-ICOS) technology. The analyzers can simultaneously measure CH_4, CO_2 and H_2O with a precision of 2 parts per billion (ppb), 300 ppb, and 200 ppb, respectively. The operational principle described here has a closed cell, through which the sample is pulled by means of a small auxiliary pump within the unit [28]. Other analyzers, such as the Li-COR LI-7700, are open path methane analyzers that operate on a single-mode, tunable, near-infrared laser. It uses Wavelength Modulation Spectroscopy (WMS) to scan the open path where a gas may become present and then demodulates it back to a reference signal to determine a concentration of CH_4 [29]. Analyzers such as these can report concentrations with a high level of precession when used in intended applications.

In Industry

Most, if not all, methane monitors used in the longwall mining industry today still utilize the CAT sensors. They are relatively cheap and robust, which makes them suitable for the application. In a study conducted to analyze response times of machine mounted methane monitors, three different MSHA approved units were used; all three units used a CAT sensor for methane detection [30]. For proper operation of the CAT sensors, the methane concentration must be below 8% and the oxygen level must be above 10%, therefore, oxygen sensors are often used in conjunction with the CAT sensors. [16]

However, as improvement in the safety systems and other technologies in mines have been on the rise, research has examined other sensor types could be more appropriate for industry or why the CAT sensors have been used and unchanged over the past decades. Specifically, IR sensors may be able to take the place of the CAT sensors. Some IR sensors, while not as many as the CAT sensors, have already been MSHA approved. An improvement in measurement range could be made if the IR sensors are implemented in industry as they have the ability to accurately measure up to 100% methane; they also do not require oxygen for measurements [31]. Some IR sensors could even provide faster response times. One study compared response times of two monitors, each containing an IR sensor, and one monitor containing a CAT sensor. One of the monitors with an IR sensor had a faster response time then the monitor with the CAT sensor and the other had a slower response time. They determined that the response times for the IR sensors were heavily dependent on the sensor housing, which protect the sensor from hazardous environmental conditions [32]. One downfall to using the IR sensors is that the measurement accuracy could be

affected by dusty or high humidity environments [22]. The accuracy of methane measurements made by some IR sensors may also be affected by other hydrocarbons, such as ethane. The measurements made by one IR sensor in a study by Taylor et al overestimated concentration in the presence of ethane while the other was un-affected [32].

Sampling Approaches

There are various sampling methods that can be used for methane detection in longwall mining. One method used is the passive sampling method, also known as diffusion sampling. For diffusion sampling, the sensor is placed directly in the area to be monitored (sampling location) and the sample, which could be a potentially hazardous concentration of methane, passes by it via the mine ventilation already in place or by the movement of the machine on which it is mounted. Federal regulations require a methane monitor to be placed on certain mining equipment such as the longwall shearer since areas close to the face are of concern for "high" methane concentrations; the shearer could cause a frictional ignition if the dangerous methane levels are not detected and the shearer is not deenergized. Many machine-mounted methane monitors use the diffusion sampling method as they are located at the sampling location; they generally have some sort of housing to help protect them from physical damage. A study analyzed mounting locations of the methane monitor on the mining machinery, methane monitors were placed at multiple locations on the mining machine which were at various distances away from the longwall face. Since the monitors were placed directly in their corresponding sampling locations, monitors closer to the longwall face were at higher risk of physical damage. This was taken into consideration when conclusions were made for the study [33]. Federal regulations also require methane measurements to be periodically taken at various locations in the mine by a miner using a handheld methane monitor in addition to the continuously monitoring shearer sensor. Some "handheld" monitors can be attached to the miner, typically using some sort of clip, and are continuously monitoring the gas concentrations surrounding the miner. RKI Instruments makes one of these monitors and it generally operates using the diffusion sampling method, however the addition of a hand aspirator or motorized pump is optional; if one of these were added, it would then operate as an active sampler [34].

Since the passive sampling method placed the sensor directly at the sampling location, which could possibly cause risk of damage to the sensor if it were not properly protected, an active sampling method could also be used. If an active sampling method were used, the sensor can be housed at a remote location, away from physical hazards, where the sample was actively pulled from the sampling location safely to the sensor. The transport of the sample can be powered by various sampling systems (samplers). One type of sampler that could be used to pull the sample is the use of one or more air pumps. Many handheld methane monitors utilize a pump to transport a sample. The pump can either be an attachment for optional use, like for the RKI monitor mentioned previously, or the monitor can have a built-in pump [31].

Another type of sampler that could be used is an ejector which can be powered by compressed air or pressurized water; this eliminated the need for electricity or moving components at the sampler. An ejector operates using the "venturi" effect. Simple, single-stage ejectors consist of three components: a nozzle, suction chamber, and a diffuser. As the motive, or primary, pressurized fluid passes through the nozzle, its velocity increases, creating a vacuum in the suction chamber. This motive fluid can be a gas, vapor, or liquid. This low-pressure region causes the suction, or secondary, fluid to be pulled into the suction chamber and mix with the primary fluid as it enters the diffuser, from which the mixture exits the ejector [35]. In the application of using an ejector as

a sampler for methane detection, the secondary fluid would be the sampled air transported from the area of interest to the remotely located node.

The sampler(s) could theoretically be placed at any location(s) with a tube(s) connecting the sampler to the sensor location. Another tube could be attached at the sensor location and lead to the sampling location. This was beneficial for sampling in restricted areas that are un-accessible to miners or sampling in locations containing physical hazards that could cause sensor damage. One downfall to the active sampling method, however, is that there could be a significant measurement delay time depending on the distance between the sensor location and the sampling location since there would be a "travel" time associated with the sample travelling from one location to the other. It is ideal for this time to be minimized to provide time-sensitive measurements.

4.2 Initial Design and Sensor Selection

The original proposed monitoring system consisted of an active venturi driven housing that would contain the methane sensor and some filtration material. The housing unit would have consisted of some robust noncorrosive material that could adequately house the sensors and withstand the harsh mining conditions. Figure 4.2.2 shows the proposed design.

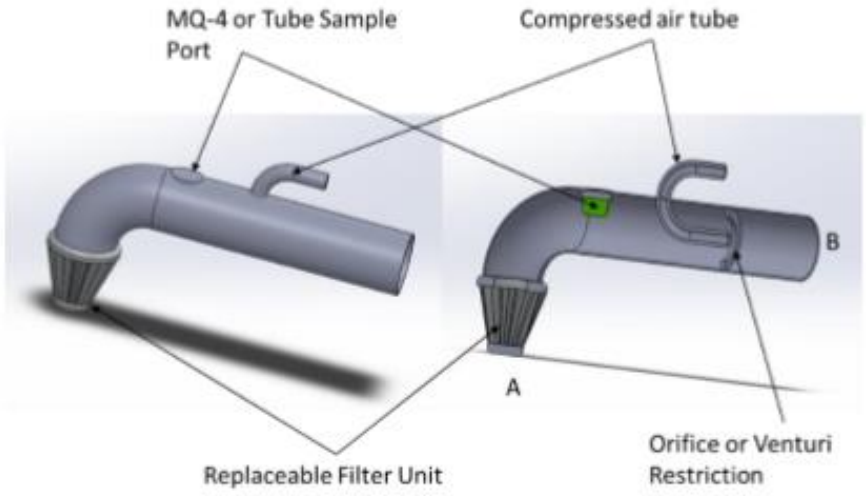

Figure 4.2.1: Original proposed design for a sampling unit.

The MQ-4 Sensor (MOS)

The first sensor selected for the MWS was the MQ-4 methane sensor, which is a metal-oxide sensor (MOS). This sensor is low cost (~$5). Figure 4.2.3 shows the provided data sheet for the MOS that contains the power requirements and operational limitations. For wiring and replacement of the MOS, an additional wiring "chip" was purchased that accommodated the six prongs of the individual sensor and created a wiring harness. This reduced the wiring configuration to take in ±5 V from a power supply, and signal wire that was connected to the data acquisition device. The manufacturers also recommended a load resistor of 4.7 kΩ be placed between the ground and signal wire. Upon further development of calibration strategies, the 4.7 kΩ resistor was replaced with an 8.77 kΩ. This load resistance helped vary the high and low detection limits of the sensor, this allowed for more accuracy within these regions. The 8.77 kΩ was selected to extend the upper limit of the sensor's response range to 2% methane for calibrations. Due to the sensor's nonlinear

response, advanced calibration strategies were developed to maintain accuracy throughout the entire detectible range.

Model			MQ-4
Sensor Type			Semiconductor
Standard Encapsulation			Bakelite, Metal cap
Target Gas			Methane
Detection range			300～10000ppm(CH_4)
Standard Circuit Conditions	Loop Voltage	V_c	≤24V DC
	Heater Voltage	V_H	5.0V±0.1V AC or DC
	Load Resistance	R_L	Adjustable
Sensor character under standard test conditions	Heater Resistance	R_H	26Ω±3Ω(room tem.)
	Heater consumption	P_H	≤950mW
	Sensitivity	S	Rs(in air)/Rs(in 5000ppmCH_4)≥5
	Output Voltage	Vs	2.5V～4.0V (in 5000ppm CH_4)
	Concentration Slope	α	≤0.6($R_{5000ppm}$/$R_{1000ppm}$ CH_4)
Standard test conditions	Tem. Humidity		20℃±2℃; 55%±5%RH
	Standard test circuit		Vc:5.0V±0.1V; V_H:5.0V±0.1V
	Preheat time		Over 48 hours

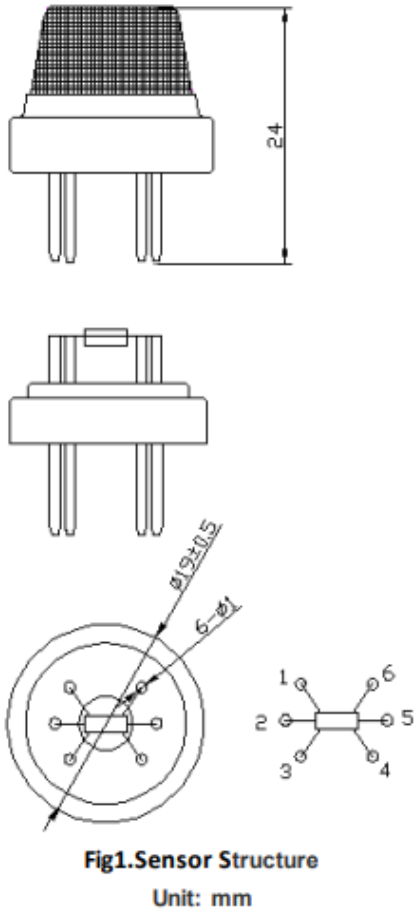

Fig1.Sensor Structure

Unit: mm

Figure 4.2.2: MQ-4 sensor specifications.

The Dynament Sensor (IRS)

The Dynament sensor, which was an infrared sensor (IRS), was initially selected to be a secondary methane sensor due to its larger range of operation and since it was less affected by climate conditions as the MOS. The IRS is a moderately low-cost sensor (~$150). The product purchased for the initial design comes equipped with an explosion proof housing and necessary filters to protect the sensor in harsh conditions. The housing contained the necessary wiring for power and signal processing and was wired into a connection terminal for easy removal during testing. The IRS included a linear factory calibration for a targeted range of methane; in this case 0-5% by volume. Figures 4.2.4 and 4.2.5 provide the IRS specifications.

GENERAL SPECIFICATION	
Operating Voltage Range:	3.0 – 5.0 V d.c.
Operating Current:	Average current 15mA. See graph on page 7
Operating temperature range:	-20°C to +50°C (-4°F to 122°F)
Warm up time:	To final zero ± 2% of full scale: 1 minute @ 20°C (68°F) ambient
Storage temperature range:	-20°C to +50°C (-4°F to 122°F)
Humidity range:	0 to 95% RH non-condensing.
Digital signal format:	8 data bits, 1 stop bit, no parity. 2.8V logic level
Standard baud rates:	38,400, 19,200, 9600, 4800
User configurable parameters:	Full-scale value, resolution, Sensor 'zero' function Sensor 'span' function
MTBF:	> 5 years
Weight:	15 grams
Pressure	± 5% of the calibration pressure to maintain the accuracy limits

HYDROCARBON CHANNEL SPECIFICATION	
Methane measuring range:	0-5%, 0-100% volume or both
Hydrocarbon measuring range	0-100% LEL equivalent
Resolution:	0.01% for readings up to 5% volume methane 0.1% for readings from 5% up to 100% volume methane 0.01% propane for all readings
Accuracy:	± 10% of the reading @ 20°C (68°F), 1 bar pressure, applied gas.
Response Time T_{90}:	<30s @ 20°C (68°F) ambient
Zero Repeatability:	± 1% of full scale @ 20°C (68°F) ambient
Span Repeatability:	± 2% of full scale @ 20°C (68°F) ambient
Long term zero drift:	± 1% of full scale per month @20°C (68°F) ambient, (max ± 3% of full scale per year)
Temperature performance: * May not be applicable when using gas cross-reference factors	± 0.1% volume or ± 10% of reading up to 50% of full scale, ± 15% of reading from 50% to 100% of full scale, or 2% of full scale whichever is greater over the range -20°C to +50°C (-4°F to 122°F)
User configurable parameters and functions:	Sensor 'zero' function Sensor 'span' function Over-range value

Figure 4.2.3: Dynament sensor specifications.

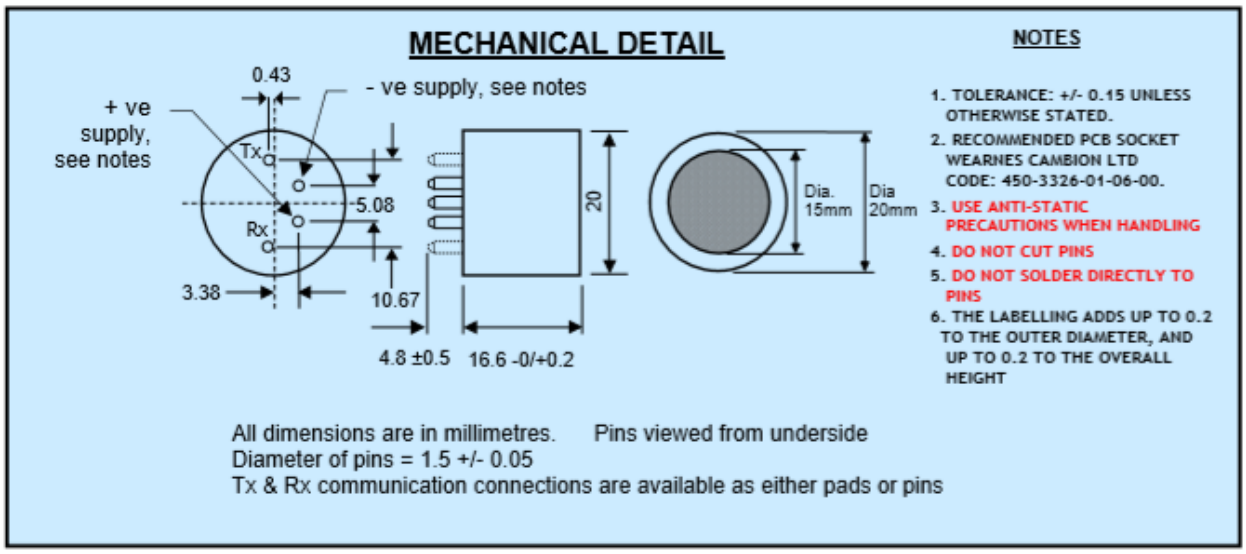

Figure 4.2.4: Dynament sensor diagram.

Sampling System

As initially proposed, a stainless-steel tube was purchased to house the MOS and IRS for experimental testing. Figure 4.2.6 shows the dimensions of the tube. A cap was threaded onto one end of the stainless-steel tube that contained a Yor-Lok fitting for connection of Teflon tubing that supplies either the gas sample or for connection to an auxiliary pump to pull a sample through.

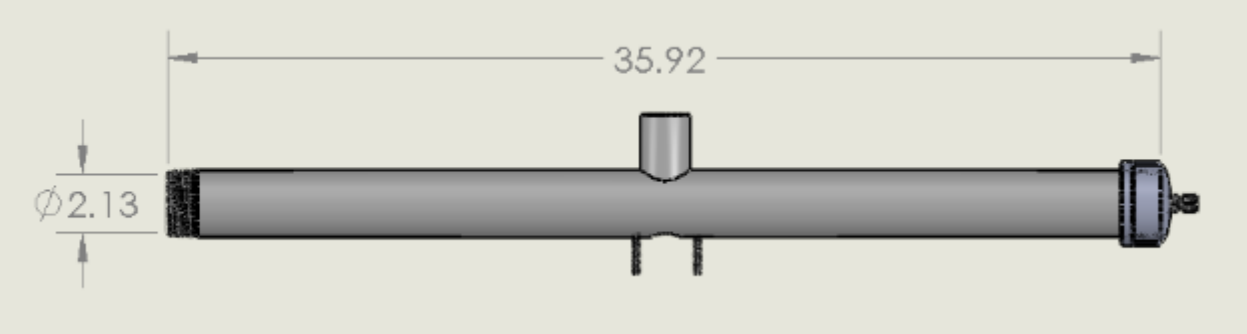

Figure 4.2.5: Initial design of the proposed sampling system for the methane watchdog monitor. Dimensional units [in].

The stainless-steel tube was then modified to house both the MOS and IRS so that the sensor heads would be adequately exposed to the flow in the tube. Two holes were drilled adjacently halfway down the tube 0.47 m (1.54 ft from the entrance) to fit the respective dimensions of each sensor. Since the IRS was equipped with a stainless-steel housing, the housing was modified and welded to the sampling tube so that the sensor could still be fitted and sealed to minimize leaking. The MOS required additional means of securing and sealing due to its profile. We found that the MOS was susceptible to leaking through the construction of the sensor itself. To combat this, electronics potting epoxy was used to fill and seal the back of the sensor. After several different gasket materials and approaches of mounting the sensor to the sampling tube were tested, an O-ring was selected to seat in between the sensor and tube. Two threaded rods were welded in line with the sensor head inlet of the tube for securing the MOS onto the O-ring. Leak proofing the sampling

apparatus was crucial to protect against sample dilution and false readings. Figure 4.2.7 shows the initial design with the sensors mounted in place.

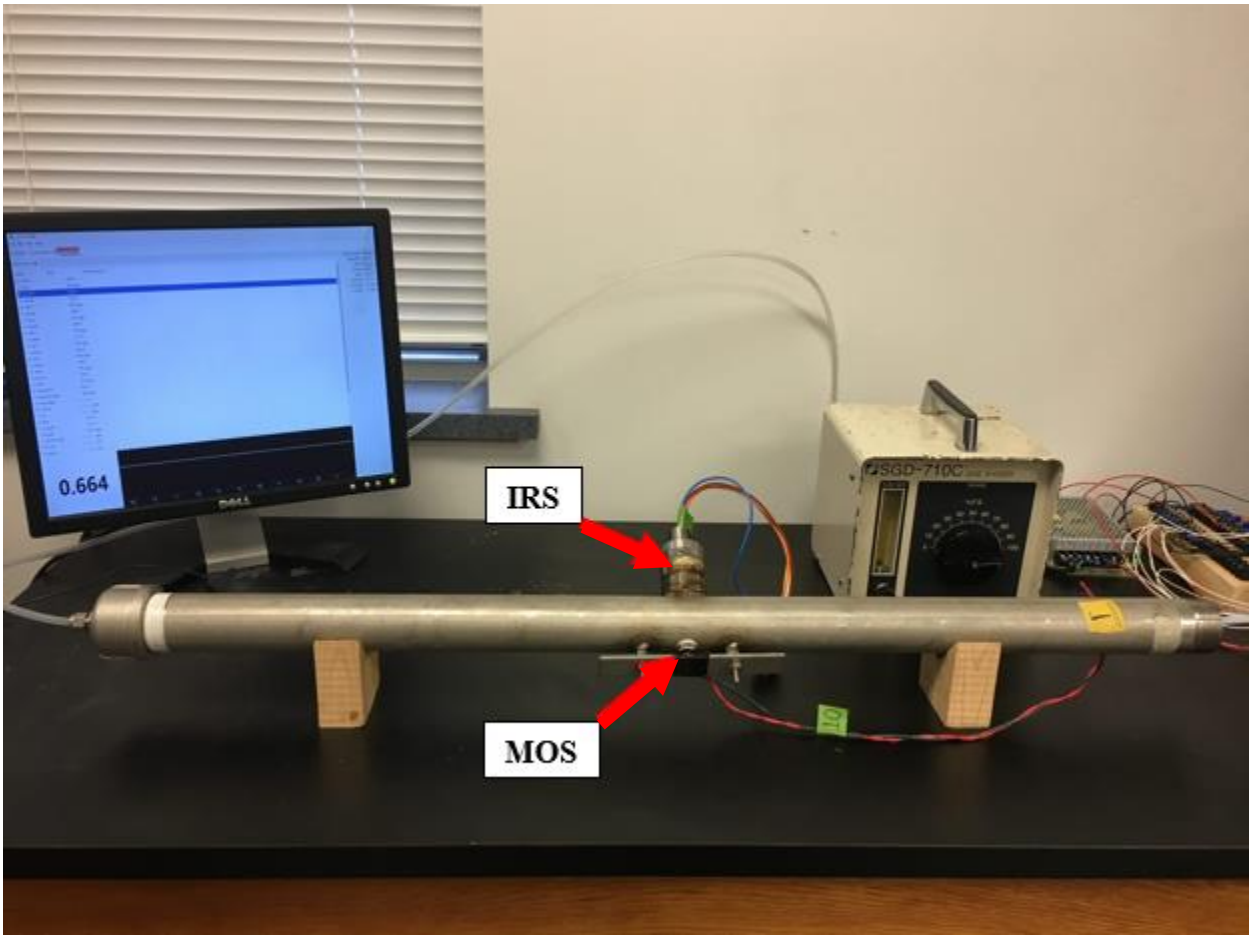

Figure 4.2.6: Initial sampling unit design.

Data Acquisition/Signal Processing

The MOS and IRS were powered from an external 5V power supply and communicated with a desktop computer. The raw signals of the sensors first passed through a data acquisition device (ICP DAS: PET 7019Z) which relayed information to a computer via ethernet. This device was also compatible with thermocouples, which were also implemented to monitor sample temperatures. Additionally, an environmental condition monitoring device by OMEGA measured barometric pressure, temperature, and humidity. It was included as a standard reference for background conditions when collecting data. To record and view the collected data and parameters, an in-house software (Scimitar) was used on the desktop. This software enabled calibrations and control of desired parametric variables.

4.3 Second Generation Design

Once the initial methane sampling unit was subjected to various laboratory procedures to test for sensor response and calibrations, a significant sampling delay time as well as climate effects on the CH_4 sensors became apparent. The delay time was a direct consequence of the large inner diameter of the stainless-steel pipe used for the initial design. To combat system response times

and minimize bulk of design, a new approach was taken, and a second-generation design was conceived. The architecture of the new design consisted of a centrally located unit (node) that contained the methane sensors as well as environmental sensors to combat climate effects. The sample was collected from a discrete location, away from the unit. The sampling tube consisted of a reduced inner diameter flexible line that significantly reduced sampling delays by increasing sample velocity.

Two Sampling Locations per Node

After initial testing, we determined that each node should consist of two sampling locations, one near the face (shield tip) and one near the gob. Having two sampling locations for each node allowed for a greater number of sampling locations without increasing the number of sampling units; this helped make the system more cost effective. The sampling node alternated sampling between the two locations at a prescribed time interval and was controlled by a three-way valve. When the valve was energized, the node sampled from the gob and when it was deenergized, the node sampled from the face. We assumed a default status at the mining face would be beneficial for enhanced safety even in the case of a disabled valve. The sample traveled through a 2.1 m (7 ft) tube from the sampling location to the node. The end of each tube at the sampling locations was connected to an enclosed filter to protect against coal dust and water droplets. Figure 4.3.1 shows the two sampling locations per node configuration.

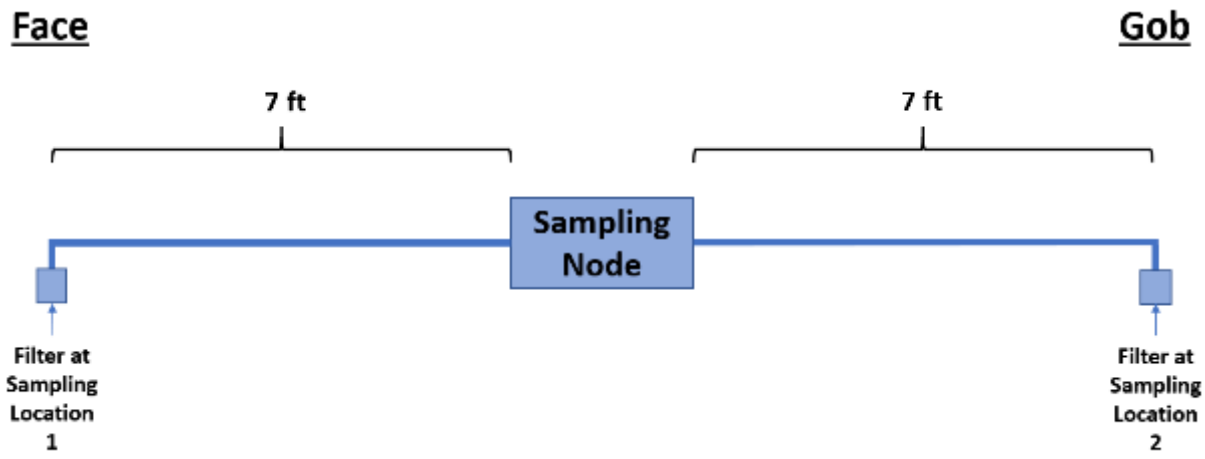

Figure 4.3.1: Two sampling locations at each node configuration.

Filtration Requirements

Three filters were purchased for experimental evaluation after an initial assessment of commercially available filters. All three filters were pleated and varied in geometry. These geometries consisted of a conical, cylindrical, and flat/cassette type structures. Table 4.3.1 includes the individual filter details. Filters were assessed on several criteria that would be crucial to the performance and integrity of the filter in the harsh environment of a coal mine. Due to the presence of water and coal dust associated with mining, it was imperative that the filtration system performed effectively and efficiently as to not affect or damage any internal sensors. Therefore, a series of tests were administered to each filter that assessed the effects of pressure losses over the system due to water and coal dust loading on the filter media.

Table 4.3.1: List of filters selected for experimental testing.

Filter	Geometry	Effective Filtration Area [m^2]
Spectre	Conical	0.0102
McMaster Carr	Cylindrical	0.0147
Solberg	Flat	0.0185

Effects of pressure due to flow rate

The first test consisted of baseline measurements, where air was pulled through each filter by a pump. A pressure measurement device (Heise) was used to measure the resulting differential pressure (pressure drop) across the filter media at various flow rates. These tests were performed at flowrates of 1, 2, 3, and 4 standard liters per minute (slpm) (0.035, 0.071, 0.106, and 0.141 standard cubic feet per minute (scfm)); which covered the proposed sampling rate of roughly 2 slpm (0.071 scfm). Results are found in Table 4.3.2.

Table 4.3.2: Examination of flow restriction across dry unloaded filter at various flow rates. Units [inH2O]. 1 inH2O = 0.03609 psi.

Filter	4 slpm	3 slpm	2 slpm	1 slpm
Spectre	1.041	0.655	0.341	0.126
McMaster Carr	0.012	0.008	0.006	0.004
Solberg	0.032	0.022	0.015	0.008

Effects of pressure due to dust loading

To assess the effects of dust accumulation on the individual filters, a procedure to accelerate the cake formation on the filter media was used to simulate effective filtration life. This experiment correlated the amount of coal dust loaded to a resulting pressure drop that would ultimately lead to a reduction in sampling flow. To more accurately mimic the cake formation of coal dust on each of the filter's media, an apparatus was designed to effectively suspend coal dust within the proximity of a filter that actively sampled the dust laden air. This not only allowed for uniform dust loading but also enabled control of how much coal dust was added to the filter. From a review of literature, an average daily coal dust loading was found to be 0.144 g/day which equated to 1.008 grams per week. The filter was initially weighed before entering the dust loading apparatus and weighed after to achieve a simulated 1 weeks' worth of coal dust. This procedure was carried out for each filter and the results are reported in Tables 4.3.3 - 4.3.5.

Dust Loading Simulation Results

Table 4.3.3: Evaluation of coal dust on Spectre Filter (Blue). Initial weight of filter: 53.7g. Effective filtration area: 0.0102 m^2.

Time	Loading [g]	Pressure @3.5 slpm [inH_2O]	Pressure @3 slpm [inH_2O]	Pressure @2 slpm [inH_2O]	Pressure @1 slpm [inH_2O]
1 day	0.1	1.560	1.218	0.652	0.240
1 week	1	1.605	1.224	0.626	0.202
2 weeks	2	1.592	1.240	0.639	0.211
3 weeks	3	1.625	1.267	0.670	0.222
4 weeks	4	1.707	1.348	0.721	0.249

Table 4.3.4: Evaluation of coal dust on Cylindrical Filter (White). Initial weight of filter: 65.2g. Effective filtration area: 0.0147 m^2.

Time	Loading [g]	Pressure @3.5 slpm [inH_2O]	Pressure @3 slpm [inH_2O]	Pressure @2 slpm [inH_2O]	Pressure @1 slpm [inH_2O]
1 day	0.1	0.010	0.008	0.005	0.003
1 week	1	0.012	0.010	0.006	0.003
2 weeks	2	0.013	0.011	0.007	0.003
3 weeks	3	0.027	0.023	0.015	0.007
4 weeks	4	0.037	0.031	0.020	0.010

Table 4.3.5: Evaluation of coal dust on Solberg Filter (Black). Initial weight of filter: 14.1g. Effective filtration area: 0.0185 m^2.

Time	Loading [g]	Pressure @3.5 slpm [inH_2O]	Pressure @3 slpm [inH_2O]	Pressure @2 slpm [inH_2O]	Pressure @1 slpm [inH_2O]
1 day	0.1	0.028	0.022	0.014	0.006
1 week	1	0.043	0.035	0.022	0.010
2 weeks	2	0.052	0.043	0.027	0.013
3 weeks	3	0.082	0.067	0.043	0.020
4 weeks	4	0.138	0.115	0.074	0.036

Effects of pressure due to water loading

Following the coal dust loading simulation, a similar procedure was conducted that assessed the flow restriction due to the presence of water on the filter media. The coal dust on the filter from the previous experiment was mostly removed. The remaining coal dust was accounted for and included in the initial weight of the filter before water was added. Similar to the dust loading procedure, water was incrementally added to the filter and a new weight was recorded. The results are reflected in the Tables 4.3.6-4.3.8.

Table 4.3.6: Evaluation of wetted Spectre Filter (Blue). Initial weight of filter: 54.6g. Effective filtration area: 0.0102 m^2.

Loading [g]	Pressure @3.5 slpm [inH_2O]	Pressure @3 slpm [inH_2O]	Pressure @2 slpm [inH_2O]	Pressure @1 slpm [inH_2O]
0 (dry)	1.543	1.218	0.624	0.196
0.1	1.607	1.216	0.644	0.199
0.4	1.616	1.219	0.633	0.208
1.8	1.643	1.231	0.639	0.206

Table 4.3.7: Evaluation of wetted Cylindrical Filter (White). Initial weight of filter: 66.2g. Effective filtration area: 0.0147 m^2.

Loading [g]	Pressure @3.5 slpm [inH_2O]	Pressure @3 slpm [inH_2O]	Pressure @2 slpm [inH_2O]	Pressure @1 slpm [inH_2O]
0 (dry)	0.010	0.008	0.005	0.002
0.1	0.010	0.008	0.005	0.002
0.5	0.010	0.008	0.005	0.002
1.8	0.011	0.009	0.006	0.002
11.6	0.023	0.019	0.011	0.005

Table 4.3.8: Evaluation of wetted Solberg Filter (Black). Initial weight of filter: 14.4g. Effective filtration area: 0.0185 m^2.

Loading [g]	Pressure @3.5 slpm [inH_2O]	Pressure @3 slpm [inH_2O]	Pressure @2 slpm [inH_2O]	Pressure @1 slpm [inH_2O]
0 (dry)	0.057	0.047	0.030	0.014
0.1	0.056	0.046	0.029	0.013
0.4	0.055	0.046	0.030	0.014
1.8	0.068	0.056	0.036	0.017

Filter Selection Summary

From the data collected, all three filters performed within desired limitations. No significant contribution to flow restriction (pressure drop) was measured throughout both the dust and water loading simulations. From the three filters initially evaluated, the Solberg filter was selected for the for the MWS prototype that was deployed for full scale data collection. The flat pleated filter cassette was housed in a protective metal two-piece construction that allowed for easy removal and replacement, see Figure 4.3.2. In addition, the housing served to block water and spray impingement. However, its dead volume may contribute to artificial "sample diffusion" which is discussed later. These design features coupled with the satisfactory performance from the coal mine simulation tests made this filter a favorable option.

Figure 4.3.2: Solberg Filter selected for final design.

Environmental Sensor Requirements for Corrections

During initial testing of the MOS and IRS, RH, and temperature were found to substantially impact the MOS and slightly impact the IRS responses. Therefore, we determined that a RH sensor and thermocouple should be included in each sampling unit along with the CH_4 sensors. This enabled application of both RH and temperature corrections. A pressure sensor was also added into the sampling unit to determine when the filter needed changed; as the coal debris caked onto the filter, the absolute pressure would drop. Figure 4.3.3 shows the three "new" sensors (RH, temperature, and pressure). The temperature sensor is a Type-T thermocouple with a 7.62 cm (3 in) probe.

Figure 4.3.3: RH sensor (left), temperature sensor (middle), and pressure sensor (right) [36] [37] [38].

Aluminum Sensor Block

An aluminum sensor block was designed and machined to house all five sensors (RH sensor, temperature sensor, pressure sensor, and MOS, and IRS). A 3-D model of the sensor block can be seen in Figure 4.3.4 and a picture of all five sensors mounted in the block can be seen in Figure 4.3.5.

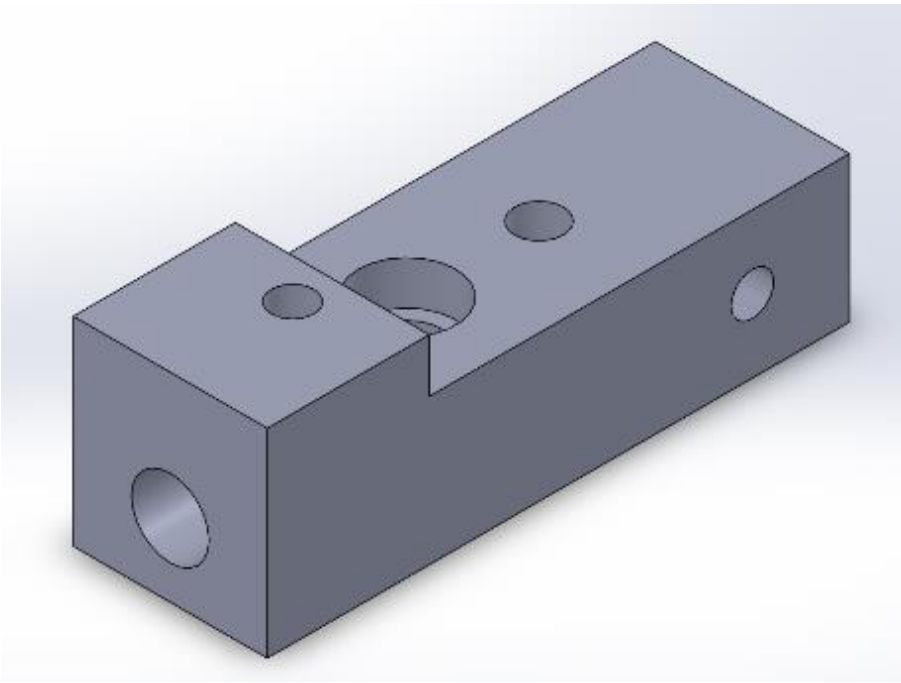

Figure 4.3.4: 3-D model of aluminum sensor block.

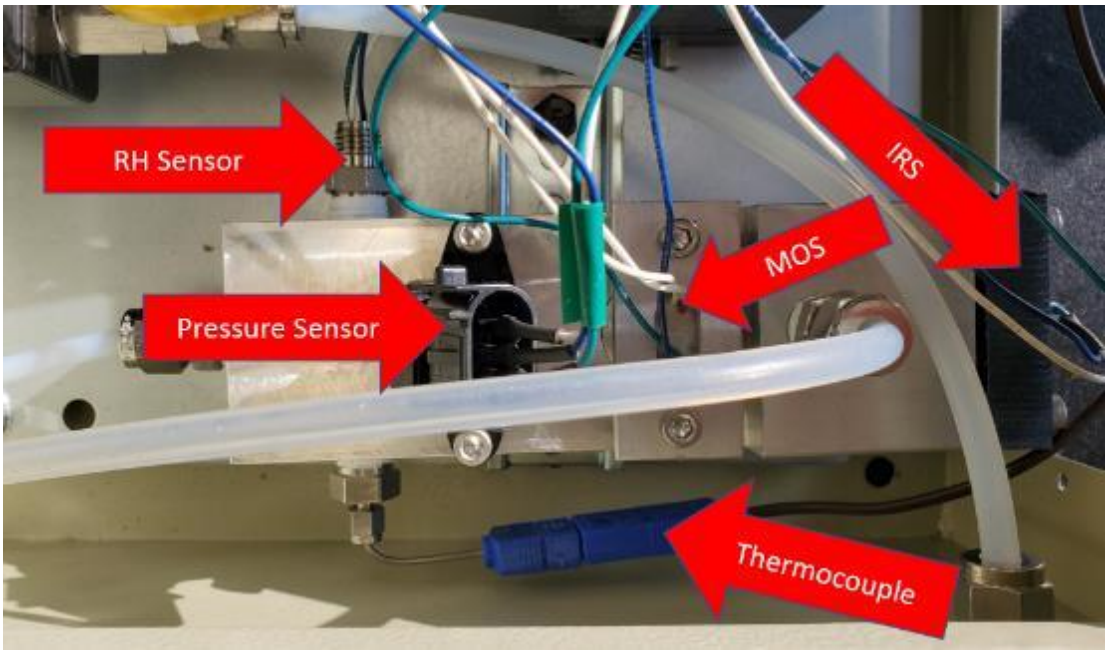

Figure 4.3.5: Sensor placement in aluminum block.

Sampling Unit Design

Each sampling unit consisted of a steel box which housed the aluminum sensor block containing the five sensors as well as other components for power, data collection, and communication with the CPH. Table 4.3.9 contains a list of all components inside the sampling unit.

Table 4.3.9: Components housed within each sampling box (node).

Item	Picture of Component	Description
Sensor Block		The aluminum sensor block houses the IRS, MOS, RH sensor, thermocouple, and pressure sensor and has one inlet and one outlet which are connected to the sampling tubes; this allows the sample to flow through the sensor block, past all five sensors.
3-Way Valve	 [39]	The 3-way valve is a direct acting solenoid valve and controls the location that the sample is being pulled from Inlet 1 or Inlet 2, either from the face or from the gob. (see the "Two Sampling Locations per Node" section) The valve is powered by the 24VDC power supply.
24VDC to 5VDC Power Converter		The converter has an input of 24VDC, from the external power source, and an output of 5VDC, which is needed to power most sensors in the unit.

Terminal Blocks (one 24 VDC and one 5VDC)		The terminal blocks are bridged in a way that one can supply 24VDC power and one can supply 5VDC power. All components that require power in the unit are connected to the terminal block corresponding to their power input specification. The 24VDC terminal block is powered directly from the external power source and the 5VDC power strip is powered by the output of the converter.
ICP CON	 [40]	The ICP CON is a data acquisition unit by ICP DAS. It has 8 analog input (AI) channels and 4 digital output (DO) channels and is powered by the 24VDC power supply. All sensors are connected to the AI channels and the valve is connected to a relay and is controlled through a DI channel. The ICP CON sends the sensors' signals to the computer where they can be post processed and the computer sends signals to the ICP CON to control the valve via ethernet.
Relay	 [41]	The relay receives the DI signal from the ICP CON and controls the power supplied to the valve.
Temperature Transmitter (4-20mA)	 [42]	Since the ICP CON being used does not have a thermocouple input, a transmitter is needed which converts the thermocouple signal into signal of 4-20mA. This transmitter is powered by the 24VDC power supply.
Sampling Tubes		Sampling tubes (0.25in PTFE Tubing) are connected to inlet and outlet locations throughout the box. They are connected from each of the unit inlets to the corresponding valve inlet, from the valve outlet to the sensor block inlet, and from the sensor block outlet to the outlet of the unit.
Ethernet Connection Ports		Two ethernet connection ports were mounted through the back side of the unit. The ICP CON "in" and "out" ethernet ports are connected to the respective connection port. The ethernet "in" and "out" connection ports allow the units to be "Daisy-Chained" together where only the first unit is directly connected to the computer.
Through Panel Terminal Block		The through panel terminal block is mounted through the back side of the unit. The external 24VDC power source is connected to the side of the terminal on the outside of the unit. The 24VDC power strip is connected to the side of the terminal on the inside of the unit; all components in the unit can then be powered

Figure 4.3.6 shows a 3-D model, made in SOLIDWORKS™, of the sampling unit with the location of each of the components as well as the direction of the sample flow through the unit; the sampling tubes and direction of flow are represented by the blue arrows and the green-dashed lines represent the ethernet cables. Figure 4.3.7 shows one of the 10 sampling units assembled with the components. While the box itself would likely not be approved for use in the mine, it was selected to be comparable in size to a final product. It should be metallic, sealable, and as small as possible to reduce issues associated with installation in a real mine.

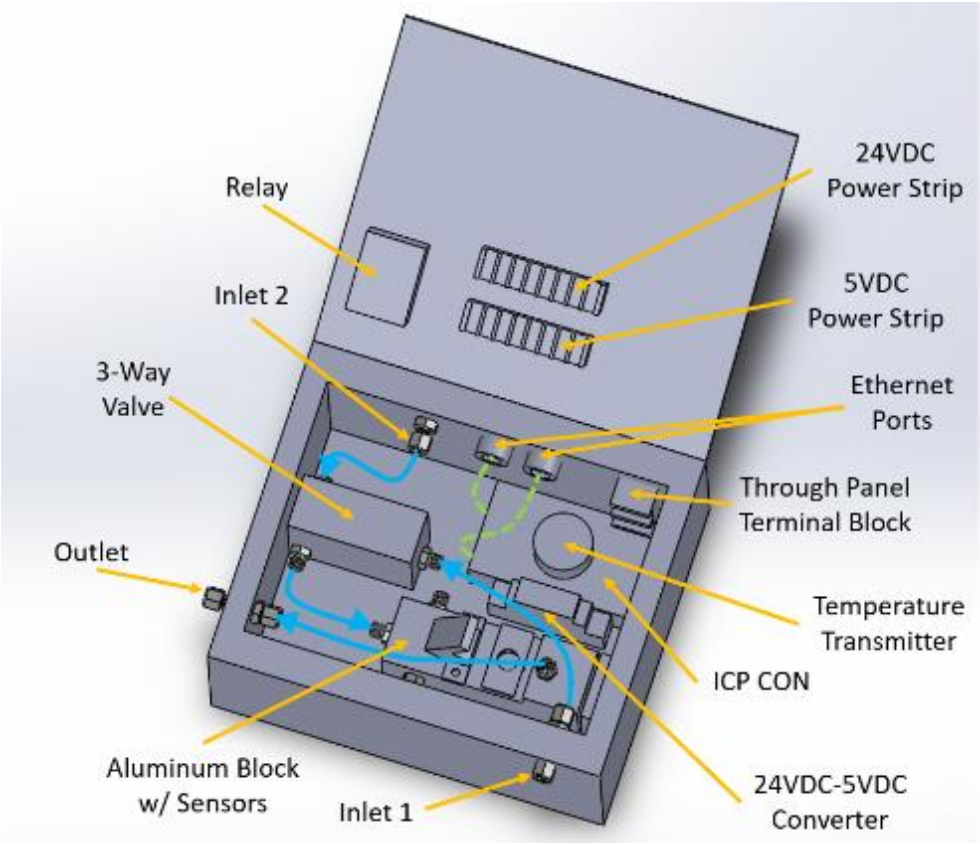

Figure 4.3.6: 3-D model of sampling unit with components.

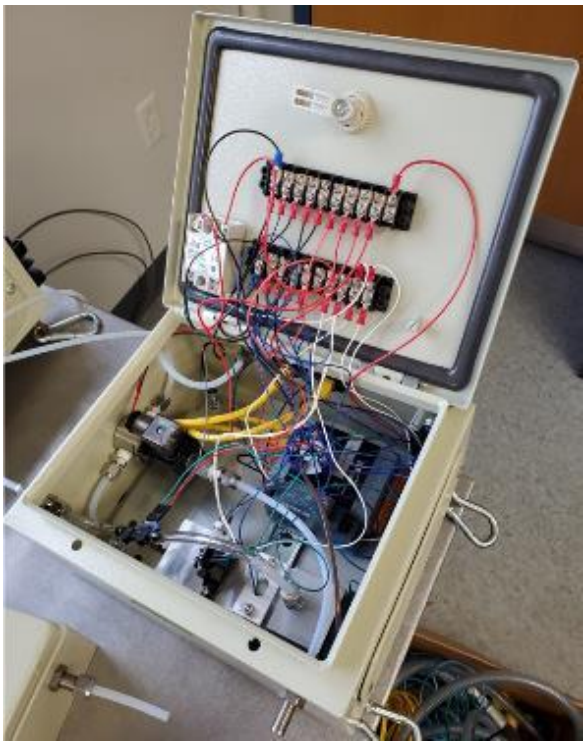

Figure 4.3.7: Assembled sampling unit.

All ten sampling units were "daisy-chained" together with ethernet cables, where only the first box was directly connected to the CPH. The power supply was connected in the same manor using 2-gauge wire. Figure 4.3.8 shows a diagram of this set up where the yellow lines represent the ethernet cables, the red lines represent the positive wire of the power supply, and the black lines represent the negative wires. Note that the diagram only shows an example with five sampling units; all ten units were connected this way.

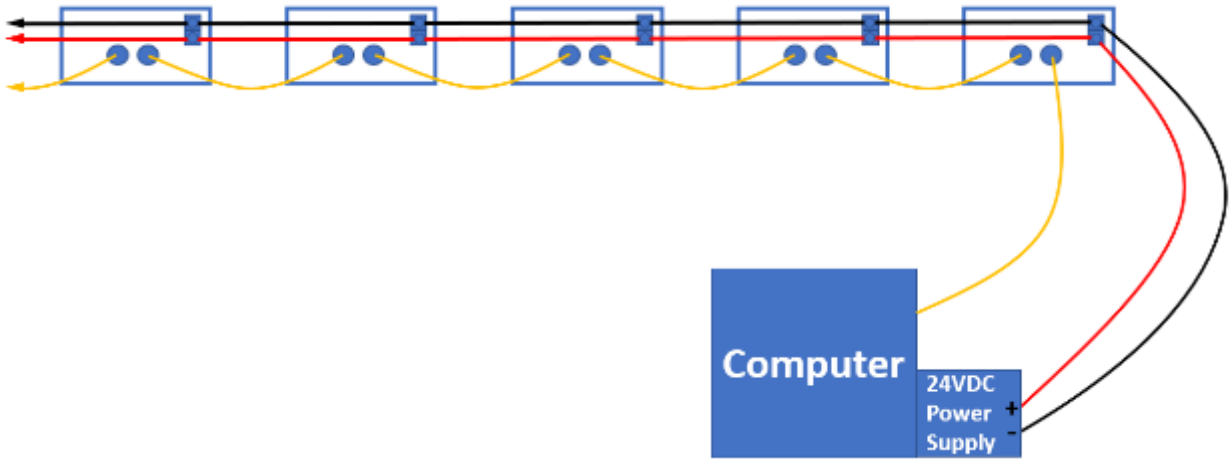

Figure 4.3.8: Diagram of "daisy-chain" connection of sampling units.

Additional Sensors (Flow and Air Velocity)

Since a goal of the proposed system was to ultimately be integrated for possible control of shearer and ventilation speeds, an anemometer was needed to measure wind speed for the semi-full-scale testing and demonstrations. Note that continuous wind measurements would improve mine safety and enable estimates of methane flow rates. A 3-cup anemometer was selected primarily for their low cost. Two were obtained and mounted on two of the sampling units, see Figure 4.3.9. Another additional sensor integrated at this stage was a flow sensor; one flow sensor was integrated into each sampling unit. Both the anemometer and flow sensors, were powered by the 5 VDC power supply and were connected to an analog input channel in their respective sampling unit so the signals were measured, recorded, and interpreted at the CPH. After initial testing of the entire system using a manifold system to pull a sample through multiple sampling units at a time, which is further discussed in a later section, we determined that flow sensors would be useful and would make it easier to keep sampling rates of the multiple units relatively similar and consistent. A section of the outlet tube from the sensor block leading out of the sampling system was removed and replaced with the flow sensor; see Figure 4.3.10 (all other sensors are in the same position as in Figure 4.3.5).

Figure 4.3.9: 3-Cup anemometer mounted on sampling unit.

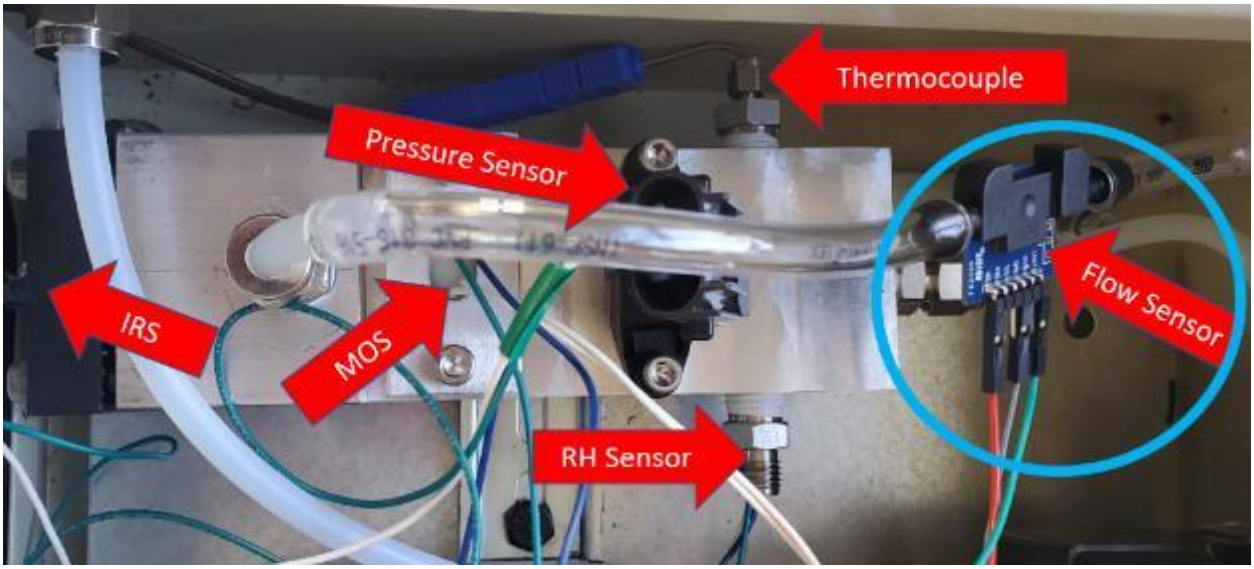

Figure 4.3.10: Addition of flow sensor to the sampling unit.

Water Ejector Design

An ejector was designed to provide an active sampling method for the MWS. We determined that compressed air was not readily available, and that passive sampling would be plagued with variable flow rates, water sprays, and particulate matter. However, in our initial discussion with industry workers, it was determined that water upwards of 689.5 kPa (100 psig) was available throughout mines. In order to reduce moving components, use available resources, and to use a mine safe method, we focused on development of a water powered ejector.

Figure 4.3.11 shows an example of a general ejector with some of the components labelled, where "High Pressure" is the motive fluid inlet, "Low Pressure" is suction fluid inlet, and "Intermediate Pressure" is the outlet. The main operating principle of an ejector was the Bernoulli Principle; as a motive fluid of high pressure moved though the nozzle, the exit velocity of the motive fluid increased, causing the pressure to drop. This caused the suction fluid to move toward the area of low pressure created by the motive fluid exiting the nozzle. As the suction fluid moved to the area of low pressure, it mixed with the motive fluid while entering the mixing chamber. The mixture then travelled through the diffuser and exited the ejector.

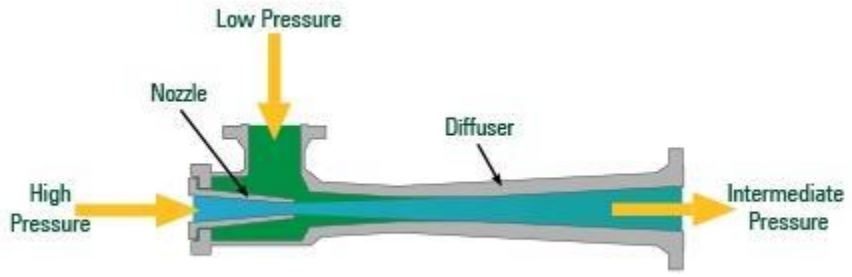

Figure 4.3.11: Basic ejector with labels [43].

Design Methods

The ejector for the proposed system was designed based on the assumption that water supply systems currently implemented in longwall mines could be used to provide water as the motive fluid of the ejector. The ejector would be placed downstream of a node's sampling system and the low-pressure port would serve as the motive force though the sensor block and components. We originally thought that the water pressure being supplied to each shield, where the ejectors would also be supplied from, was around 689.5 kPa (100 psig), which was a design parameter used. The ejector was designed where the methane (CH_4) – air mixture is the suction fluid; the sample fluid being pulled into the ejector. The ejector was designed to minimize water consumption and maximize suction pressure. The goal was maintaining an air flowrate of around 2 slpm (0.071 scfm) at the estimated pressure drop due to the sampling system (including a filter and coal dust caking to the filter). The pressure drop was determined through additional testing and it was determined that at a flowrate of 2 slpm (0.071 scfm), the maximum pressure drop due to the system for one sampling box was approximately 1.4 kPa (0.2 psig, 5.55 inH_2O), which corresponded to the suction pressure needed to overcome this pressure drop. Initially, an ejector was designed solely from calculations and recommendations from "Ejectors and Jet Pumps – Design and Performance for Incompressible Liquid Flow." Calculations and iterations were performed using MATLAB®. The code used for these can be found in Appendix A. This initial design was drawn in SOLIDWORKS™, 3-D printed, and tested. We found experimentally that the addition of a constant cross-sectional component at the ejector outlet increased the ejector performance. This was found by placing 7.9 mm (5/16 in) diameter tubing of various lengths into the outlet of the ejector; a tube length of 76.2 (3 in) yielded the best results. A new ejector was designed in SOLIDWORKS™ to mimic the tube inserted into the ejector; the outlet diameter was changed to the inner diameter of the 7.9 mm (5/16 in) tubing and a 76.2 mm (3 in) constant cross-sectional segment was added at the diffuser outlet. Other dimensions that were found using the design recommendations, including nozzle diameter, nozzle length, nozzle angle, mixing chamber diameter and length, diffuser angle, and distance from nozzle tip to the beginning of the mixing chamber, remained the same as the initial design. The water and air inlet diameters were set to be the same size as the inner diameter of the tubing (3.2 mm (0.125 in)). Table 4.3.10 shows the final design dimensions and an engineering drawing with dimensions is found in Appendix B.

Table 4.3.10: Designed ejector dimensions.

Nozzle Diameter (in)	0.0447
Nozzle Angle (degrees)	18
Mixing Chamber Diameter (in)	0.0869
Mixing Chamber Length (in)	0.6081
Diffuser Angle (degrees)	8
Diffuser Outlet Diameter (in)	0.18
Gap between nozzle outlet and mixing chamber inlet (in)	0.0447
Constant Cross-Section Segment after Diffuser (in)	3
Water Inlet Diameter (in)	0.125
Air inlet Diameter (in)	0.125

The new design was modelled and printed in two parts: the "base" part and the "diffuser/constant cross-sectional segment" part. The "base" part consisted of the water and air inlets, the nozzle,

the suction chamber, and the mixing chamber; this part can be seen in Figure 4.3.12. The “diffuser/constant cross-sectional segment” part consisted of the diffuser and the constant cross-sectional segment that was added to mimic the tube; this part can be seen in Figure 4.3.13. Figure 4.3.14 shows a cross-sectional view of the assembly of the two parts and labels of the ejector components.

Figure 4.3.12: "Base" part.

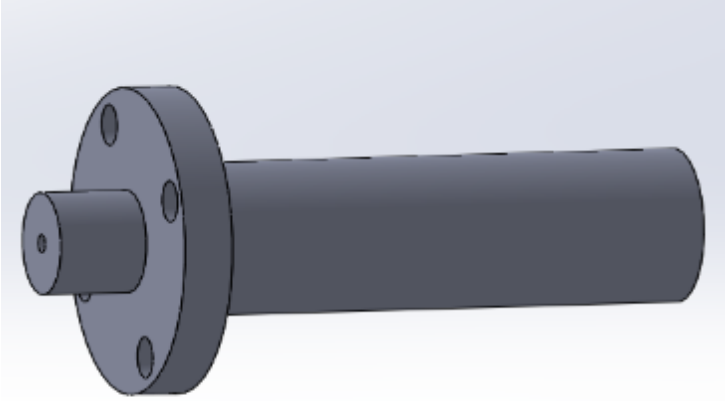

Figure 4.3.13: "Diffuser/constant cross-sectional segment" part.

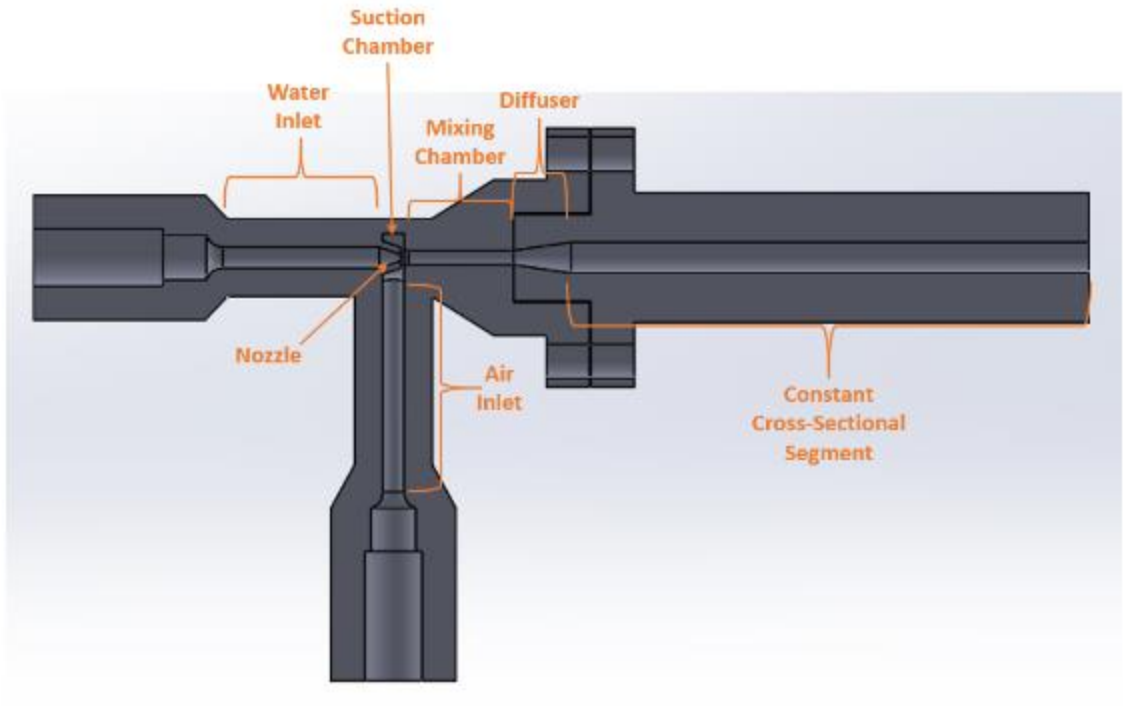

Figure 4.3.14: Cross-sectional view of ejector model with labels.

The two parts of the new ejector design were printed on a Formlabs® sla 3-D printer. Due to printing uncertainties, the nozzle diameter had to be re-drilled. The drill bit used was 1.17 mm (0.046 in) because it was the closest to the design diameter. The two parts were then connected via machine screws and nuts. The water and air inlet tubes were attached with 3.2 mm (0.125 in) NPT to 6.4 mm (0.25 in) compression fittings. The printed and assembled ejector can be seen in Figure 4.3.15.

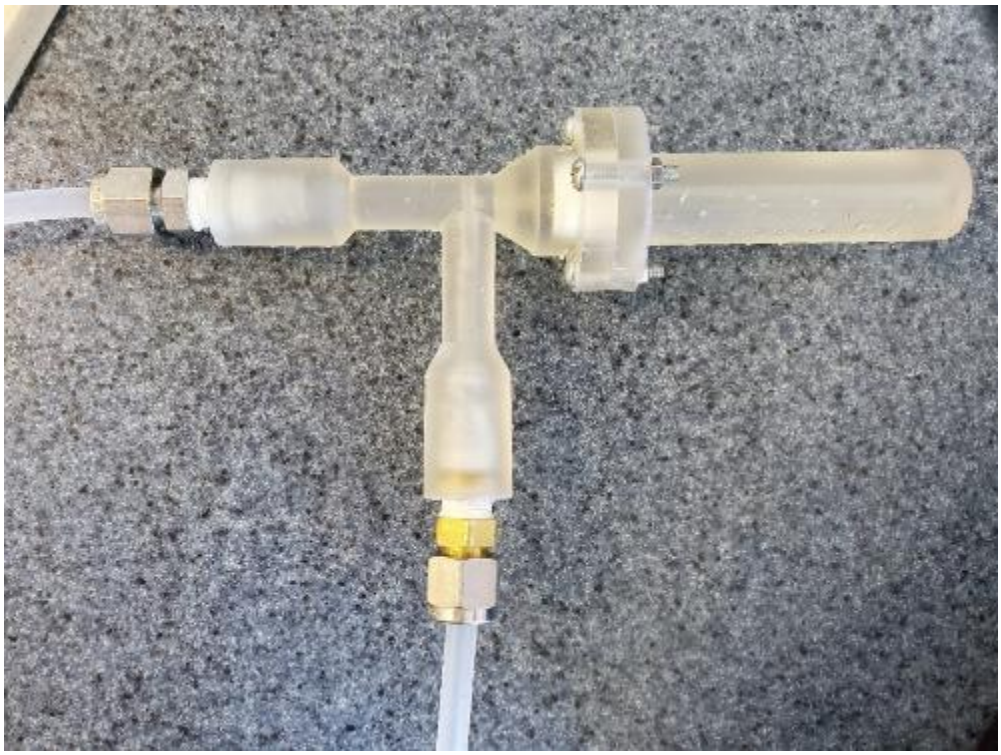

Figure 4.3.15: Printed and assembled ejector.

The ejector was then tested at water inlet pressures of 517.1, 586.1, 655.0 kPa (75, 85, and 95 psig). The results from these tests showed that the ejector had two different, distinct curves over the range of operation. It seemed that at some point of air restriction (suction pressure) the operation curve of the ejector changed, and the performance increased; it should be noted that this point changed for each operational water pressure. We suspected that this threshold may be caused due to cavitation within the suction chamber. These results are shown in Figures 4.3.16 – 4.3.18 where the blue line represents the high curve, the orange line represents the low curve, and the gray line in Figure 4.3.16 represents a curve that was obtained from a CFD model of the ejector. The model tended to over-predict, as expected. However, if the high curve was extended downward to the right (lower suction pressures), it approached the model curve. This could be because the model did not account for cavitation or other phenomena occurring at lower suction pressure before the curve switched (low curve). The water flowrates at each operational water pressure as well as the water flowrate from the CFD model were also recorded and can be seen in Table 4.3.11.

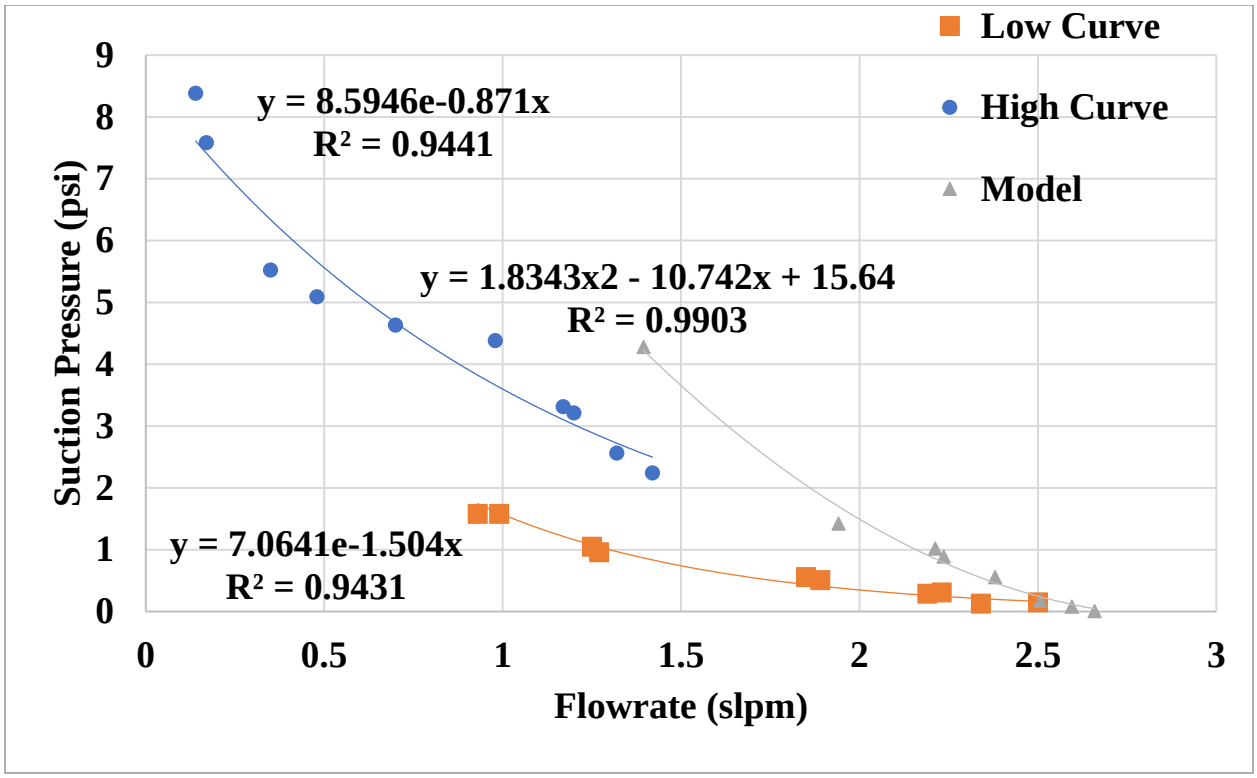

Figure 4.3.16: Ejector results at 75 psig water pressure.

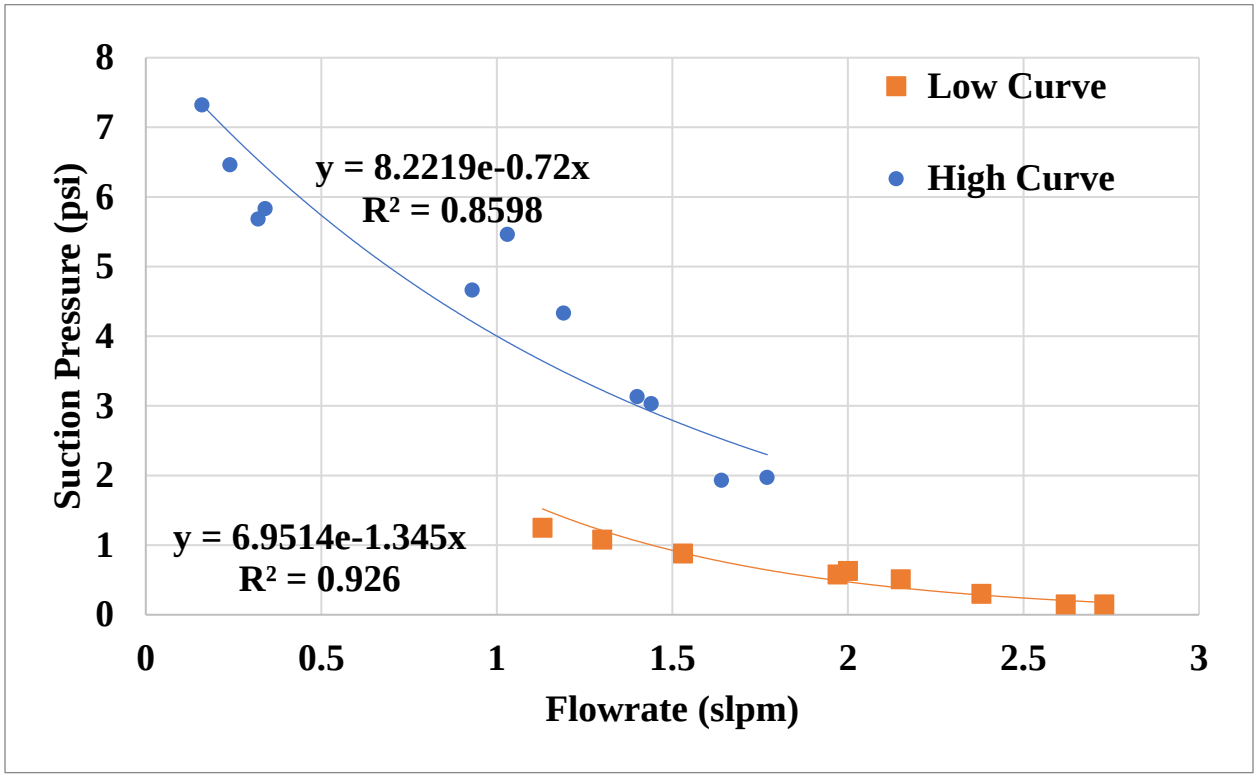

Figure 4.3.17: Ejector results at 85 psig water pressure.

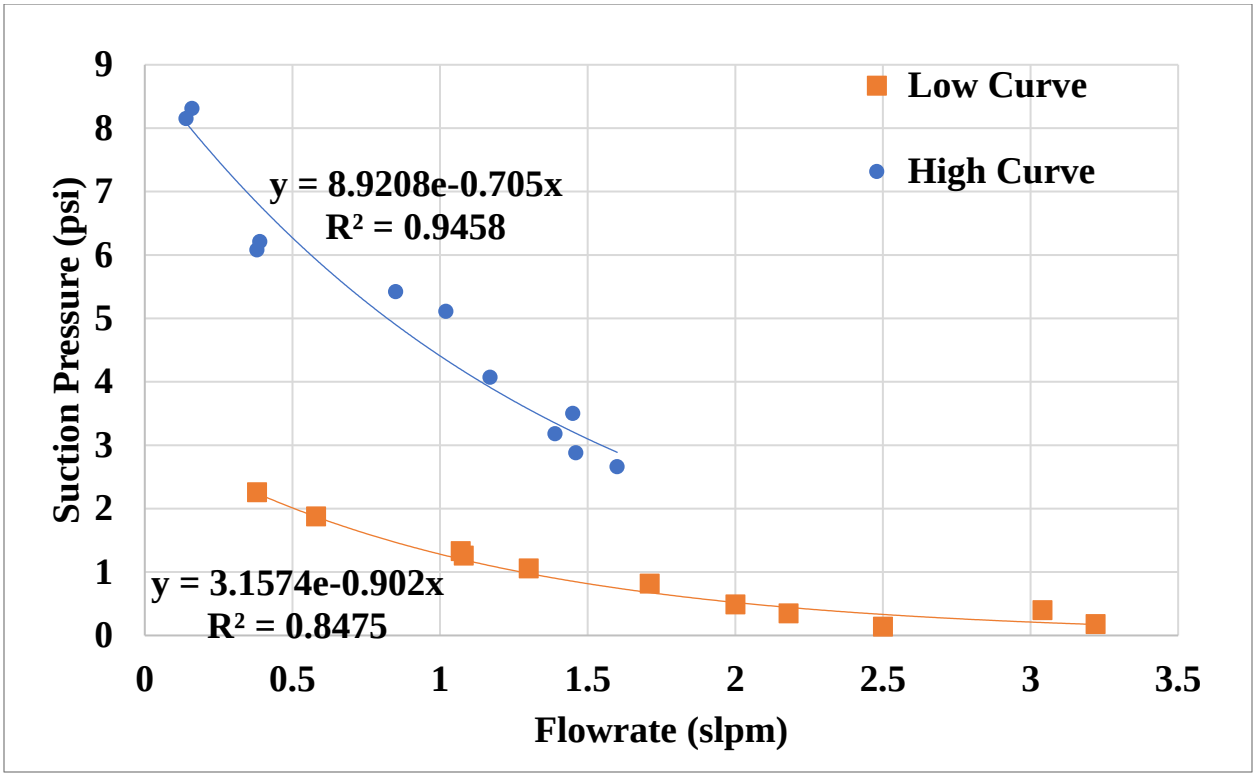

Figure 4.3.18: Ejector results at 95 psig water pressure.

Table 4.3.11: Water flowrates at various pressures.

Water Pressure	Water Flowrate (LPM)
Experimental – 75 psig	1.77
Experimental – 85 psig	1.89
Experimental – 95 psig	1.89
Model – 70 psig	1.55

Based on the trendline equation for the low curve in Figure 4.3.16, a flowrate of 2 slpm (0.071 scfm) could be achieved at suction pressures of approximately 2.4, 3.2, 3.6 kPa (0.35 psig, 0.47 psig, and 0.52 psig) for water pressures of 517.1, 586.1, 655.0 kPa (75, 85, and 95 psig), respectively. Therefore, the pressure drop of 1.4 kPa (0.2 psig) due to the sampling system could be overcome using this ejector at all water pressures tested.

Ejector Summary

After deciding to use a water ejector as the sampler for each sampling unit, an initial design was made utilizing guidelines and recommendations from "Ejectors and Jet Pumps – Design and Performance for Incompressible Liquid Flow". The ejector was designed to achieve a sample flowrate of at least 2 slpm (0.071 scfm) through the sampling system at one node; this included the sampling unit along with the 2.1 m (7 ft) tubing and the filter (including dust and water loading for "worse" case scenario). It also included any pressure from transport of the sample through

various fittings. The pressure drop caused by the sampling system at one node was measured to be around 1.4 kPa (0.2 psig). It was also ideal that the water flowrate be as low as possible while maintaining the suction pressure and flowrate requirements. The initial ejector design was 3-D printed and tested in the laboratory. We determined, experimentally, that extending the constant cross-sectional area at the outlet improved the ejector performance. Modifications were made based on the results from the experimentation and then the "new" design was printed and tested at three different water supply pressures, 517.1, 586.1, 655.0 kPa (75, 85, and 95 psig). Using compressed water of less than 689.5 kPa (100 psig), the ejectors provided sample flow rates of up to 2 slpm (0.071 scfm) with minimum water consumption of ~1.9 lpm (~0.5 gpm). The new design showed improved performance, as expected, and met the ejector flowrate and suction pressure requirements. However, the ejector had two distinct performance curves, a "low" and "high" curve, which transitioned from one to the other at a certain suction pressure; this transition point varied based on the water supply pressure. Since the flowrate and suction pressure requirements were satisfied at all water supply pressures tested, we recommended that the ejector be operated using a 517.1 kPa (75 psig) water supply pressure as this would prolong the life of the 3-D printed ejector as well as allow for less water consumption than if the ejector were operated at a higher pressure.

4.4 Sensor Calibrations and Verifications

As previously discussed, there were multiple sensors housed within the sensor block of each sampling unit. Each of the sensors were either calibrated or verified with additional laboratory equipment. Table 4.4.1 includes a summary of all sensors implemented at each sampling node. Figure 4.3.10, in a previous section, presents an overview of the sampling block housed within the sealed sampling unit.

Table 4.4.1: Sensors and equipment used in the calibration and verification methods.

Measurement Type	Sensor in Sampling Unit	Verification Analyzers/Equipment
CH_4 (Primary)	Dynament Infrared Sensor (IRS)	UGGA (OA-ICOS)
CH_4 (Secondary)	MQ-4 Metal-Oxide Sensor (MOS)	UGGA (OA-ICOS)
Relative Humidity of Sample	Honeywell HIH-4602-L Series	Edgetech DewMaster (Chilled Mirror)
Sampling Temperature	Thermocouple (K-type)	Omega iBTHX
Absolute Sampling Pressure	Manifold Air Pressure (MAP)	Heise
Sample Flow Rate	-	Mass Flow Controller (Alicat)
Desired CH_4 Concentration	-	Gas Divider (Horiba SGD-710C)
Mine Ventilation Flow	Anemometer (3-cup transducer)	WindSonic 2-D Ultrasonic Anemometer

Humidity Control of Sample

Two Horiba gas dividers (GDs) were used to control both CH_4 and humidity in the sample for sensor verifications. Both GDs operated on the same source of Ultra Zero Air (UZA) as the dilution gas, and a specified concentration of CH_4 (from a calibration gas cylinder) as the component gas.

One GD was used to control the CH_4 concentration of a dry sample and the other GD controlled the CH_4 of a wet sample. Both samples (dry and wet) were joined at a 4-way flooded junction. One GD output the dry sample directly to the flooded junction, while the other output the sample to the bubbler, where humidity was added (wet sample). A mass flow controller (MFC) was connected to the outlet of each gas divider to independently control the flow rates of the dry and wet samples. The humidity was controlled by adjusting each of the GDs flowrates with the two MFC's to the setpoints corresponding to the desired humidity.

Delivery of Sample

The GDs directed the samples to the flooded junction where the positive pressure was vented to atmosphere through an open junction end. The remaining junction port was connected to the sampling box. The primary flow of the sample was driven by a positive displacement pump and manifold system connected to all the sampling boxes. The pump created a negative pressure and pulled the controlled mixture through the 4-way flooded intersection. The sum of the two flowrates from the GDs were set higher than the flow of the pump to ensure no atmospheric air entered the sample. An Ultraportable Greenhouse Gas Analyzer (UGGA) was then connected to the exit of the sampling box on a T-fitting. The UGGA contained an internal pump by which it pulled in its own sample at a flowrate of about 0.5 slpm (0.018 scfm). The UGGA was used to verify methane concentrations upstream. Figure 4.4.1 shows a schematic of the humidity control and sampling system setup.

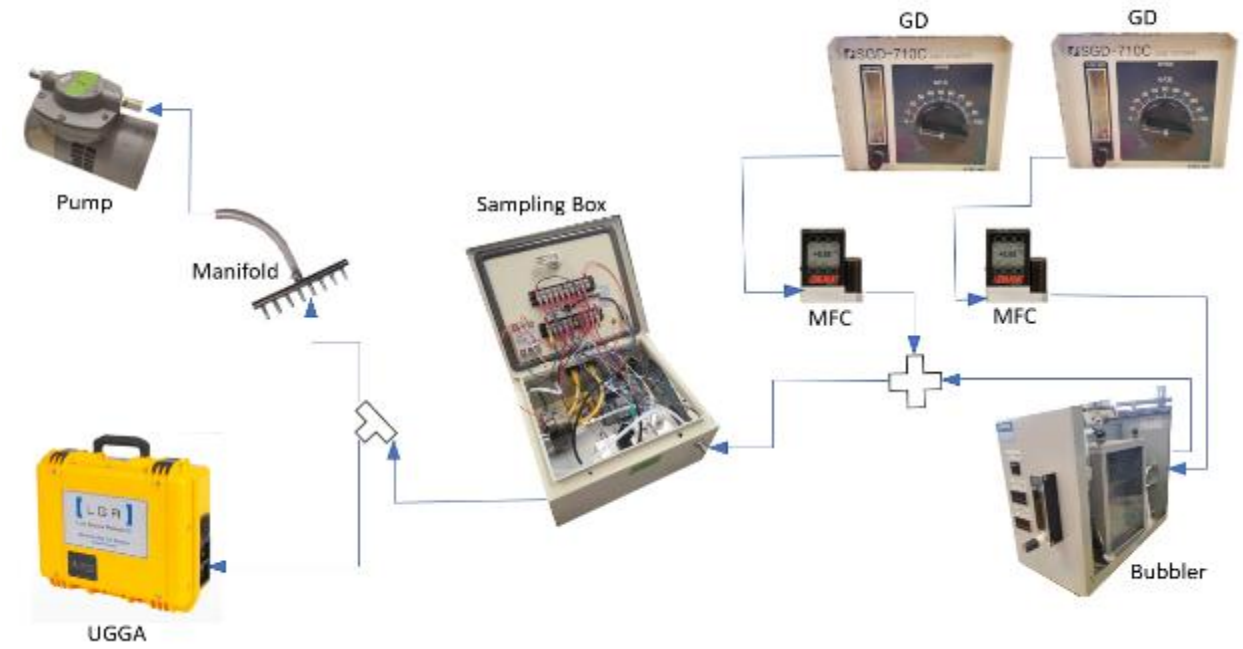

Figure 4.4.1: Setup for IRS and MOS calibration and verification.

Preliminary/Reference Analyzers

Edgetech DewMaster (RH Sensors)

Relative humidity (RH) sensors in the sampling box were verified and calibrated against an Edgetech DewMaster chilled mirror hygrometer, see Figure 4.4.2. The Edgetech measured three parameters as set by the user. For the calibrations performed for the RH sensors in the sampling

box and the UGGA, the Edgetech was set to measure either RH, temperature, and pressure or H_2O concentration in ppm, temperature, and pressure.

Figure 4.4.2: Edgetech DewMaster [44].

Heise (Pressure Sensors)

Leak tests were performed, and pressure sensors were verified and calibrated with a pressure calibrator unit (Heise), utilizing a specific module for absolute pressure. The Heise is pictured in Figure 4.4.3.

Figure 4.4.3: Heise [45].

UGGA (MOS and IRS)

For methane verification, the UGGA (shown in Figure 4.4.4) was proposed as the reference source for the sample exiting the sensor box.

Figure 4.4.4: UGGA [28].

Since higher H_2O concentrations (up to 100% RH) were likely in the mines, an internal and external calibration of the UGGA was conducted at a known CH_4 concentration of 20,100 parts

per million (ppm) as well as a known water (H_2O) concentration of 24,000 ppm. Humidity was added to the sample by means of the methods listed above. The external calibration was applied to CH_4 measurements greater than 1500 ppm; it was determined that the external calibration was not necessary at lower concentrations (less than 1500 ppm). For this calibration, as well as any other calibration performed where the GDs were used, the GD corrected values were calculated. These values were calculated to compensate for viscosity differences from the dilution gas to the component gas, since the operational principle of the GD is a pressure/flow driven mechanism. The composition gas inlet pressure to the divider was set to 144.8 kPa (21 psig) at the 100% cut point and the dilution gas inlet pressure set to 117.2 kPa (17 psig) at the 0% cut point. Since H_2O was added to the sample, the GD corrected values were subsequently corrected based on the amount of H_2O present; this correction was performed using Eq. 4.4.1 where the GD corrected value (in ppm) is the known CH_4 concentration directed through the GDs based on the component gas used and the H_2O Concentration (in ppm) was determined by the Edgetech DewMaster chilled mirror hydrometer, mentioned in more detail in the next section.

$$Actual\ CH_4\ Concentration = GD\ Corrected\ Value * \left(1 - \frac{H_2O\ Concentration}{1000000}\right) \quad \textbf{Eq. 4.4.1}$$

The verification for the UGGA calibration can be seen in Figures 4.4.18 and 4.4.19 and in Table 4.4.*4*.

Alicat MFC (Flow Sensors)

Calibrations of the flow sensors in each box were verified using an ALICAT mass flow controller (MFC). The MFC can be seen in Figure 4.4.5.

Figure 4.4.5: MFC used for flow sensor verification.

WindSonic (3-Cup Anemometers)

Measured wind speeds were collected with the WindSonic 2-D ultrasonic anemometer, herein referred to as the WindSonic (shown in Figure 4.4.6) and used as reference for the two 3-cup anemometers mounted to the sampling boxes 2 and 9.

Figure 4.4.6: WindSonic 2-D ultrasonic anemometer [46].

Calibration Methods

RH Sensors

The RH sensors used in the sampling boxes were calibrated using the two GDs and bubbler set up as described above to control humidity and with the Edgetech as the reference analyzer. The Edgetech measured a RH value that was then converted to an H_2O concentration in ppm based on the temperature and pressure, which were also measured by the Edgetech (Eq. 4.4.2 – 4.4.4). The ppm values for H_2O concentration were then used to calculate the expected RH values for the sensors based on the temperature and pressure measurements within the sensor block (Eq. 4.4.5 – 4.4.7); the RH sensors were calibrated with respect to these values. It should also be noted that the calibration occurred at 23 °C (73.4 °F) while the manufacturer's calibration and temperature compensation were at 25 °C (77.0 °F), therefore the calibration was offset by two so that the temperature compensation equation given by the manufacturer was used.

$$P_{g_E} = 0.00014{T_E}^2 - 0.00686T_E + 0.17603 \quad \textbf{Eq. 4.4.2}$$

$$P_{v_E} = \left(\frac{RH_E}{100}\right) * P_{g_E} \quad \textbf{Eq. 4.4.3}$$

$$PPMv_E = \frac{Pv_E}{P_E} * 1000000 \quad \textbf{Eq. 4.4.4}$$

$$Pg_{RHS} = 0.00014{T_T}^2 - 0.00686T_T + 0.17603 \quad \textbf{Eq. 4.4.5}$$

$$Pv_{RHS} = \frac{PPM_E}{P_{RHS}} \quad \textbf{Eq. 4.4.6}$$

$$RH_S = \frac{P_{vS}}{P_{g_S}} * 100 \quad \textbf{Eq. 4.4.7}$$

Where the subscripts "E", "RHS", and "T" denote the Edgetech, RH sensor in the sampling box, and the thermocouple in the sampling box, respectively, P_g is the saturation pressure (psia), P_v is

the partial pressure of water vapor (psia), T is the sample dry bulb temperature (°F), PPMv is the humidity (PPM), and RH is the relative humidity. The results reflecting the calibration procedures for the RH sensors are shown in Figures 4.4.20 and 4.4.21 and in Table 4.4.5.

Pressure Sensors

The pressure sensors were calibrated using a hand pump to control pressure, and the Heise absolute pressure module was used as the reference. The results reflecting the calibration procedures for the pressure sensors can be seen in Figures 4.4.22 and 4.4.23 and in Table 4.4.6.

Methane Sensors (MOS and IRS)

Effects of Temperature, Pressure, RH, and Flowrate on the CH_4 Sensors

In order to calibrate the MOS and IRS, the effects of climate (temperature, RH, and pressure) and flowrate of the sample on the sensors were analyzed. To initially test the climate effects on the sensors, a testing apparatus which consisted of a test chamber where climate could be modified by using an air conditioner to either heat or cool the test chamber volume and various methods were used to vary the humidity. A MOS and an IRS were both mounted in a metal tube along with a thermocouple to measure temperature near the sensor locations. The section of the tube containing the open end and all of the sensors was placed inside the test chamber; the rest of the tube extended through a hole in the test chamber where it was connected to a pump which pulled the sample through the tube. An Omega iBTHX was also placed in the testing apparatus to measure temperature, RH, and pressure of the test chamber volume. The testing apparatus set-up can be seen in Figure 4.4.7.

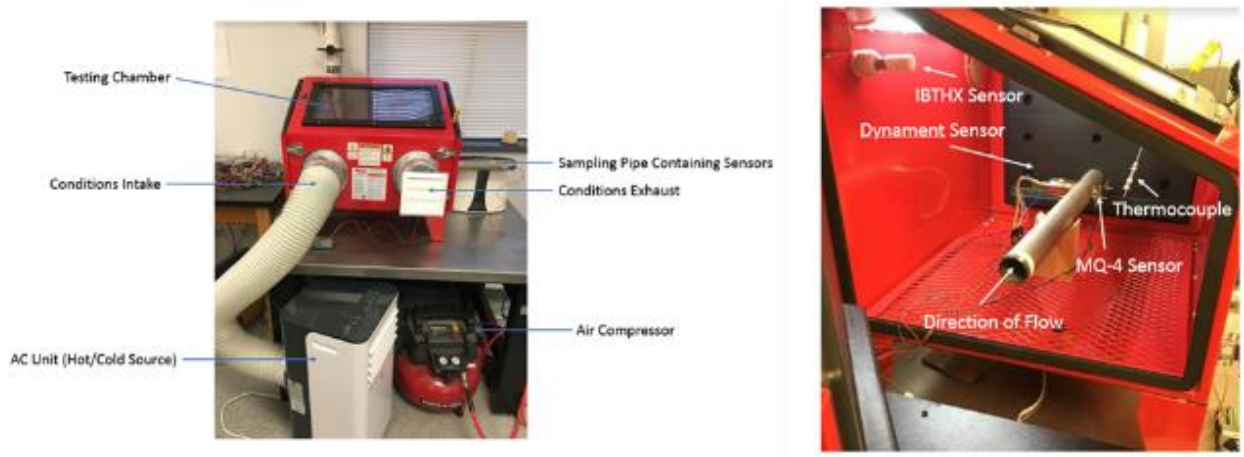

Figure 4.4.7: Left – test chamber with equipment, right – inside of test chamber.

Initial tests were completed to determine if temperature had a significant effect on the sensors' responses. Three tests were performed at three different temperature ranges. It should be noted that the temperature range represented the variation of temperature over the span of the test. A 2.01% CH_4 calibration gas bottle and a GD were used to supply methane at the tube inlet at ten different CH_4 concentration points. In these three tests, the conditions in the box were not directly being sampled, however the temperature variations in the test chamber also caused a change in temperature in the sample over the time it took for the sample to reach the sensors. The thermocouple located in the tube near the MOS and IRS was the temperature reference for these tests. The results of the three tests for the MOS and IRS are shown in Figures 4.4.8 and 4.4.9,

respectively. Temperature has a more significant effect on the MOS than the IRS, especially at lower CH_4 concentrations.

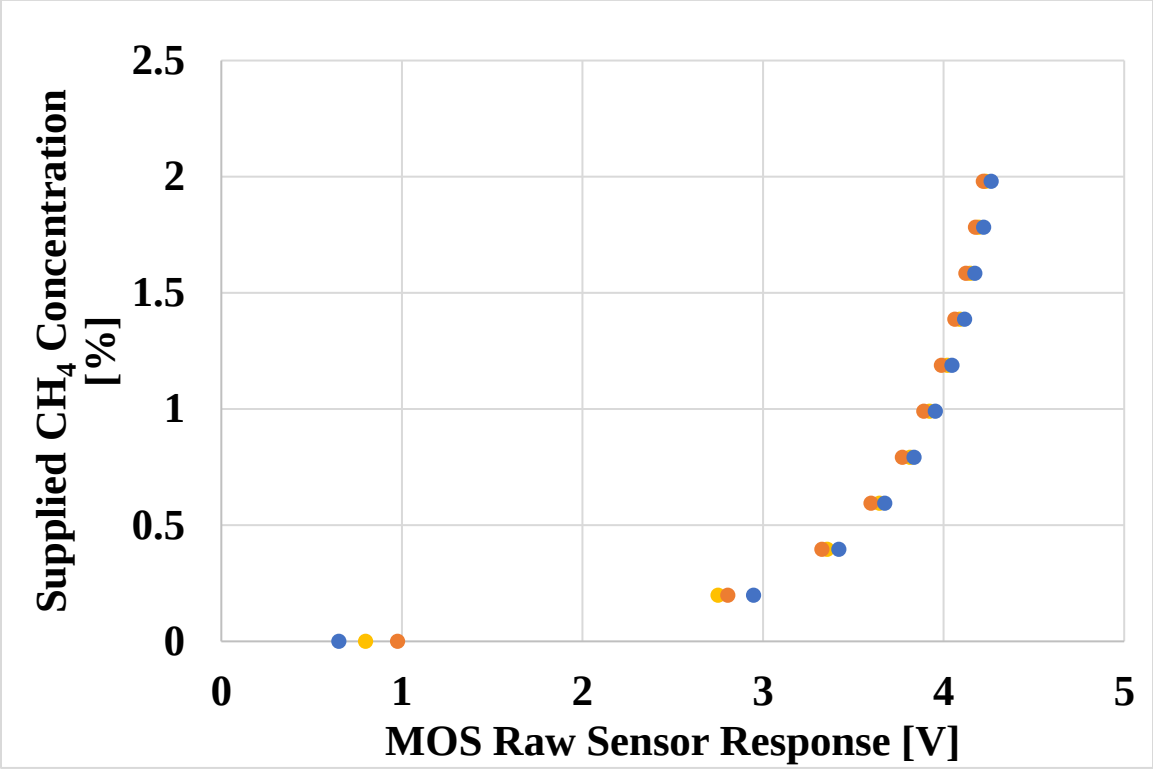

Figure 4.4.8: Initial testing to determine temperature effects on the mos.

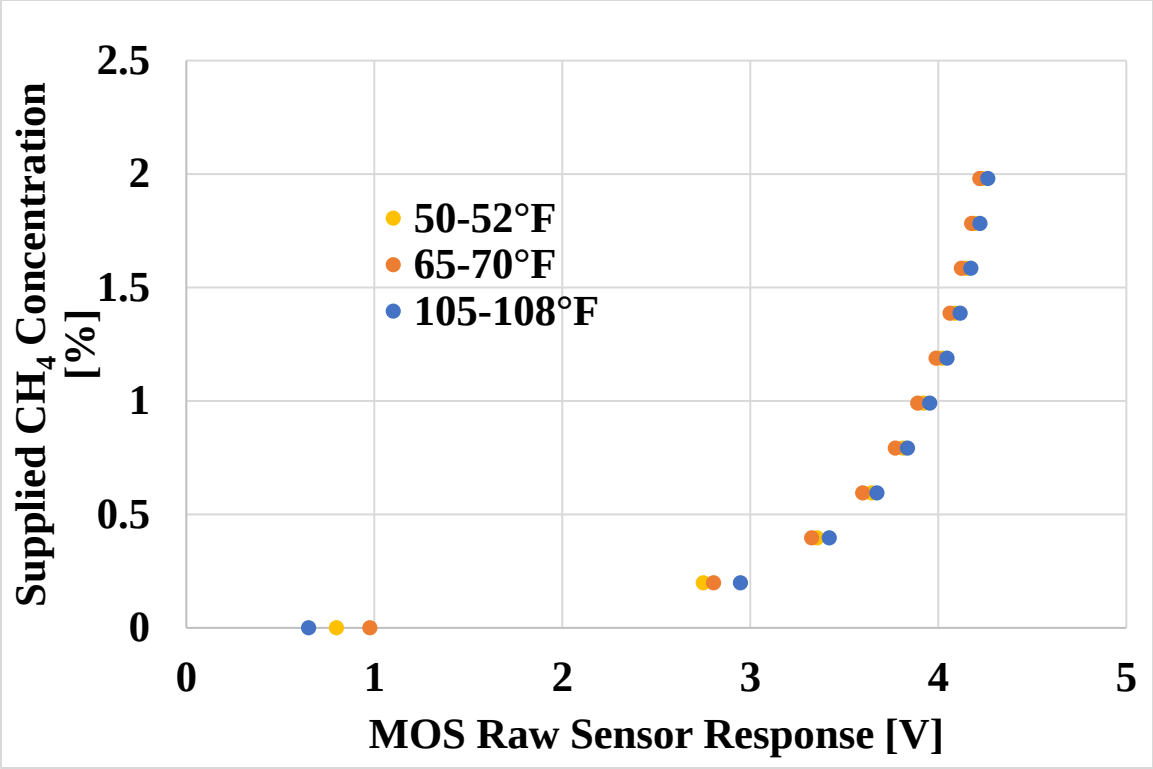

Figure 4.4.9: Initial testing to determine temperature effects on the IRS.

An initial test to analyze effects of humidity on the MOS and IRS was also performed in the test chamber. One MOS and one IRS were suspended in the test chamber and the humidity in the chamber was continuously increased over the duration of the test using a humidifier. It should be noted that this test was at room temperature and there was no CH_4 added. Four data points were gathered by taking 100 second averages of the raw responses for the MOS and IRS at various times during the test; the same time averages were taken for the RH values measured by the iBTHX. The raw responses of the sensors were used along with their manufacturer specified output range to find the percent of the total response for each sensor. These percent values were then plotted against the RH to show the humidity effects. The results of this test are shown in Figure 4.4.10. A linear trendline was plotted for each data set in order to better show the RH effect on the sensors; a higher sloping line corresponded to a greater humidity effect. The MOS were more impacted by humidity than the IRS since the trendline for the MOS had a greater slope.

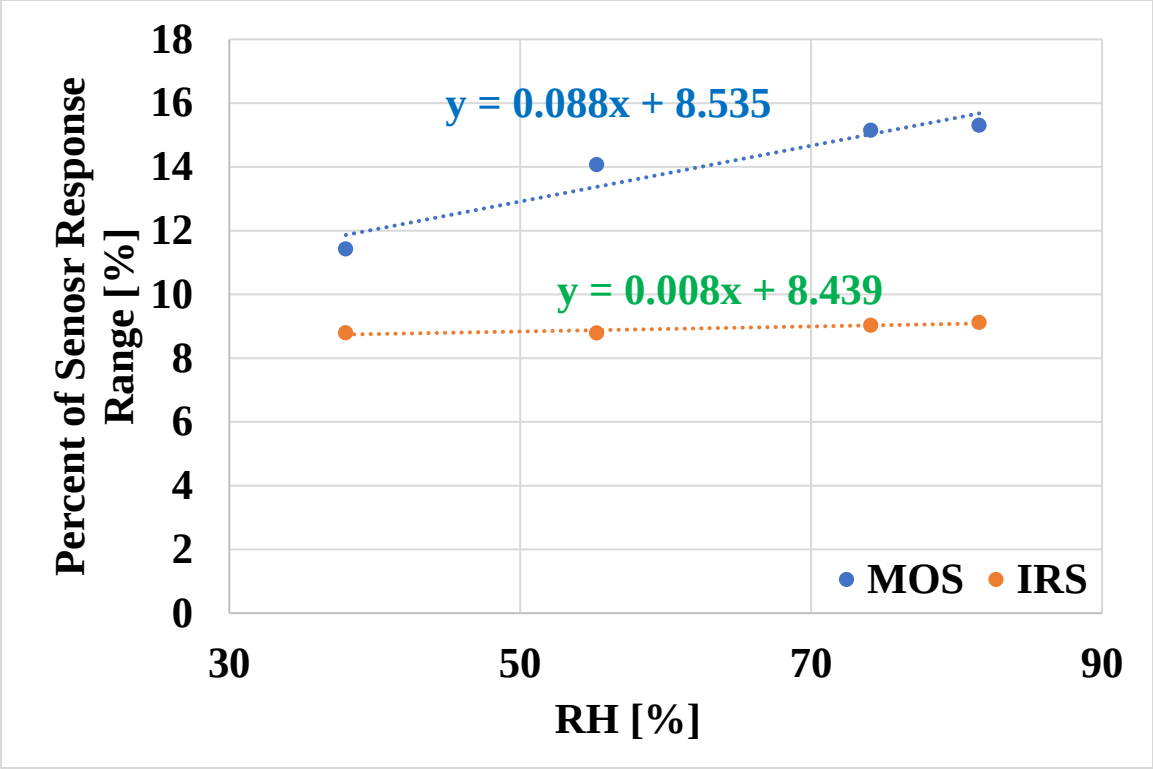

Figure 4.4.10: Humidity effects on MOS and IRS raw responses.

To analyze the effects of pressure on the MOS and IRS responses, a test was performed where a 2.02% CH_4 calibration gas bottle and a GD were used to flow 1% CH_4 through the aluminum sensor block, which housed the sensors, and a valve was placed between the GD and sensor block inlet to control the pressure. The pressure was incrementally decreased during the test and was measured by the pressure sensor in the sensor block. Figure 4.4.11 shows the results from this test; initial calibrations were applied to the sensors prior to this test, therefore the sensor response in percent CH_4 was used to compare pressure effects. The IRS was more affected by pressure than the MOS. However, based on additional testing, the absolute pressure of the system when in operation should always be, at least, above 89.6 kPa (13 psia) unless there was a major issue, such as a clogged sampling tube. Therefore, the plot has was "zoomed" into the area above 89.6 (13 psia) (Figure 4.4.12); from this new region of interest, we determined that pressure effects could be neglected for both sensors.

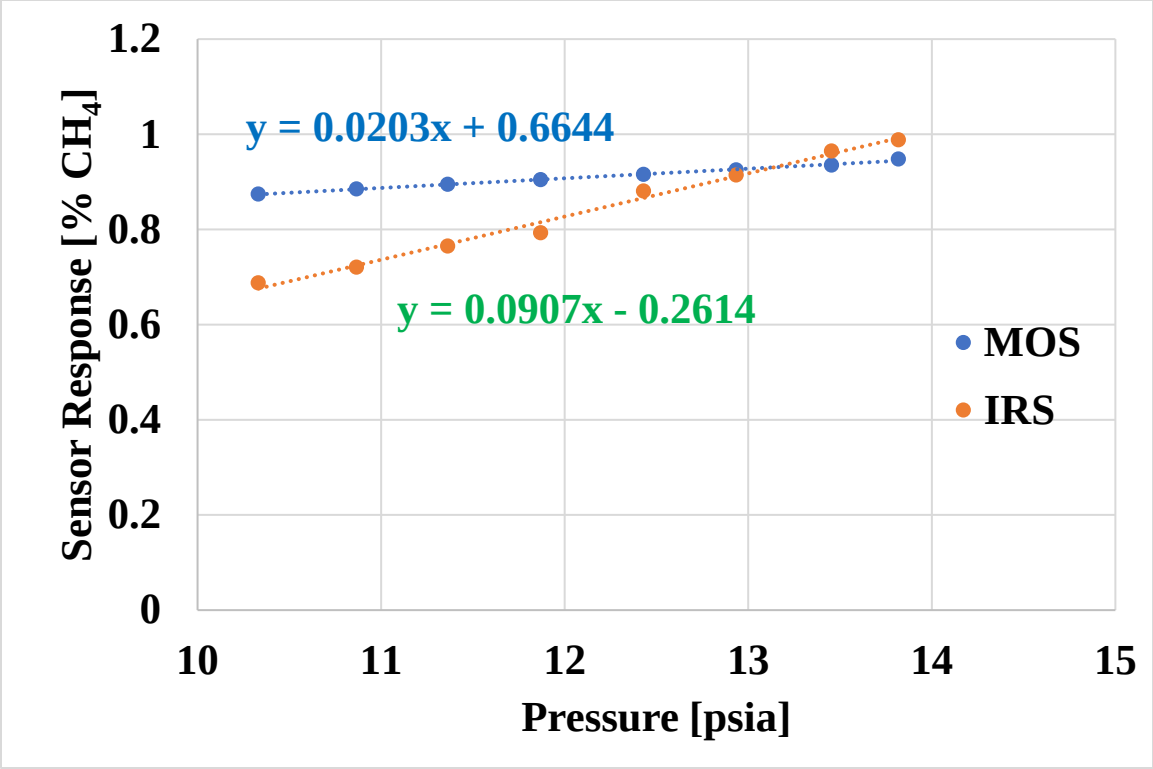

Figure 4.4.11: Pressure effects on MOS and IRS response with ~1% CH_4 supplied.

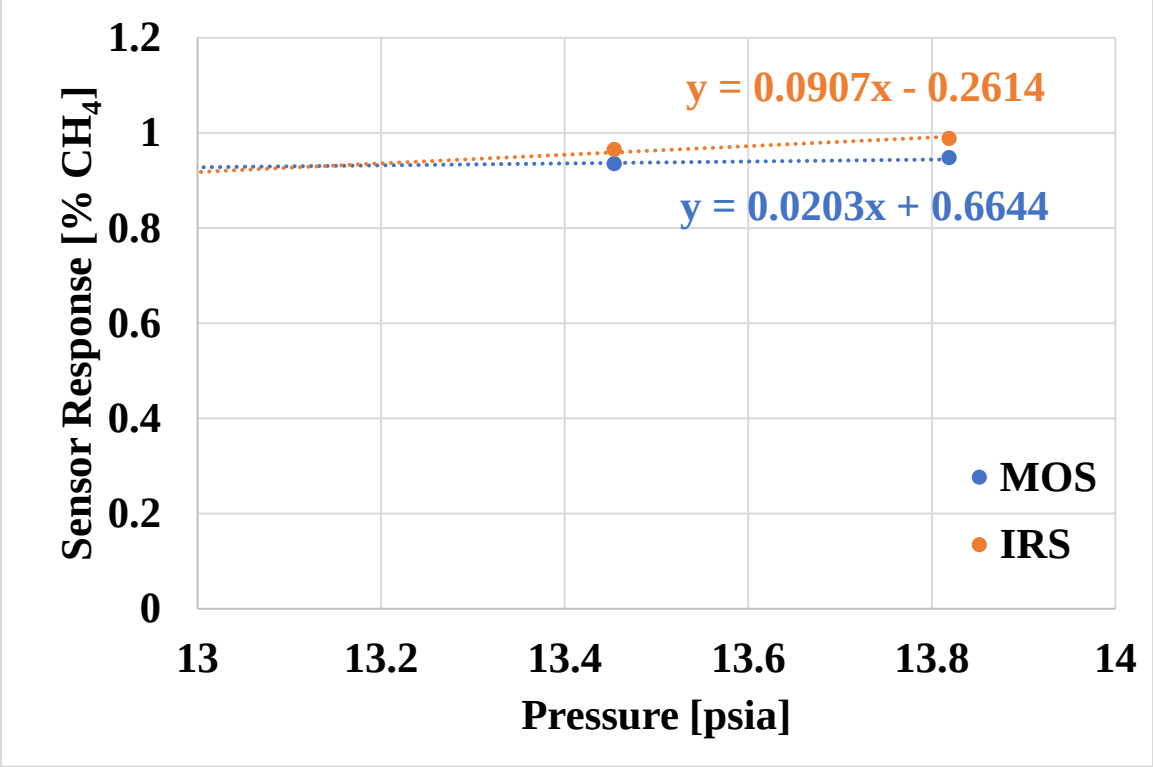

Figure 4.4.12: Pressure effects on MOS and IRS response "zoomed" in to expected minimum system pressure when in operation.

To test the effects of sample flowrate on the MOS and IRS, a 2.02% CH_4 calibration gas bottle and a GD were used to flow 1% methane through the aluminum sensor block which housed the sensors. The flowrate of the sample was increased in increments of approximately 0.5 slpm (0.018 scfm) from 1 slpm (0.035 scfm) up to 3.5 slpm (0.124 scfm) over the duration of the test. Results showed that the neither of the sensors' responses were significantly affected by the sample flowrates between 1 and 3.5 slpm (0.035 and 0.124 scfm), see Figure 4.4.13. Trendlines have been added for each data set to show that the effect of the flowrate on sensor response was negligible; both trendline slopes are near zero.

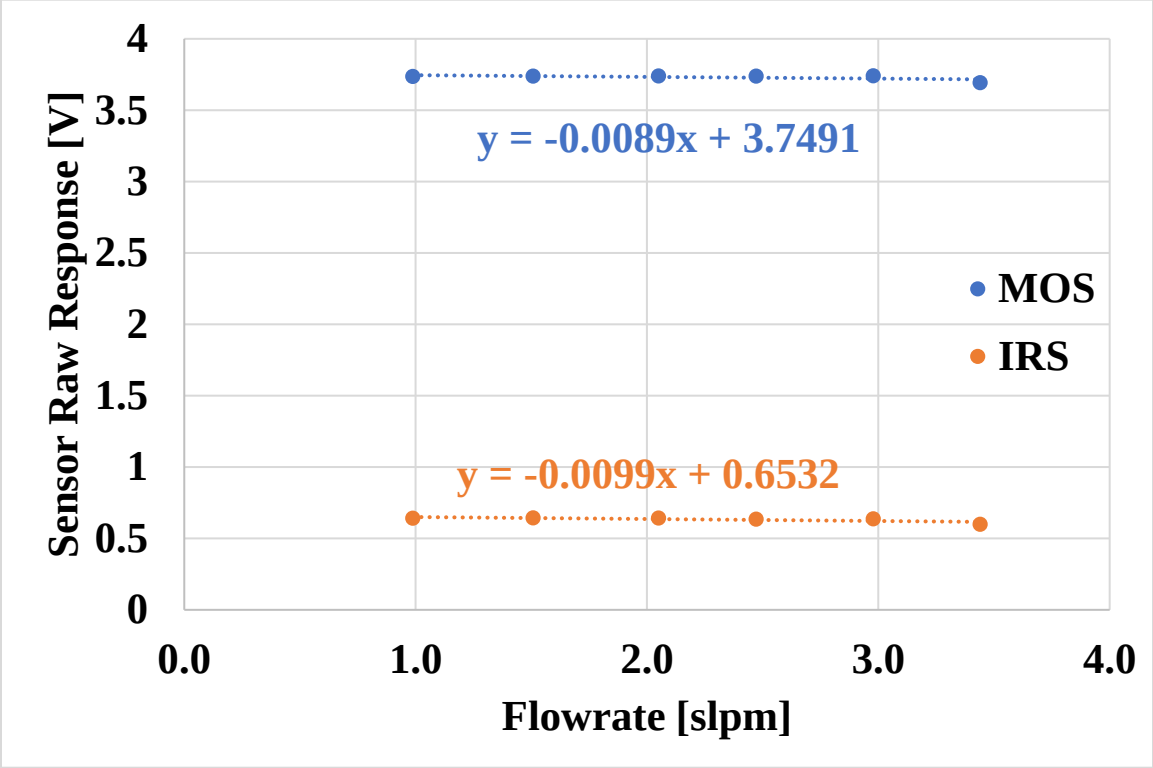

Figure 4.4.13: Flowrate effects on MOS and IRS raw responses.

Dynament Sensors (IRS)

The IRS had a linear response to the respective methane concentrations. An initial 20-point calibration was performed utilizing a 2.01% CH_4 bottle for the first ten points and a 0.2475% CH_4 bottle for the second ten points; both bottles were divided with UZA using the GD to obtain the 20 calibration points. Figure 4.4.14 shows an example of a calibration curve for an IRS where the dry calibration equation is shown in the red rectangle.

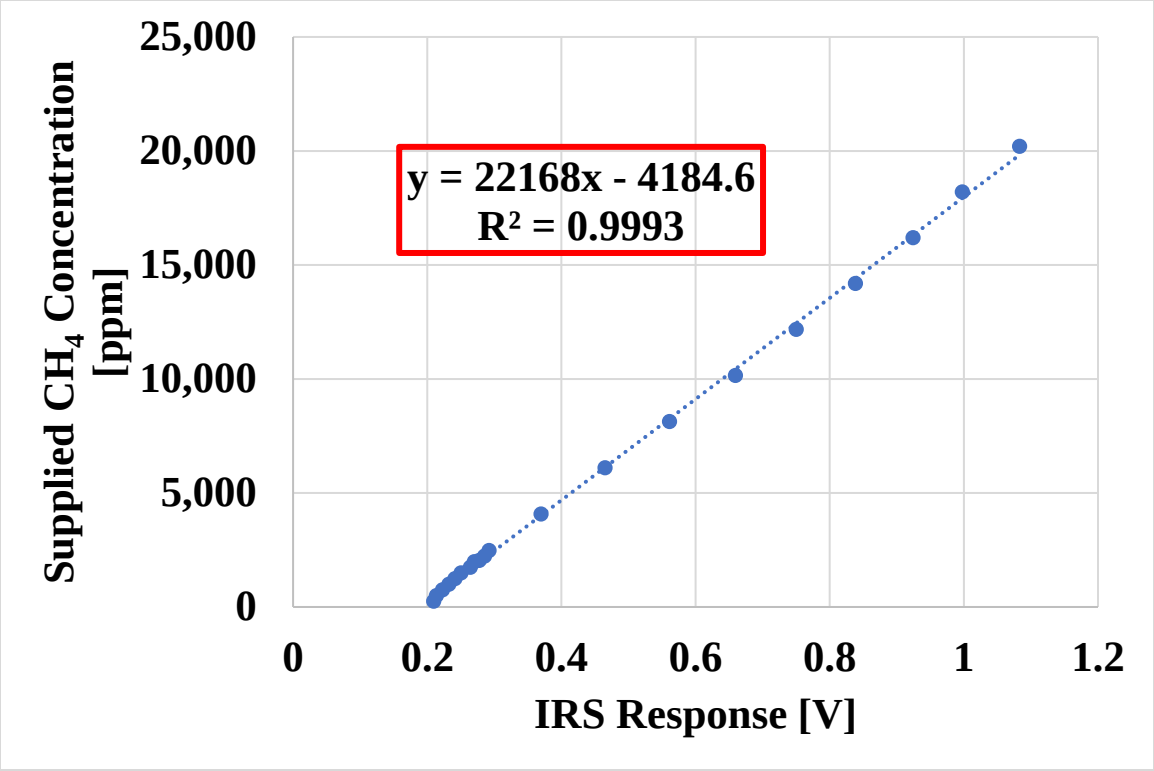

Figure 4.4.14: Example of IRS 20-Point dry calibration curve and equation.

This calibration contained no humidity in the sample; therefore, an additional correction calibration was performed to ensure acceptable error at all humidity conditions. To derive the correction factors, the previous calibration was conducted with the addition of humidity by means of the two GDs combining a wet and dry sample to a desired relative humidity (setup shown in Figure 4.4.1). Three different correction factors were calculated for different ranges of the IRS raw response. A set of correction factors was calculated using one IRS and then applied to all ten IRS; these corrections used absolute humidity ratio to account for RH, temperature, and pressure. The equations used to calculate the absolute humidity ratio are shown in Eq. 4.4.5, 4.4.8, and 4.4.9. The calibrated RH sensor, temperature sensor and pressure sensor in the sampling box were referenced for these calculations and a corrected methane concentration value was computed from the base calibration.

$$P_{v_{RHS}} = \left(\frac{RH_{RHS}}{100}\right) * P_{g_{RHS}} \qquad \textbf{Eq. 4.4.8}$$

$$\omega = \frac{0.622 * P_{v_{RHS}}}{P_{ps} - P_{v_{RHS}}} \qquad \textbf{Eq. 4.4.9}$$

Where Pg, Pv, T, RH, and the subscripts "RHS" and "T" are the same as in Eqs. 2-7, the subscript "ps" denotes the pressure sensor in the sampling box, P is the absolute pressure (psia), and ω is the absolute humidity ratio (lb/lbdryair).

The corrections applied to compensate for RH, temperature, and pressure were a set of various raw response ranges and absolute humidity ratio ω ranges. The results for the humidity calibration tests were plotted and can be seen in Figure 4.4.15. Each line represents one test at a certain CH_4

concentration while the humidity was varied; the trendline equations are shown next to the right of the trendlines and are outlined corresponding to their respective test. These trendline equations were used to determine the correction factors for the various ranges.

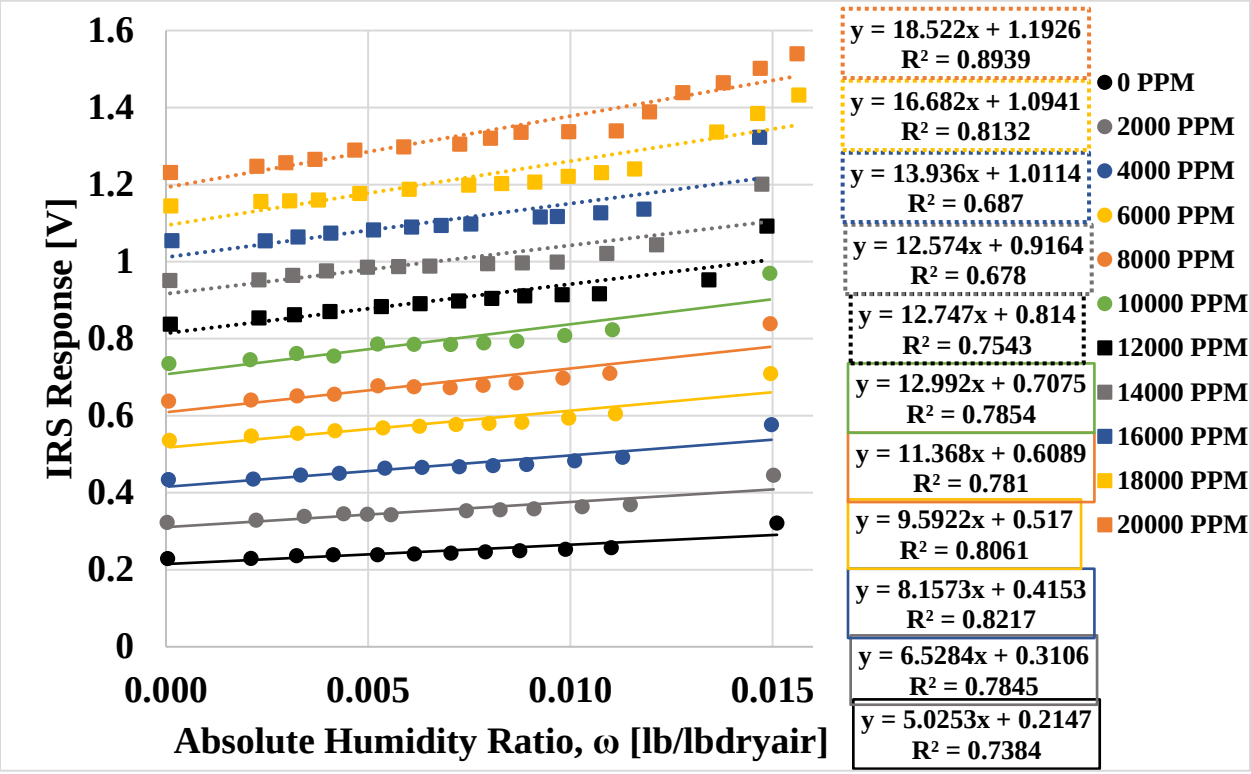

Figure 4.4.15: IRS plot used for humidity calibration corrections.

The correction factors for the various ranges for the IRS can be seen in Table 4.4.2 where the factors, k and c, are used in Eq. 4.4.10 to calculate the corrected voltage which is then used in the individual dry calibration equation pertaining to the specific sensor.

$$V_{corrected} = V - k * \omega - c \qquad \textbf{Eq. 4.4.10}$$

In this equation, $V_{corrected}$ is the corrected voltage to be used in the dry calibration equations, V is the raw sensor response voltage, and ω is the absolute humidity ratio.

Table 4.4.2: IRS calibration correction factors.

Raw Response Range	k
V < 0.3	1.5
0.3 ≤ V < 0.6	2.5
V ≥ 0.6	5

MQ-4 Sensors (MOS)

Unlike the IRS, the MOS did not have a linear response relationship to CH_4 concentration; this caused calibration of these sensors to be more challenging. An initial 20-point calibration was performed for each MOS with dry CH_4 concentrated gas out of two calibration gas bottles as was completed for the IRS. In attempts to calibrate the sensors above their recommended range of operation (up to 1% CH_4) two exponential calibration equations were found for each sensor, one for lower concentrations (less than 1%) and one for higher concentrations (greater than 1%); an example of these calibration curves can be seen in Figure 4.4.16 where the calibration equation for higher concentrations is shown in the solid-orange rectangle and the calibration equation for the lower concentrations is shown in the dashed-blue rectangle.

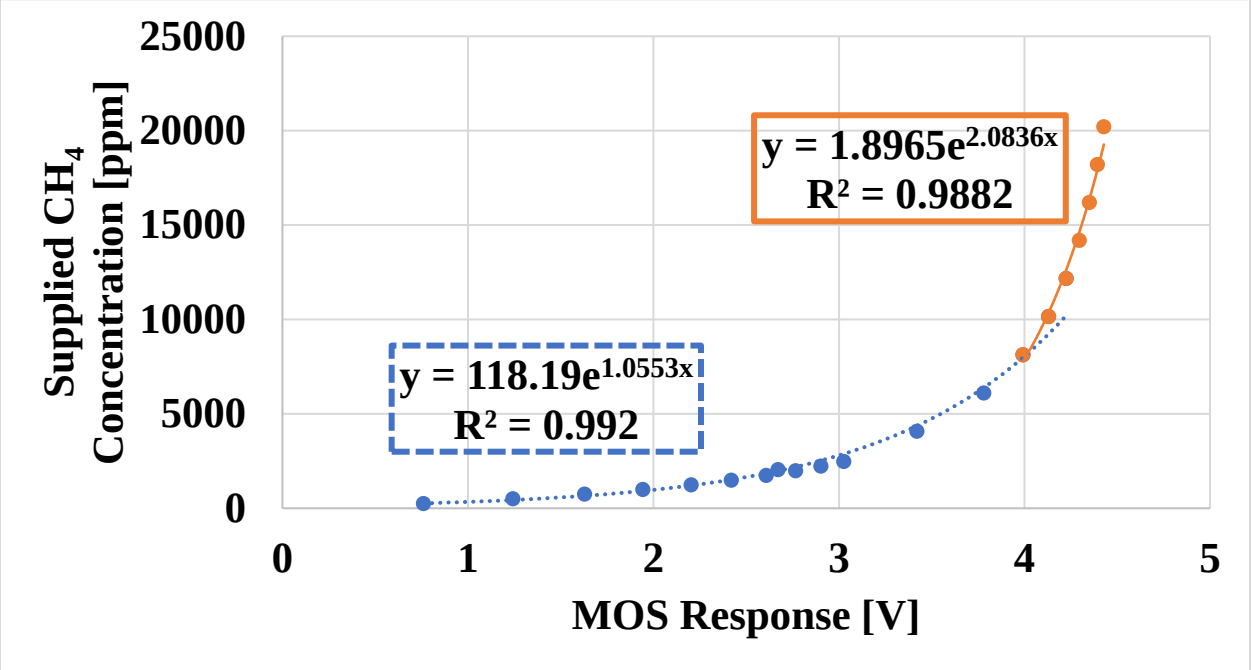

Figure 4.4.16: Example of MOS 20-Point dry calibration curve and equation.

Tests where humidity was added to the sample were also performed the same way as for the IRS. We found that different humidity correction factors were required for different ranges of humidity as well as for different ranges of CH_4 concentration. One set of humidity correction factors for the different humidity and CH_4 concentrations ranges was found using one MOS and then it was applied to all ten MOS.

The set of correction factors for the MOS had a greater number of ranges than for the IRS due to the complexity of their responses. The ranges were determined using the plot of the humidity tests performed, like for the IRS; this plot can be seen in Figure 4.4.17. It should be noted that the 14,000 ppm and 18,000 ppm tests have been omitted to provide a clearer plot.

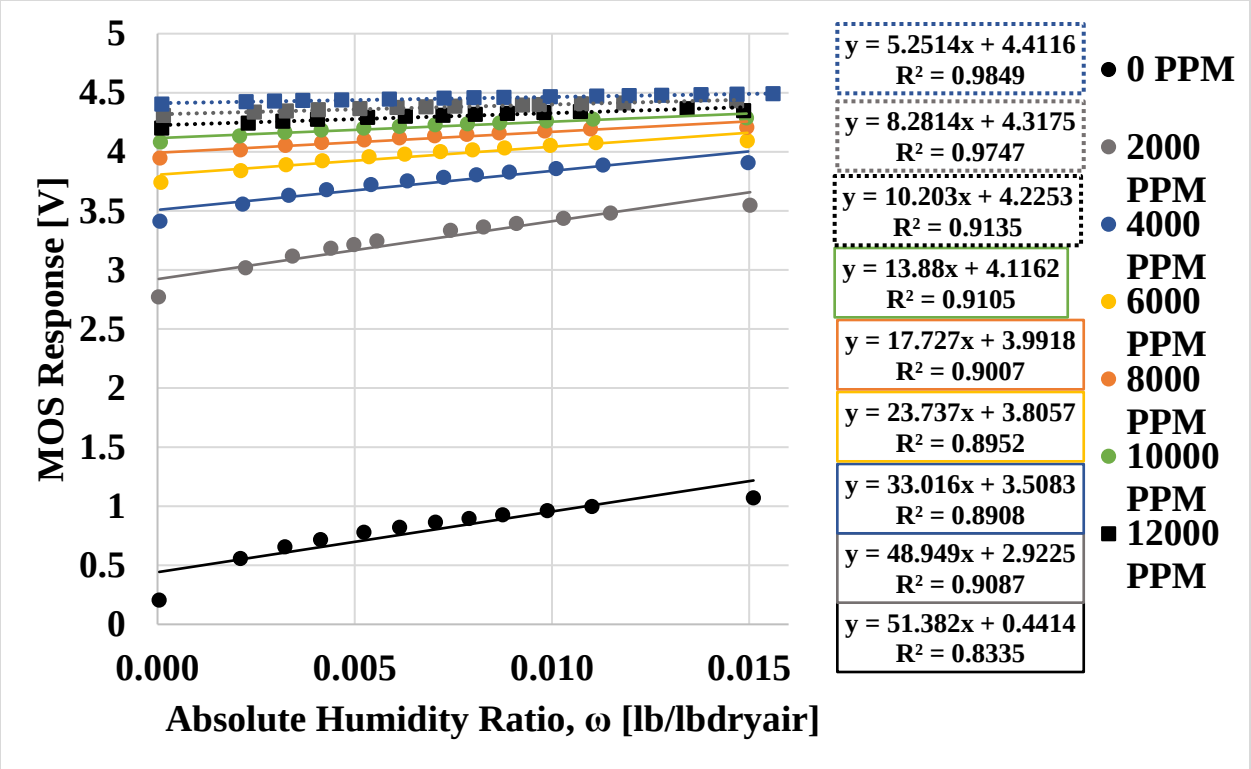

Figure 4.4.17: MOS plot used for humidity calibration corrections.

The correction factors for the various ranges for the MOS can be seen in Table 4.4.3. These factors applied to the same equation as for the IRS (Eq. 4.4.10) to calculate the corrected voltage to be used in the dry calibration equations.

Table 4.4.3: MOS calibration correction factors.

Raw Response Range [V]	ω ≤ 0.005		ω > 0.005	
	k	c	k	c
V < 3.3	70	0.1	80	0.1
3.3 ≤ V < 3.5	50	0.09	60	0.09
3.5≤ V < 3.75	40	0.05	55	0.05
3.75 ≤ V < 3.9	39	0.035	45	0.035
3.9 ≤ V < 4.0	32	0.035	37	0.035
4.0 ≤ V <4.1	25	0.035	35	0.035
4.1 ≤ V <4.23	13	0	18	0
4.23 ≤ V < 4.3	9.5	0	12	0
4.3 ≤ V <4.4	8.8	0	10	0
4.4 ≤ V < 4.5	7	0	7	0
V ≥ 4.4	4	0	4	0

Flow Sensors

The calibration for the flow sensors was given in the data sheet. This calibration can be seen in Eq. 4.4.11 where the flowrate is in slpm and V is the raw response voltage of the sensor.

$$Flowrate = 2 * V \quad \textbf{Eq. 4.4.11}$$

3-Cup Anemometers

The calibration used for the 3-cup anemometers was the original calibration given by the manufacturer based on the specific sensor parameters. The equation for this calibration can be seen in Eq. 4.4.12 where the V is the raw sensor response voltage and "wind speed" is in meters per second (m/s). It should be noted that the starting/minimum wind speed for the operation of these anemometers is 0.5 m/s (98.4 fpm).

$$wind\ speed = 9V \quad \textbf{Eq. 4.4.12}$$

Verification Results

Defining Error

The equation used to calculate the percent error is shown in Eq. 4.4.13. For the UGGA and IRS, the "actual" value was the calculated CH_4 concentration based on GD corrected values and the humidity corrections, and the "measured" value is the measured CH_4 concentration. The "actual" values were the measurements taken by the Edgetech and Heise for the RH and pressure sensors, respectively. The "measured" values for the RH and pressure sensors were their respective measurements.

$$\%\ Error = \left(\frac{measured - actual}{actual}\right) * 100 \quad \textbf{Eq. 4.4.13}$$

Methane Analyzer (UGGA)

Figure 4.4.18 shows the results of the calibration test performed on the UGGA from which the external calibration equation was obtained. Figure 4.4.19 and Table 4.4.4 show the verification of the UGGA calibration by comparing the UGGA measured values to the supplied CH_4 concentration (GD corrected values); percent error values can be seen in Table 4.4.4.

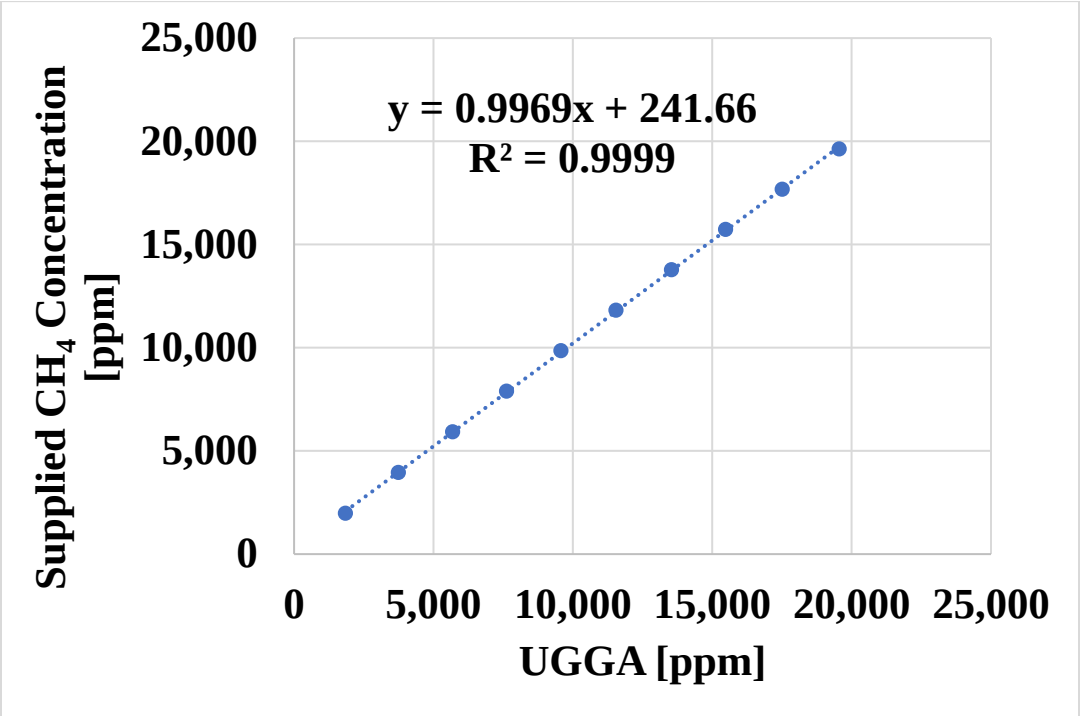

Figure 4.4.18: Calibration performed on the UGGA using a 2.01% (20,100 ppm) CH_4 bottle.

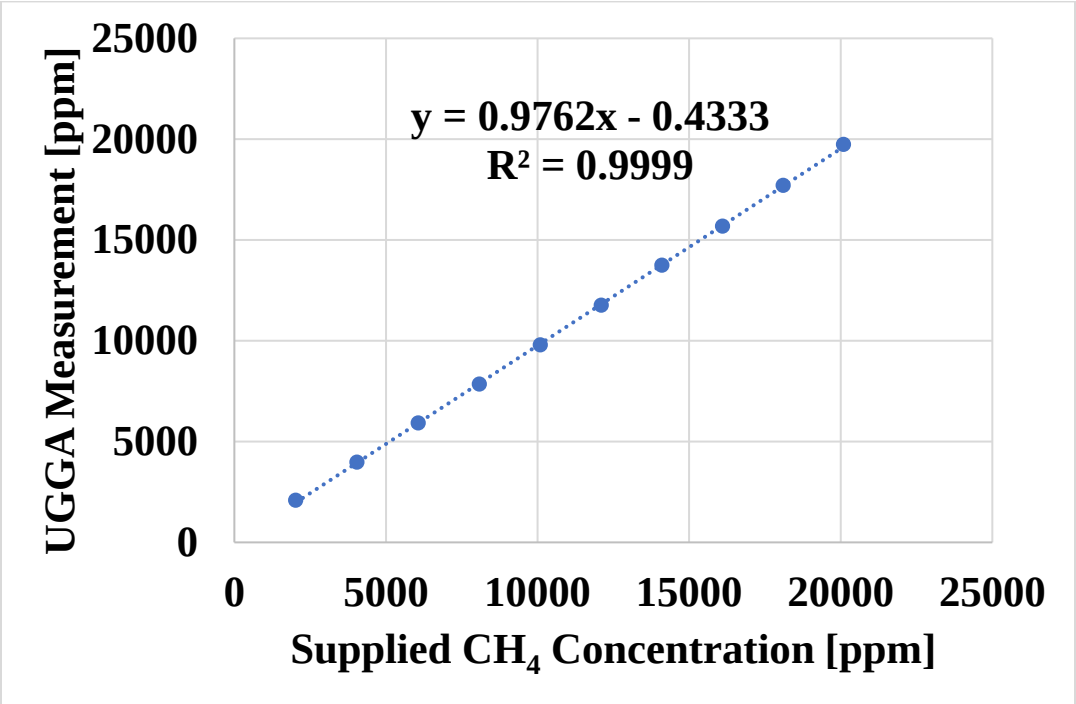

Figure 4.4.19: UGGA calibration verification after external calibration was applied.

Table 4.4.4: UGGA Calibration Results Verified to GD Corrected Values.

UGGA CH_4 [ppm]	Supplied CH_4 Concentration [ppm]	Error [%]
2032	2027	0.233
4059	4051	0.213
6102	6070	0.520
8132	8086	0.572
10,161	10,098	0.627
12,158	12,106	0.426
14,178	14,110	0.484
16,196	16,111	0.531
18,193	18,107	0.473
20,221	20,100	0.603

Relative Humidity Sensors

Figure 4.4.20 shows the results of the calibration test performed for the RH sensors from which the calibration equation was obtained. Figure 4.4.21 and Table 4.4.5 show the verification of the RH sensor calibration by comparing the measured values of the RH sensor to the measured values of the Edgetech; percent error values are in Table 4.4.5.

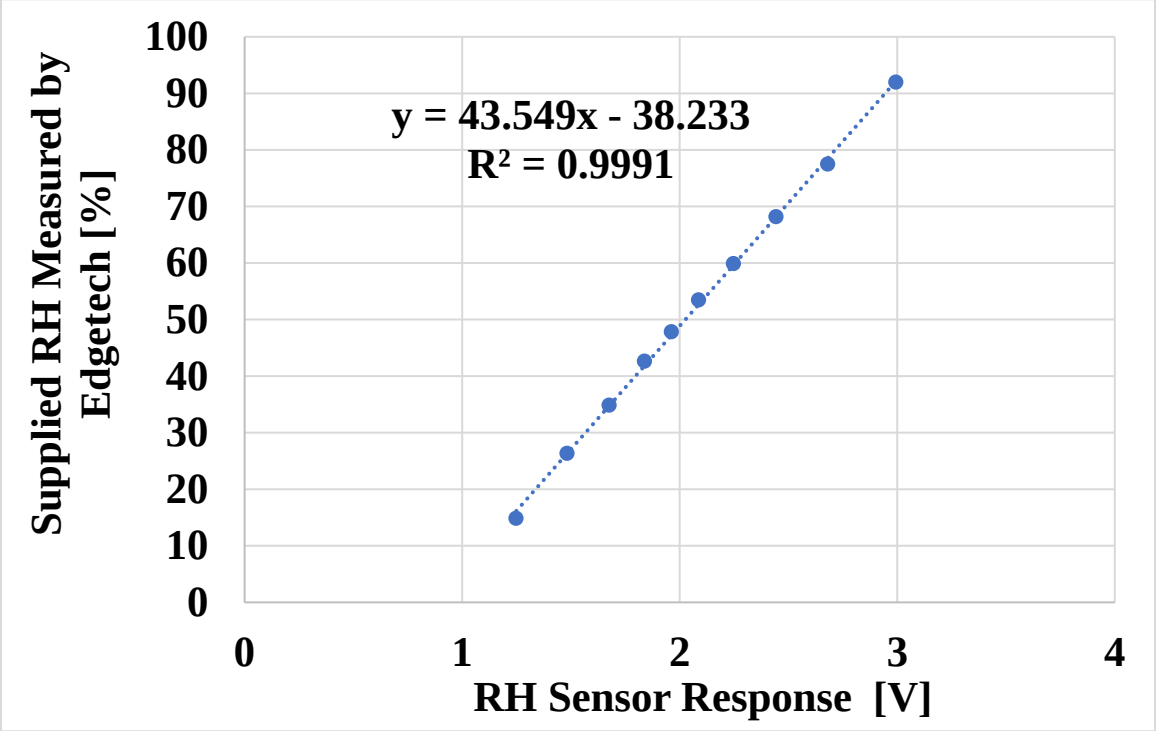

Figure 4.4.20: Calibration curve for the RH sensors at 23 °C using the Edgetech as reference for RH supplied.

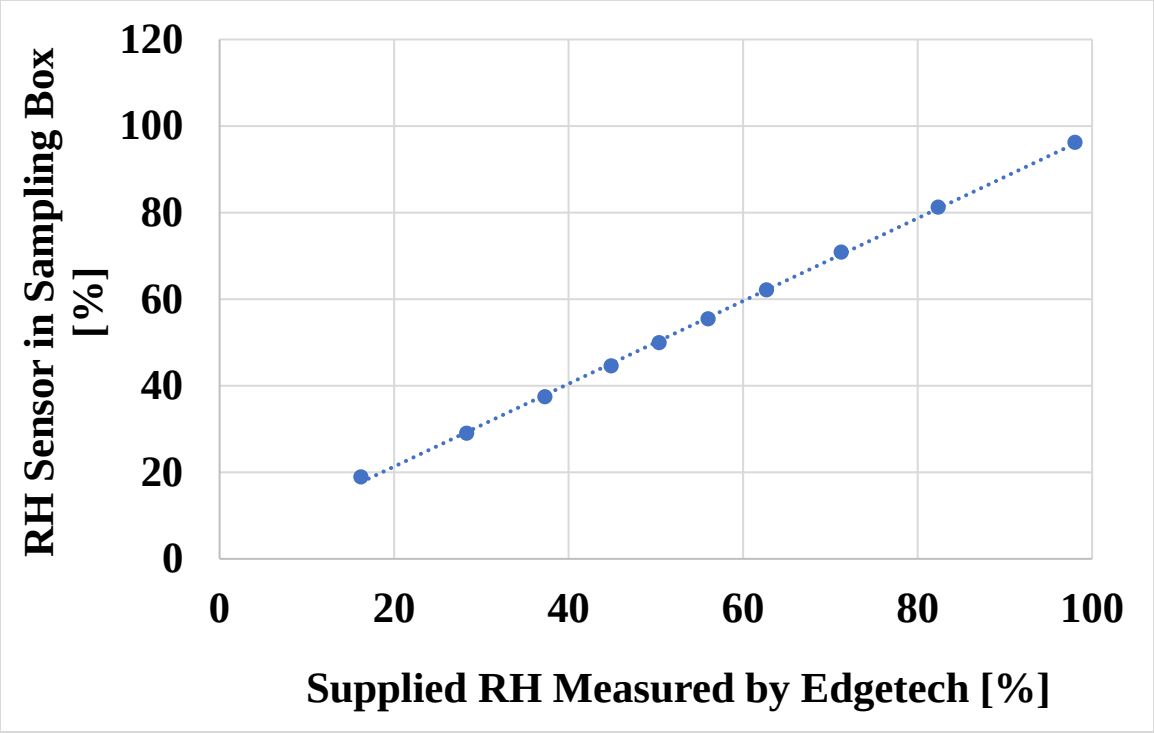

Figure 4.4.21: RH Sensor calibration verified with Edgetech.

Table 4.4.5: RH values reported by RH sensor and compared to the Edgetech.

RH Sensor [%]	Edgetech RH [%]	Error [%]
18.9	16.2	16.6
29.0	28.3	2.33
37.4	37.3	0.353
44.6	44.9	0.751
49.9	50.4	0.955
55.4	56.0	1.07
62.1	62.7	0.910
70.8	71.3	0.615
81.2	82.4	1.40
96.2	98.1	1.92

Pressure Sensors

Figure 4.4.22 shows the results of the calibration test performed for the pressure sensors from which the calibration equation was obtained. Figure 4.4.23 and Table 4.4.6 show the verification of the pressure sensor calibration by comparing the measured values of the pressure sensor to the measured values of the Heise; percent error values are in Table 4.4.6.

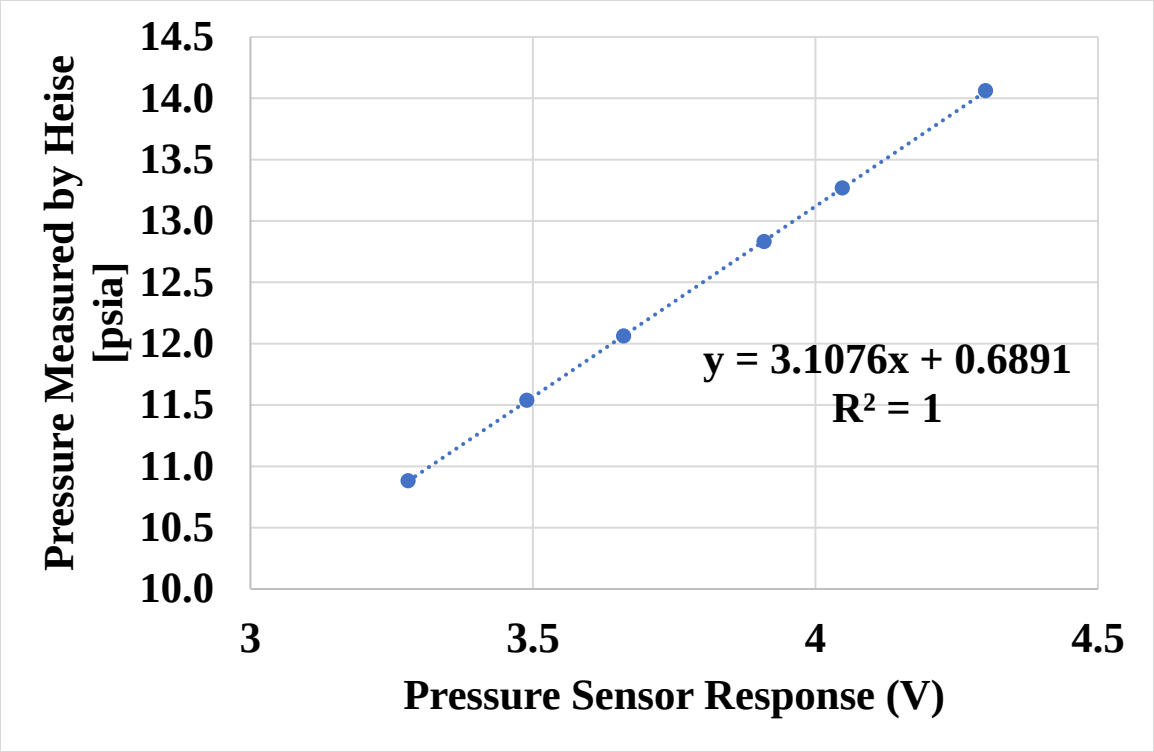

Figure 4.4.22: Calibration curve for the pressure sensors using Heise as static pressure reference.

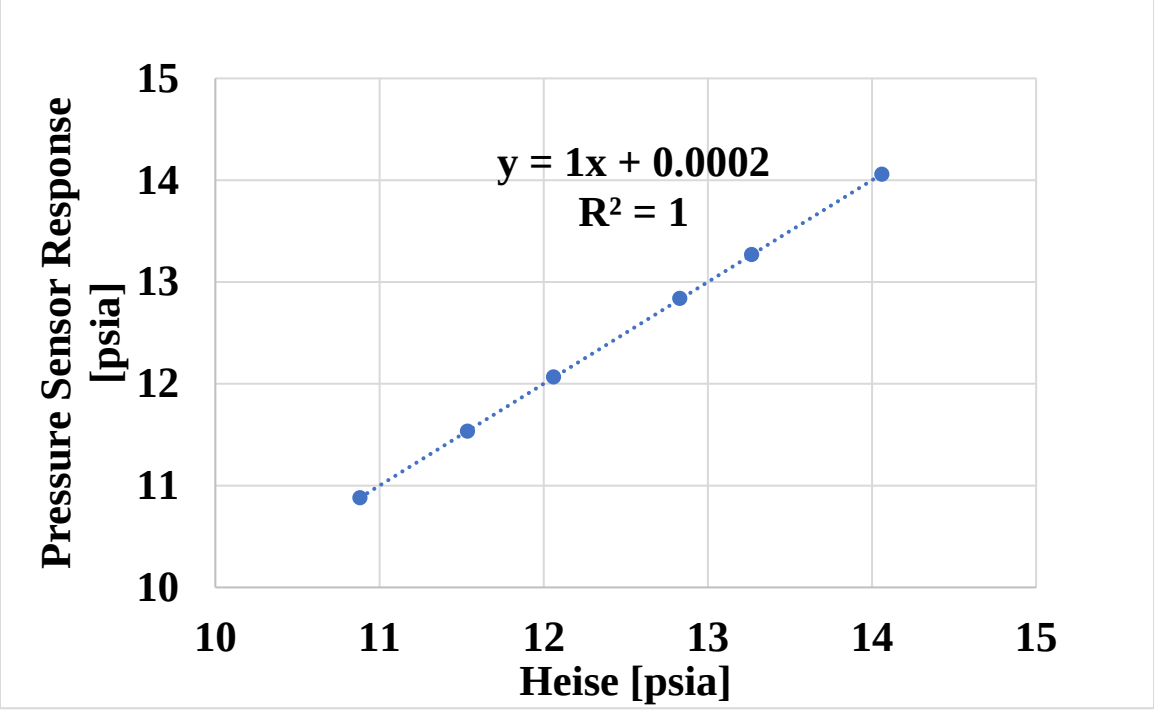

Figure 4.4.23: Pressure sensor calibration verification with Heise.

Table 4.4.6: Pressure sensor compared to Heise measurements.

Pressure Sensor [psia]	Heise [psia]	Error [%]
13.79	14.06	1.91
13.03	13.27	1.79
12.61	12.83	1.70
11.86	12.06	1.64
11.35	11.54	1.64
10.71	10.88	1.54

Methane Sensors (IRS and MOS)

To verify that all IRS and MOS were reading accurately at various CH_4 and H_2O concentrations, each sensor was exposed to three different H_2O concentrations and four different CH_4 concentrations measured in ppm. The IRS percent errors for each of these tests were found with respect to the calculated CH_4 concentration based on the GD corrected values as well as the H_2O concentration as shown in Tables 4.4.7 – 4.4.16, one table for each IRS.

The percent error values were highest at lower CH_4 concentration (1200 ppm) with the highest percent error being 26.55% for IRS 5 at the highest humidity tested. Note that the program targets the use of the low-cost sensor network to identify and detect when concentrations approach 10,000 ppm or 1% methane due to regulation set points at 1 and 1.5%.

Table 4.4.7: Humidity effect error on IRS 1 with respect to reference gas corrected values.

Percent Error [%]					
Box 1		**Methane Concentration [ppm]**			
		1200	**4000**	**12,000**	**20,000**
H_2O Concentration [ppm]	**6000**	2.34	0.476	4.65	3.84
	15,000	8.09	5.73	4.45	4.37
	25,000	0.243	1.99	1.22	5.49

Table 4.4.8: Humidity effect error on IRS 2 with respect to reference gas corrected values.

Percent Error [%]					
Box 2		**Methane Concentration [ppm]**			
		1200	**4000**	**12,000**	**20,000**
H_2O Concentration [ppm]	**6000**	5.07	3.86	2.19	3.65
	15,000	1.40	1.69	4.58	5.40
	25,000	6.93	0.863	0.414	5.04

Table 4.4.9: Humidity effect error on IRS 3 with respect to reference gas corrected values.

Percent Error [%]					
Box 3		Methane Concentration [ppm]			
		1200	4000	12,000	20,000
H_2O Concentration [ppm]	6000	0.913	8.60	4.62	4.38
	15,000	1.03	2.43	3.94	3.82
	25,000	7.43	3.45	1.69	3.27

Table 4.4.10: Humidity effect error on IRS 4 with respect to reference gas corrected values.

Percent Error [%]					
Box 4		Methane Concentration [ppm]			
		1200	4000	12,000	20,000
H_2O Concentration [ppm]	6000	18.6	7.41	4.03	4.63
	15,000	5.12	5.23	5.82	5.33
	25,000	21.9	3.38	1.73	5.13

Table 4.4.11: Humidity effect error on IRS 5 with respect to reference gas corrected values.

Percent Error [%]					
Box 5		Methane Concentration [ppm]			
		1200	4000	12,000	20,000
H_2O Concentration [ppm]	6000	18.08	3.48	5.98	3.78
	15,000	10.62	3.10	4.51	5.04
	25,000	26.55	3.84	0.843	5.40

Table 4.4.12: Humidity effect error on IRS 6 with respect to reference gas corrected values.

Percent Error [%]					
Box 6		Methane Concentration [ppm]			
		1200	4000	12,000	20,000
H_2O Concentration [ppm]	6000	3.67	1.53	3.96	3.40
	15,000	0.634	0.389	2.79	2.47
	25,000	8.90	4.44	0.04	1.77

Table 4.4.13: Humidity effect error on IRS 7 with respect to reference gas corrected values.

Percent Error [%]					
Box 7		Methane Concentration [ppm]			
		1200	4000	12,000	20,000
H_2O Concentration [ppm]	6000	12.86	2.66	2.73	2.77
	15,000	12.18	0.492	4.03	4.37
	25,000	23.30	4.57	0.176	3.20

Table 4.4.14: Humidity effect error on IRS 8 with respect to reference gas corrected values.

Percent Error [%]					
Box 8		Methane Concentration [ppm]			
		1200	4000	12,000	20,000
H_2O Concentration [ppm]	6000	16.8	2.28	4.10	5.73
	15,000	11.1	5.74	3.76	5.33
	25,000	23.7	4.64	5.44	7.37

Table 4.4.15: Humidity effect error on IRS 9 with respect to reference gas corrected values.

Percent Error [%]					
Box 9		Methane Concentration [ppm]			
		1200	4000	12,000	20,000
H_2O Concentration [ppm]	6000	6.72	0.876	2.20	2.49
	15,000	8.36	5.15	2.32	3.56
	25,000	20.4	2.48	0.740	4.60

Table 4.4.16: Humidity effect error on IRS 10 with respect to reference gas corrected values.

Percent Error [%]					
Box 10		Methane Concentration [ppm]			
		1200	4000	12,000	20,000
H_2O Concentration [ppm]	6000	14.7	7.40	3.75	0.96
	15,000	27.7	16.1	5.54	3.64
	25,000	13.2	10.4	2.98	5.27

Since the UGGA was the reference device when testing transitions to a scale demonstration, the IRS as well as the MOS measurements were compared to the UGGA measurements by calculating the percent difference. Tables 4.4.17 – 4.4.26 show the IRS and MOS measurements compared to the UGGA measurements. The percent difference was found using Eq. 4.4.14**,** where the "measured1" value was either the IRS or MOS and the "measured2" value was the UGGA.

$$\%\, Difference = \left(\frac{measured1 - measured2}{\frac{measured1 + measured2}{2}} \right) * 100 \qquad \textbf{Eq. 4.4.14}$$

The percent difference values have been highlighted where anything less than 10% is green, values between 10-15% are yellow, and values above 15% are red. All the "red" values were seen in the tests at the lowest CH_4 concentration (1200 ppm). It should be noted the percent differences are absolute value in these tables; the percent difference values were both positive and negative.

Table 4.4.17: MOS 1 and IRS 1 compared to the UGGA measurement.

Approximate H_2O Concentration	MOS	IRS	UGGA	Percent Difference between MOS and UGGA	Percent Difference between IRS and UGGA
[ppm]	[ppm]	[ppm]	[ppm]	[%]	[%]
6000	1457	1202	1139	24.52	5.37
	4804	4007	4028	17.56	0.53
	13,276	12,592	11,833	11.50	6.22
	20,196	20,744	19,584	3.08	5.75
15,000	1481	1122	1185	22.23	5.44
	4842	4216	4171	14.89	1.09
	12,979	12,447	11,827	9.29	5.11
	19,263	20,651	19,514	1.30	5.66
25,000	1801	1204	1159	43.40	3.86
	4262	4025	4055	4.98	0.73
	12,041	11,939	11,598	3.74	2.89
	19,852	20,658	19,279	2.93	6.90

Table 4.4.18: MOS 2 and IRS 2 compared to the UGGA measurement.

Approximate H_2O Concentration	MOS	IRS	UGGA	Percent Difference between MOS and UGGA	Percent Difference between IRS and UGGA
[ppm]	[ppm]	[ppm]	[ppm]	[%]	[%]
6000	1453	1293	1149	23.38	11.81
	4868	3872	4062	18.05	4.78
	14,217	12,300	11,831	18.32	3.88
	20,560	20,713	19,659	4.48	5.22
15,000	1297	1205	1206	7.22	0.12
	4390	4058	4189	4.68	3.19
	12,347	12,473	11,907	3.63	4.64
	17,989	20,873	19,605	8.60	6.26
25,000	1223	1291	1173	4.11	9.56
	3599	3917	4074	12.37	3.93
	10,687	11,854	11,660	8.70	1.65
	15,687	20,590	19,366	20.99	6.13

Table 4.4.19: MOS 3 and IRS 3 compared to the UGGA measurement.

Approximate H_2O Concentration	MOS	IRS	UGGA	Percent Difference between MOS and UGGA	Percent Difference between IRS and UGGA
[ppm]	[ppm]	[ppm]	[ppm]	[%]	[%]
6000	1433	1220	1187	18.81	2.76
	4351	3674	3688	16.48	0.40
	12,954	12,568	11,917	8.33	5.31
	19,821	20,821	19,794	0.13	5.06
15,000	1703	1237	1231	32.16	0.45
	4186	4092	4228	1.00	3.25
	12,321	12,411	11,969	2.90	3.63
	18,907	20,582	19,782	4.52	3.96
25,000	1605	1302	1207	28.31	7.53
	4889	4092	4122	17.02	0.73
	11,353	12,019	11,747	3.41	2.29
	17,760	20,270	19,625	9.98	3.23

Table 4.4.20: MOS 4 and IRS 4 compared to the UGGA measurement.

Approximate H_2O Concentration	MOS	IRS	UGGA	Percent Difference between MOS and UGGA	Percent Difference between IRS and UGGA
[ppm]	[ppm]	[ppm]	[ppm]	[%]	[%]
6000	1466	1460	1185	21.17	20.78
	4659	4328	4119	12.30	4.93
	12,709	12,526	11,852	6.98	5.53
	18,949	20,916	19,701	3.89	5.98
15,000	1525	1286	1235	20.99	3.99
	4360	4203	4215	3.38	0.29
	11,698	12,631	11,937	2.02	5.66
	17,364	20,877	19,651	12.36	6.05
25,000	1595	1474	1199	28.33	20.55
	3951	4088	4074	3.06	0.35
	10,383	12,020	11,675	11.72	2.91
	15,514	20,626	19,426	22.39	5.99

Table 4.4.21: MOS 5 and IRS 5 compared to the UGGA measurement.

Approximate H_2O Concentration	MOS	IRS	UGGA	Percent Difference between MOS and UGGA	Percent Difference between IRS and UGGA
[ppm]	[ppm]	[ppm]	[ppm]	[%]	[%]
6000	1508	1454	1200	22.80	19.14
	5011	4167	4170	18.33	0.07
	13,757	12,755	11,993	13.70	6.16
	19,923	20,740	19,867	0.28	4.30
15,000	1699	1352	1247	30.64	8.08
	4920	4121	4222	15.27	2.43
	13,167	12,483	11,992	9.34	4.02
	18,917	20,838	19,793	4.53	5.14
25,000	2098	1531	1218	53.10	22.76
	4465	4106	4104	8.43	0.04
	12,183	11,919	11,769	3.46	1.26
	17,650	20,690	19,566	10.30	5.59

Table 4.4.22: MOS 6 and IRS 6 compared to the UGGA measurement.

Approximate H_2O Concentration	MOS	IRS	UGGA	Percent Difference between MOS and UGGA	Percent Difference between IRS and UGGA
[ppm]	[ppm]	[ppm]	[ppm]	[%]	[%]
6000	1379	1276	1173	16.17	8.44
	4874	4088	4104	17.16	0.38
	13,045	12,512	11,932	8.91	4.74
	19,191	20,661	19,708	2.66	4.72
15,000	1532	1231	1236	21.40	0.37
	4792	3984	4184	13.55	4.90
	11,274	12,285	11,909	5.47	3.11
	17,832	20,332	19,631	9.60	3.51
25,000	1729	1319	1202	35.97	9.28
	3904	3783	4066	4.05	7.21
	11,428	11,835	11,673	2.13	1.38
	15,807	19,985	19,424	20.53	2.85

Table 4.4.23: MOS 7 and IRS 7 compared to the UGGA measurement.

Approximate H_2O Concentration	MOS	IRS	UGGA	Percent Difference between MOS and UGGA	Percent Difference between IRS and UGGA
[ppm]	[ppm]	[ppm]	[ppm]	[%]	[%]
6000	1471	1389	1198	20.51	14.81
	4766	4132	4171	13.31	0.95
	13,305	12,358	11,996	10.35	2.97
	19,328	20,527	20,009	3.46	2.55
15,000	1484	1372	1242	17.73	9.91
	4794	4014	4233	12.44	5.29
	12,527	12,420	12,077	3.65	2.80
	18,437	20,693	19,911	7.68	3.85
25,000	1777	1492	1212	37.80	20.71
	4251	3775	4110	3.37	8.51
	11,723	11,800	11,831	0.92	0.26
	17,196	20,256	19,701	13.58	2.78

Table 4.4.24: MOS 8 and IRS 8 compared to the UGGA measurement.

Approximate H_2O Concentration	MOS	IRS	UGGA	Percent Difference between MOS and UGGA	Percent Difference between IRS and UGGA
[ppm]	[ppm]	[ppm]	[ppm]	[%]	[%]
6000	1199	1438	1191	0.66	18.79
	4486	4119	4089	9.27	0.74
	11,718	12,529	11,775	0.48	6.21
	17,521	21,126	19,574	11.07	7.63
15,000	1383	1360	1231	11.63	9.96
	4347	4224	4160	4.39	1.51
	11,424	12,387	11,789	3.14	4.95
	16,879	20,879	19,447	14.14	7.10
25,000	1605	1497	1208	28.22	21.41
	3977	4132	4030	1.33	2.51
	10,654	12,444	11,535	7.95	7.57
	15,609	21,037	19,206	20.67	9.10

Table 4.4.25: MOS 9 and IRS 9 compared to the UGGA measurement.

Approximate H_2O Concentration	MOS	IRS	UGGA	Percent Difference between MOS and UGGA	Percent Difference between IRS and UGGA
[ppm]	[ppm]	[ppm]	[ppm]	[%]	[%]
6000	1226	1314	1184	3.51	10.38
	4082	4061	3962	3.00	2.48
	11,895	12,298	11,788	0.90	4.23
	17,691	20,477	19,492	9.69	4.93
15,000	1234	1324	1235	0.10	6.97
	4189	4199	4144	1.09	1.32
	11,533	12,214	11,794	2.24	3.49
	16,901	20,528	19,493	14.24	5.17
25,000	1296	1454	1214	6.55	18.04
	3716	4044	4032	8.18	0.28
	10,533	11,880	11,607	9.70	2.33
	15,552	20,492	19,278	21.40	6.10

Table 4.4.26: MOS 10 and IRS 10 compared to the UGGA measurement.

Approximate H_2O Concentration	MOS	IRS	UGGA	Percent Difference between MOS and UGGA	Percent Difference between IRS and UGGA
[ppm]	[ppm]	[ppm]	[ppm]	[%]	[%]
6000	1506	1412	1147	26.99	20.69
	4919	4325	3951	21.82	9.04
	14,808	12,484	11,695	23.50	6.53
	21,619	20,172	19,397	10.84	3.92
15,000	1727	1562	1236	33.13	23.34
	5484	4641	4111	28.62	12.10
	14,525	12,613	11,782	20.85	6.81
	20,762	20,564	19,452	6.51	5.56
25,000	2076	1369	1220	51.97	11.50
	4561	4364	4014	12.76	8.36
	13,231	12,158	11,555	13.52	5.08
	21,015	20,638	19,215	8.95	7.14

From these tables and the tests for all four CH_4 concentrations 87.5% of the IRS and 50% of the MOS percent difference values were below 10%. If the 1200 ppm tests are omitted, about 95% of the IRS and 53% of the MOS percent difference values were below 10%. With the 1200 ppm tests

omitted, all the IRS percent difference values were below 13%. The IRS were more accurate than the MOS when a single humidity correction was applied to all ten sensors. Due to the complexity and variety of the MOS responses, a humidity correction may need to be made specifically for each sensor to provide better accuracy. We also believed that if MOS were calibrated only to lower CH_4 concentrations, such as concentrations below 2000 ppm that the IRS may not respond to, higher accuracy would be able to be achieved.

Flow Sensors

The calibration for the flow sensors was verified by testing one of the ten sensors at various flowrates and comparing it to the MFC. A positive displacement pump was used to provide the flow and a valve was attached at the outlet of the pump to throttle it down in order to supply different flowrates. The results of this test can be seen in Table 4.4.27 and Figure 4.4.24. Additional research should focus on a reduction in these errors.

Table 4.4.27: Flow sensor verification with MFC.

MFC	Flow Sensor	Percent Error
slpm	**slpm**	**%**
3.53	3.86	9.62
3.00	3.34	11.35
1.94	2.09	7.68
1.02	0.82	-19.98

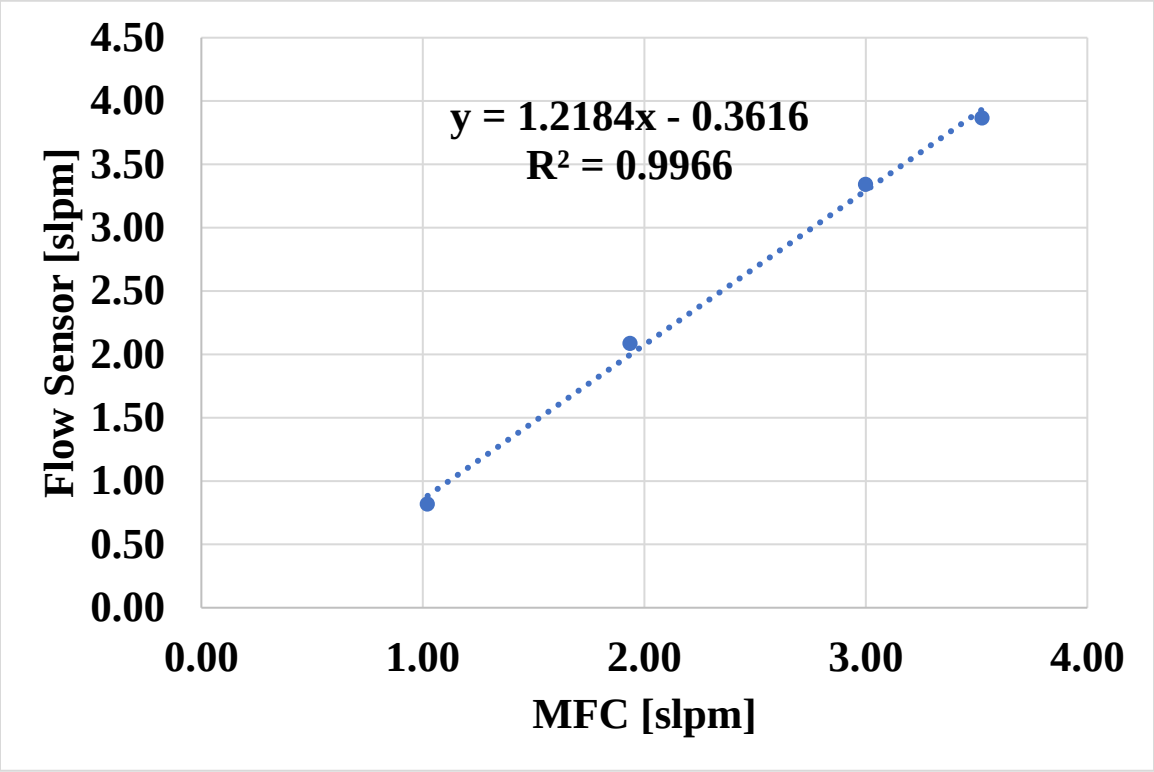

Figure 4.4.24: Flow sensor verification with MFC.

3-Cup Anemometers

The manufacturers calibration for the 3-cup anemometers was verified using the WindSonic as reference. During the verification tests, the WindSonic was aligned with one of the 3-Cup anemometers and both sensors were enclosed in a cardboard tunnel (one inlet and one outlet). Air flow was supplied at four different velocities to the inlet using an air conditioning (AC) unit. The results of the tests can be seen in Table 4.4.28, where the wind velocity measurements of the 3-cup anemometer are compared to the measurements of the WindSonic by calculating a percent error for the four different velocity points. Based in these four points, it seemed that the percent error increased as the velocity decreased, moving closer to the minimum operational velocity of the 3-cup anemometer.

Table 4.4.28: 3-Cup anemometer verification with the WindSonic.

WindSonic [m/s]	**3-Cup Anemometer [m/s]**	**Error [%]**
3.46	3.58	3.57
2.34	2.49	6.02
1.96	2.16	10.55
1.24	1.54	24.74

4.5 Full System Operations

Mock Mine Facility

WVU's research wind tunnel was utilized for a scaled demonstration and evaluation of the newly developed multi-nodal MWS. The tunnel was used as a "mock" mine in attempts to model possible longwall mining scenarios that mimicked methane release and dispersion. Federal regulations require electrical equipment around the shearer (current single monitoring point) to be manually deenergized at 1% methane, the cutting mechanism to be automatically deenergized at 1.5% methane, and all electrical equipment be automatically deenergized at 2% methane. As such methane concentrations in the range of 1-2% would occupy the sampling regions in the mock mine to ensure the system is working properly within the operational and required limits [22]. It should be noted that all methane concentrations are on a volume basis.

To more accurately represent the dimensions of a typical longwall mine, the wind tunnel was sectioned by placing a 30.5 by 6.1 m (100 by 20 ft) piece of plastic 2.4 m (8 ft) from the ground to act as the roof of the mine. The height of the roof was determined based on the maximum and minimum height of a shield, fully extended and fully collapsed, respectively. The dimensions for one type of shield typically used in industry were obtained from Swanson Industries. The maximum height of the fully extended shield was 3.0 m (10 ft) and the minimum height, fully collapsed, was approximately 1.2 m (4 ft) therefore, the roof height of the mock mine should be between 1.2 and 3.0 m (4 and 10 ft). The roof height was also limited by the wind tunnel entry door. For these reasons, a mock mine roof height of 2.4 m (8 ft) was used. The plastic laid across ten "T" structures that were constructed by various lengths of 50.8 by 101.6 mm (2 in by 4 in) pieces of wood (as seen in Figure 4.5.1). The cross-sectional area of the mock mine was approximately 4.9 by 2.4 m (16 by 8 ft), making the experimental volume approximately 373.8 m^3

(13,200 ft^3). The prototype MWS was installed in the mock mine. The system consisted of ten sampling nodes outfitted with various sensors: two types of methane sensors (Metal Oxide and Infrared), a flow sensor, a temperature sensor, a relative humidity (RH) sensor, and a pressure sensor. The ten sampling units were evenly spaced along the 30.5 m (100 ft) wind tunnel (one at each node and mounted near the roof, 2.4 (8 ft) from the ground, at the center of the cross section. Each node had the ability to sample from both the face and gob sides (not simultaneously) 2.1 (7 ft) from each side of the node, perpendicular to the flow. Figure 4.5.1 shows a couple views of the mock mine with the MWS installed.

Figure 4.5.1: Mock mine with MWS installed.

Ultimately, the integration of monitoring atmospheric flow rates in the coal mine (longwall face) would be beneficial in the case of the proposed system. Issues with accurately measuring wind speed among the everyday operations of an underground coal mine may be difficult due to spatial limitations and structural integrity. For system demonstrations and data collection, two 3-cup anemometers were implemented into the design of sampling boxes two and nine to measure wind velocities near the beginning (HG) and exit (TG) of the mock mine. Figure 4.5.2 shows the anemometer mounted at Node 2. The measurements of these 3-cup anemometers were referenced to the standard (WindSonic) which placed in-line with the 3-cup anemometers and at the center of the wind tunnel for various tests. Due to poor circulation of air throughout the mock mine from the fans and natural causes beyond our control (i.e. gusts of wind), wind speeds were generally below the minimum operational wind speeds and were inconsistent. Since the 3-cup anemometers operated on a momentum driven principle, consistent and sufficient wind speeds were required for more practicality.

Figure 4.5.2: Cup anemometer mounted on sampling unit at Node 2.

While the proposed sampling method for the system was the use of water ejectors, due to the lack of water access at the mock site, two positive displacement diaphragm pumps were used in conjunction with two manifolds to induce sample flows; each pump controlled the flow through five sampling units. The sampling flowrates for each node were controlled to approximately 2 slpm (0.071 scfm) by adjusting the valves on the manifolds and by throttling the pump with a valve that was placed at the outlet. The pumps and manifolds were then mounted on the "T" structure of nodes 3 and 8, as shown in Figure 4.5.3.

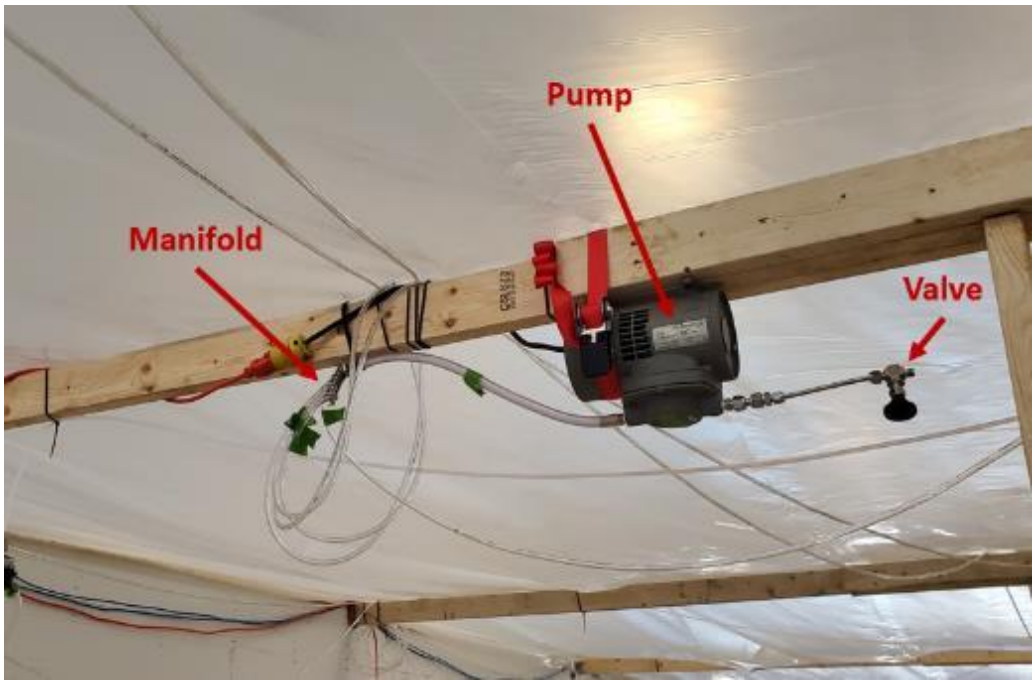

Figure 4.5.3: Pump and manifold mounted to the "T" structure.

All the sampling units were “daisy-chained” together via low voltage ethernet communication cables to obtain connectivity and communication between all the sampling units to the CPH. The CPH was an industrial computer housed in a steel box, along with the 24 VDC power supply used to power the entire MWS. The CPH had the ability to process input analog signals and display desired parameters on a user interface (such as CH_4 concentrations at each node) as well as send and receive digital signals to control the 3-way valves in each unit and the relay which controlled the alarm. Figure 4.5.4 shows the CPH and its placement in the mock mine.

Figure 4.5.4: CPH in mock mine.

Baseline Characterizations and Data Collection

Baseline Tests (Temperature, RH, Pressure)

To attain measurements of ambient conditions, baseline tests were completed without the presence of methane; these tests measured temperature, RH, and pressure in the mock mine. Many of these tests were recorded overnight or over the period of 2-3 days. Also, all tests that involved the presence of methane were recorded for a period long enough to obtain baseline conditions before methane was introduced. Temperature, RH, and pressure were measured in each of the ten sampling units as well as by an Omega iBTHX which was placed on the face side at the middle of the mock mine (at the door) near the roof. Figure 4.5.5 shows a picture of the iBTHX (left) and its location in the mock mine (right).

Figure 4.5.5: iBTHX and its location in the mock mine.

Baseline Results

There were ten "long term" tests recorded at the mock mine where temperature, RH, and pressure were recorded in each of the ten sampling units as well as with the iBTHX for reference. During these tests, the MWS sampled ambient conditions (no CH_4 was supplied). It was known prior to these tests that the temperature inside the sensor block was generally higher than that of the surrounding ambient environment. This was most likely due to the heated operation of the MOS. Since the volume in the block was small, the heat emitted from the MOS increased the temperature of the sample. This rise in temperature also impacted the RH inside of the sensor block. There should be a slight decrease in pressure, when the MWS is in operation, due to the flow; therefore, the pressure in the sampling box would be slightly lower than the ambient pressure measured by the iBTHX. Figure 4.5.6 shows the temperature, RH, and pressure, respectively, for one of the "long-term" tests. The measurements of temperature were generally higher, RH lower, and pressure just slightly lower for all ten sampling nodes than for the iBTHX, as expected. These relationships were seen in all the "long-term" tests.

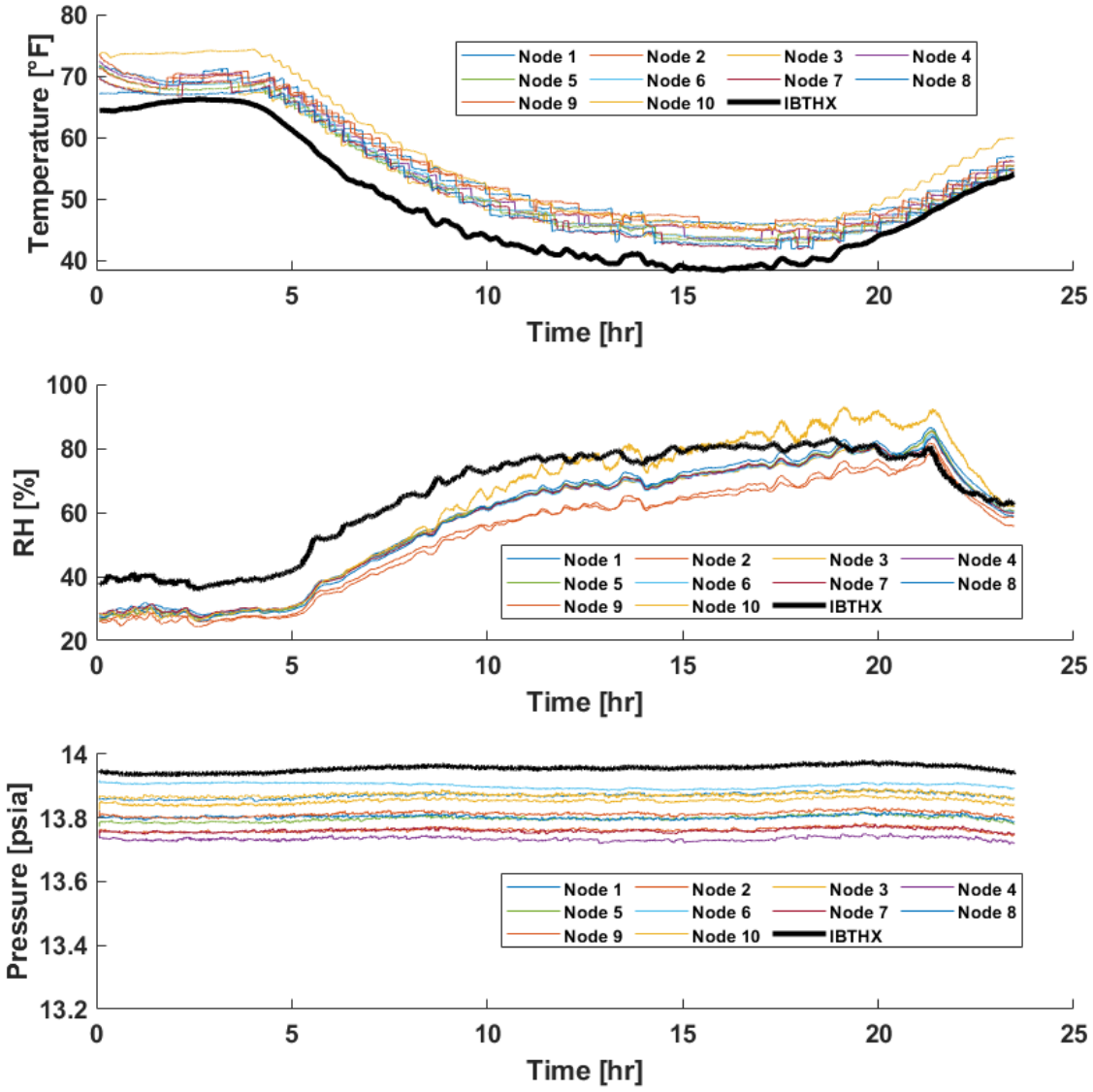

Figure 4.5.6: Temperature, RH, and pressure during a long-term test (test 5).

System Response Characterization Methods

Response Times

Two methods were used to analyze system response times when exposed to CH_4. The rise and decay times of the system were found for each test using both the MOS and IRS responses as reference. During these tests, methane at a known concentration of 2.03% (from a calibration gas

bottle) was supplied to the desired sampling location(s). Method 1 supplied methane to 5 sampling locations at a time through a tubing network, while Method 2 examined a single sampling location.

Method 1

Method 1 consisted of a network of tubing for which supplied methane to one of four groups of sampling locations at a time; each group consisted of 5 sampling locations. The placement of these sampling locations (face or gob) can be seen in Figure 4.5.7. This system consisted of four manifolds, each with a single inlet and five outlets, for a total of 20 supplied sampling locations. The first manifold supplied CH_4 to sampling locations 1-5, the second to sampling locations 6-10, the third to sampling locations 11-15, and the last to sampling locations 16-20. The CH_4 supply was directed to one manifold at a time (5 sampling locations); this action was controlled by a system of three 3-way valves, see Figure 4.5.7. The "true" and "false" at each valve represented the direction of the flow when the valve was powered on and off, respectively. For example, if all valves were powered off, sampling locations 11-15 received the sample of CH_4. The length of the tubing that the CH_4 was supplied through was approximately 19.8 m (65 ft) from the 3-way valve system to the sampling location of interest. Before the test began, the CH_4 supply was turned on to purge the tubing to ensure it was flooded with methane; the tubing was then placed into the filter of the respective sampling location. It should be noted that the outer diameter of the tube was less than the inner diameter of the filter inlet, thus it was served as a flooded probe to ensure the system was not over pressurized – which would have impacted the response time. The recording of the test was started before the supply of CH_4 was initiated to record background conditions before supplying the CH_4. The CH_4 was then supplied to each sampling location at a flowrate lower than the sampling flowrates of each box to alleviate the chance of effecting the response time due to the CH_4 supply rate; the remaining portion of the sample was pulled from ambient. The flowrate of the CH_4 was regulated by a mass flow controller (MFC) that was connected directly to a pressure regulator on the methane gas bottle. The time in which the CH_4 supply was initiated (start time, t_{start}) and the time at which the CH_4 supply was ceased (stop time, t_{stop}) were either controlled and referenced by the MFC or by the 3-way valve system. There were two tests performed where the MFC was referenced for start and stop times and two tests where the valves were referenced. Note that there was no noticeable difference between either method, therefore they have been grouped together to form one set of four tests for assessment of the rise and decay times.

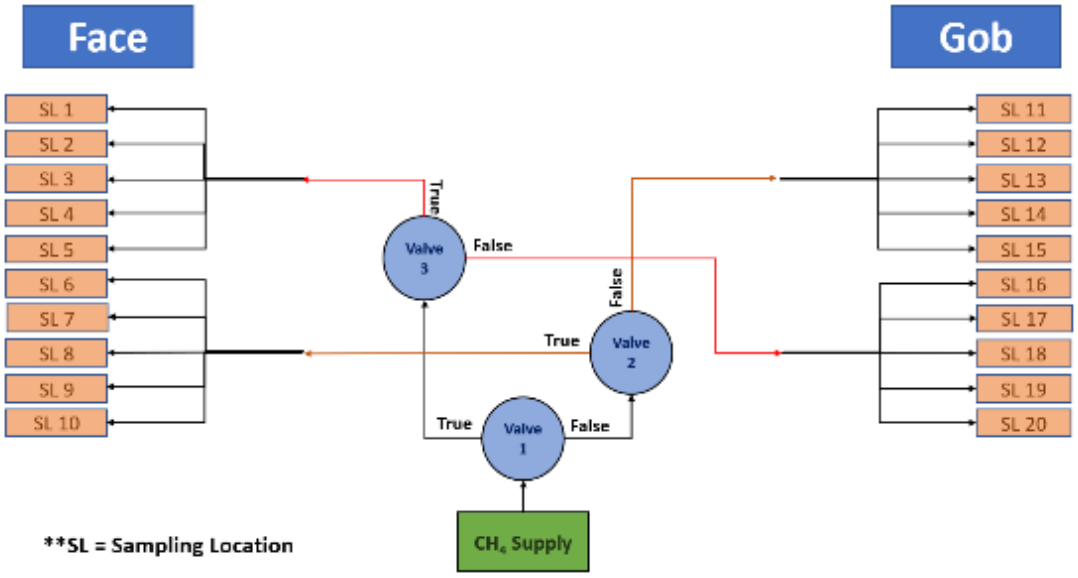

Figure 4.5.7: Valve setup for the supply of methane using a "flooded" probe approach used in both Methods 1 and 2.

The rise and decay times of the system were determined based on the responses of both the MOS and IRS. The rise time was characterized as the time it took a sensor (MOS or IRS) to reach 90% of its total response once the CH_4 supply was initiated (t_{start}). Taylor et al and Zhang et al conducted research that analyzed response times of sensors and both studies used 90% of the response when calculating the rise times of the sensors; therefore, we used a value of 90%. The total response was determined by taking an average (30-60 seconds) of the sensor response before CH_4 was supplied (background conditions), averaging the peak sensor response and then taking the difference of the two averages and multiplying by 0.9. The decay time was characterized as the time, once the CH_4 supply is stopped (t_{stop}), to drop below 90% of the total response and was within 5% of the background average; this was the same background average that was used to determine the rise time. It should be noted that the raw sensor response (voltage) was used in all calculations. Figure 4.5.8 shows an example of the MOS and IRS raw responses to help visualize how the rise and decay times were calculated.

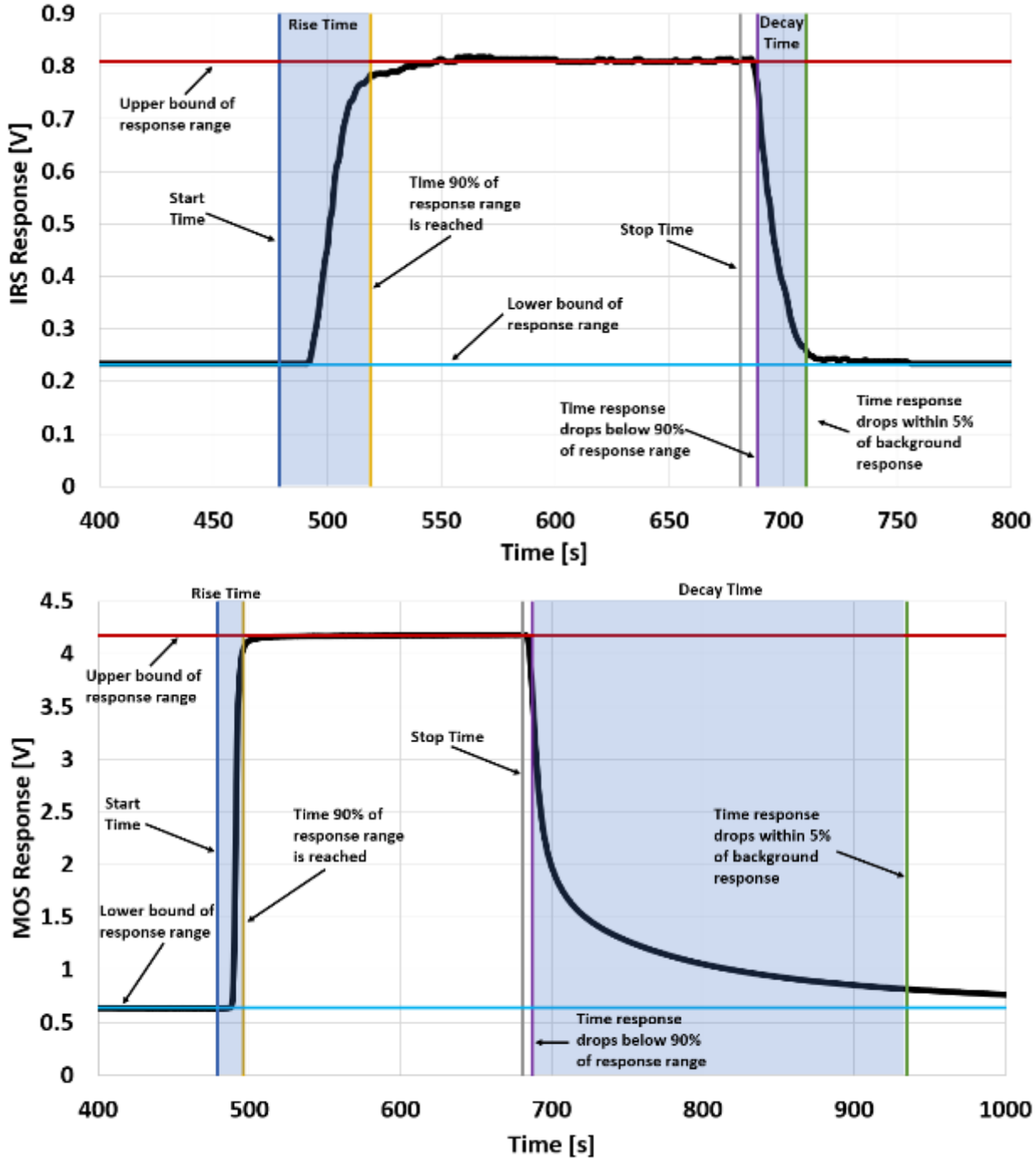

Figure 4.5.8: Example of MOS and IRS raw responses to help visualize rise and decay times.

After the rise and decay times for each test were found, the results for both the MOS and IRS were averaged to calculate an average rise time and an average decay time for type of sensor. We originally thought that the CH_4 supply tube was flooded prior to the start of the test (i.e. no diffusion) and the filter was filled with ambient air; meaning that at the start time the CH_4 supply

immediately began to flood the filter, replacing the ambient air with the CH_4 concentrated gas. However, after initially viewing the results, we determined this was likely not the case; discussed in more detail in the "Results and Discussion" section. To further analyze the accuracy of these results, the results of Method 2 were used for comparison.

Method 2

Method 2 was performed where the MFC was placed directly at the filter of sampling location 5. A tube of approximately 0.3 m (1 ft) was attached to the MFC and inserted into the filter; Figure 4.5.9 shows this setup. It should be noted that the outer diameter of the tube was less than the inner diameter of the filter inlet, thus it acted as a flooded probe to ensure the system was not over pressurized – which would have impacted the response time. This method was repeated 4 times with 4 different supply flowrates: 3, 1.4, 1.3, and 1.2 slpm (0.106, 0.049, 0.046, and 0.042 scfm).

This method was used to ensure the CH_4 was being supplied to the filter as soon as the MFC was turned on; this was assumed because the 0.3 m (1 ft) CH_4 supply tube was considered negligible compared to the 19.8 m (65 ft) of supply tubing used in Method 1. A similar method of averaging (as for Method 1) was used to calculate the rise and decay times.

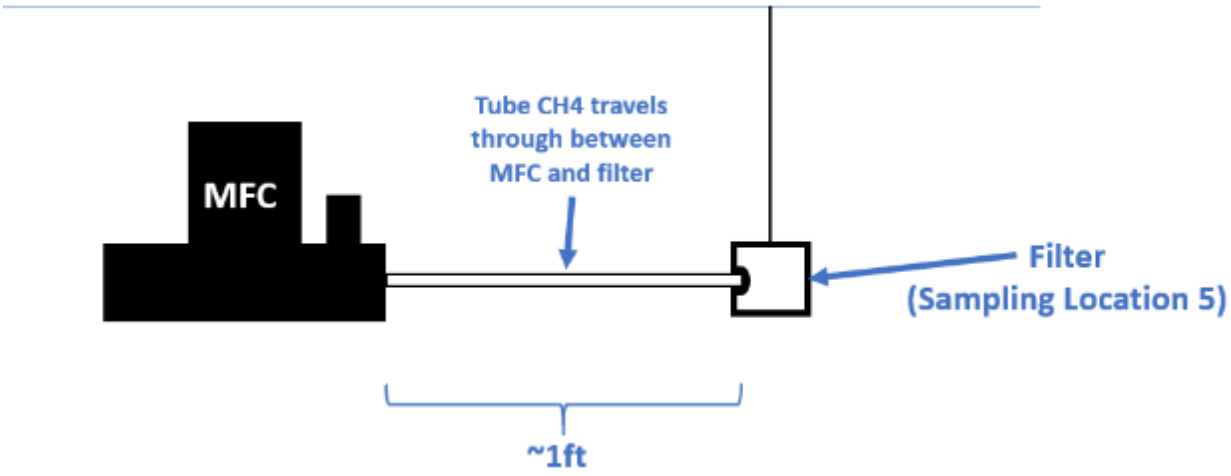

Figure 4.5.9: Method 2 setup.

Tests Conducted Using the FFS

Initial attempts were made to locally increase the presence of methane to the desired limits by leaking 2% calibration gas (methane) at various flow rates and release points. We determined a proximity of a few inches was necessary overcome dilution of the gas within the mock section. Therefore, we used WVU's full flow sampling system (FFS), pictured in Figure 4.5.10, operating in reverse to deliver dilute methane plumes directly near the filter inlet at the sampling location as well as to increase the concentration of methane and its flowrate. The system utilized a blower that coupled a dilute flow measurement section containing a mass air flow (MAF) sensor, temperature sensor, and the ultra-portable greenhouse gas analyzer (UGGA) used for varying methane emissions into the mock mine. Corrugated tubing of about 7.6 m (25 ft) was placed on the outlet of the measurement tube to increase mobility and control the position of the methane leak. About 30.5 m (100 ft) of tubing was placed on the inlet of the blower to allow dilution air to be pulled

from outside of the test section to avoid recirculation. The FFS system allowed for an elevated level of methane to enter the system at a controlled flow rate; for which it then diluted to the desired concentration and was discharged at a greater volumetric flow rate to test section.

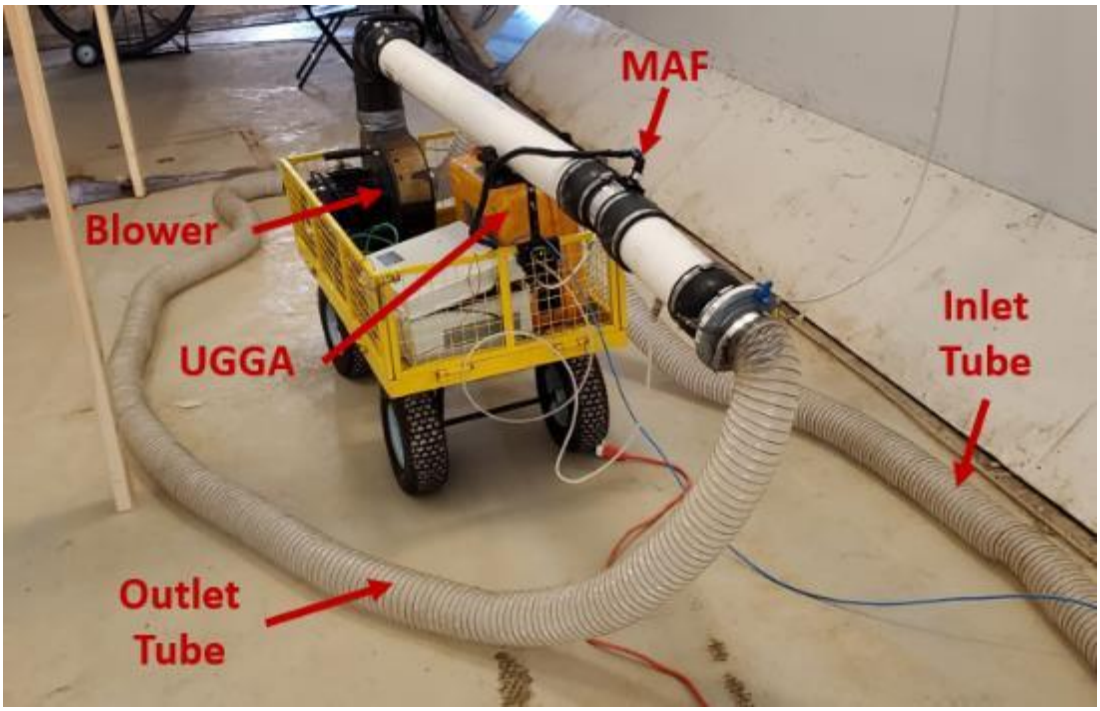

Figure 4.5.10: Use of the FFS system for creation of high volumetric flow rates of lower concentration methane.

Type 1 – Constant Immobilized Leak with Low Ventilation

For this test, only the fan located at the TG of the test section was on to help direct and pull flow through the wind tunnel. It should be noted that any outside variables to the test section, such as weather, were directly associated with the conditions inside the test section and may have contributed to variances to the ideal scenarios throughout the tests being described. The FFS was then placed at the HG with its flow directed down the test section, parallel to the face of the longwall. The release point is fixed 2.1 m (7 ft) before Node 1 at a height of 0.9 m (3 ft) from the ground, as shown in Figure 4.5.11. After collecting background responses of the system (prior to the presence of methane), methane from the pure bottle was injected into the intake flow of the FFS at a setpoint which corresponded to a desired diluted concentration. Most of these tests consisted of a 2% leak of methane into the test section at a flow rate of 2832 slpm (100 scfm)). A higher concentration of 6% was also conducted. The 2% leak described above was left constant for the remaining duration of the tests.

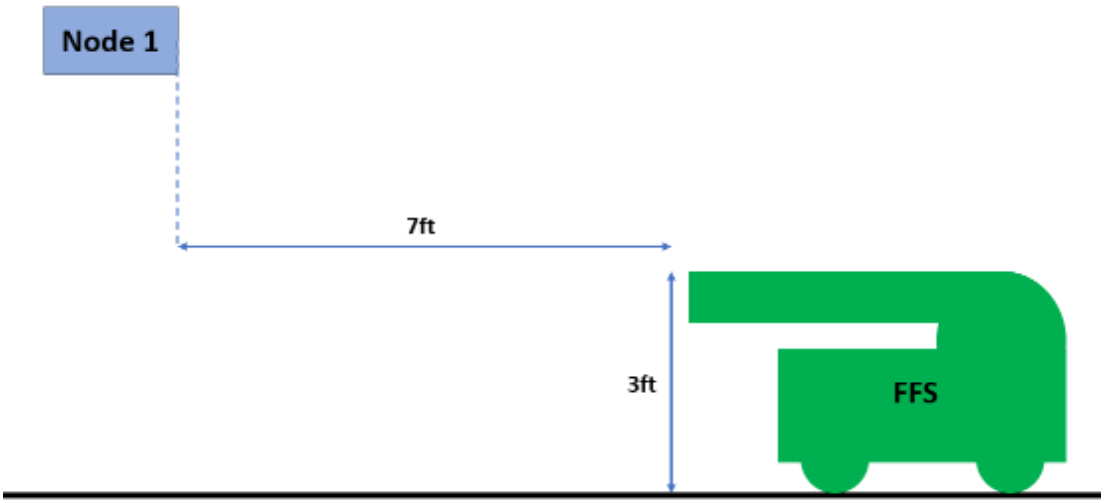

Figure 4.5.11: Location of FFS.

**Various configurations of these tests were conducted such as switching valves back and forth and placing the methane leak closer to either the face or gob side.

Type 2 – Constant Immobilized Leak with Increased Ventilation

These tests were conducted similarly as the ones in the previous section with the addition of a fan at the HG. The additional fan was implemented in attempts to increase and better control the flow through the mock mine section. Once again, the FFS was used to release a known concentration of methane to the test section at the HG.

Type 3 – Methane Released Directly Near the Sampling Locations (Filters)

Due to the detection limits of the infrared sensor (IRS), a local, detectable, methane concentration was unable to be achieved with the immobilized leak methods mentioned above. To evaluate the sensors responses within their operational range, the FFS was placed directly near each individual filter at the sampling location to ensure the desired concentration was present. The FFS flow containing the methane was held approximately a 0.3 m (1 ft) from each filter for around a minute, allowing the sensor to reach a full response. These tests were conducted with 2% methane by volume from the FFS as referenced by the UGGA. In proper operating conditions, the UGGA measured with an uncertainty of around +/-5%. Figure 4.5.12 shows a visualization for the setup of a Type 3 test for one sampling location.

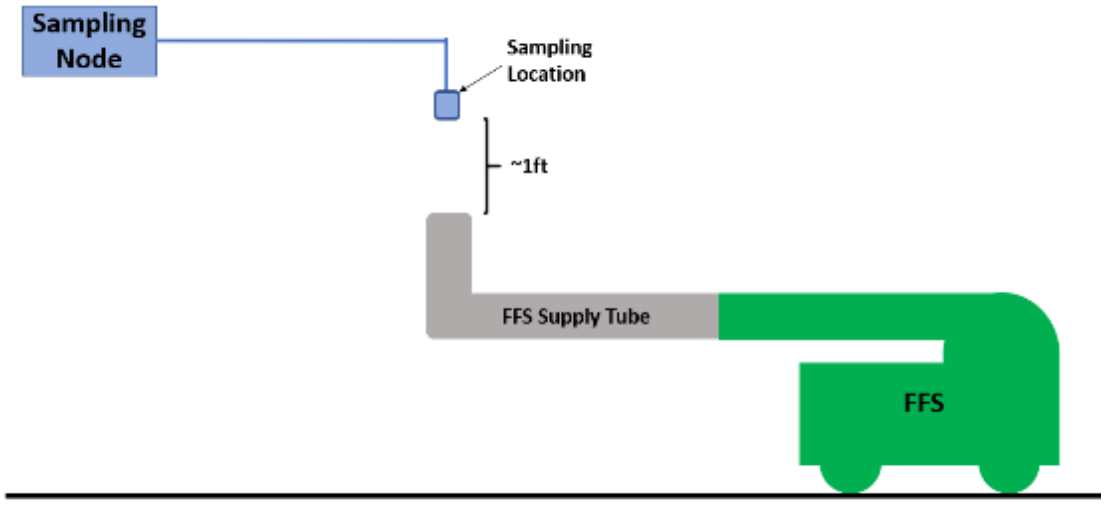

Figure 4.5.12: Type 3 Test - Visualization for one sampling location.

Type 4 - Methane Released Directly Near the Sampling Locations (Filters) and Continuously Moving

As in the previous section, the FFS was placed about 0.3 m (1 ft) away from each filter. However, in these tests, the FFS was continuously moving past each sampling location at a slow walking speed; it was never stationary at a sampling location for an extended period. A diagram showing this test can be seen in Figure 4.5.13.

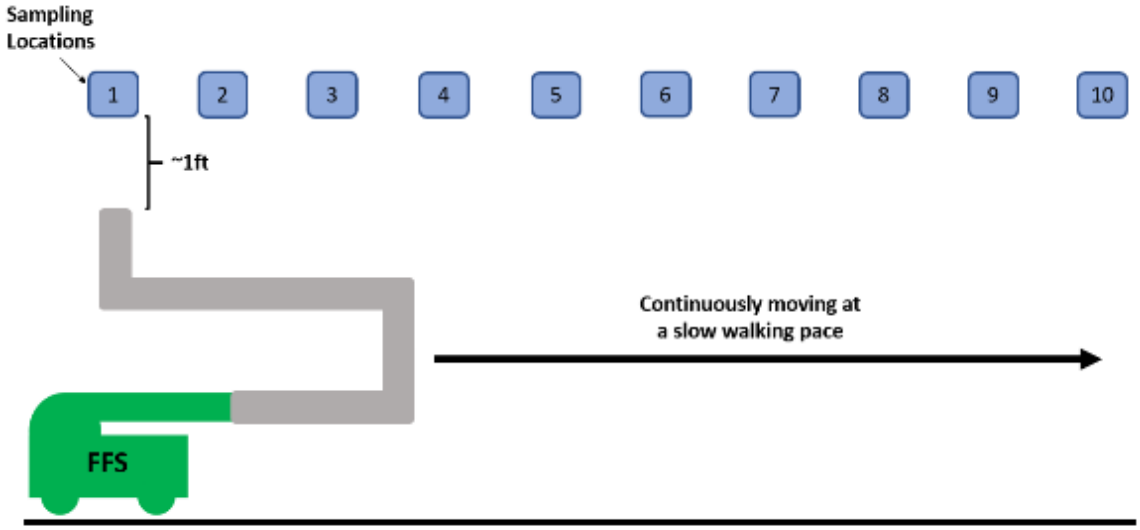

Figure 4.5.13: Type 4 Test - Visualization of set-up relay/alarm testing.

Alarm/Relay Control

A major objective was to improve mine safety by including the ability to deenergize equipment. Physical disconnections would be through notification of operators and through software control. The MWS included both an audible and visual alarm to notify operators, and the capabilities to

control isolated relays. To test that the relay control worked properly, a program was written that turned a relay on and off and activated an alarm whenever any of the IRS measured over 1% methane concentration. Figure 4.5.14 shows a scenario when an IRS sensor exceeded the 1% threshold; in this example, IRS 1 ("Dynament 1" in the picture) was exposed to a CH_4 concentration above 1% to set off the alarm. Figure 4.5.15 shows an example of what the interface looks like when an alarm is set off; when an alarm is triggered, the "Gauge" block in the "Alarm" group turns red (shown in the red circle) and the message box displays which node triggered the alarm (shown in the blue rectangle). In this example, "Dynament 1" represents node 1.

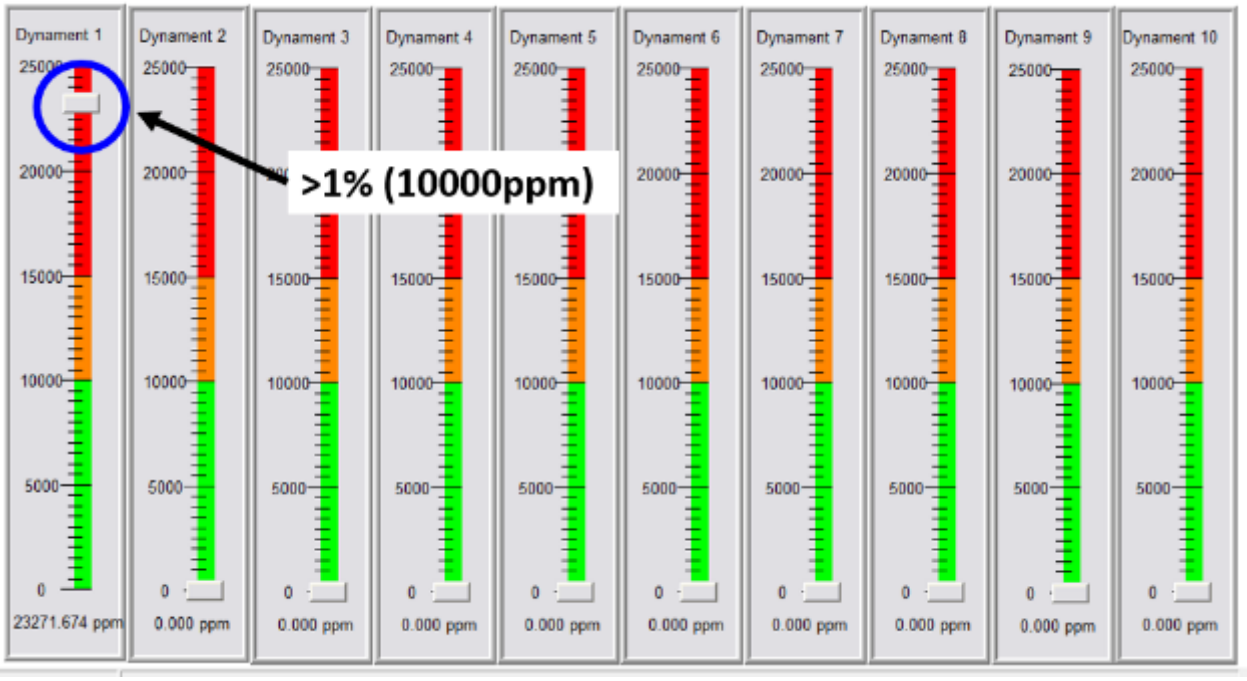

Figure 4.5.14: CPH interface showing IRS 1 measuring a CH_4 concentration above the 1% threshold.

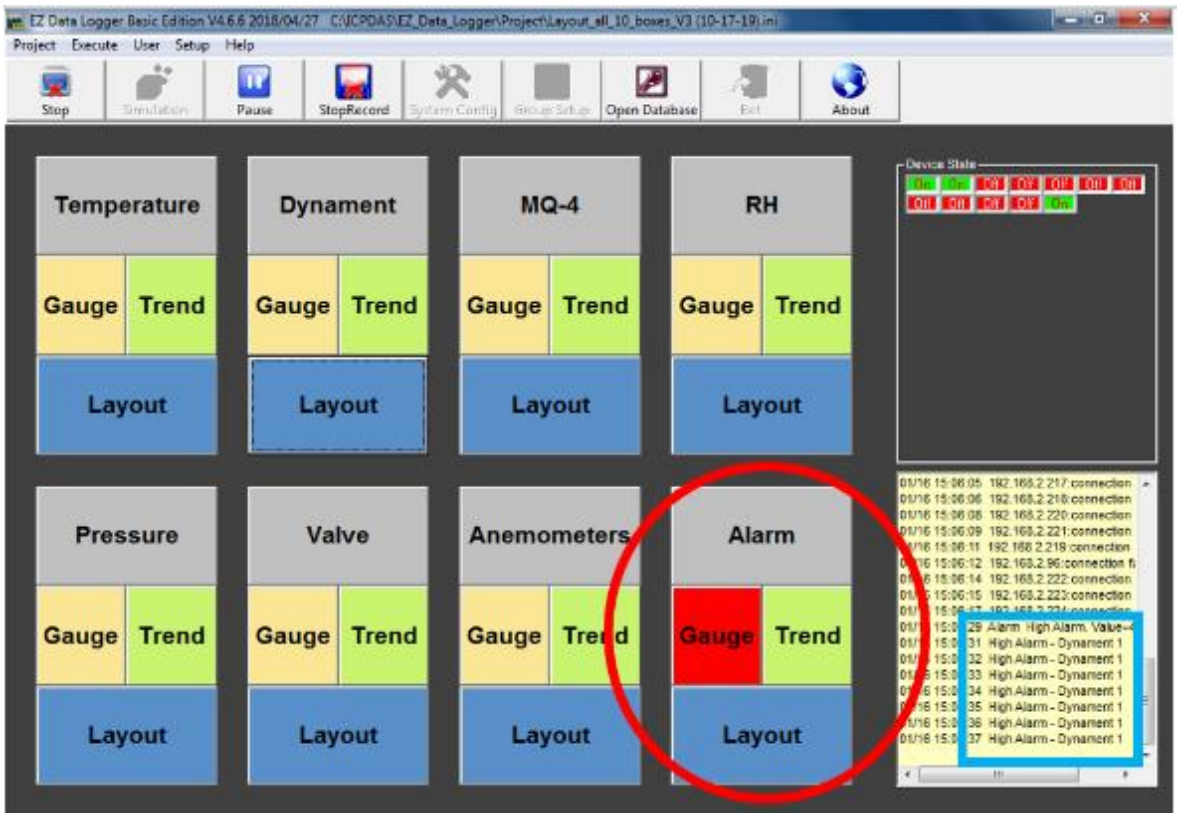

Figure 4.5.15: CPH interface when alarm was active.

In this test, the FFS was used to supply CH_4 to each sampling location on the gob side; one sampling location was supplied with approximately 2% methane until the sensor measured high enough to turn on the relay and set off the alarm. The supply was then taken away until the sensor's response decayed to below 1% and the relay was turned off; this was completed for all ten nodes.

System Response Characterization Results

Response Times

The four tests performed using Method 2 supplied the CH_4 sample to the filter at four different flowrates. There was not a distinct correlation of supply flowrate to the response times. Table 4.5.1 shows the resulting response times for the MOS and IRS of node 5.

Table 4.5.1: Method 2 comparison of response times at different supply flowrates.

	3 slpm		**1.4 slpm**		**1.3 slpm**		**1.2 slpm**	
	MOS	**IRS**	**MOS**	**IRS**	**MOS**	**IRS**	**MOS**	**IRS**
Rise Time [s]	8	28	8	29	10	30	9	27
Decay Time [s]	142	20	122	22	120	22	151	24

Since there did not seem to be a correlation between the supply flowrates used and the response times, the results from the four tests which used Method 2 were also used to compare to the results

of Method 1. The averages of the rise and decay times for both the MOS and IRS of the four tests using Method 1 as well as for the four tests using Method 2 are found in Table 4.5.2; since Method 2 occurred on a nodal basis, only averages for the face sampling location 5 were presented to allow for comparison of the two methods. The assumptions made for Method 1 were first brought into question when we noticed that the decay times for some sampling locations were much different than others. Figure 4.5.16 shows an example to help visualize this effect and includes the raw response as well as the calibrated response as a CH_4 concentration in a percent by volume. Figure 4.5.16 shows that the response of the MOS at sampling location 1 did not fall back down to the background response after being exposed to the CH_4 supply as the other four appeared to; it seemed to get "hung-up" at a CH_4 concentration of around 0.09% for approximately 200 seconds after the other sensor responses dropped close to the background concentration; this drop is shown in the circles in each plot of Figure 4.5.16. Since the response of the MOS at sampling location 1 "hung-up" at a higher concentration and then eventually dropped to meet the rest, we suspected that the majority of the CH_4 diffusing from the supply tube was being pulled/sampled by box 1 (the box associated with sampling location 1).

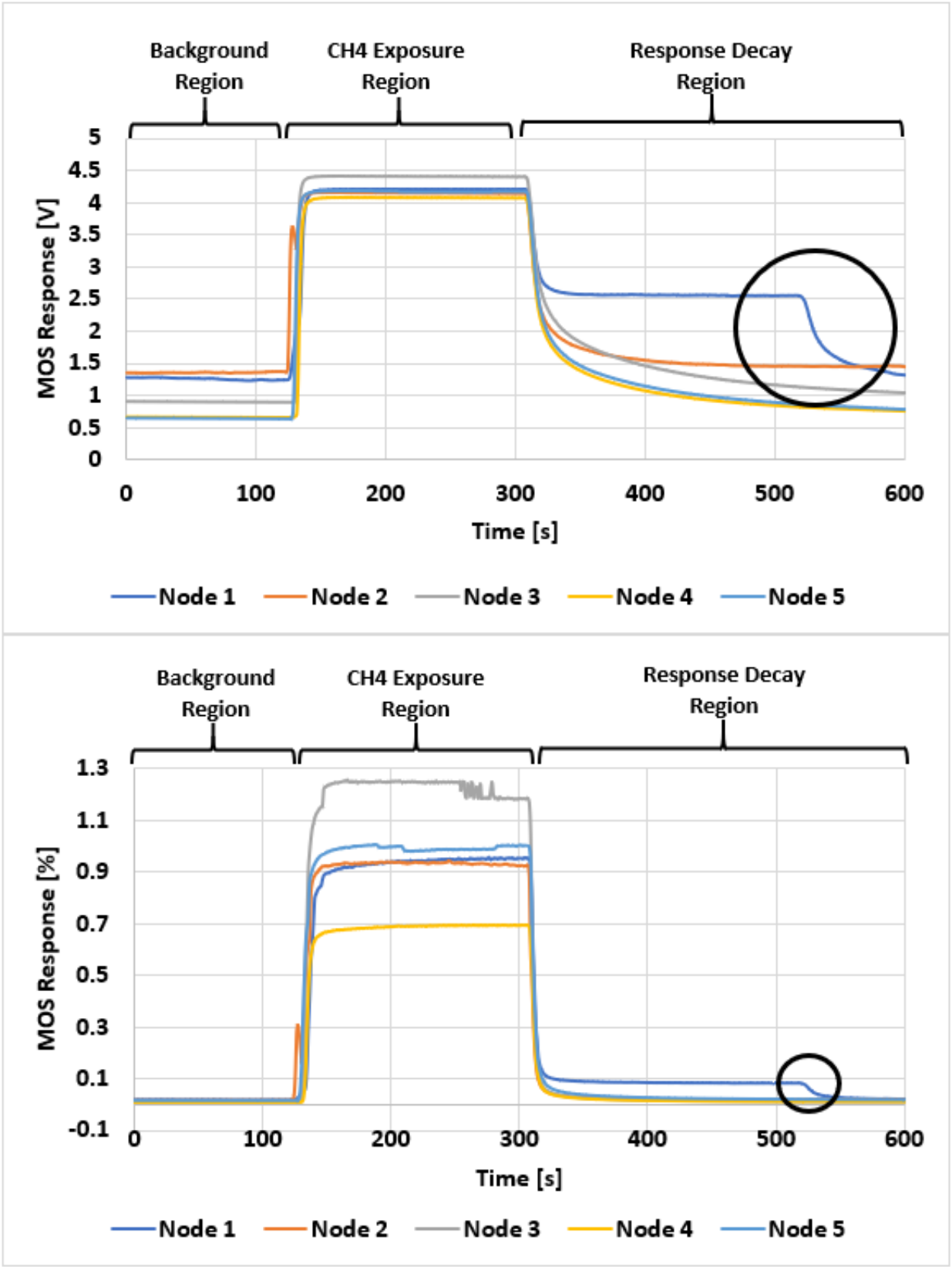

Figure 4.5.16: Example of MOS response for sampling locations 1-5 using method 1.

The rise times for Method 1 were greater than those of Method 2 for both the MOS and IRS, as shown in Table 4.5.2. However, the response times of Method 2 were aligned with those of current sensors used in mining applications as presented in literature.

Table 4.5.2: Rise and decay times for both methods and the difference between them.

	Method 1		**Method 2**		**Differences**	
	MOS	**IRS**	**MOS**	**IRS**	**MOS**	**IRS**
Rise Time [s]	13.75	32.25	9	28.25	4.75	4
Decay Time [s]	239.5	21	129.3	22.25	110.3	-1.25

We determined that the greater rise times for Method 1 were due to the diffusion or leaking of the CH_4 concentrated gas from the CH_4 supply tubing that led to each sampling location; if this occurred, CH_4 was not immediately supplied to the filter at the sampling location at the start time, as previously assumed. This meant that when the test started and the CH_4 supply was turned on, the CH_4 concentrated sample travelled through a portion, if not all, of the 19.8 m (65 ft) of tubing before reaching the filter at the sampling location, which then increased the rise time. Method 2 eliminated this issue because the CH_4 supply tube that extends from the MFC to the filter at the sampling location is only 0.3 m (1 ft) as opposed to 19.8 m (65 ft).

We also believed that the diffusion of the CH_4 concentrated gas from the tube after the supply was turned off, in Method 1, was the reason the decay time for the MOS was higher for Method 1 than for Method 2. If the CH_4 slowly diffused from the end of the supply tube, the sample would still contain trace amounts of CH_4 that the MOS detected. It appeared that the differences in the two methods had little to no effect on the decay time for the IRS, which supported this hypothesis. This was most likely because the amount of CH_4 in the sample after the supply had been turned off (the amount due to diffusion) was at the lower end of the IRS detection range, unlike the MOS. If we assumed that the highest CH_4 concentration that was sampled after the stop time was 0.09%, like for sampling location 1 in Figure 4.5.16, this concentration was most likely too low for the IRS sensor to detect.

Tests Conducted Using the FFS

Type 1 and Type 2

Figure 4.5.17 – 4.5.19 show Type 1 tests, while Figure 4.5.20 – 4.5.22 show Type 2 tests. For these tests, a CH_4 concentration of approximately 2% was leaked at a rate of 2832 slpm (100 scfm). The metal oxide sensor (MOS) responses for the Type 2 (two fans) tests were noticeably "smoother" than those of Type 1 (one fan). Note the concentrations in the test section achieved with these types of tests were too low for the IRS's to respond. Figure 4.5.17 and Figure 4.5.20 show the MOS responses over the duration of the tests. Figure 4.5.18 and Figure 4.5.21 show a zoomed in portion of the respective test to show the sensors' initial responses. It should be noted that, for better visualization of the response order, all MOS raw responses have each been offset to show approximately zero when background data is being collected at the beginning of the test. These figures (easier seen in the zoomed in figures) also show the order in which the sensors responded, note that the leak was set nearest node 1 and aimed downstream. For Type 2 tests, the sensors seemed to consistently respond in order from node 1 to 10 (this order is labeled with numbered circles in Figure 4.5.21), while for the Type 1 tests, the order of response is more difficult to

determine. It should be noted that CH_4 was supplied to the face sampling locations for the tests shown in all figures for test Types 1-4.

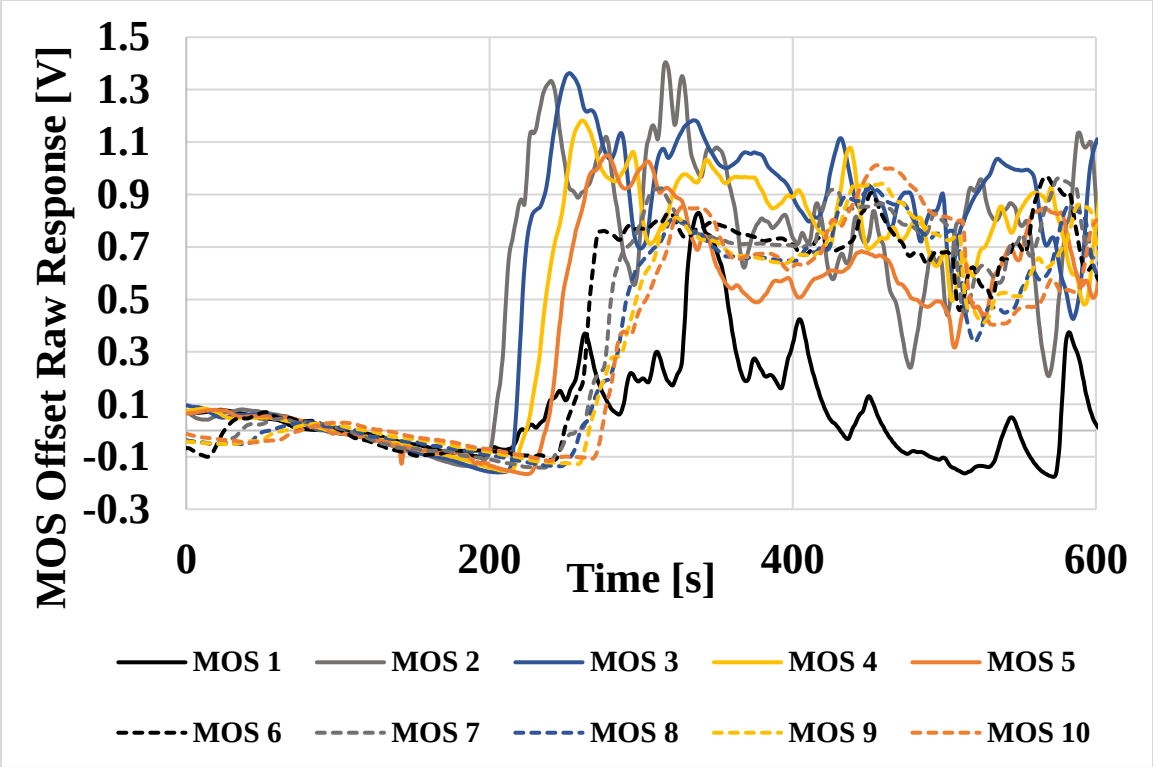

Figure 4.5.17: Type 1 Test - MOS offset raw responses for sampling locations 1-10.

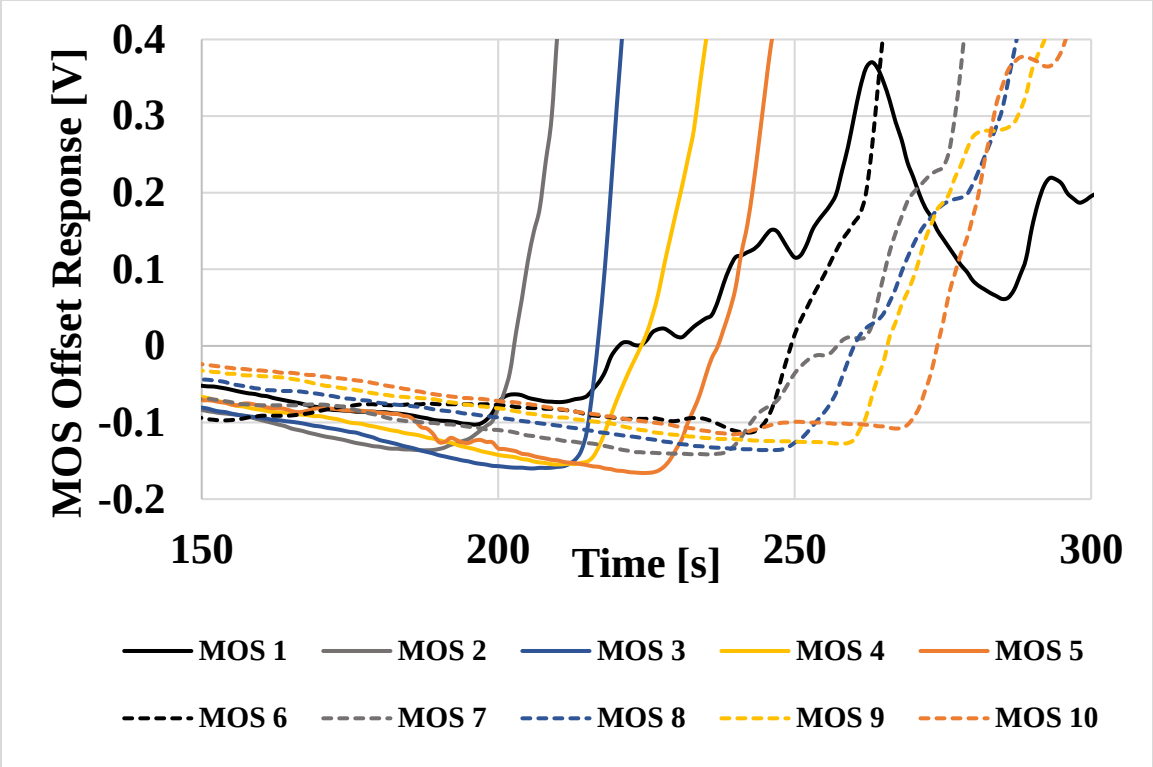

Figure 4.5.18: Type 1 Test – MOS offset raw response zoomed into initial response.

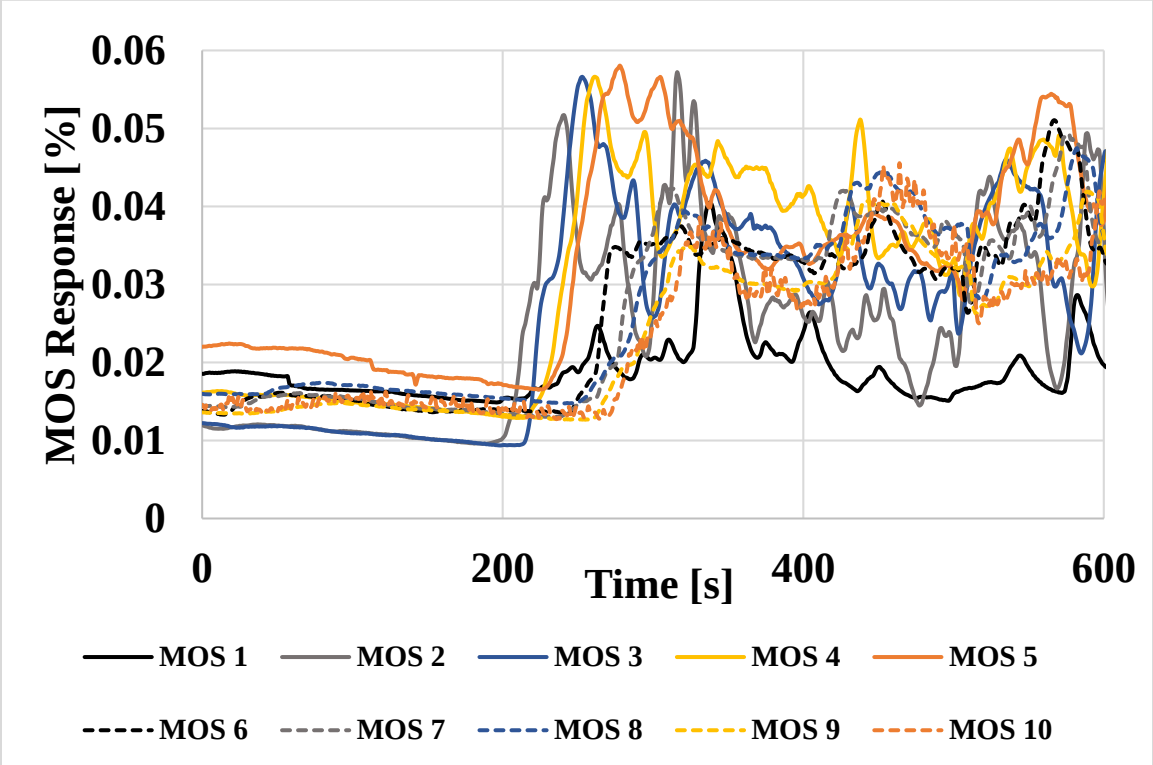

Figure 4.5.19: Type 1 Test – MOS responses for sampling locations 1-10.

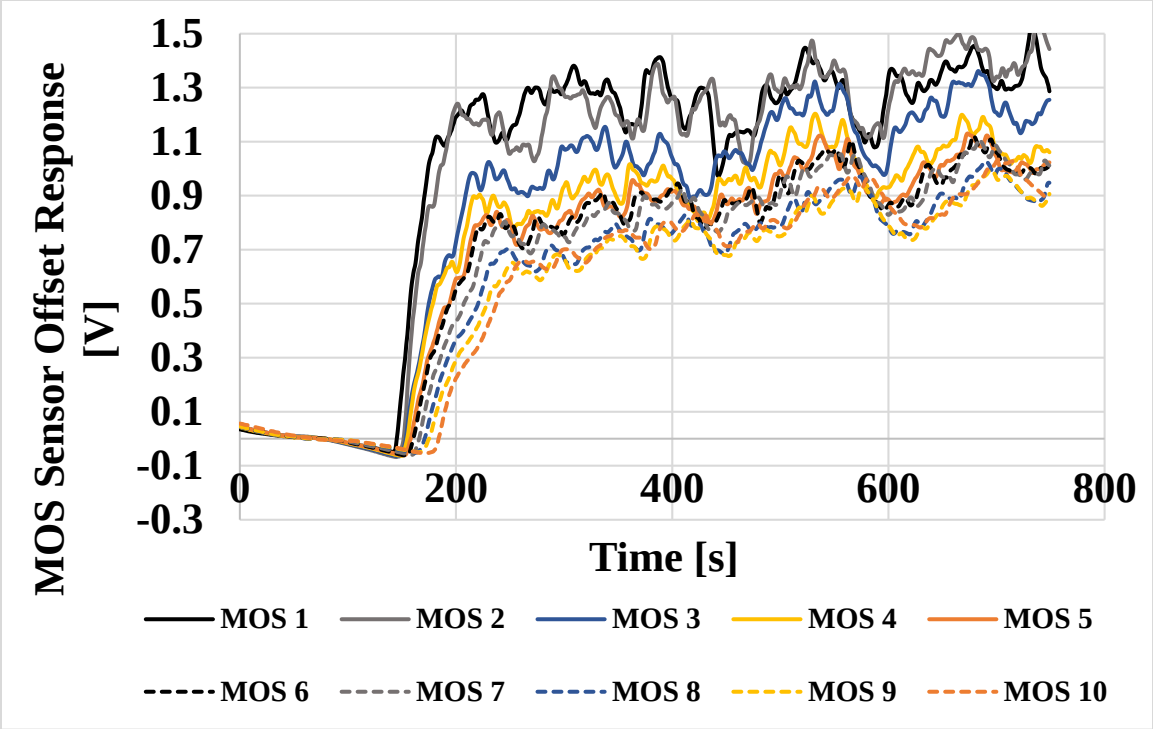

Figure 4.5.20: Type 2 Test – MOS offset raw responses for sampling locations 1-10.

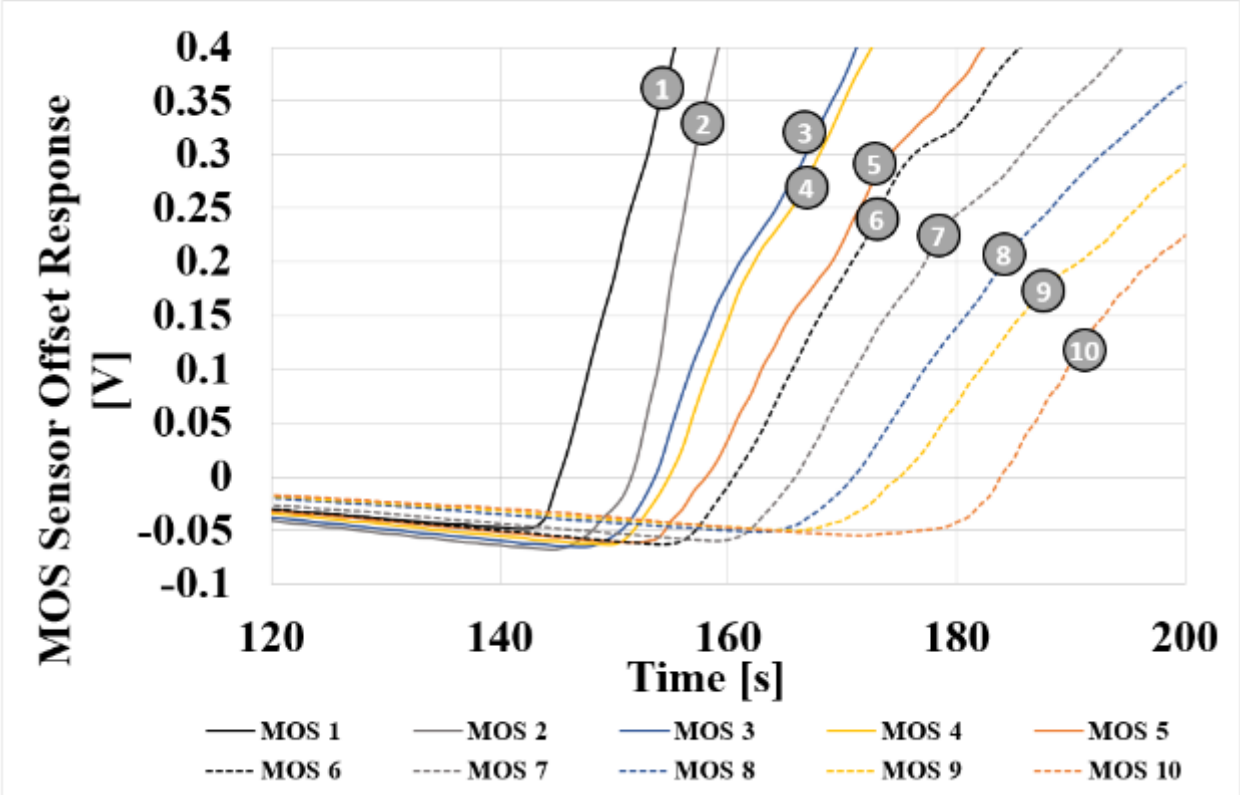

Figure 4.5.21: Type 2 Test – MOS offset raw responses zoomed into initial response.

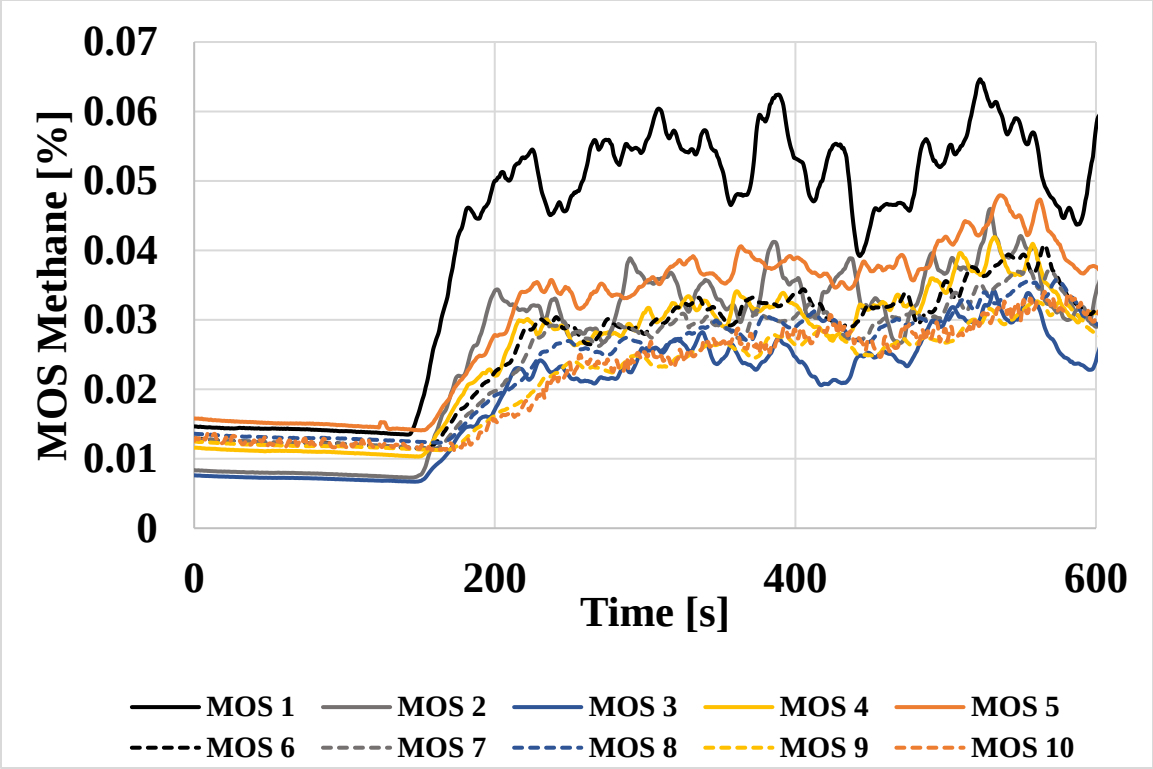

Figure 4.5.22: Type 2 Test – MOS responses for sampling locations 1-10.

The average of each response between 400 and 600 seconds was taken and can be seen in Figure 4.5.23. There appeared to be a general decrease in concentration as the CH_4 leak progressed from node 1 to node 10; this would make sense as the amount of dilution and mixing would increase as the CH_4 moved progressively further away from the leak location.

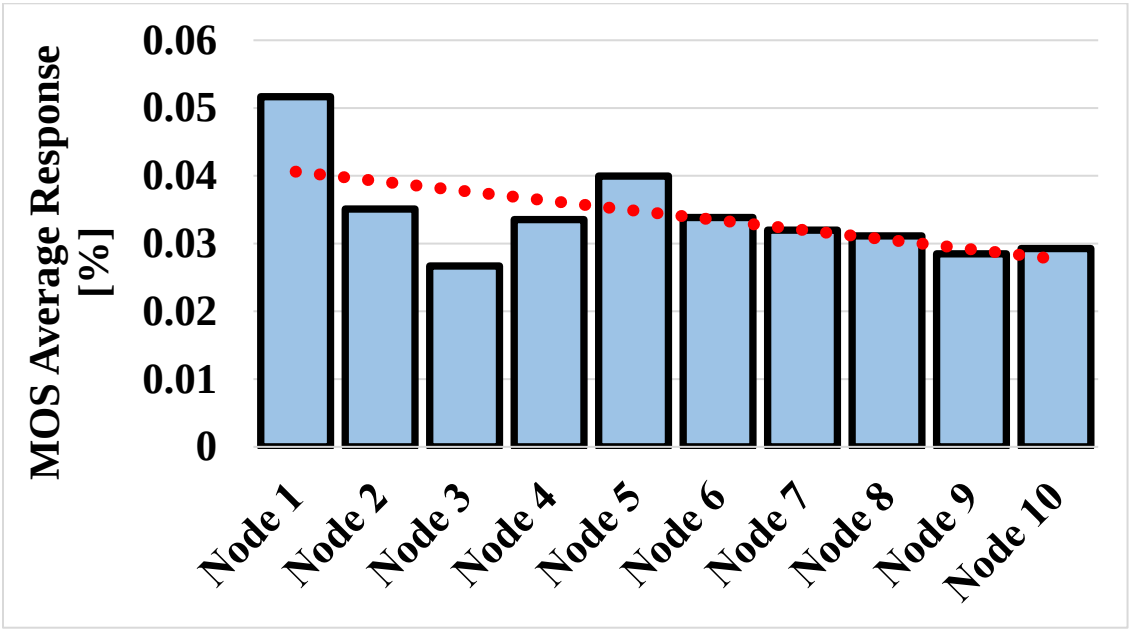

Figure 4.5.23: MOS response averages for nodes 1-10.

Type 3 and Type 4

As previously stated, approximately 2832 slpm (100 scfm) of 2% methane was "leaked" into the mock mine and diffused quickly before reaching the sampling locations. As such, the IRS sensors, which are more responsive and accurate nearer the control set points, did not show clear trends for tests of Type 1 and 2. Therefore, Type 3 and 4 tests were completed to assess both methane sensors. The responses of the IRS and MOS for a Type 3 test can be seen in Figure 4.5.24 and Figure 4.5.25, respectively. To analyze the responses of the IRS and MOS, 20 second averages were taken at the peak response of each sensor; peak responses can be seen in Table 4.5.3 along with the percent difference between them. The percent difference values are highlighted with green, yellow, and red; where green represents a percent difference lower than 10% ("good"), yellow represents a percent difference between 10% and 20%, and red represents a percent difference above 20% ("bad"). Out of the ten sampling nodes, seven were green, two were yellow, and only one was red. It should be noted that due to the shorter response times of the MOS, there was more fluctuation in concentration at the peaks than for the IRS; they are able to respond quicker to the inconsistencies of the CH_4 concentration of the sample

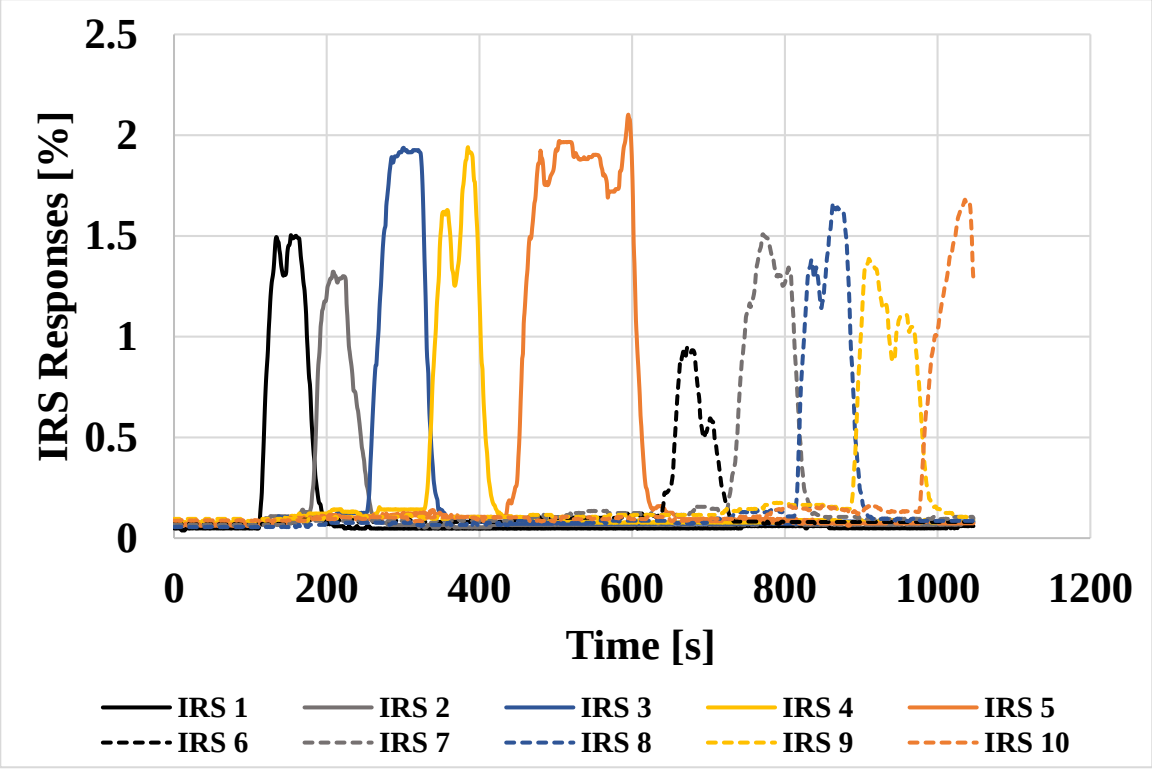

Figure 4.5.24: Type 3 test - IRS responses for sampling locations 1-10.

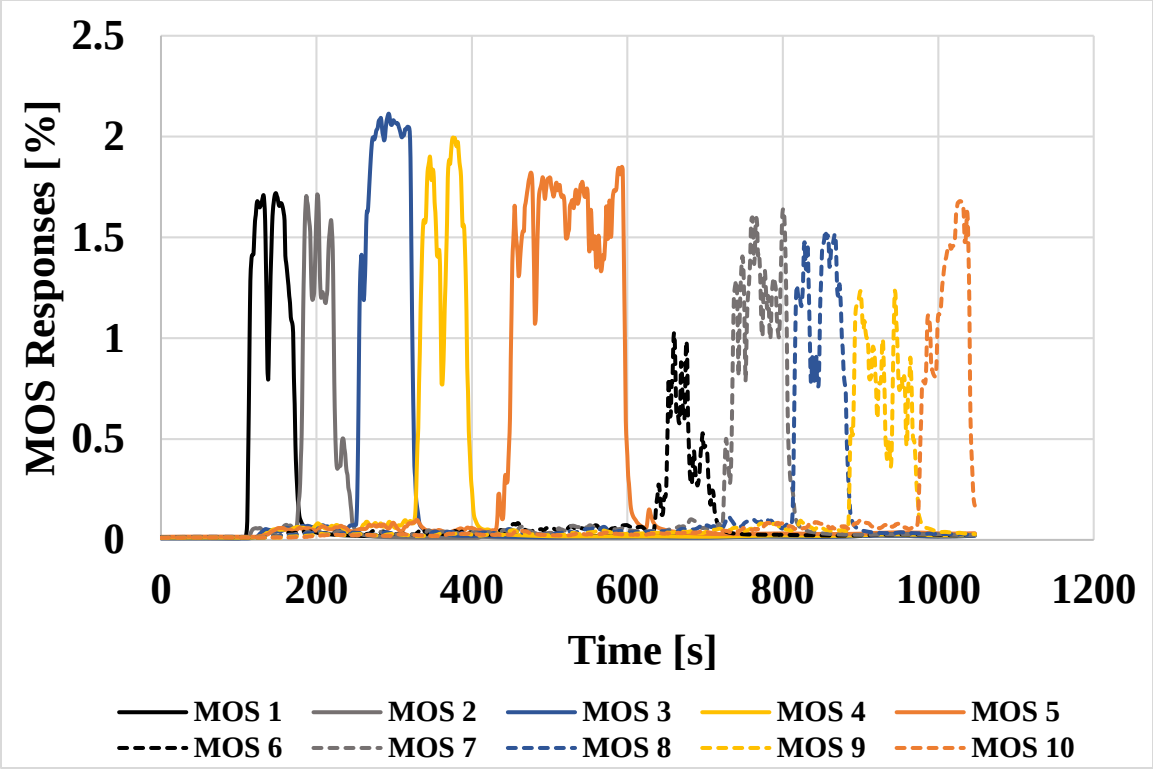

Figure 4.5.25: Type 3 test - MOS responses for Sampling Locations 1-10.

Table 4.5.3: Type 3 Test - Percent difference between peak responses (20 s averages) of MOS and IRS.

Sampling Node #	Average Response		Percent Difference
	MOS	IRS	
	[ppm]	[ppm]	[%]
1	15,008	14,064	-6.49
2	13,626	12,672	-7.25
3	20,629	19,108	-7.66
4	14,889	14,357	-3.64
5	17,466	19,441	10.70
6	7696	8536	10.35
7	13,115	14,464	9.78
8	14,135	14,280	1.02
9	10,188	12,518	20.52
10	14,901	16,190	8.30

In further analyses of these results, we attempted to determine why node 9 had a relatively high percent difference. We examined covariance with other variables such as RH, temperature, and pressure but found none. Another factor taken into consideration was the greater response time for the IRS; if this were the issue, it would be expected that the IRS measurement would be lower than

that of the MOS. However, this was not the case, the MOS measurement was lower. Therefore, it was believed that the high percent difference was due to issues either with the MOS sensor itself.

Figure 4.5.26 and Figure 4.5.27 show the responses of the IRS and MOS for a Type 4 test. The peak response values were calculated, see Table 4.5.4. The responses for the MOS were generally higher than for the IRS. This was most likely due to the shorter response times for the MOS; the IRS may not respond quick enough to see the full concentration of the sample before the CH_4 supply source has moved past the sampling location. Note, we address this issue of signal response from delay and diffusion in the future research section.

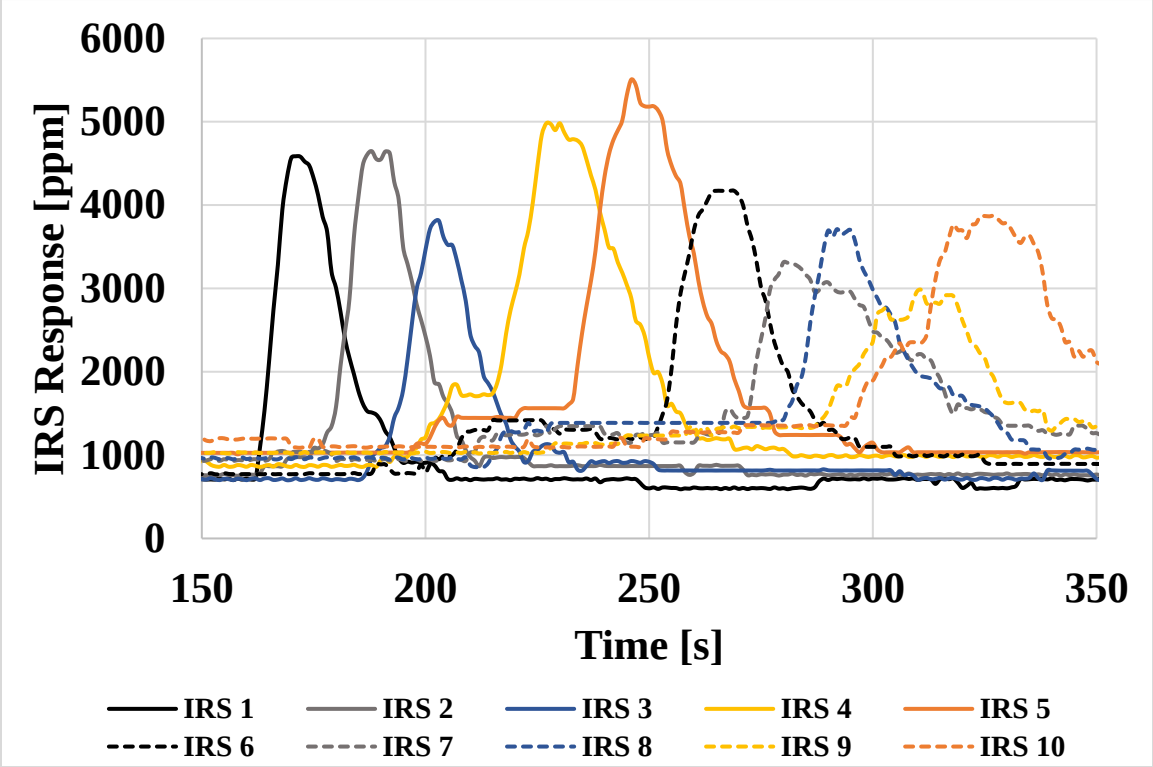

Figure 4.5.26: Type 4 test - IRS responses for sampling locations 1-10.

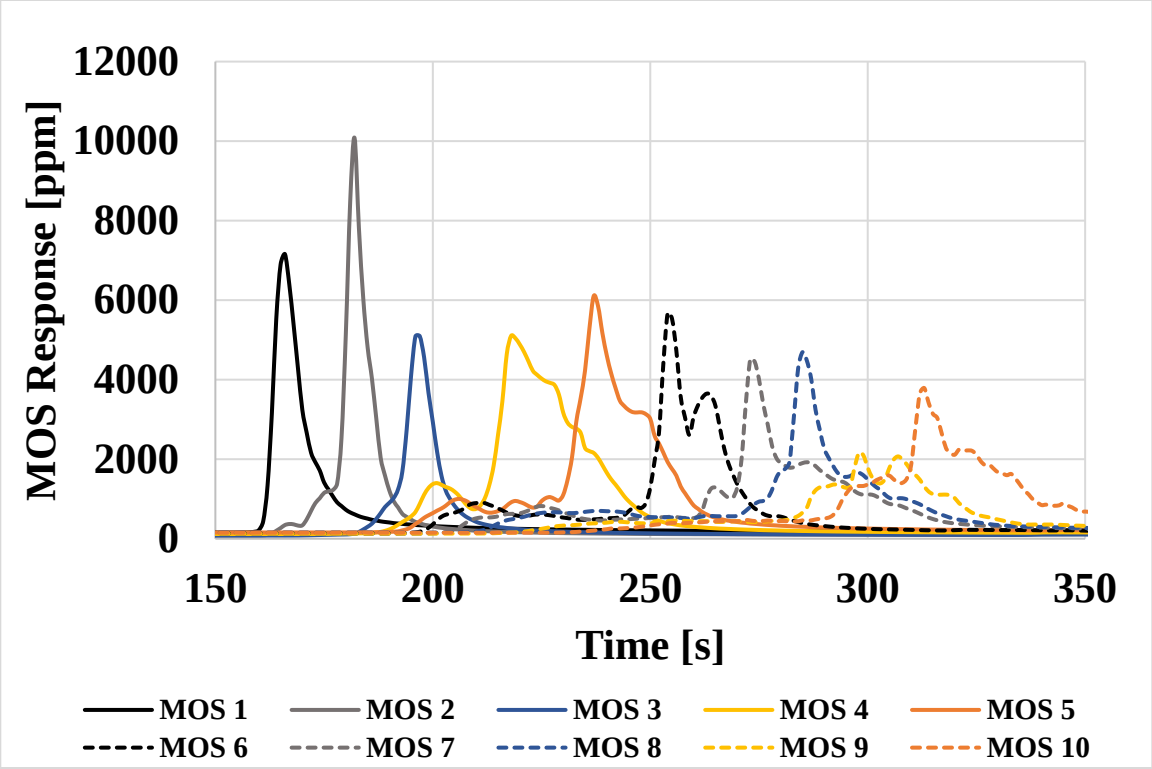

Figure 4.5.27: Type 4 test - MOS responses for sampling locations 1-10.

Table 4.5.4: Type 4 Test - Peak responses of MOS and IRS.

	Peak Response	
Sampling Node #	**MOS [ppm]**	**IRS [ppm]**
1	7157	4586
2	10,083	4647
3	5094	3812
4	5102	4983
5	6106	5506
6	5668	4172
7	4515	3312
8	4691	3712
9	2161	2973
10	3790	3870

Alarm/Relay Control

Figure 4.5.28 shows the results of the alarm tests. When each sensor responded above and then dropped below the threshold of 1% methane, the relay was turned on and off, respectively. The shaded region on the plot represents the time where the relay was turned on. It should be noted that there was a connection issue with node 8 that was resolved for subsequent tests.

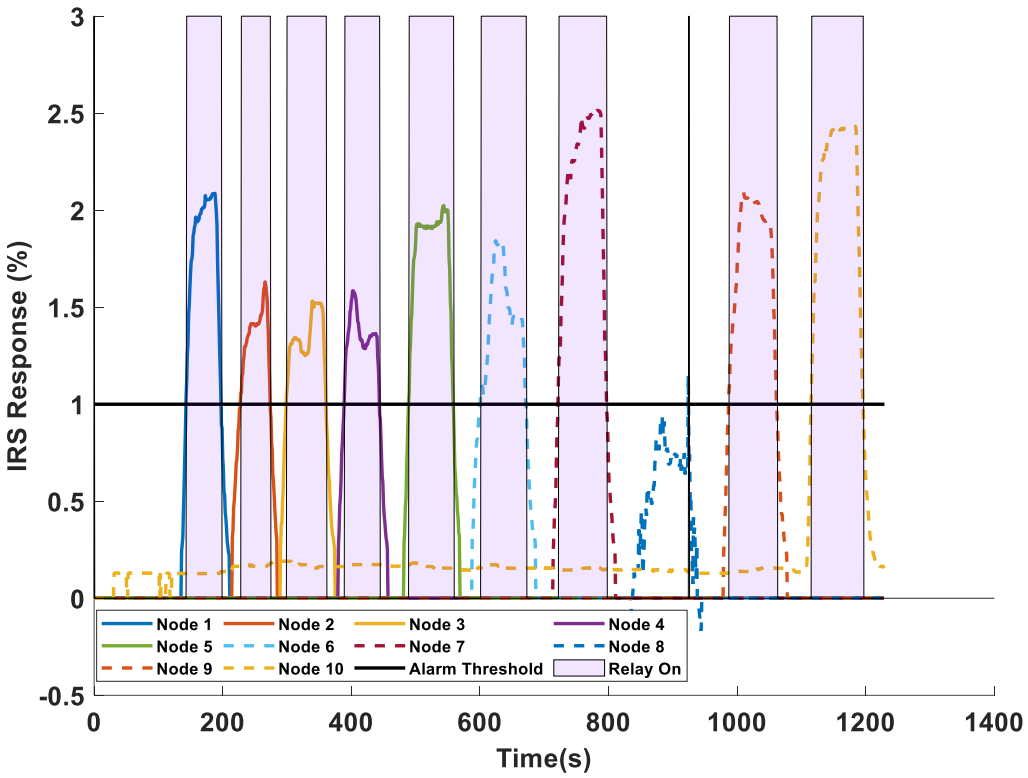

Figure 4.5.28: Visualization of relay control.

System Characterization Summary

Overall, deploying and testing the MWS in the mock mine was successful. While certain testing conditions were not ideal to accurately represent a longwall mine, such as wind speed and dust loading, conclusions of the operating abilities of the system were made. Testing in the mock mine confirmed the limits and capabilities of the two CH_4 sensors (MOS and IRS) and why it was beneficial to employ both types in the system. The rise/decay time testing along with the testing utilizing the FFS confirmed the limitations of the IRS like its long response time, compared the MOS and its inability to detect CH_4 concentrations less then approximately 0.1%. Even though the IRS have these limitations, they were crucial for the MWS since they were more accurate at the methane concentration used for control. The IRS were also less impacted by sample conditions such as RH and temperature, which are major variables in a longwall mine. Although the MOS had lower accuracy, their short response times were beneficial to the system for rapid identification of low concentration changes. We believe that higher accuracy could be achieved for the MOS if they were only calibrated to lower CH_4 concentrations. Since the MOS were designed for CH_4 concentrations up to 1%, higher accuracy could be achieved if calibrations were made only up to this limit; there was greater resolution in the sensor response under 1%. The MOS could also, solely, be used to compensate for the lower detection limit of the IRS and be calibrated only up to that limit (about 0.1%); correction factors for RH, temperature, and pressure could also be made based on the lower calibration range to further improve accuracy. This would provide a larger response range of the overall system. Future research should expand on these possibilities.

4.6 System Modeling

We developed basic 1-D and 3-D models to evaluate a limited number of scenarios that could occur during production in a longwall coal mine. These models allowed us to define various parameters using available literature so that events that may lead to halted production or accidents were examined. A major portion of future research focuses on using a version of the prototype MWS as a method to control system variables such as ventilation rate or shearer speed. Our initial models can be further refined and serve as a tool leading to a safer and more productive environment and second-generation continuous monitoring system. A system such as this will also alleviate the burden and limitations of the routine hand checks while increasing accuracy of measurements.

A 1-D model was developed to simulate various methane fluxes (emissions sources) along the longwall to better understand methane concentration development and interaction with production. Because methane checks are only periodically conducted over the course of a regular shift, we hypothesized that elevated levels of methane that go unnoticed could contribute to mine disasters. If these accumulations occur in-between routine hand checks, the shearer may progress into an unexpected highly concentrated area and operate here during the shearer sensor response time (10-30 seconds). Such a scenario would cause a shutdown at best or an accident at worst. The model presented here aimed to generate these scenarios and we assessed the capabilities of the MWS. These initial insights also allowed us to gain an understanding of future research that would enable mitigation of such scenarios.

Background Emissions

Methane can enter the longwall from a number of sources. Though methane was known to reside in the previous workings or the gob, it was also instantaneously released from the face as a result of shearing and fracturing the coal. The model's first source accounted for the naturally occurring methane flux from the exposed coal face. At first, the shearer and production were neglected, and a methane profile was generated as a function of ventilation rate and the naturally occurring flux of methane along the entire long wall face. A baseline methane emission rate of 0.02 m^3/s (50 cfm) was reported in a previous study [11]. This value was reported prior to the start of production; therefore, it was assumed to be the result of only flux from the exposed coal face. The baseline emission rate was then divided by the exposed surface area of coal along the longwall to obtain the methane flux rate. The surface area was defined by the number of shields and an average face height. This source served to create a background or baseline concentration prior to production. The length of the longwall was defined as 300 m (984 ft) with a constant ventilation rate of 21.2 m^3/s (45,000 cfm). These values were obtained from average data observed in literature and Table 4.6.1 presents the summaries. An example of a resultant profile from a constant ventilation and methane emission rate can be seen in Figure 4.6.1.

Table 4.6.1: Table of values assumed for modeling and simulation [10], [11], [12].

Parameter	Value
Ventilation Rate	21.2 m^3/s (45,000 cfm)
CH_4 Emission Rate	0.02 m^3/s (50 cfm)
Shearer Velocity (Production Rate)	0.28 fps (0.0838 m/s)
Longwall Length	300 m (984 ft)
Longwall Width	4.9 m (16 ft)
Longwall Height	1.8 m (5.9 ft)
Shield Width	1.7 m (5.74 ft)

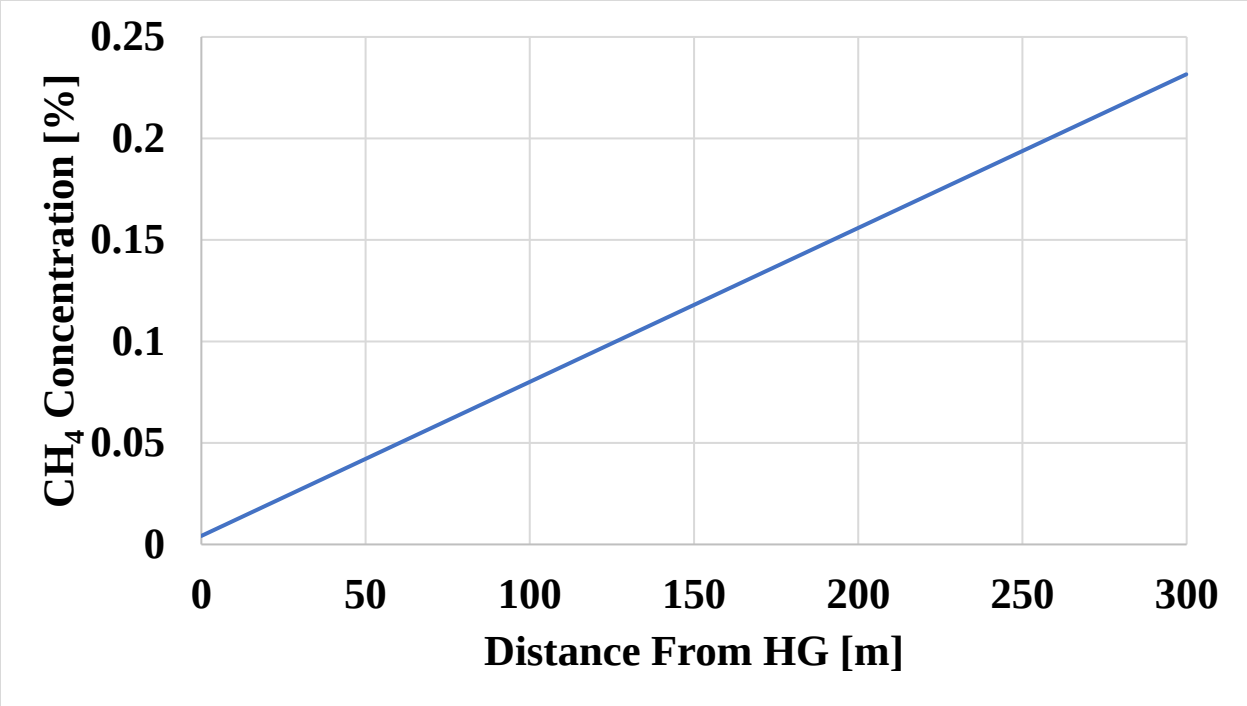

Figure 4.6.1: Methane concentration profile along the longwall due to a constant flux derived from a baseline emission rate of 0.0236 m^3/s (50 cfm).

A previous study in the Pittsburgh Coalbed deployed three methane sensors to measure methane along the face during production. The sensors were evenly spaced, along a 315 m (1032 ft) longwall face with an average coal thickness of 2.2 m (7.2 ft) [10]. Data were collected for both HG to TG and TG to HG passes and were averaged over the day. Single pass data were plotted, and a linear regression was used to obtain a predictive model equation. This equation was used to reconstruct the data and plot the results as a function of percent CH_4. The ventilation rate in their study was reported as 23.6 m^3/s (50,000 cfm). Figure 4.6.2 depicts the reconstructed plot containing the new equation.

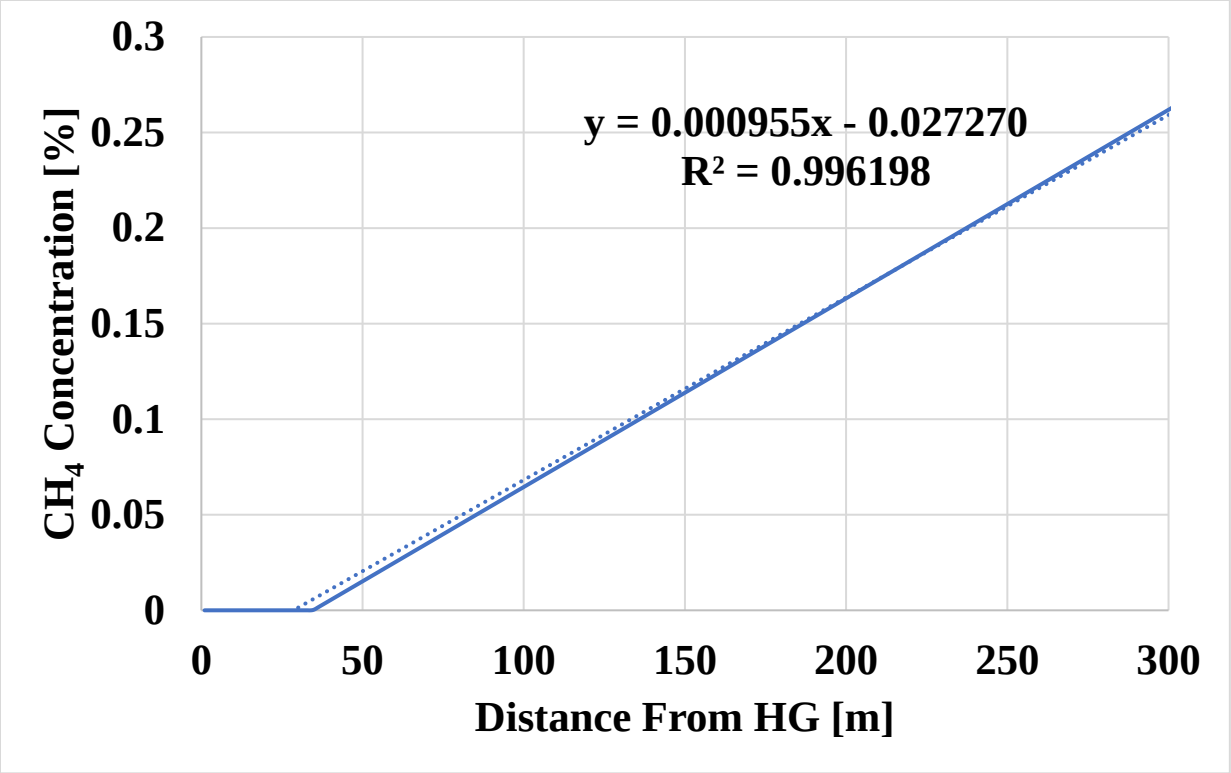

Figure 4.6.2: Single pass methane emission profile collected from Pittsburgh Coalbed in percent methane [10].

The numerically obtained results were formed from an ideal scenario. Methane emissions increased linearly with distance from the HG as a result of constant ventilation (major assumption) and flux rates. It was believed that differences in ventilation rates and the addition of production from the experimentally collected results that the emissions appeared to be higher.

Influence of Shearer and Ventilation Rate on Downwind Methane Concentrations

Exceeding regulated methane emissions within the longwall may be a result of increased production rates. To assess the relationship between the coal production and methane emissions, an analysis was conducted with varying production rates to calculate expected downwind methane concentrations. If a correlation existed, and a downwind concentration were predicted from the shearers current operational rate (production rate), then there may be an optimal production rate that guarantees methane emissions never exceed regulatory limits. The methane concentration downwind at any given moment and location was a function of both the background emissions and the methane released from the production of coal. The following analysis was completed to assess the correlation of production rate to methane emissions.

The formulation of emissions due to production rate was based on the following:

- A volumetric methane content per square foot of coal cut was assumed to be 0.0152 $m^3/s/m^2$ (3 cfm/ft^2).
- Height of cut by shearer is equal to 1.8 m (6 ft); average longwall height used in prior work.
- Constant ventilation rate of 21.24 m^3/s (45,000 cfm).
- Background emissions at a desired location were acquired from the previous analysis.

All rates were converted to seconds in the following calculations to simplify analysis and presentation (Eq. 4.6.1). An average constant shearer rate of 0.0838 m/s (0.275 fps) was first used to obtain an expected emission profile from normal production data [11]. To arrive at an instantaneous emission rate that was a function of production, a unit area of coal produced each second was derived from the shearer rate. This area was derived from (Eq. 4.6.2 and 4.6.3), using the height of cut and a length equal to the integration of shearer velocity. The volumetric methane content of 0.02 $m^3/s/m^2$ (3 cfm/ft^2) was then multiplied by the derived area in (Eq. 4.6.4) to produce a methane emission rate (cfs). A resulting concentration was created in (Eq. 4.6.5) from the ratio of methane emissions to the ventilation at that time. The procedure mentioned here can be further explained in the example calculation found below.

$$Volumetric\ Methane\ Content\ of\ Coal = 3\,\frac{cfm}{ft^2} * \left(\frac{1\,min}{60\,sec}\right) = 0.05\,\frac{cfs}{ft^2} \quad \textbf{Eq. 4.6.1}$$

$$\Delta x = \int_0^1 V_{shearer}\,dx = \int_0^1 0.275\,dx = 0.275\,ft \quad \textbf{Eq. 4.6.2}$$

$$Area\ of\ coal\ cut\ per\ second = h * \Delta x = 6 * 0.275 = 1.65\,ft^2 \quad \textbf{Eq. 4.6.3}$$

$$Methane\ Emitted = Volumetric\ Methane\ Content\ of\ Coal * Area\ per\ second = 0.05 * 1.65 = 0.0825\,cfs \quad \textbf{Eq. 4.6.4}$$

$$\%\ Methane = \frac{Methane\ Emitted}{Ventilation} = \frac{0.0825}{750} = 0.011\% \quad \textbf{Eq. 4.6.5}$$

The resulting methane concentration derived from the example above represented the methane concentration produced from shearing coal per unite time. If the shearer moved at a constant rate, then the resulting concentration would be the same for every second in time. Furthermore, the concentration due to production would be the same at any location downwind of the shearer, since in this basic model the methane emitted from production was added to the background emissions and ventilation flow remained constant.

Methane emissions that were a result of cutting coal were first assessed at the TG, where background emissions were typically at their highest. Studies noted, “Production delays due to increasing methane concentrations were most common when the shearer was near the TG” [20]. This trend was also confirmed in the multi-dimensional models presented later. The MWS would enable continuously monitoring at the TG and ensure that downwind emissions never exceeded 1%, which should enable production to proceed without interruption anywhere in the longwall. After computing the expected emissions from an average production rate of 0.08 m/s (0.275 fps), it was noted that the resulting concentration yielded only a small increase compared to the baseline methane flux. In other words, the concentration profile along the face tended to be dominated by the background/baseline flux and the fixed ventilation rate. Table 4.6.2 and Figure 4.6.3 present the expected methane concentrations at various production rates with a fixed ventilation rate of 2.4 m/s (7.80 fps) for ten locations along the mine. The background concentrations that were expected at each of the ten nodes were also reported. Finally, the total resulting concentration containing

both background and shearer emissions were shown. It should be noted that the results shown here do not account for a time varying release of methane from the freshly cut coal. Furthermore, the continued emission contributions as the coal is transported along the face on the conveyor belt are not accounted for. This could likely be a significant contributor that requires additional attention. Further research should estimate the impact these additional roles play on downwind concentrations.

Table 4.6.2: Effects of production rates on methane concentrations along the longwall. Resulting concentrations contain both background and newly formed methane as a result of production.

Node #	Distance from HG	Background CH_4 Concentration	CH_4 Concentration [%]				
			Shearer Velocity (Production Rate)				
	m (ft)	[%]	0.01 m/s (0.03 fps)	0.05 m/s (0.16 fps)	0.1 m/s (0.33 fps)	0.3 m/s (0.98 fps)	0.5 m/s (1.64 fps)
1	30 (98.4)	0.027	0.028	0.033	0.04	0.065	0.091
2	60 (196.9)	0.05	0.051	0.056	0.063	0.088	0.114
3	90 (295.3)	0.072	0.074	0.079	0.085	0.111	0.137
4	120 (393.7)	0.095	0.097	0.102	0.108	0.134	0.159
5	150 (492.1)	0.118	0.119	0.124	0.131	0.156	0.182
6	180 (590.6)	0.141	0.142	0.147	0.154	0.179	0.205
7	210 (689.0)	0.163	0.165	0.17	0.176	0.202	0.228
8	240 (787.4)	0.186	0.188	0.193	0.199	0.225	0.25
9	270 (885.8)	0.209	0.21	0.215	0.222	0.247	0.273
10	300 (984.3)	0.232	0.233	0.238	0.244	0.27	0.296

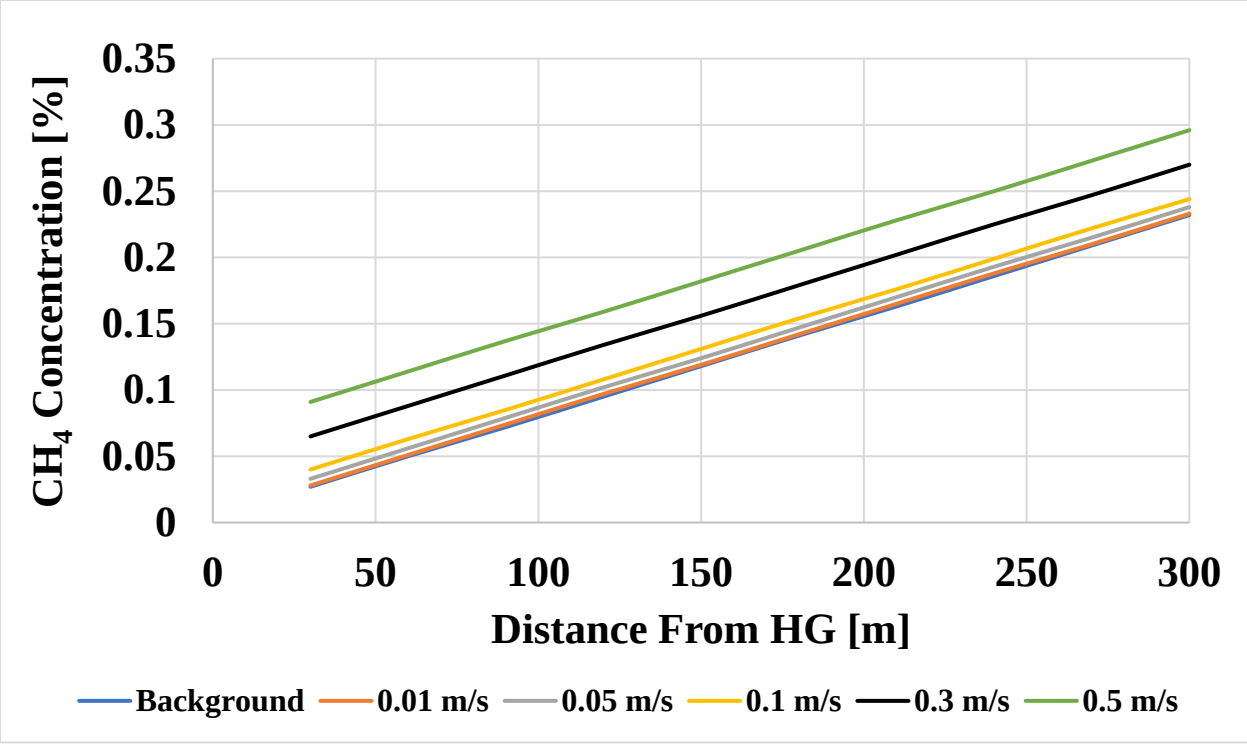

Figure 4.6.3: Graphical plot of data from Table 4.6.2. Fixed average ventilation rate with various shearer rates.

In addition, we initially modeled the impacts of ventilation rate. The ventilation rate dominated the background concentration profile, which we showed to be much larger than the methane release as a result of cutting coal as you approach the TG (based on limited available literature). Since the natural flux was constant over the entire surface area of exposed coal, any fluctuation in ventilation rate will directly influence the downwind concentrations. To assess the influence of ventilation rate on background methane concentrations, a similar analysis was completed that varied ventilation rates while excluding the dependence of production rates. Table 4.6.3 and Figure 4.6.4 present the results. The slopes of the lines in Figure 4.6.4 represent the increased methane concentrations that were present at nodes across the longwall face. This slope and its derivatives over time could serve to provide valuable insight to improve longwall safety by predicting future emissions well before any regulatory or safety threshold. As a result, continuous monitoring of ventilation rate coupled with production may be crucial to predicting an event and optimizing control.

Table 4.6.3: Effects of ventilation rates on methane concentrations along the longwall (no production).

Node #	Location	CH_4 Concentration [%]				
		Ventilation Rate				
	m (ft)	0.5 m/s (1.6 fps)	1 m/s (3.3 fps)	2 m/s (6.6 fps)	3 m/s (9.8 fps)	4 m/s (13.1 fps)
1	30 (98.4)	0.535	0.139	0.037	0.018	0.011
2	60 (196.9)	1.047	0.268	0.069	0.032	0.019
3	90 (295.3)	1.556	0.396	0.102	0.046	0.027
4	120 (393.7)	2.063	0.525	0.134	0.061	0.035
5	150 (492.1)	2.567	0.653	0.166	0.075	0.043
6	180 (590.6)	3.068	0.781	0.198	0.089	0.051
7	210 (689.0)	3.567	0.909	0.230	0.104	0.059
8	240 (787.4)	4.063	1.037	0.263	0.118	0.067
9	270 (885.8)	4.557	1.164	0.295	0.132	0.075
10	300 (984.3)	5.048	1.292	0.327	0.147	0.083

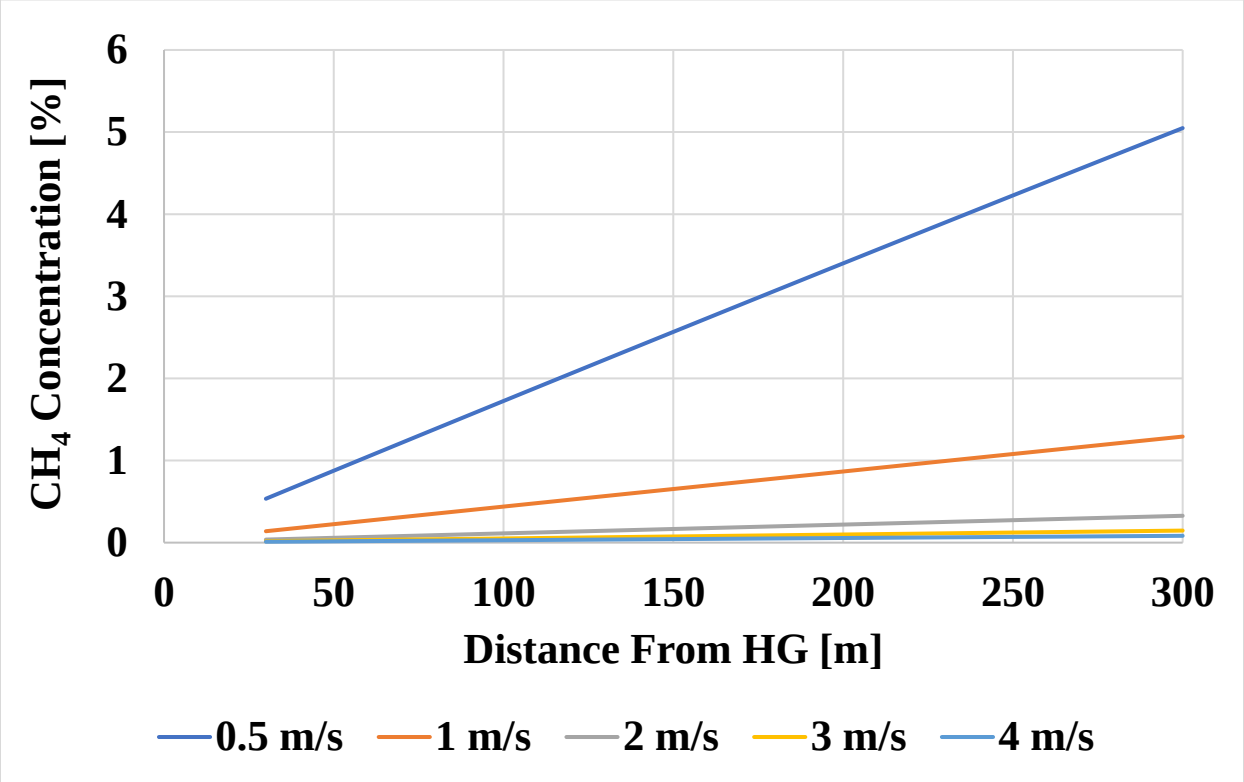

Figure 4.6.4: Graphical representation of data from Table 4.6.3. Impact of varying ventilation rate on methane concentrations.

Our first model assumed that the cross-sectional area and ventilation flow rate were constant from the HG to the TG. However, literature has shown the ventilation velocity near the longwall face

varies over the length of the longwall due to ventilation losses to other areas, like behind the shields in the gob. A plot showing the distribution of ventilation velocities along a longwall face was found in "Investigations of Ventilation Airflow Characteristics on a Longwall Face—A Computational Approach" [2]. It should be noted that in this specific investigation, the longwall length was 200 m (656 ft) and the height was 3.5 m (11.5 ft); the plot was generated from a model which was first verified by field ventilation survey data. A plot digitizer software was then used to obtain data from the figure of this plot, which was provided in the paper. These data were then implemented into the longwall model to calculate the CH_4 concentration at each node over the time it takes the shearer to complete a HG to TG pass at a constant rate.

Figure 4.6.5 shows the results for locations at node 1 and node 10. Near the end of the longwall, about 10-15 m (32.8-49.2 ft) away from the TG, the ventilation velocity dropped dramatically, causing an increase in the CH_4 concentration; this was one reason why areas near the TG were of major concern for CH_4 ignition related accidents. It should also be noted that this model accounted for the time it took for the CH_4 emitted due to production (at the shearer location) to reach the location of interest (nodes 1 and 10 in this case). Note, once the shearer passed a certain location, the CH_4 concentration at that location dropped back to the background concentration. This drop can be seen on the line for node 1 at approximately 70 seconds where the CH_4 concentration instantly drops and remains constant for the duration; at this time, the shearer passed the location of node 1, which was at 30 m (98.4 ft). We note again that our initial basic model assumed instantaneous mixing within each analysis section. Future work, including CFD modeling, should be used to develop mixing and diffusion coefficients.

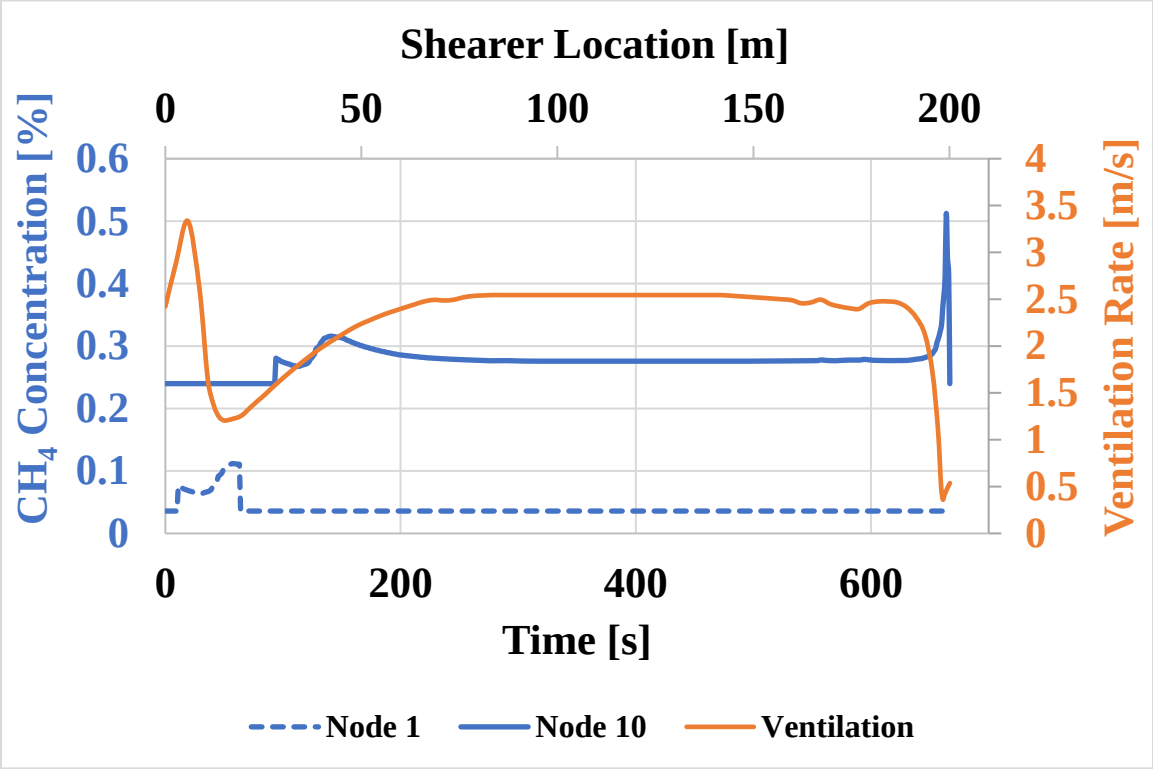

Figure 4.6.5: CH_4 concentrations at Nodes 1 and 10 as the shearer makes a HG-TG pass using ventilation data along the longwall face.

The current design of the MWS consisted of two anemometers, the first on the sampling unit mounted at node 2 and the second at node 9. These would be located near current ventilation check points at the HG and TG of the longwall. The units were actively measuring wind speeds (ventilation rate) at the wind tunnel testing facility where full scale data were collected for the rest of the system. However, ventilation rates were not sufficient in the test section to predict or correlate any relationship between downwind emissions and local velocities. It appears that the continuously monitoring wind speeds function of the MWS while recording air flow patterns along the longwall may have many benefits. The fluctuations in supplied air to the longwall may also help correlate deficiencies or problematic areas throughout the mine that are related to current mining practices within longwall production. Future research should include a cost benefit analysis. Sonic anemometers are very accurate and if cost effective options exist, these should be implemented to account for multi-dimensional velocity measurements. Cup anemometers (as used in the first-generation prototype) or vane/blade anemometers currently used in handheld units could also be implemented. However, we noted that continuous deployment could impact these methods since they contained moving components. Future efforts should assess these issues.

High Emitting Events

Once a background methane concentration profile was obtained, more specific outcomes or events were integrated into the model to further analyze the severity of an event. Methane was known to accumulate near the TG of the longwall, since it was the farthest location from the fresh air source and flow rates may be lost to the permeable gob area. This accumulation of the methane made it a particularly hazardous area to operate the shearer. Furthermore, a high emitting source of methane may occur elsewhere along the longwall; whether it be swept out from the gob, or a fracture that has become exposed from a previous cut. These events will then add to the currently existing background concentration and accelerate the methane plume formation. Such high emitting sources were added into the simulation and a resultant methane profile was generated. The model used here references distance with respect to shield number, where shield 171 represents 300 m (985 ft). Figure 4.6.6 shows a resulting methane concentration profile that is a result of a high emitting event that occurs at shield 107. The constant naturally occurring methane flux before and after the event was defined as the background emission rate from the 0.02 m^3/s (50 cfm).

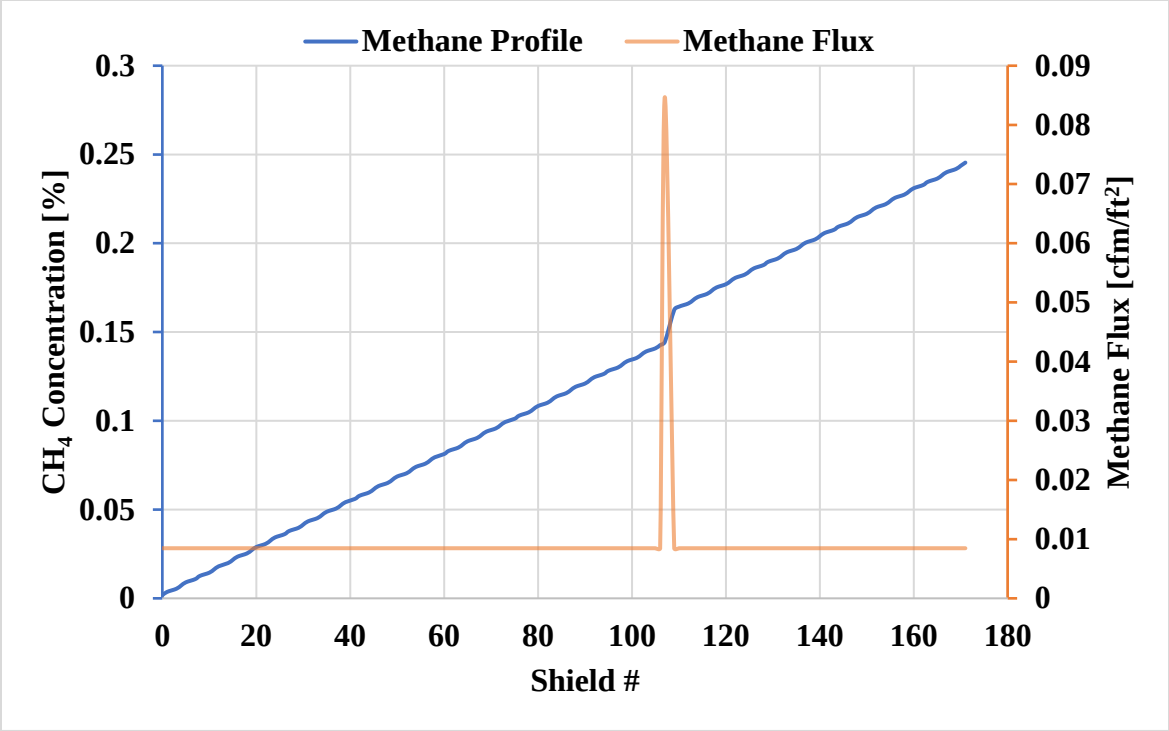

Figure 4.6.6: High emitting event that occurs at shield 107.

Methane and Shearer Interaction

By simultaneously referencing the shearer's location with respect to the fixed nodal network, the methane profiles generated from the specific events mentioned above can be overlaid to show their respective locations. This meant that an exact time and location that an ignition may occur could be predicted and thus prevented. The model contained initial condition features that allowed the shearer's initial location to be selected at any point across the face. This allowed us to evaluate specific time sensitive scenarios that contributed to the effectiveness of the control strategy. A plot of the shearer's location with respect to time is shown in Figure 4.6.7. This simplified approach assumed the shearer was operated at a constant rate of 0.1 m/s (0.275 fps) and turnaround time was neglected at the HG and TG. A more realistic shearer schedule should be developed in the future from literature and new data to better assess the MWS and its methane prediction model.

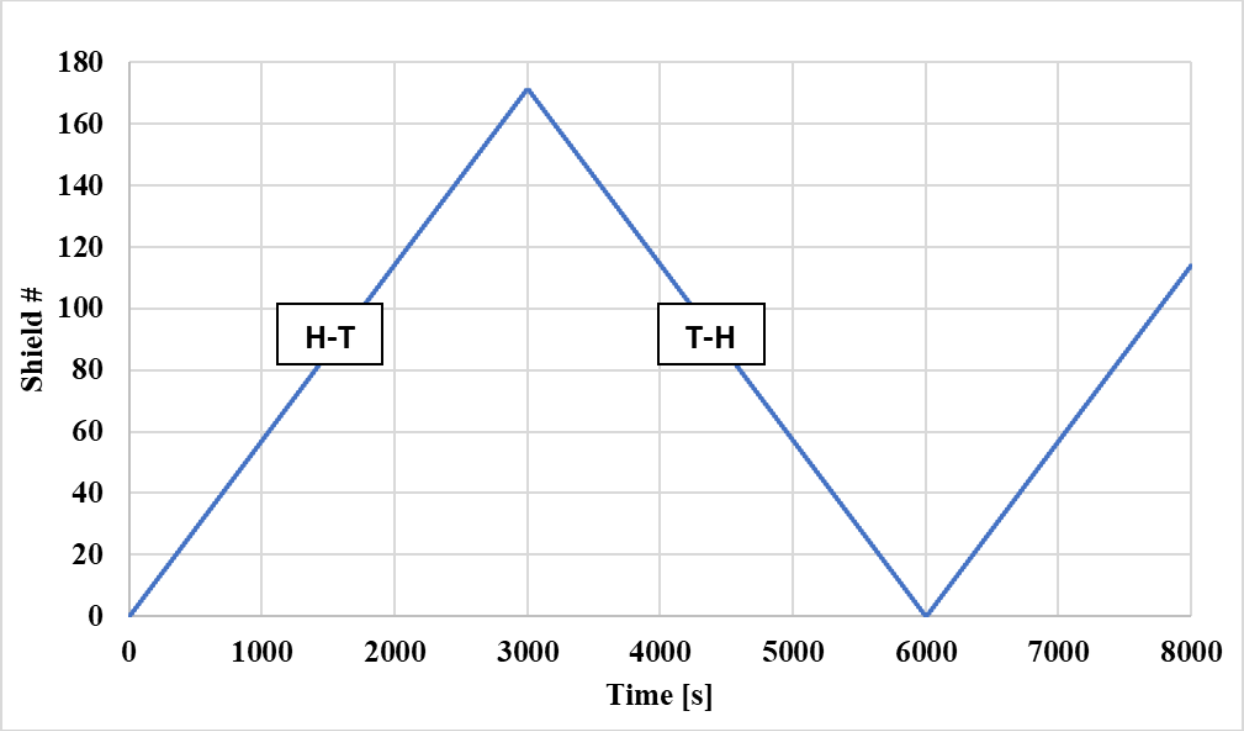

Figure 4.6.7: Shearer tracking with time and respect to shield number in longwall being mined.

With the shearer's location now accounted for, a plume of some high concentration (> 1%) can be combined to predict time and locations of unexpected stoppages as they interacted with the shearer. An analysis was conducted to generate the intersection time and locations from various initial plume and shearer locations throughout the longwall. For this analysis, we assumed that a plume of high concentration methane (>1%) had already developed and then traversed the longwall. A few initial starting locations were selected as well as constant velocities for the shearer and plume. In Case 1 (Table 4.6.4), the plume and shearer moved in the same direction. The plumes initial location was held constant while the shearer was located near each quarter of the longwall length. The final location in the table denotes the distance between two consecutive nodes of the MWS system (30 m (98 ft)). For Case 2 (Table 4.6.5), the shearer and plume moved in the opposite direction. The shearers initial location as kept constant at the TG, as it would begin back towards the HG where the plumes initial location was varied at each quarter of the longwall. The ventilation rate was a constant rate of 2 m/s (6.56 fps) for Cases 1 and 2. Cases 3 and 4 (Tables 4.6.6 and 4.6.7) were initialized exactly the same way as Cases 1 and 2; however, the ventilation rate was reduced to 1 m/s (3.28 fps). An average shearer or production rate was defined as 0.1 m/s (0.275 fps). The longwall length was also fixed at 300 m (985 ft). These constant values were initialized into the model and a few scenarios were evaluated for intersection time and location.

Table 4.6.4: Case 1: Plume and Shearer are moving in same direction (HG-TG).

Shearer's Initial Location [m] / shield #	Plume Initial Location [m] / shield #	Time Elapse [sec]	Location of Intersection [m] / shield #
280 / 160	0 / 1	149	296 H-T / 169
150 / 86	0 / 1	80	158 H-T / 90
75 / 43	0 / 1	41	80 H-T / 46
30 / 17	0 / 1	17	32 H-T / 18

Figure 4.6.8 presents a graphical representation of the data collected from the first scenario in Case 1. The x-axis represents time where the y-axis denotes the position along the longwall. The location of the plume and shearer on the y-axis at T=0 seconds (x-axis) is the initial location at the start of the simulation. For this case, the simulation was terminated when the plume and shearer intersect at T=149 seconds. Figure 4.6.9 is a visual representation of the plume and shearer interaction.

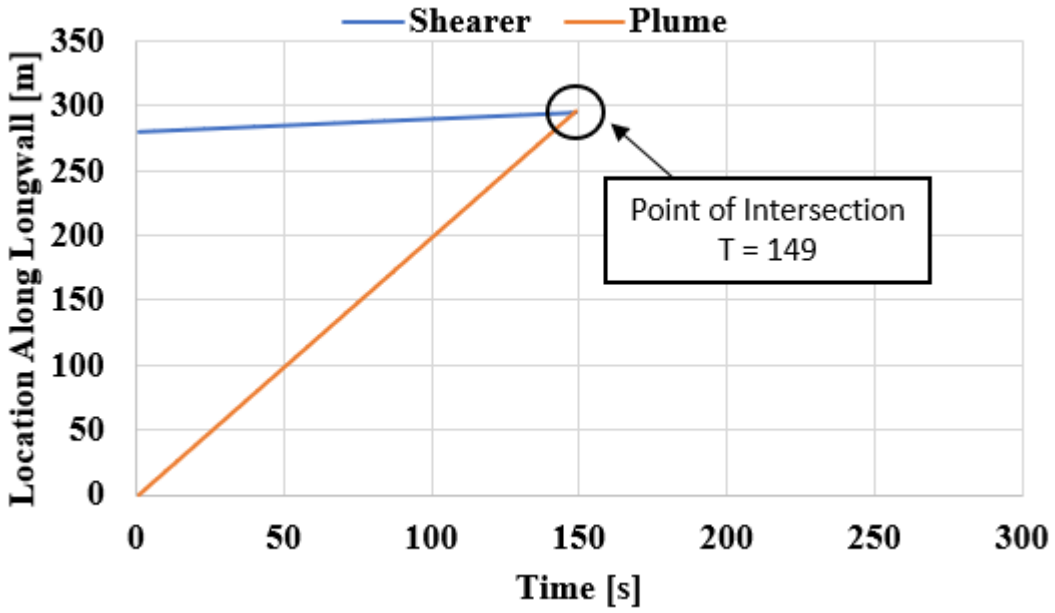

Figure 4.6.8: Shearer and Plume intersection scenario. Shearer rate 0.1 m/s. Plume rate 2 m/s. Shearer initial location: 280 meters HG-TG. Plume initial location: 0 meters HG-TG.

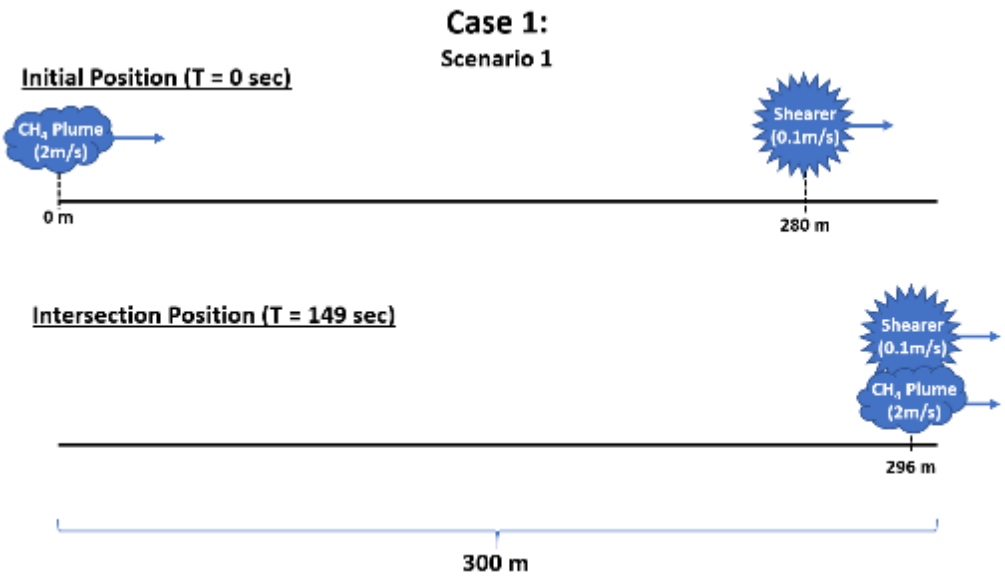

Figure 4.6.9: Visualization of Case 1: Scenario 1.

Table 4.6.5: Case 2: Plume and Shearer are moving towards each other (opposite directions).

Shearer's Initial Location [m]	Plume initial Location [m] / shield #	Time Elapse [sec]	Location of Intersection [m] / shield #
300 / 171	0 / 1	144	286 TG-HG / 163
300 / 171	150 / 86	73	294 TG-HG / 168
300 / 171	225 / 129	37	297 TG-HG / 170
300 / 171	270 / 154	16	300 TG-HG / 171

Table 4.6.6: Case 3: Plume velocity reduced to 1 m/s. Initial locations same as Case 1.

Shearer's Initial Location [m] / shield #	Plume Initial Location [m] / shield #	Time Elapse [sec]	Location of Intersection [m] / shield #
280 / 160	0 / 1	292	291 TG-HG / 166
150 / 86	0 / 1	168	167 HG-TG / 96
75 / 43	0 / 1	85	84 HG-TG / 48
30 / 17	0 / 1	35	34 HG-TG / 20

Table 4.6.7: Case 4: Plume velocity reduced to 1 m/s. Initial locations same as Case 2.

Shearer's Initial Location [m] / shield #	Plume initial Location [m] / shield #	Time Elapse [sec]	Location of Intersection [m] / shield #
300 / 171	0 / 1	274	273 TG-HG / 156
300 / 171	150 / 86	138	287 TG-HG / 164
300 / 171	225 / 129	70	294 TG-HG / 168
300 / 171	270 / 154	29	298 TG-HG / 170

Basic 2-D and 3-D CFD Analyses

In these studies, Ansys's CFD package Fluent was used to model both 2-D and 3-D flow scenarios in a longwall coal mine. The aim of these studies was to further predict and validate gathered information found in previous works; as well as provide some visual insight to methane distributions with a turbulent model more realistically represented dispersion characteristics. Simple geometries were selected for the current first-generation models to reduce the computational burden and need for complicated mesh.

2-D Longwall Section

In this model, a rectangle with a length of 257 m (843 ft) and a width of 4.7 m (15.4 ft) was used to define the average longwall production area. Boundary conditions were set such that air entered along the left (HG) and CH_4 entered along the entire bottom length to represent the natural flux of methane from the exposed coal along the face. Thus, 4.6.10 is an overhead planform view. Direction of flow is from left to right (x-axis, long wall face length) and the height (y-axis, bottom face, top shield rear near gob) represents width of the width of the shields. A mesh study was performed until a final refined version produced repeatable results. The 2-D model was performed with the reported boundary conditions found in Table 4.6.8, and a simulation time of 200 seconds was used to ensure steady state results were achieved. Figure 4.6.10 shows the resultant concentration contour along the length of the longwall from the 2-D simulation.

Table 4.6.8: Boundary conditions for 2-D and 3-D simulation.

Boundary Condition	Value
Entry ventilation rate	2 m/s
Methane emission rate	0.000043 m/s
Mesh construction	1100x20 divisions

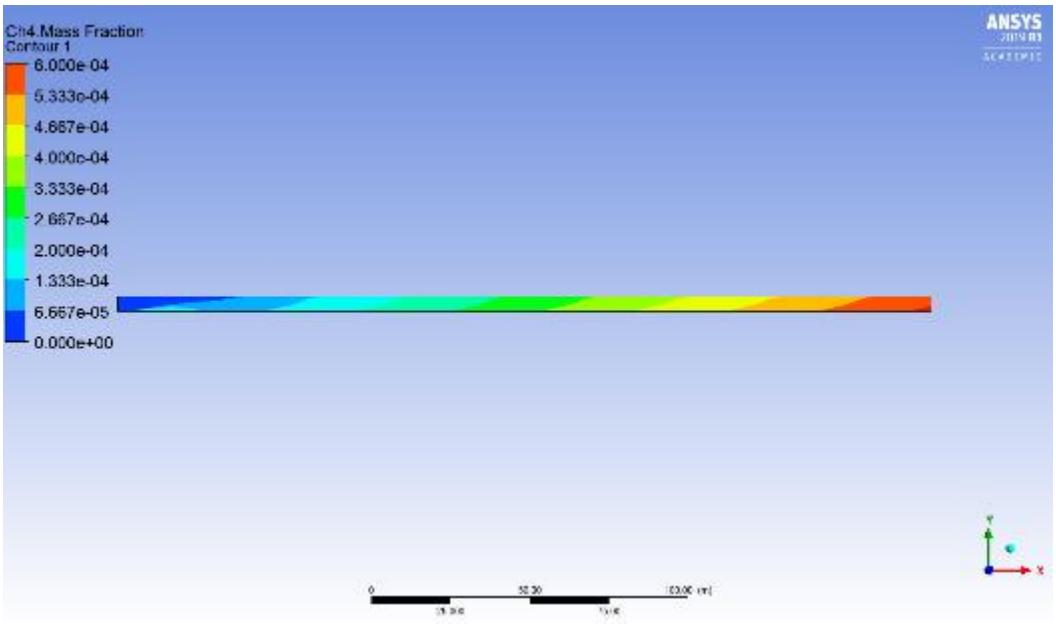

Figure 4.6.10: Resultant methane concentration contours from 2-D CFD analyses.

Figure 4.6.11 depicts the maximum generated concentration data plotted with respect to the location along the longwall (nearest the face). This plot shows the maximum concentration occurred at the TG, and that the profile demonstrates a linear or first order trend similar to the 1-D study previously conducted.

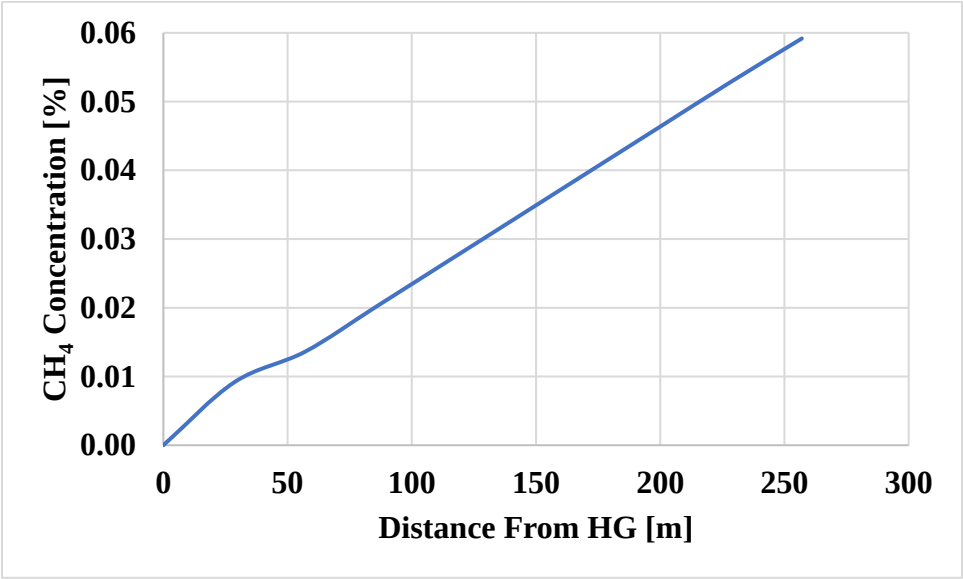

Figure 4.6.11: 2-D simulation results plotted with respect to distance along the longwall.

3-D Longwall Section

A 3-D model was constructed to better capture the effective geometry of the longwall section. In a real production area of a longwall, the geometry is rather complex due to all the shield components, shearer, and pan line. However, we simplified the geometry to generally depict a flow domain for the methane concentration study. Figure 4.6.12 presents the modeled longwall section used in this analysis.

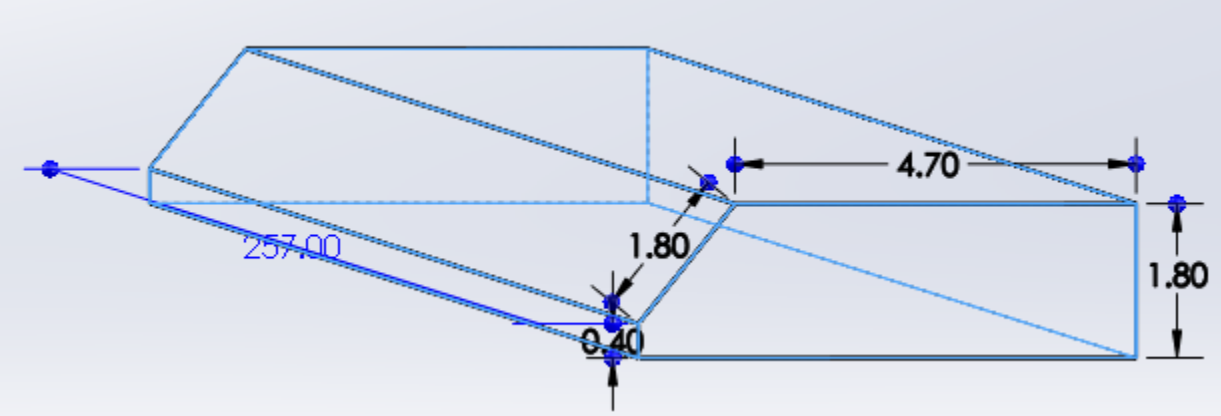

Figure 4.6.12: Longwall geometry created for 3-D simulation.

A similar setup of the 2-D model was used in the 3-D simulation with the adoption of the new geometry. The same 2-D boundary condition values were used and defined similarly to that of an actual longwall section. Fresh air entered the HG as a velocity inlet and methane was continuously emitted along the "face" to mimic the natural desorption of exposed coal from recent production activities. Figures 4.6.13 and 4.6.14 depict the methane concentration contours in both the axial and cross-sectional planes of the longwall model following the simulation.

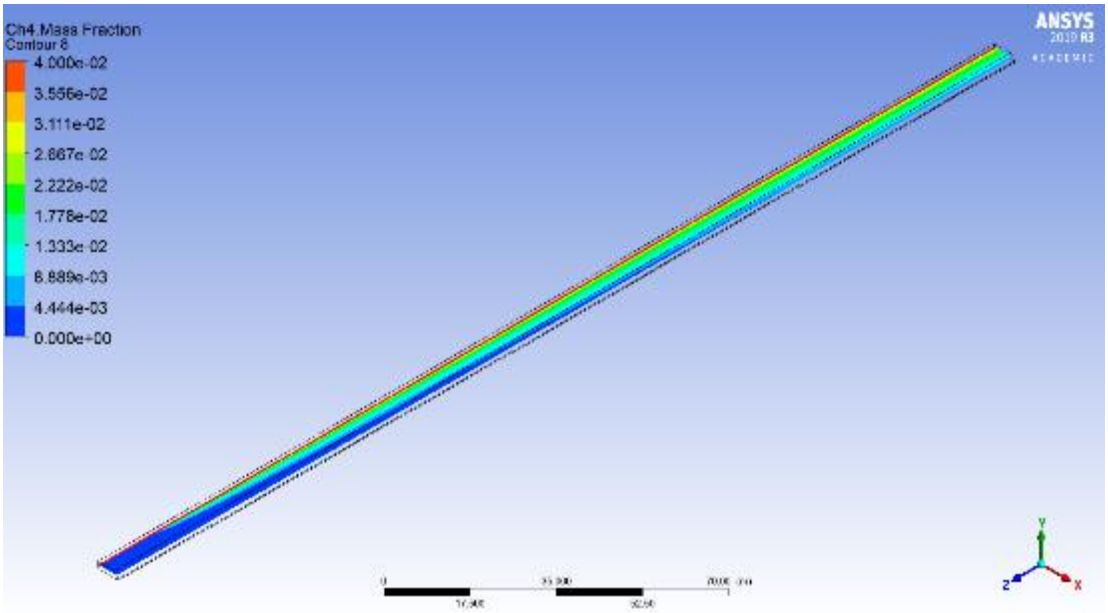

Figure 4.6.13: Top view of the inner sectional methane concentration profile generated from the 3-D simulation.

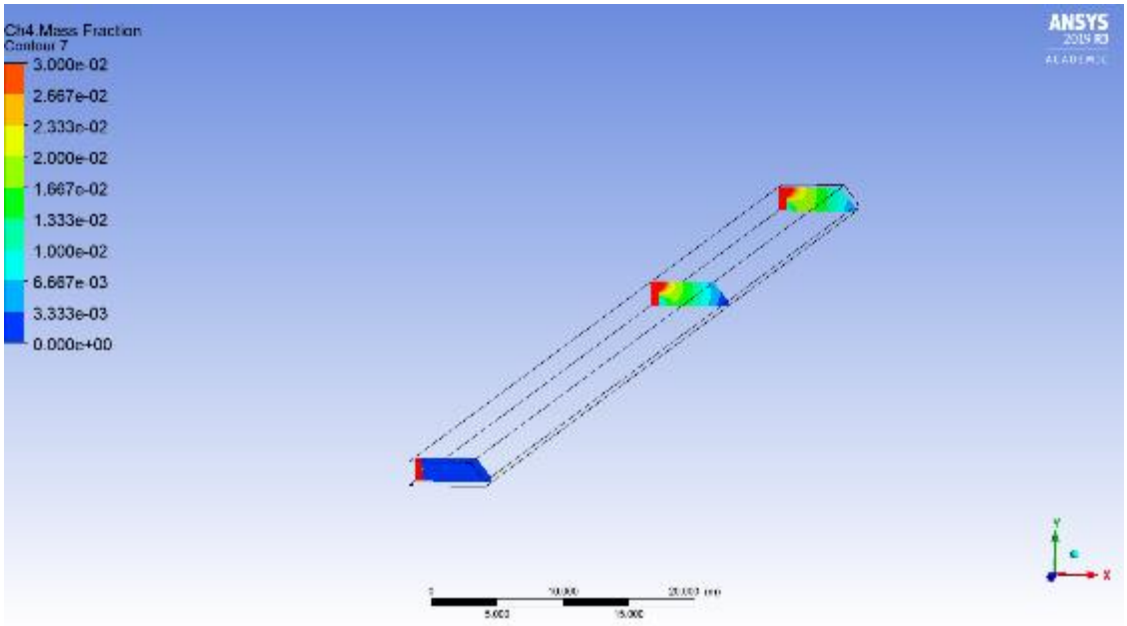

Figure 4.6.14: Cross-sectional views of the methane propagation from the face of the longwall.

The velocity magnitude throughout the longwall model was also graphed to assess its behavior as a result of the geometry. Figure 4.6.15 contains the velocity contours at three cross-sectional areas of the longwall: the HG (near), middle, and TG (far). The velocity graphs helped assess areas of the model that experience resistance to flow. Areas of insufficient flow may lead to inadequate dilution of local methane emissions and contribute to hazardous areas.

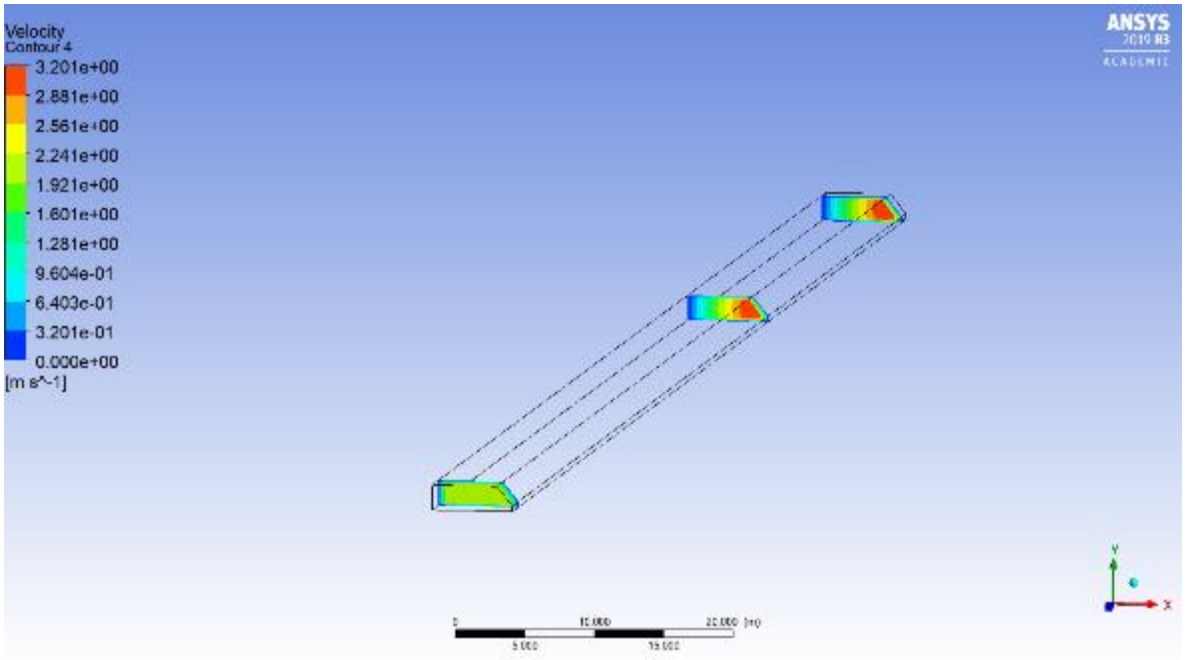

Figure 4.6.15: Velocity profiles at the entry, middle, and tailgate sections of the longwall model.

Multi-dimensional CFD models were created to further assess methane distributions in the longwall section of a coal mine. Boundary conditions similar to those used in the 1-D analyses were defined in these models examine spatial and geometric contributors to downwind methane concentrations. Results obtained from these simple domain models shows consistency with previous studies and current analysis presented earlier in the report; where emission profiles demonstrated positive linear trend towards the tailgate at which emissions reached their maximum. To further capture flow characteristics and fully define the most significant contributors to flow behavior and methane plume formation in the longwall, the current geometries can be further developed to incorporate major components found within the longwall section. Also, by extending the boundaries to include more realistic entry and exit splits, as well as the gob region, a more complete analysis could be conducted to assess methane measurements as the proposed sampling locations.

Modeling Conclusions

The development of a model and simulation for the multi-nodal detection system was a valuable resource in evaluating events in the coal mine. The results obtained from the model can be coupled with the currently developed MWS to optimize system response and inform node placement. The first-generation model presented here aimed to predict initial background concentrations and transport times under a few general assumptions. Characteristics such as dispersion and mixing of the methane as it entered the longwall play a key role in time scales and distribution profiles. The absence of these key characteristics in the first generalized model may inaccurately represent the severity of a scenario depicted in the results. Naturally, if these characteristics could be more accurately modeled, the time to intersection of the shearer and a dangerous methane plume could be extended. Currently, the T90 response times for a detection node in the MWS are around 10 seconds for the MOS and 30 seconds for the IRS. The intersection times obtained from the shearer and plume analysis appear to be on the same order as the response times of the system where a maximal intersection time was found to be 151 seconds. However, this analysis could be considered a “worse-case-scenario” situation since the ventilation rates (plume velocities) were held constant along the entire longwall. Figure 4.6.5 shows the fluctuation of the ventilation rates across the longwall face. More accurate representation of the ventilation rates could also extend the time to interaction of the shearer and plume. These results of the shearer and plume analysis compared to the system response times revealed two initial characteristics of the system and model that require attention in future work: a more accurate representation of methane mixing and dispersion as it is introduced to the ventilation air, and the reduction of the system response time. Attempts to improve system response times in future research could include minimizing the dead volume in the sampling block, improving sampler design to increase sample flowrates, or modifying tubing dimensions in order to reduce sample transport time. Another way to improve system response time may include the use of a new methane sensor that possesses a shortened response time.

Methane formation is a continuous function of several parameters known in both the mining production and methane/air interaction. This highlights the importance of using a “smart” system that the MWS embodies. A “smart” system could calculate the first and second derivatives both with respect to time and distance (between nodes). Such a predictive method would alleviate the response time limitations imposed by even an optimized sampler system. Having the ability to differentiate concentrations between nodes over the entire longwall can help construct correlations among the production and environmental parameters; as well as predict downwind emissions

before they occur. Predictive methods such as these are a significant way to prevent accidents while reducing downtime as a result of unplanned stoppages. Well-developed models would serve as valuable tools used among production industries to more accurately predict and prevent unwanted events. Data driven methods aid in the behavioral study of a system to assess the most efficient shearer velocity (production rate for a given ventilation rate) while abiding by the number one objective, safety.

5.0 Summary of Accomplishments

5.1 Key Design Findings

Some relatively major design modifications were made from the initial proposed design of the system. We determined that along with the MOS originally proposed, the addition of an IRS would help improve the accuracy of the CH_4 concentration measurements. We later found that the implementation of both CH_4 sensors together could provide a more accurate and larger measurement range due to the range limitations of each sensor. While testing these CH_4 sensors, we found that climate corrections were necessary to improve accuracy, especially for the MOS. In order to apply these corrections, RH, temperature, and pressure sensors were added to the design to measure the climate of the sample. These sensors were also beneficial to the design because of the lack of climate data available for longwall mines. If this system were eventually deployed in an actual mine, RH, temperature, and pressure will consistently be recorded; this would aid future research related to longwall mining. A flow sensor was also added to each sampling unit to ensure proper flow of the sample was consistent and that there were no issues that could be restricting the flow such as a clogged filter or ejector failure. One of the goals of the system was the eventual control of variables such as ventilation speeds. As such, two 3-cup anemometers were also integrated into the system in order to measure the wind speed. The ability to measure wind speed would allow the system to decide whether the ventilation speed should be increased to clear out areas of "high" CH_4 concentrations or if the ventilation speed could be lowered (reducing energy consumption and improving miner comfort.

One key component of the final prototype, not originally included, was the design and manufacturing of an aluminum sensor block which housed the two CH_4 sensors, a RH sensor, a temperature sensor, and a pressure sensor. The sampling block had one inlet and one outlet for the sample to flow through, passing all five sensors. Since the volume of cross-sectional flow area through the block was much smaller than of the original tube design, the delay time was significantly reduced which improved response time. The sensor block, along with all other components required for each unit, were mounted in a steel box which had through ports for power, communication, and the sample tubes. The method of a sealed and self-contained sensing node could easily be modified for node future MSHA certifications.

Another key component of the final design was the ability of each sampling unit (node) to sample from two locations (not simultaneously), near the face or near the gob. The sampling location can be alternated at a prescribed time interval. This allowed for only one sampling unit at each node with maintaining the ability to pull a sample from both the face and the gob via tubes. The ends of each tube included filters to avoid clogging of the sampling tubes or damaging of the sensors due to coal debris and moisture. The sampling location was controlled by a 3-way solenoid valve which was also mounted in the sampling unit.

Many modifications were made to the initial design of the MWS to improve the overall system as well as to ease the MSHA certification process in the future. Even with these modifications, the system remains cost effective and was believed to be very valuable in the improvement of longwall mining safety along with providing useful data for future longwall mining research.

5.2 Experimental Validations

Experimental validations of the MWS were made in a mock mine setup at a wind tunnel at the WVU JW Ruby Research Farm. A mock mine was constructed inside the tunnel to mimic the

longwall mine cross-sectional dimensions. Since the tunnel was only 30.5 m (100 ft) long, a sampling unit was placed at each node, which were spaced 3 m (10 ft) apart in a line near the center of the tunnel at the roof; each of the sampling tubes attached to the units were mounted in their respective location either at the "face" or "gob" side of the mock mine.

Once the MWS was in place, various experiments were conducted. Some "long-term" testing was completed over spans of a day to a few days to verify baseline data for RH, temperature, and pressure and assure all units were measuring similar values for these parameters; no CH_4 was introduced during these tests. Other experiments were conducted where CH_4 was introduced to analyze the response of the system, including response times, as well as to test the alarm system. During some of these experiments, fans were used at the HG and TG of the mock mine in attempts to simulate the ventilation in a longwall mine, however, minimum ventilation speeds could not be achieved and controlled as a major factor of the wind speeds through the tunnel were related to natural gusts of wind entering the tunnel from outside. Even though wind speeds were not ideal, the experiments were informative. For the majority of the tests performed, the FFS was used to supply the desired methane concentration at a specific location. To analyze the overall system response, the FFS was first setup to supply CH_4 at the HG with the supply directed downstream, towards the TG. These tests were named Type 1 and Type 2 tests where the fans were either of off or on, respectively. The Type 2 tests (fans on) showed "smoother" results than for Type 1 tests and the response order of the units was more easily distinguished; the units responded in order from nodes 1-10.

While these tests were beneficial in analyzing the response order of the system, the CH_4 concentrations achievable with this method were too low for the IRS to detect, therefore, other types of tests (Type 3 and Type 4) were performed to analyze the responses of the IRS. During the Type 3 and Type 4 tests, the FFS supplied CH_4 near each sampling location along the "face". For the Type 3 tests, the CH_4 was supplied near the sampling location for approximately one minute while for the Type 4 tests, the CH_4 supply traversed the section at a near constant walking speed. These tests were also used to compare the response of the MOS to the IRS. The alarm system was also tested by using the FFS to supply CH_4 at a concentration above 1% to each sampling location along the face, one at a time to assure that the alarm was set off when the concentration exceeded 1% at any location. This test confirmed that the alarm system was worked properly.

Another set of tests were performed to analyze the system response time by directly supplying a 2% CH_4 concentration to each sampling location along the face. This was achieved using two methods; the first method (Method 1) allowed the sample to be sent to multiple sampling locations at once by using a manifold system with ~10.7 m (~35 ft) supply tubes (one for each manifold) leading from the area where the gas bottles were located to the respective manifold and 7.6 m (25 ft) supply tubes leading from each outlet of the manifold to their respective sampling location filter (a total of 18.3 m (~60 ft) of supply tubing from the "start" location to the filter). The supply was controlled by a system of three 3-way valves that were located with the gas bottles. Originally, we assumed that once the CH_4 concentrated gas filled the supply tubes, it remained there even when flow ceased, meaning no diffusion from the filled line when off. However, in analyzing the results, using MOS and IRS responses to characterize the rise and decay times, it seemed that that assumption was not accurate due to some of the sensor decay responses.

After issues with the Method 1 were determined, a second method (Method 2) to analyze system response times was used. For Method 2, the CH_4 concentrated gas was directly supplied to a

sampling location via a supply tube leading from the gas bottle to an MFC, which controlled the flowrate, and a 0.3 m (1ft) long tube exiting the MFC which was inserted directly into the filter at the sampling location. For this method, the MFC controlled the flow and could be referenced as the start and stop times. Once the flow was initiated, the sample only had to travel through the 0.3 m (1 ft) tube leading into the filter, which was negligible compared to the 18.3 m (60 ft) of supply tubing used in Method 1. The results of the two methods were compared to each other and it was determined that there were issues with Method 1 and the results of Method 2 more accurately represented the system response times.

Based on the results of Method 2, the average system response rise time was 8.75 seconds based on the MOS response and 28.5 seconds based on the IRS response, while the average system response decay time was 133.75 seconds based on the MOS response and 22 seconds based on the IRS response. The extended MOS delay time was due to the lower detection limits of the IRS; the MOS detected lower concentrations that the IRS did not. Overall, the testing performed at the mock mine were informative. The results from these tests were adequate to initially validate the operation of the MWS.

5.3 Modeling Accomplishments

A first-generation model was successfully developed to predict methane concentration across the long wall and verified with literature. This model was used in conjunction with the currently designed MWS to assess a few scenarios that may be expected in a full-scale deployment. The model also provided us with a useful tool to aid in further constructing the systems logical “smart” control scheme. The control strategy and learning features of the MWS are key elements in promoting a safe and productive work environment that the system embodies. Data were collected from previous relevant studies to define the boundary conditions of the modeled longwall coal mine. A simplified first order analysis was conducted to generate expected methane concentrations along the length of the longwall face that are a function of both natural release from exposed coal and production. These methane fluxes were coupled with ventilation and production rates to further assess the dependence of the two.

We found that ventilation rate was a more significant contributor to downwind methane concentrations than production rate. Fluctuations in fresh air, or lack thereof at the TG, created high concentration areas that would lead to unexpected delay times. Due to periodic ventilation checks, these events may go undetected, and therefore shows the benefits of a continuously monitoring system that incorporated these measurements. Our first model generated these scenarios and evaluated the resulting concentration profiles downwind. These events and key parameters of a working longwall mines created insight to further development of the system and its control strategy. The model also simulated the tracking of the shearer as a function of production rate. This allowed the MWS to always know where the shearer was along the longwall at any given time from a safe remote location of the CPH. Simple constant shearer rates were used in the current analysis to predict interaction time and locations of a highly concentrated (> 1%) methane plume with the shearer; given their respective initial locations and rates. The effectiveness of the MWS system was determined by the array of units and their system response time. The model provided an environment to define these parameters and analyze the individual variables to reduce system limitations and produce desired results. We also developed basic 2-D and 3-D models to account for more realistic dispersion though they were simple. However, general trends tended to match those with literature.

6.0 Dissemination Efforts and Highlights

6.1 Intellectual Property

It is our belief that the MWS represents intellectual property. Therefore, to date we have not sought public dissemination on the MWS design beyond the proposal and interim report. Pursuant to IP and patentability, the initial date of public disclosure could make future protections difficult. Dr. Nigel Clark completed an initial patent search and found no patents that would appear to in any way infringe on the system developed herein. Reviewed patents included US Patents 6,158,240; 3,683,255; 10,089,848; 8,692,997; 5,611,844 which relate to methane, but none was considered as relevant in nature to the Methane Watchdog System (MWS). Additionally, literature from NIOSH, other researchers, and the CDC were reviewed without significant findings. Therefore, the MWS likely represents a novel method and therefore intellectual property (IP). As such, we selected to focus on IP protections prior to public dissemination. Note: we had originally submitted an abstract for a conference but did not follow through with this public disclosure.

Appendix C includes the final invention disclosure that was filed on 11/26/2019 and enabled on 12/05/2019. The disclosure includes a detailed description of the system along with general straw claims. The invention disclosure underwent a commercial assessment by an external party - TreMonti Consulting - and its subsequent score warranted a full review by the WVU Technology Transfer Assessment Committee (TTAC). The research team was informed on January 22nd, 2020 that the university has elected to file a provisional patent for the MWS. We subsequently met with patent attorney Dr. Randy Schoen on February 27th, 2020 to review a draft provisional. A provisional patent will be used to establish a priority date and once filed; public dissemination can occur. A provisional patent lasts for 12 months and during this time period, WVU will work to assess commercial interest as necessary to file a full utility patent. We note that the commercial assessment recommended researchers continue to work on further development and refinement of the system. We have identified key areas of future research in Section 8 below and if funded will address these issues to ensure commercial viability on a path towards deployment. Once the provisional patent is filed, we will reach out to industry to assess their common interest in commercialization and deployment. Such industry would likely be represented by Sensors Inc, a worldwide leader in portable emissions measurement systems; energy companies (such as Murray or CONSOL), shield manufacturers (such as Caterpillar and Komatsu) and shield maintenance and repair companies such as Swanson Industries.

6.2 Expected Theses

Multiple undergraduate and graduate students have benefited from this research. Two students will focus on different aspects of the project for partial fulfillment of the requirements for their Master's Degrees. This will include the publication of two theses. Ms. Amber Barr's thesis will focus on the overall design of the system. Dependent on future funding, she has also proposed to focus on optimization of the sampling methods based on the use of highly compressed water streams for explosion proof ejector samplers. Dependent upon funding and additional research Ms. Barr is expected to graduate in August or December of 2020. Mr. Brian Cappellini's thesis will focus on reduced order modeling of the system and its possible benefits as a novel method to control either mining ventilation or shearer velocity. Dependent upon future funding, Mr. Cappellini may also focus on advanced modeling as he is expected to graduate in December of 2020 or May 2021.

6.3 Public Dissemination – Future

We already have material and text gathered for extensive publication of the MWS, and the fundamental and applied research that supported the development. We plan to publish one article focused on the overall design of the system, its deployment in the wind tunnel, and some example data from that deployment. We have identified the International Journal of Mining Science and Technology or the International Journal of Coal Science and Technology as suitable publication venues.

Second, we also plan to present a general paper at an annual conference, with more emphasis on the wind tunnel installation, and a discussion of the design decisions that led to the present MWS. This will likely be given at the Thirty-Seventh Annual International Pittsburgh Coal Conference or the International Symposium on Mine Safety Science and Engineering (expected in 2020/2021)

Third, we intend to publish the research and design related to the sampling system, including modeling of the ejector, and response of the system to varied line lengths and diameters. This paper will also include the necessity for sampling filters, the influence of dead volume at the filter, and the influence of dead volume at the point of methane sensor installation. This paper will present the basic system response, using modeling of dead volumes as stirred tanks, and modeling of tube flow with velocity and axial dispersion. This will provide theoretical response information. This will be submitted to a journal such as Flow Measurement and Instrumentation (Elsevier) or Instrumentation Science & Technology (Taylor & Francis).

We plan a fourth paper to demonstrate our first foray into early prediction of a methane cloud, using simulation of the cloud and the sensor system to produce a suite of signal that is processed to provide safety and control information. In particular, we will publish on the ability of the system to distinguish normal versus action scenarios as a function of time, as the cloud evolves. This fourth paper will also address the ability of the system to assess its own health, in terms of leaks and sensor failures, and to provide a best available decision under constraint of a failure. The paper may also extend to determining reasonable sampling point spacing for reliable detection. This would be suited to a journal such as Measurement (Elsevier).

7.0 Conclusions and Impact Assessment

Under this program a first-generation prototype Methane Watchdog System (MWS) was developed, aimed at improving mine health and safety. This system included ten nodes capable of sampling from 20 different locations. Ten locations were at the face, and ten at the gob. This was enabled through use of a single water powered ejector at each node. The ejector embodied an explosion-proof method to create a sampling flow without the use of any electricity or moving components. The ejector created the negative pressure to sample from non-central locations that would otherwise be deemed too dangerous. Tubes extended from the node to the rear and front of the shields and each termination included an enclosed filter to protect components and lines from coal dust and water sprays.

The nodes housed all sensors and necessary electrical components within its sealed enclosure. Each node included two methane sensors (one MOS and one IRS) and temperature, relative humidity, pressure, and flow sensors. These additional sensors increase the accuracy of the low-cost methane sensors and enabled additional capabilities. Ten data sets were recorded continuously at 1 Hz, switching sampling as programmed between pairs of locations. Each node was powered using low voltage DC power that would be available in longwall shields and communication occurred through conventional low voltage ethernet cabling similar to the communication between shields. The design vision anticipated future integration of the system with shields, as one deployment option.

All ten nodes communicated with a remotely located Central Processing Hub (CPH). The CPH was an industrial solid-state computer with touch screen and data recording capabilities. The CPH converted analog and digital signals from each node to meaningful engineering units through a variety of signal conversions and stored calibrations. This conversion included the correction of methane sensor data. The CPH also had the capability to process the signals and present alarms, de-energize equipment and manage production rates in the interests of safety through its various output channels.

The functionality of the prototype system was demonstrated at a mock mine facility 30.5 m (100 ft) in length. This facility was established in a wind tunnel originally configured to examine exhaust plumes. The wind tunnel ceiling was lowered to represent anticipated height in a working mine. During the demonstration, a basic CPH program was verified to successfully complete the following objectives:

- interpret and present in useful engineering units, signals from over 60 sensors,
- control multiple relays (1-per node) to switch sampling between the face and the gob,
- control isolated relays that could deenergize mine equipment,
- display on screen and sound audible alarms when nodes exceeded a threshold (e.g. 1% methane by volume), and
- record sensor data during unmanned operation.

In addition to these objectives, research was also conducted to select appropriate filters to be installed at each sampling point to protect nodal sensors from particles and droplets while minimizing pressure drops. Such attributes enable sampling from near the gob and face at locations that would be dangerous to sample during in-use operations.

A vacuum was needed to draw gas from the sampling locations to the nodes, where the gas was exposed to the sensors. To satisfy a commitment to minimize ignition sources from the MWS, water-based ejectors or eductors were chosen for this purpose. Pressurized water is available underground at longwall applications. Modeling provided ejector design parameters in relation to sampling tube length and bore. The ejectors were verified on the bench and then incorporated into the system. Using compressed water of less than 689.5 kPa (100 psig), the ejectors provided sample flow rates of up to 2 slpm (0.071 scfm) with minimum water consumption of ~1.9 lpm (~0.5 gpm). Such an approach was inherently explosion proof and uses no moving components which would be prone to failure under extreme conditions encountered in longwall mining operations.

Based on our discussions and review of shield operations with industry, these attributes should enable easy integration of the MWS within current shields. This is a major beneficial impact, since shields have long lives and are typically rebuilt or refurbished for continuing service. A retrofit methane monitoring system could be installed during surface repairs or even in the mines themselves. Much as shields are connect with quick disconnect houses and connectors, so to would the final version of the MWS, enabling easy plug-and-play integration and easy modularity. We note that in discussions with CPH manufacturer, its current model could likely include communication up to nearly 250 nodes.

Nodal response times were determined for metal oxide sensors (MOS) and infrared sensors (IRS) of 9 and 32 seconds, respectively. These values were on the same order as response times for machine mounted and handheld methanometers. While some may see this as a lack of improvement over current technologies, basic 1-D, 2-D, and 3-D models were used to highlight cases in which the MWS would be capable of setting alarms well before the shearer or miners themselves entered dangerous methane plumes. These benefits were due to the continuous monitoring from the nodal network that would be distributed across the entire longwall face, especially near the tailgate where methane plumes or clouds often reach their peak concentrations. In addition, a handheld unit would require a miner to be within a dangerous plume for 10-30 seconds before their alarm would sound. The distributed network would report these dangerous scenarios across the face at the remote CPH, providing an increased level of mine safety. In addition, we note that mines require periodic methane and windspeed measurements at specified intervals and locations. Deployment of the MWS would alleviate any human error associated with missing or delayed data collection.

Our efforts require additional public dissemination and collaboration with industry. However, during our research we found a dearth of intellectual property (IP) associated with technologies and sensor networks to improve mine safety. Along with independent reviewers and the West Virginia University Office of Technology Transfer, we concluded that the MWS likely represents multiple sources of IP. We are moving forward with a provisional patent to protect this IP broadly before extensive public dissemination of our findings. We feel that our current prototype system and results have demonstrated an acceptable reduction to practice; however, we have conclusively highlighted key areas that should be addressed in Section 8.

Ultimately, to improve mine health and safety and provide real beneficial impacts, the MWS must be deployed in active longwall mines. This could be achieved through partnership with mines, shield manufacturers, or regulating agencies. Before the system is deployed, our highlighted areas of future research must be addressed to enable the full capabilities of a distributed methane monitoring system. These recommendations are summarized in the proceeding section.

8.0 Recommendations for Future Work

During this 18-month program, we have designed, developed and demonstrated a complete prototype MWS. A major task we had proposed to conduct in this project was a demonstration to industry members. This was delayed due our realization that the system could be a commercially viable system that represents new intellectual property. Therefore, we have avoided public disclosures and have concentrated on protecting the IP. However, an invention disclosure has been filed and provisional patent language is in a final editing stage. Intent is to submit the provisional patent in April. This would enable us to publish and present our research and conclusions. In addition to these items, our research has highlighted 7 key areas where future research should focus. We seek additional funding to focus the following key areas of future research.

8.1 Signal Sharpening

In addition to sensor response time, our final prototype design causes additional sampling time delay and a diffusion of the sample in the tube from the sampling location to the node. The sampling time delay represents the time it takes for the encountered methane plume concentration to travel from the inlet of the remotely place filter (near gob or shield tip) to the methane sensor locations within the sampling block. The diffusion effect occurs primarily in two regions – the filter housing itself and the sampling block volume. There is also net axial diffusion during flow through the tube. Redesign of the sampling block could reduce delay. However, numerical methods exist to reverse some of the effects of both sample delay and diffusion. This issue is quite a common yet overlooked issue for gas sampling systems whose goal focuses on continuous real time measurements within transient gas flows. One of the present investigators has previously studied this area of signal recreation or sharpening and has published on the subject [47 and 48]. A mechanistic model would be developed and consist of the following three components, in sequence:

a. A filter and filter housing

b. A tube from the filter housing to the sampling block

c. The sensor block: a dead volume containing a sensor

These components are of importance in identifying the measurement response time to a rise or fall in methane concentration at the sampling point. It is reasonable to treat the tubes in an idealized fashion, with no axial mixing. In other words, a pulse of methane ingested at the tube entrance will leave the tube as the same pulse, neglecting axial mixing. Without granular flow modeling for the filter and sensor enclosures, it is reasonable to treat these two dead volumes as well-mixed zones, with the same concentration throughout.

For the filter volume, therefore

$$\frac{dY_F(t)}{dt} = \left(\frac{Q}{V_F}\right)(Y_i(t) - Y_o(t)) \qquad \textbf{Eq. 8.1.1.}$$

where Y is the concentration, the subscript ‘i’ is into the filter, ‘o’ the concentration out of the filter, and ‘F’ the well mixed concentration of the filter. Assuming no axial mixing within the tube, the outlet of the tube will be shifted by a time constant ‘t_c’.

$$Y_{T,o}(t + t_c) = Y_{T,i}(t) \qquad \textbf{Eq. 8.1.2.}$$

where the subscript T,o is the concentration at the outlet and T,i is the concentration of the inlet of the tube – $Y_F(t)$. The measurement volume, denoted by SB for the sensor block, has a response similar to that of the filter volume

$$\frac{dY_{SB}(t)}{dt} = \left(\frac{Q}{V_{SB}}\right)(Y_i(t) - Y_o(t)) \qquad \textbf{Eq. 8.1.3.}$$

In addition, the sensor itself has a response, which may be characterized by an exponential rise in response to a step change:

$$\frac{dY_S(t)}{dt} = (k)(Y_{SB}(t) - Y_S(t)) \qquad \textbf{Eq. 8.1.4.}$$

where k is the time constant of sensor response. The resulting measurement that is recorded will represent one delay and three exponential responses relative to the concentration in the sampling zone (plume passing filter). The three exponential responses in series will resemble a gamma function (in response to a narrow pulse), characterized by no immediate response, a rapid rise to a maximum, and a long tail returning to the baseline value. Note, see the T90 rise time versus decay times in Table 4.5.2. If all three responses have the same time constant, the result will be a perfect gamma function.

It is imperative that detection of a dangerous concentration of methane in the sensor area should be both reliable and rapid. There is no way to address the time delay due to tube flow other than by shortening tubes and raising the flow velocity. However, for the response due to dead volumes, it is possible to infer a step rise in concentration from the time-varying sensor response. More broadly, the sensor response can be transformed to yield a prediction of the concentration history at the sampling point, yielding a faster decision on setting an alarm. The decision to set an alarm relies on confidence in the time-varying accuracy of the signal and a measure of the variability of the system due to fouling, sensor deterioration and flow variation – ideally the system would be time invariant. Further analysis and modeling are needed to explore the ability to anticipate high "sharpened" concentrations. In addition to these methods, the Principal Investigator recently supervised a master's student who examined delay and diffusion issues for low concentration methane analyzers [49]. Figure 8.8.1 shows an example of an analyzer with a delay and diffusion compared to the "real" spatial concentration of methane. Figure 8.1.2 shows a recreated signal using an artificial neural network. Where volumes and time delays can be reduced, they should be, but in the limiting cases, their impacts should be accounted for in an algorithm deployed in the CPH.

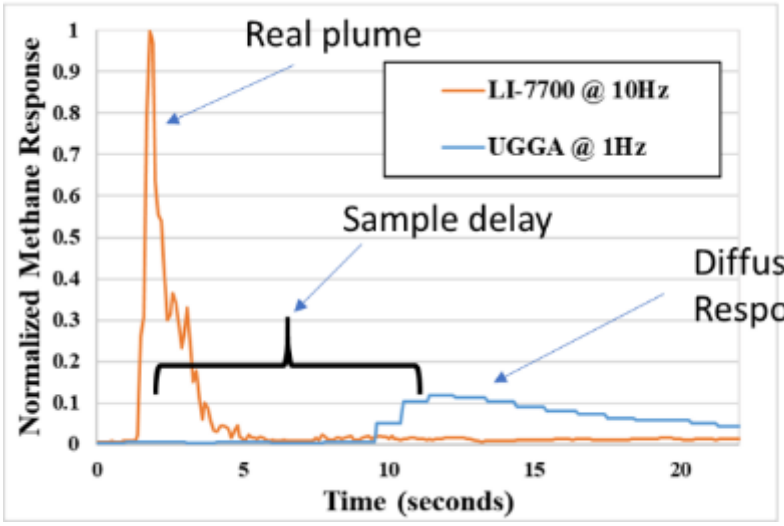

Figure 8.1.1: Example of methane plume and signal response for system that includes time delay and diffusion of the signal [49].

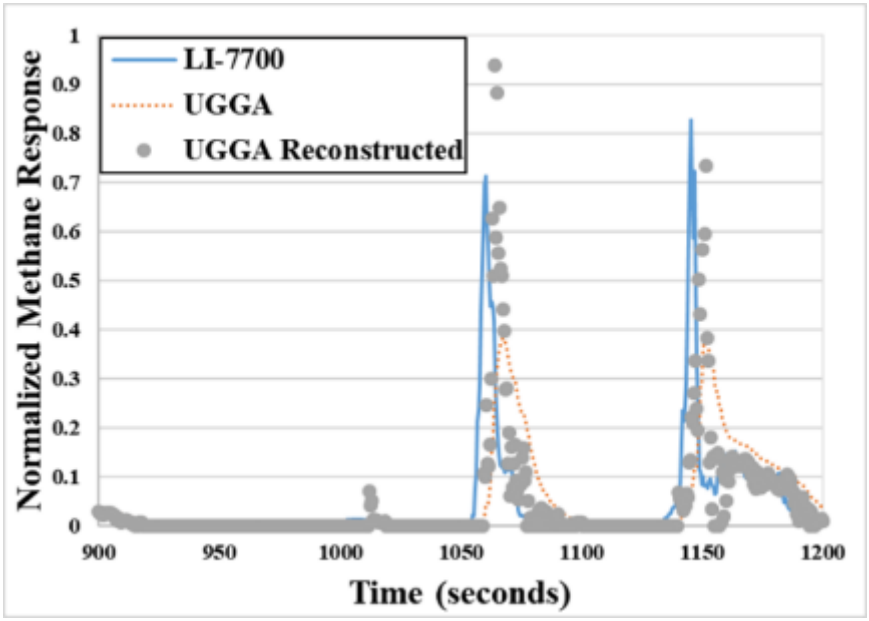

Figure 8.1.2: Use of artificial neural network to reconstruct a sharpened methane signal [49].

8.2 Sensor Modifications

It is beneficial to use both the MOS and IRS together in the system since there are advantages and disadvantages to each. The MOS do not offer high accuracy. We believed that accuracy of the MOS would be improved if their calibrations were made only to lower CH_4 concentrations closer to their recommended operating limit (<1% CH_4). Since the IRS have been deemed accurate and reliable for measurements above around 0.2% CH_4, which is above their lower detectable limit, the MOS could be calibrated only to focus on measurements up to 0.2% CH_4 to compensate for the limitations of the IRS; this would also aid in improving the RH, temperature, and pressure

corrections for the MOS. Further, an optimized blend of information from the two sensors can be proposed as a function of their ranges of calibration.

Another improvement that could be made pertaining to the CH_4 sensors would be to consider the implementation of a different, single, CH_4 sensor to replace the IRS and MOS in each sampling unit. We have a long-standing relationship with researchers at Sensors, Inc [50]. Sensors is a worldwide leader in the production of portable emissions measurement systems (PEMS) and is a producer of integrated systems and components. We are currently collaborating with Sensors on other methane related technology development and recently renewed a Non-Disclosure Agreement (NDA) with them. Once the final report is submitted, we plan to seek permission to release our findings to Sensors to determine if they might offer providing additional sensor expertise to our system.

8.3 Advanced Control and Modeling

We have conducted some basic modeling to show the initial benefits of implementing the MWS. These scenarios utilized experimentally obtained response times and data gathered from literature to examine a variety of scenarios to highlight the pre-emptive alerts provided by the MWS. The current MWS provides multiple local and global digital outputs that could be used to isolated, intrinsically safe relays to stop or de-energize equipment. It is realized that beyond digital control, the system could output signals to modify operational activity such as for control of a ventilation on demand (VOD) system. However, we realize that VOD systems would yield their own response time and are not commonly available.

Alternative to VOD, the MWS could also pre-emptively alter the shearer speed to enable slower, yet continuous production. Studies have shown that gassy mine seams can often experience work stoppage down-times of 50%. Methane can be emitted from the gob area, the floor/ceiling, and the face. In addition, multiple references recognize that the primary source of methane is the mining of coal at the face. With the capability to understand the time varying methane concentration across the entire face in near real time, the shearer velocity profile could be modified based on historical data to ensure that work stoppages are avoided without changing the ventilation rates. There may exist optimum mining shearer velocity profiles that yield higher production rates compared to conventional fast mining until a stoppage is required. We propose to conduct additional modeling targeted on the following two key areas with focus on multiple variables:

1. Additional scenario modeling (0-, 1-, and 3-D)
    a. Additional ventilation velocities (higher and lower)
    b. Additional methane flux rates to mimic conditions of multiple area and point source emitters
2. Assessment of closed-loop, feed-back control of shearer velocity based on historical pass data
    a. Examination of slower velocity rates on production versus digital on-/off-mining until the 1% threshold
    b. Impact of sharpening model and derivatives for predictive control
3. Sensor signal characterized in model to replicate and reconstruct varying methane concentrations
    a. Study concentration time scales

8.4 Advanced Sampler Design

Based on our original discussions with mine workers and foreman from the region, we targeted the use of low-pressure water to power our ejectors. They estimated that water represented a good energy source, but that pressure used at wash stations was around 100 psig. However, we later met with a shield repair company to obtain data on current shields. From discussion, we determine that the water supply pressure to the shields is often much higher (up to ~1000 psig). They stated that their shop facility could produce up to about 400 psig, but that such an amount was adequate to check all spray nozzles. Since this discovery occurred later in the project and a sampler (ejector) design was already made, we propose that sampler design could be improved in the future where the higher supply pressure is utilized.

We note that upon review of the interim report, feedback from the Alpha Foundation showed concern regarding the additional water consumption of the MWS. This warrants further examination of pressures above 100 psig and less than 1000 psig. A high-pressure ejector can reduce water consumption by an order of magnitude. In addition, more centralized ejectors or a single ejector system may be capable of producing enough flow and suction pressure to power all sample boxes within the MWS. If possible, such a centralized approach could permit water recovery and reuse, offsetting any associated penalties with the addition of the system. Also, if water pressures are always consistently this high, pressure regulation should be added to the design.

8.5 Shield Integration

Integration of the MWS into shield design is of central importance for future acceptance and deployment. One known modification is the conversion of the system to operate on 12 VDC as opposed to 24 VDC. Based on discussion with shield repair companies, many systems in the US and region use standard 12 VDC for onboard electronics. Note that our selection of 24 VDC enabled a reduced current flow. Solid state 12 to 24 VDC and 24 to 12 VDC converters are common off-the-shelf components.

We propose that water supply for the samplers be branched off the water supply that is already sent to each shield for high pressure sprays. Note multiple options exist and must be considered – direct use of high-pressure shield water, pressure regulation, design of choked flow for application to a variety of pressures experienced in mines, or centralization of water ejectors. Figure 8.5.1 shows three umbilicals that connect each of the shields together. The blue hose is for the compressed water. The others are electrical and hydraulic hoses.

Initial assessment of the integration of the system into the shields was made during a trip to the shield repair company. They provided additional information such as actual dimensions (schematics and diagrams) of typical shields that are currently used in industry. During the tour at the facility, they also showed a recently implemented proximity sensing system which was meant to keep track of where miners were standing or walking to improve safety. The proximity sensing control unit integrated into a shield can be seen in the red circle in Figure 8.5.1. This central location could support installation of nodes on shields without the proximity units. The integration of the MWS into the shields would be a similar process as the proximity sensing units and the sampling units (nodes) of the MWS are similar in size. Figure 8.5.2 expected locations at the front shield tip and the rear of the shield. For a retrofit system, a stainless tube or Teflon tube would run to the filters installed in the highlighted areas. Future shields could include a recessed cavity for sampling like those used for water nozzles. The right of Figure 8.5.2 also highlights the rear of the

shield in the fully collapsed position. There is adequate room to install the selected filter in this area and pathways exist for the sampling tube. Success of the MWS is predicated on deploying the system both in a retrofit mode and as an OEM integration into new shields.

Figure 8.5.1: New prototype proximity sensor system installed on a shield at a local repair facility.

Figure 8.5.2: Shield that was examined by the team at a local repair facility. Left: highlighted front tip area for the face sample location. Right: highlighted location of possible gob region sampling area.

8.6 Deployment in More Realistic Mock Mine

A further goal of additional research and verification is to deploy the MWS into an actual longwall coal mine. It is understood that there are many steps of MSHA certification required of the entire system. Full-scale testing has been performed at the mock mine set-up at the WVU JW Ruby Research Farm wind tunnel. Additional full-scale testing in a mine simulation facility with more controllable parameters would be beneficial to enable further optimization and demonstration of the MWS. A potential test facility has been identified for future full-scale testing of the system, namely the Mine Training Center located in Core, WV, about ten miles from the University. We visited the Training Center to tour the facility and determine if it would be an adequate test site. The Center has an above ground simulated mine, shown in Figure 8.6.1, that is used for mine training and certifications, mostly related to fire safety. Figure 8.6.2 shows an aerial view of the center from Google Maps Satellite view to help visualize the orientation of the simulated mine (circled in red). The front section is the longest at about 103 m (340 ft). While this is shorter than real long walls of 304 m (1000 ft) or more, it would be over three times the length of the mock facility we used previously at the wind tunnel.

Figure 8.6.1: Simulated mine at WVU's Mine Training Center. Left: front entrance on longest section. Right: rear tailgate entrance.

Figure 8.6.2: Satellite view of simulated mine at WVU's Mine Training Center.

In addition to providing a realistic length scale, the system is also representative of common mine heights and includes a moderately sized diesel-powered suction fan to simulate ventilation. This fan is expected to pull approximately 23.5 m^3/s (50,000 cfm) and can be seen in Figure 8.6.3. While this would be on the lower end of flows for longwalls it would enable more realistic experiments to be conducted compared to our previous use of axial fans at the wind tunnel. Deployment and testing in this simulated mine would be a major step to deployment in a production longwall mine.

Figure 8.6.3: Diesel powered fan used for ventilation in the simulated mine at WVU's Mine Training Center.

8.7 Summary of Future Work

The present investigators will prepare and submit a request for additional resources to perform the key elements of this research over a period of 18 months. In addition, we will advance the provisional patent to a full nonprovisional submission. We estimate this work could be completed for an initial cost estimate of between $208,000 to $240,000. In summary, the objectives of the future research are:

1.) Examine and develop methods to create sharpened sensor responses in real time to enable predictive control.

2.) Collaborate with Sensors, Inc. and others to assess additional sensor modifications that offer further reductions in system response time or improved accuracy.

3.) Conduct modeling and experimental research to further optimize ejector design for reductions in water consumption.

4.) Develop a shield integration plan thought additional co-operative visits and discussions with industry.

5.) Conduct larger scale system research and demonstrations at the Mine Training Center in Core, WV.

In addition, future work will also include public dissemination through journal and conference publications in order to the highlight this important work funded by the Alpha Foundation.

9.0 References

[1] Utah Labor Commission, *Test Preparation Study Guide for Coal Mine Certification: Underground Fire Boss* **2010**; https://laborcommission.utah.gov/wp-content/uploads/2019/11/Fire-Boss.pdf.

[2] Wang, Z.; Ren, T.; Ma, L.; Zhang, J. Investigations of Ventilation Airflow Characteristics on a Longwall Face—a Computational Approach. *Energies* **2018**, *11* (6), 1564–1564 DOI: 10.3390/en11061564.

[3] CFR: Title 30 Part 75; https://ecfr.io/Title-30/pt30.1.75.

[4] Cecala, A.B.; Zimmer, J.; and Thimons, E. Determination Of Optimal Longwall Face Methane Monitoring Locations. *Society for Mining, Metallurgy, and Exploration.* **1993**.

[5] Ozdeniz, H.; Sivrikaya, O.; and Sensogut, C.; Investigation of Spontaneous Combustion of Coal in Underground Coal Mining. In *Mine Planning and Equipment Selection*; Drebenstedt, C., Singhal, R., Eds.; Springer International Publishing Switzerland **2014**; pp 637.

[6] Colinet, J.; National Institute for Occupational Safety and Health. Office for Mine Safety and Health Research. *Best Practices for Dust Control in Metal/nonmetal Mining*; Information Circular, 9521; Department of Health and Human Services, Centers for Disease Control and Prevention, National Institute for Occupational Safety and Health, Office of Mine Safety and Health Research: Pittsburgh, PA, **2010**.

[7] Peng, F. F.; Wang, W. G. Respirable Dust Concentration Distribution Model on Longwall Faces — Multiple Dust Source Approach. *Powder Technology* **1994**, *79* (2), 121–133 DOI: 10.1016/0032-5910(94)02817-6.

[8] Sapko, M. J.; Cashdollar, K. L.; Green, G. M.; Sixth International Symposium on Hazards Prevention and Mitigation of Industrial Explosions ISHPMIE Halifax Nova Scotia Canada 20060827-20060901. Coal Dust Particle Size Survey of Us Mines. *Journal of Loss Prevention in the Process Industries* **2007**, *20* (4-6), 616–620 DOI: 10.1016/j.jlp.2007.04.014.

[9] Barone TL; Patts JR; Janisko SJ; Colinet JF; Patts LD; Beck TW; Mischler SE. Sampling and Analysis Method for Measuring Airborne Coal Dust Mass in Mixtures with Limestone (rock) Dust. *Journal of Occupational and Environmental Hygiene* **2016**, *13* (4), 284–292 DOI: 10.1080/15459624.2015.1116694.

[10] Schatzel, S.; Mutmansky, Jan. Prediction of Longwall Methane Emissions and the Associated Consequences of Increasing Longwall Face Lengths: A Case Study in the Pittsburgh Coalbed. In *Prediction of Longwall Methane Emissions and the Associated*

Consequences of Increasing Longwall Face Lengths: A Case Study in the Pittsburgh Coalbed; **2006**; pp 375–381.

[11] Diamond, W. P.; Garcia, F.; Pittsburgh Research Laboratory (National Institute for Occupational Safety and Health). *Prediction of Longwall Methane Emissions : An Evaluation of the Influence of Mining Practices on Gas Emissions and Methane Control Systems*; Report of Investigations, 9649; U.S. Dept. of Health and Human Services, Public Health Service, Centers for Disease Control and Prevention, National Institute for Occupational Safety and Health, Pittsburgh Research Laboratory: Pittsburgh, Pa., **1999**.

[12] Krickovic, S.; Findlay, C.; United States. Bureau of Mines. *Methane Emission Rate Studies in a Central Pennsylvania Mine*; Report of Investigations, 7591; U.S. Dept. of the Interior, Bureau of Mines: Pittsburgh, Pa., **1971**.

[13] Diamond, W. P. *Methane Control for Underground Coal Mines*; Information Circular; U.S. Dept. of the Interior, Bureau of Mines: Washington, DC, **1994**.

[14] Colorado School of Mines, "Coal Mining Methods"; https://mining.mines.edu/.

[15] Noack, K. Control of Gas Emissions in Underground Coal Mines. *International Journal of Coal Geology* **1998**, *35* (1), 57–82 DOI: 10.1016/S0166-5162(97)00008-6.

[16] Kissell, F.N.; Chapter 1.—Facts About Methane That Are Important To Mine Safety. In *Handbook for Methane Control in Mining* Cincinnati. Kissell, F.N., Eds; NIOSH–Publications Dissemination: Cincinati **2006**; pp. 3.

[17] Krog RB; Schatzel SJ; Dougherty HN. Methane Emissions and Airflow Patterns along Longwall Faces and through Bleeder Ventilation Systems. *International Journal of Mining and Mineral Engineering* **2014**, *5* (4), 328–349.

[18] Schatzel SJ; Krog RB; Dougherty H. Methane Emissions and Airflow Patterns on a Longwall Face: Potential Influences from Longwall Gob Permeability Distributions on a Bleederless Longwall Panel. *Transactions of Society for Mining, Metallurgy, and Exploration, Inc* **2017**, *342* (1), 51–61 DOI: 10.19150/trans.8108.

[19] Mitchell, G.W. Longwall Mining. In *Monograph 12 - Australasian Coal Mining Practice*, **1986**, p. 340.

[20] Schatzel, S. J.; National Institute for Occupational Safety and Health; Pittsburgh Research Laboratory (National Institute for Occupational Safety and Health). *Guidelines for the Prediction and Control of Methane Emissions on Longwalls*; DHHS (NIOSH) Publication, No. 2008-114; Department of Health and Human Services, Centers for Disease Control and Prevention, National Institute for Occupational Safety and Health, Pittsburgh Research Laboratory: Pittsburgh, PA, **2008**.

[21] Tutak; Brodny. Predicting Methane Concentration in Longwall Regions Using Artificial Neural Networks. *International Journal of Environmental Research and Public Health* **2019**, *16* (8), 1406–1406 DOI: 10.3390/ijerph16081406.

[22] Sindelar, M.F. Review of Methane Monitoring and Automatic Shut-Down Regulations and Standards for Electrically Powered Underground Coal Mine Face Equipment. **2011**.

[23] Barsan, N.; Weimar, U. Fundamentals of Metal Oxide Gas Sensors. IMCS, **2012**, DOI 10.5162/IMCS2012/7.3.3.

[24] Liu X; Cheng S; Liu H; Hu S; Ning H; Zhang D. A Survey on Gas Sensing Technology. *Sensors (Switzerland)* **2012**, *12* (7), 9635–9665 DOI: 10.3390/s120709635.

[25] Operating Principle; https://www.figaro.co.jp/en/technicalinfo/principle/mos-type.html.

[26] GFG Instrumentation, AP 1018: Understanding catalytic LEL combustible gas sensor performance; http://goodforgas.com/wp-content/uploads/2013/12/AP1018_Combustible-sensor-performance_6_30_13.pdf.

[27] Khan, S.; Baliga, S. Infrared Technology for Fail-To-Safe Hydrocarbon Gas Detection; http://s7d9.scene7.com/is/content/minesafetyappliances/IR%20Gas%20Detection%20Technology%20White%20Paper.

[28] Ultraportable Gas Analyzers; http://www.lgrinc.com/analyzers/ultraportable/.

[29] LI-7700 Open Path CH4 Gas Analyzer; https://www.licor.com/env/products/eddy_covariance/LI-7700.html?gclid=EAIaIQobChMIofzJ8uGB6AIVg5OzCh3-1AMbEAAYASAAEgIKKfD_BwE.

[30] Taylor, C.; Chilton, J.; Zimmer, J. Use of a Test Box to Measure Response Times for Machine-Mounted Monitors. **2004**; https://www.cdc.gov/niosh/mining/UserFiles/works/pdfs/utbmrtmmm.pdf.

[31] Kissell, F.N.; Chapter 2.—Sampling For Methane In Mines And Tunnels. In *Handbook for Methane Control in Mining* Cincinnati. Kissell, F.N., Eds; NIOSH–Publications Dissemination: Cincinati **2006**; pp. 27.

[32] Taylor, C.; Chilton, J.; Martikainen, A. Use of infrared sensors for monitoring methane in underground mines. 12th U.S/ North American Mine Ventilation Symposium. **2008** ISBN 978-0-615-20009-5.

[33] Taylor, C. D.; Thimons, E. D.; Zimmer, J. A. Factors Affecting the Location of Methanometers on Mining Equipment. *Journal of the Mine Ventilation Society of South Africa* **2003**, *56* (1), 25–29.

[34] GX-3R Pro Five Gas Monitor; https://www.rkiinstruments.com/pdf/gx3rpro.pdf.

[35] Berkley, F.D. Ejectors Have a Wide Range of Uses. Petroleum Refiner, **1958**; https://www.graham-mfg.com/usr/pdf/techlibvacuum/25.pdf.

[36] HIH-4602-L Series; https://sensing.honeywell.com/sensors/humidity-sensors/HIH-4602-L-series.

[37] Quick Disconnect Thermocouples with Miniature Connectors; https://www.omega.com/en-us/sensors-and-sensing-equipment/temperature/sensors/thermocouple-probes/jmqss/p/TMQSS-125U-4.

[38] BWD Manifold Absolute Pressure Sensor; https://shop.advanceautoparts.com/p/bwd-manifold-absolute-pressure-sensor-ec7034/20971064-p?c3ch=PLA&c3nid=20971064-P&adtype=pla_with_promotion&product_channel=online&store_code=&gclid=EAIaIQobChMIvpuOgeq_5wIVBhgMCh3LcA9_EAQYASABEgJ0x_D_BwE&gclsrc=aw.ds.

[39] STC, 3S012-1/4A-2A-D-V 3S012 Direct Acting 3-Way Solenoid Valve; https://megadepot.com/product/stcvalve-3s012-1-4a-2a-d-v-3s012-24vac-din-coil-1-4-npt-0-115-psi-direct-acting-3-way-ss-solenoid-valve.

[40] ET-7217-10; https://www.icpdas-usa.com/et_7217_10.html.

[41] TinaWood 2PCS SSR-25DD Solid State Relay 25A 3-32V DC/5-200V DC (SSR-25DD x2); https://www.amazon.com/TinaWood-SSR-25DD-Solid-State-5-200V/dp/B07F3WGRP4/ref=sr_1_19_sspa?keywords=solid+state+module+ssr25dd&qid=1581710784&sr=8-19-spons&psc=1&spLa=ZW5jcnlwdGVkUXVhbGlmaWVyPUEzRVoyREtERlFZRTZBJmVuY3J5cHRlZElkPUEwNjA5NTM0M0dKNUZONEQ5OURZ.

[42] Intelligent RTD Thermocouple Temperature Transmitter 4-20mA Out; https://www.hicomponent.com/rtd-thermocouple-to-4-20ma-transmitter-converter.html?search=rtd.

[43] Ejector Solutions; https://www.offshore-technology.com/products/ejector-solutions/.

[44] DewMaster Chilled Mirror Hygrometer; https://edgetechinstruments.com/product/dewmaster-chilled-mirror-hygrometer/.

[45] Heise® Model Pte-1 Dual Display Lcd Handheld Digital Calibrator; http://ww.heise.com/products/calibrators/heise-model-pte-1-dual-display-lcd-handheld-digital-calibrator.cfm

[46] 1405-PK-100 Gill UltraSonic Anemometer; https://www.scientificsales.com/1405-PK-100-Gill-UltraSonic-Anemometer-p/989-4.htm.

[47] Madireddy, M. R.; Clark, N. N. Sequential Inversion Technique and Differential Coefficient Approach for Accurate Instantaneous Emissions Measurement. *International Journal of Engine Research* **2006**, *7* (6), 437–446.

[48] Clark, N.N.; Madireddy, M.; Schmid, N.A. Diffusion In Time Of Instantaneous Emissions Data, **2009**.

[49] Oliver, D.W. Implications of Sampling Methods on Geospatial Mapping of Methane Sources. MS Thesis, West Virginia University, Morgantown, WV, **2019**.

[50] Sensors Inc. Home Page; http://www.sensors-inc.com/.

10.0 Appendices

10.1 Appendix A:

MATLAB® Code For Ejector

```
P1 = (70+14.7)*6894.76; % water inlet pressure (Pa)
P2 = (-14.7+14.7)*6894.76; % suction chamber pressure (Pa)
P5 = (0+14.7)*6894.76; %discharge pressure (Pa)
Qp = 2/60000; %water volumetric flowrate (m^3/s)
Qs = 5/60000; %air volumetric flowrate (m^3/s)
den_p = 1000; %water density (kg/m^3)
den_s = 1.225; %air density (kg/m^3)
vis_p = 1.004*10^-6; %kinematic viscosity of water (m^2/s)
vis_s = 15.12*10^-6; %kinematic viscosity of air (m^2/s)
p_v = 2333.141; %vapour pressure of water at 20degC (Pa)
M = Qs/Qp;
N = (P5-P2)/(P1-P5);
eff = M*N;
C = den_s/den_p;

%% 1st Iteration
%Approximations for loss coefficients
kp = 0.05;
ks = 0.1;
km = 0.19;
kd = 0.12;

%Solving for R
a1 = (1+C*M)*(1+M)*(1+km+kd);
syms R_sym
eq = R_sym^4*a1*(N+1)+2*R_sym^3*((N+1)*(C*M^2-a1-1))-R_sym^2*((N+1)*(2*C*M^2-
a1-4)...
    -C*M^2*(1+ks)-N*(1+kp))-2*R_sym*((N+1)+N*(1+kp))+N*(1+kp);
sol = vpasolve(eq,R_sym);
R = 0.30580935919369753100849504369378;

N0 = (2*R-R^2*(1+km+kd))/((1+kp)-2*R+R^2*(1+km+kd));
a = ((2*C*R^2)/(1-R))-C*R^2*(1+km+kd)-C*(R/(1-R))^2*(1+ks);
b = -R^2*(1+C)*(1+km+kd);
c = 2*R-R^2*(1+km+kd);
M0 = (-b-sqrt(b^2-4*a*c))/(2*a);

An = Qp*(((1+kp)-C*(1+ks)*(M*R/(1-R))^2)/((P1-P2)/(0.5*den_p)))^0.5; %nozzle
cross-sectional area(m^2)
Dn = sqrt(4*An/pi()); %nozzle diameter (m)
Dn_inch = Dn*39.3701; %nozzle diameter (in)
Am = An/R; %mixing chamber cross-sectional area(m^2)
Dm = sqrt(4*Am/pi()); %mixing chamber diameter (m)
Dm_inch = Dm*39.3701; %mixing chamber diameter (in)
Lm = 7*Dm;

Mc = ((1-R)/R)*(((P2-p_v)*An^2)/(0.5*den_p*C*1.35*Qp^2))^0.5;
```

```
P2min = 0.5*den_p*C*1.35*((Qp/An)*(M*R/(1-R)))^2 + p_v;
Re_p = Qp*Dn/(An*vis_p);
Re_s = Qs*(Dm-Dn)/((Am-An)*vis_s);

%% Second Iteration
%Approximations for loss coefficients
kp = 0.08;
ks = 0.7;
km = 0.27;
kd = 0.12;

%Solving for R
a1 = (1+C*M)*(1+M)*(1+km+kd);
syms R_sym
eq = R_sym^4*a1*(N+1)+2*R_sym^3*((N+1)*(C*M^2-a1-1))-R_sym^2*((N+1)*(2*C*M^2-
a1-4)...
    -C*M^2*(1+ks)-N*(1+kp))-2*R_sym*((N+1)+N*(1+kp))+N*(1+kp);
sol = vpasolve(eq,R_sym);
R = 0.264890663185002241407331859042222;

N0 = (2*R-R^2*(1+km+kd))/((1+kp)-2*R+R^2*(1+km+kd));
a = ((2*C*R^2)/(1-R))-C*R^2*(1+km+kd)-C*(R/(1-R))^2*(1+ks);
b = -R^2*(1+C)*(1+km+kd);
c = 2*R-R^2*(1+km+kd);
M0 = (-b-sqrt(b^2-4*a*c))/(2*a);

An = Qp*(((1+kp)-C*(1+ks)*(M*R/(1-R))^2)/((P1-P2)/(0.5*den_p)))^0.5; %nozzle
cross-sectional area(m^2)
Dn = sqrt(4*An/pi()); %nozzle diameter (m)
Dn_inch = Dn*39.3701; %nozzle diameter (in)
Am = An/R; %mixing chamber cross-sectional area(m^2)
Dm = sqrt(4*Am/pi()); %mixing chamber diameter (m)
Dm_inch = Dm*39.3701; %mixing chamber diameter (in)
Lm = 7*Dm;
Lm_inch = Lm*39.3701;

Mc = ((1-R)/R)*(((P2-p_v)*An^2)/(0.5*den_p*C*1.35*Qp^2))^0.5;
P2min = 0.5*den_p*C*1.35*((Qp/An)*(M*R/(1-R)))^2 + p_v;
Re_p = Qp*Dn/(An*vis_p);
Re_s = Qs*(Dm-Dn)/((Am-An)*vis_s);

%% Geometry recommendations
%Primary Nozzle
    %Nozzle shape = concave external contour (quarter ellipse profile)
    %if nozzle must be conical, nozzle angle = 16-20 degrees
    %No sharp edges in the external profile
    %should have as thin a tip as possible
%Secondary inlet and mixing chamber inlet
    %bell-mouth inlet to mixing chamber recommended
%Primary nozzle exit to mixing chamber entry spacing
    %maximum efficiency is found with the nozzle in the plane of the mixing
chamber entrance (s = 0)
    %to prevent cavitation, recommended s = Dn
%Diffuser
    %recommended angle = 6 to 8 degrees for optimum efficiency
    %The diffuser included angle should not exceed 14 degrees
```

```
    %The ratio of the diffuser outlet area to its inlet area should not be
greater than 5
    %trumpet-shaped diffusers were found to provide markedly higher
efficiencies than conical
        %diffusers of the same length and outlet-to-inlet area ratio
    %The junction between the mixing chamber exit and the diffuser inlet
should be radiused
```

10.2 Appendix B:

Engineering Drawing For Ejector

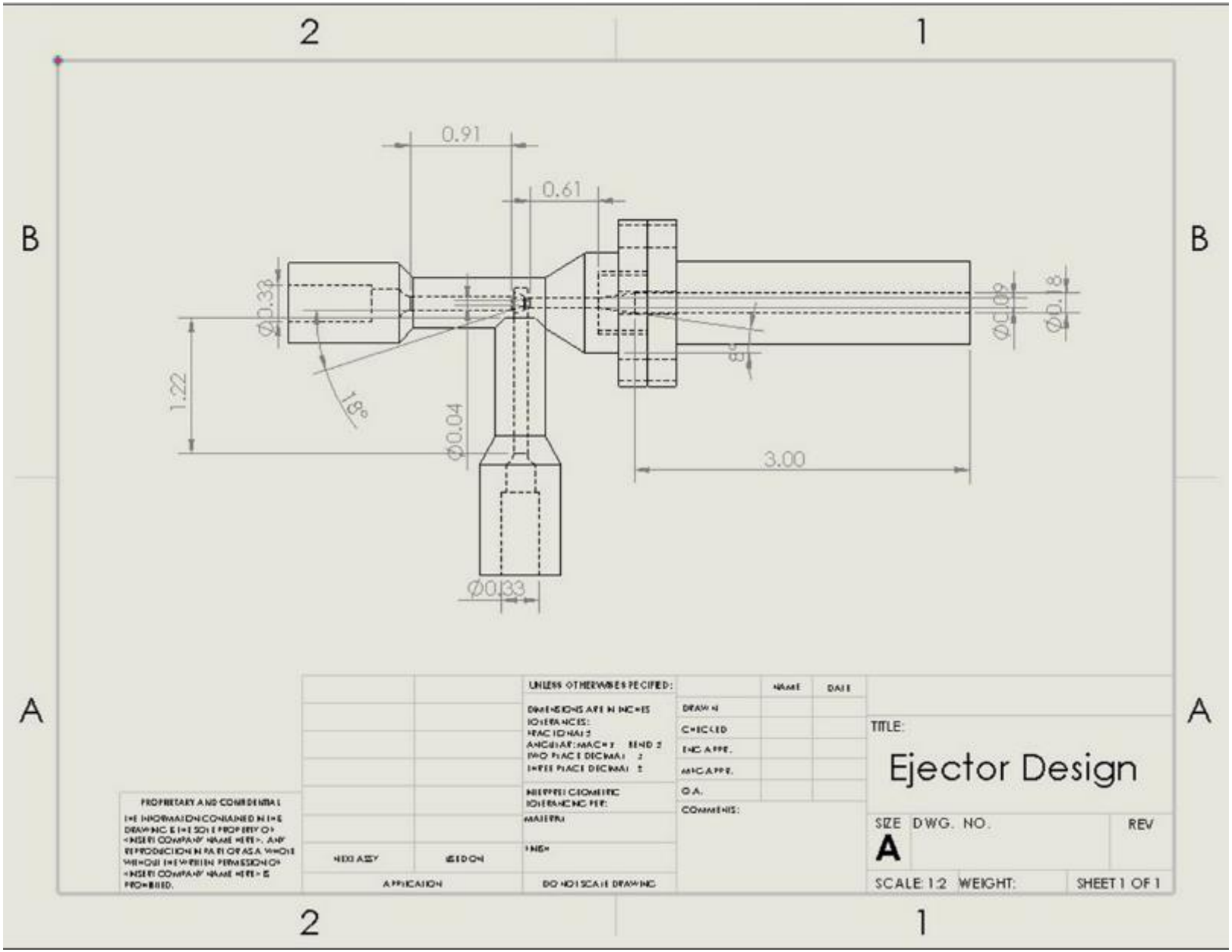
2
1
B
A
0.91
0.61
Ø0.38
1.22
18°
Ø0.04
Ø0.33
3.00
8°
Ø0.09
Ø0.18
UNLESS OTHERWISE SPECIFIED:
DRAWN
CHECKED
ENG APPR.
MFG APPR.
Q.A.
COMMENTS:
NAME
DATE
TITLE:
Ejector Design
SIZE
A
DWG. NO.
REV
SCALE: 1:2
WEIGHT:
SHEET 1 OF 1
PROPRIETARY AND CONFIDENTIAL
NEXT ASSY
USED ON
APPLICATION
DO NOT SCALE DRAWING

10.3 Appendix C:

Methane Watchdog System Invention Disclosure

WEST VIRGINIA UNIVERSITY OFFICE OF TECHNOLOGY TRANSFER **Phone** 304.293.7539 **Fax** 304.293.3224 **Email** TechnologyTransfer@mail.wvu.edu	*Submit the complete **hard copy** of this invention disclosure with **wet-ink signatures** along with the assignment form with **notarized wet-signatures** to:* Office of Technology Transfer PO Box 6224, Rm 721 886 Chestnut Ridge Rd Morgantown, WV 26506-6224	**WVU OTT Use Only**		
		File No.	**Date Submitted**	**Date Enabled**
			11/26/2019	

WEST VIRGINIA UNIVERSITY INVENTION DISCLOSURE AND ASSIGNMENT FORM

Shaded Fields Indicate a Required Entry	Further instructions are available at: https://techtransfer.research.wvu.edu/forms

A. TITLE OF INVENTION

Provide a brief (5 to 10 word) description of the invention:

Methane Watchdog System, A Cost-Effective Approach to Longwall Methane Monitoring and Control

B. INVENTOR(S)

Provide the following information for each inventor. Percent (%) Contribution from all inventors must add up to 100%. Percent (%) Contribution will be used to determine future royalty disbursements that may result from this invention disclosure.

	Inventor 1 (Lead)	**Inventor 2**	**Inventor 3**	**Inventor 4**
Name:	Derek Johnson, PhD, PE	Nigel Clark, PhD	Amber Barr	Brian Cappellini
Title:	Associate Professor	Research Professor	Graduate Research Assistant	Graduate Research Assistant
Department:	MAE	MAE	MAE	MAE
College or External Affiliation:	Statler	Statler	Statler	Statler
Work Phone:	304-293-5725	304-293-6547	--	--
Work Email:	derek.johnson@mail.wvu.edu	Nigel.clark@mail.wvu.edu	apb0002@mix.wvu.edu	bcappel1@mix.wvu.edu
Residential Address (No PO Box):	313 Pentress Road Pentress, WV 26544	362 Old Lock 13 Rd Morgantown, WV 26501	418 Lloyd Rd. Summit Point, WV 25446	1019 Deerwood Drive Morgantown, WV 26508
Home Phone:	304-216-6592	304-290-4004	304-376-4202	304-322-0699
Citizenship:	US	US	US	US
% Contribution:	35	35	15	15

C. ESTABLISHMENT OF INVENTION AND PUBLIC DISCLOSURE HISTORY

Provide the following information to establish the invention and its public disclosure history:

	Date	Location	Brief Description (i.e. who, what, how)
Invention Conception:	February 2018	Morgantown, WV	Nigel and Derek were notified of Alpha Foundation funding opportunity. We were requested to work with mining folks on proposal. However, Nigel and I developed the basic approach for a multi-nodal sampling system. (Words of Johnson)
Proof of Concept Established/Experimental Evidence of Invention:	Ongoing		
Planned Contract/Grant Submission(s):	March 5, 2018	Morgantown, WV	WVU RC Submission to Alpha Foundation.
First Public Disclosure(s):			Proposal above and interim report (Appendix A, Appendix B)
Upcoming Public Disclosure(s):		Morgantown, WV	1.) Possible demonstration, meeting with industry – November 2019-March 2020 2.) Final Report no later than March 31st, 2020 3.) Possible discussion, seeking level of interest – integration into Komatsu mine shields (letter of support provided, interested in "learning more"

D. SPONSORSHIP

Was the invention conceived or reduced to practice in the performance of or relating to the subject matter of a grant or contract?

Yes ☒ No ☐ *If yes, list below. Add more rows if necessary.*

Sponsor	Contract No.	Principal Investigator	WVU Grant ID No.	WVU OSP No.	Title
Alpha Foundation	CK #1023304	Derek Johnson	10023249..1007816R	18-680	Methane Watchdog System, A Cost-Effective Approach to Longwall Methane Monitoring and Control

E. SUMMARY OF INVENTION

1. Briefly <u>state the problem solved</u> by the invention:

Methane in coal mines may be released locally, particularly near the cutting head of mechanical mine machinery (typically a longwall arrangement) or from gob in a zone which has already been mined. There is an urgent need to stop production if an explosive pocket of gas is produced in an area where a cutter may be an ignition source. As an alternative to stopping production, the explosive gas may be diluted and made safe by enabling local air movement with extractors or fans or increasing ventilation. However, fixed gas monitors measure a more averaged concentration for general ventilation, and personal samplers are intended for use over a shift and move with the worker. The proposed system measures methane concentrations at reference locations, such as near a cutter head or in the future path of a cutter. The measurement system is reliable, robust and continuous

and can be interfaced directly with control systems to stop operations in an automated fashion. The system reduces the likelihood of mine fires, mine dust explosions, and worker injury or death. The approach may be extended to the measurement of concentrations of other gases in other hostile industrial environments. Accompanying the hardware of the invention, and as part of the overall method, software can be used for go/no-go decision-making, and through its intelligence, solving the added problem of ceasing production unnecessarily.

The invention is an outcome of a project funded by the Alpha Foundation, and the originating proposal is attached as Appendix A.

2. Briefly state what was invented. Is the invention a composition of matter, article of manufacture, machine, or process? How does the invention solve the problem described above? Why is the invention important and useful?

It is a method and apparatus for rapid, reliable measurements of methane concentration in a hostile environment, in one embodiment to avoid larger gas or coal dust explosions, but with broader applicability for safety applications.

3. Briefly describe how the invention differs from existing technology. Identify and expand on all its novel and unusual features. What obstacles associated with the prior art does the invention overcome? What advantages over the prior art does the invention possess?

The current embodiment, with subsystems already demonstrated at WVU (see photographs throughout), uses a sample tube to draw from the sampling point (node) and send it to an enclosed sensor or sensors, so that the sensor package (sampling unit) can be located remotely from a very hostile environment. Flow through the sample tube is drawn by a vacuum produced by an eductor or ejector, using water pressure as the driving energy source. This is an explosion-proof method of drawing the sample, and simpler pumps might be used in less hostile environments for applications beyond mining. Several sampling tubes drawing from different locations (nodes) can feed one sensor package via a sequential collector, and the sampling unit may contain multiple sensors for redundant measurement, or for optimal measurement at different ranges of concentration. Existing technology is worn on a miner's uniform, and not intended for applications close to the cutting head, where there is high vibration, water sprays and flying material. [see https://www.rkiinstruments.com/product-category/portable-gas-monitors/] Other existing technology is available packaged in hardened enclosures, but seeks to measure average methane in the environment for compliance, and is not located close to the cutter head or other areas prone to higher methane concentrations. Existing technology is not configured for rapid response to small pockets of explosive gas concentrations or usually involves methane and products of combustion around electrical and belt installations."
[https://www.cdc.gov/niosh/mining/topics/AtmosphericMonitoring.html] [See also commercial products: https://www.rkiinstruments.com/product-category/fixed-systems/]

F. PRIOR ART

1. Discuss how the problem the invention solves was addressed or solved previously. Identify and discuss the inadequacies and limitations of previous approaches and/or solutions. Attach the results of any literature searches and identify relevant references.

The Alpha Foundation, who sponsored this WVU research and development, saw the need for "Innovative Methods of Methane Detection near the Face and De-energizing the Longwall Equipment" as an identified topic. Currently, MSHA regulations require that only one methane monitor be mounted on the longwall shearer in a longwall face. The location of the monitor in a typical longwall face setting could be between 5 and 10 ft. away from the coal face and is unable to detect the zones of higher methane concentrations (near the front shield tip or near the rear of the shield), possibly explosive in nature. Therefore, current methane monitoring methods and equipment are geared toward MSHA compliance rather than local measurement.

A NIOSH document presents the monitoring basics.[https://www.cdc.gov/niosh/mining/topics/AtmosphericMonitoring.html]

A review by Kumar et al. [https://pdfs.semanticscholar.org/3893/86267931eb9ae03f4a06e71b24eb76d20d49.pdf] reviews gas detecting sensors. The current invention employs sensors as a component but does not seek to advance the sensor technology itself.

Numerous patents exist addressing methane collection or abatement, and these are not relevant.

US Patent 6,168,240 presents methane detection near the cutter of a continuous miner, and has only one independent claim, which limits application to a continuous miner and to other, specific details.

US Patent 3,683,255 describes a hydraulic drive that produces DC power for a monitoring system and does not reflect the current invention.

There are no relevant patents employing eductors or ejectors to move the methane to a sensor.

US Patent 10,089,848 addresses mine gas monitors but incorporates wireless communications as the core claim.

US Patent 8,692,997 claims a chamber, optical measurement channels, and radiation sources and detectors: it is substantially different from the present invention.

US Patent 5,611,844 draws a sample of landfill gas through a tube, but then passes it through tetraglyme for absorption: it is not relevant.

The string "methane AND concentration AND (Explosion OR explosive) AND (Mine OR Mining) AND (eductor OR Ejector)" for all fields in US PTO has yielded nothing relevant. Compared to most searches, the prior patent landscape seems vacant.

A 2006 CDC publication [https://www.cdc.gov/niosh/mining/UserFiles/works/pdfs/2006-127.pdf] presents some basic information that teaches towards certain aspects of the present system. "Restricted-space measurements can be made in two ways. First, the methane detector can be equipped with a remote "sample draw" capability. These use a small pump or hand-squeezed bulb to pull the sample through an extension probe and pass it through the detector. Some methane detectors have an accessory sampling pump that attaches to the detector; others have a built-in pump." "Machine-mounted methane monitors are mounted on certain types of mining machinery and operate continuously. These monitors are certified under 30 CFR 27, which has different requirements than the Part 22 used for portable detectors. The Part 27 requirements include a design that prevents the mining equipment from operating unless the methane monitoring system is functioning, a warning device that activates when the methane concentration is above 1.0%–1.5%, and a means to shut off power to the equipment when the methane concentration is 2.0% and above." However, several aspects of the present design are not addressed.

2. Provide a list of key words relevant to the invention that would be helpful in a prior art search:

(Coal Mine, Longwall, Cutter) PLUS (Methane, Ignition, Explosion, Ventilation) PLUS (Sampler, Controller, Ejector, Eductor, Sensor)

G. DETAILED DESCRIPTION OF INVENTION

Provide a detailed description of the invention that illustrates or demonstrates its utility. This description must provide enough detail such that a person having ordinary skill in the art can make and

use the invention. Provide support in the form of figures, data, results and/or attachments of relevant white papers as appropriate.

The proposal to Alpha Foundation is attached to describe the broad detail originally conceived [Appendix A]. Presented below are a general specification, description of a present embodiment, and draft claims.

Methane Watchdog System, A Cost-Effective Approach to Longwall Methane Monitoring and Control

Background

Fires and explosions are still the most feared hazards in underground coal mines. Thirteen of 15 coal mine disasters (i.e., accidents with 5 or more fatalities) since 1980 are resulted from fires and explosions[1]. The most recent coal mine disaster in the U.S. occurred at Upper Big Branch Mine where 29 miners lost their lives nearly instantly because of an explosion initiated by methane ignition near the tailgate of the longwall face that intensified with the participation of coal dust. Therefore, methane still presents hazardous conditions in the longwall faces where the coal is cut, loaded, and transported in much higher production rates than other mining methods used in the coal industry. In many cases, although the suspended coal dust may be explosive, or a lean mixture may be close to an explosive limit, there is no catastrophic even because a strong ignition source is required to ignite the atmosphere. Ignition of a localized pocket of richer gas can ignite a surrounding mixture. Currently methane concentrations are detected with stationary or portable handheld instruments that typically work on the principle of catalytic oxidation. The current federal standard mandates that methane concentrations be controlled under 1.0% in any active part of underground mine other than the bleeder system where up to 2% is allowed. In all working faces, powered equipment should be de-energized when 1.0% methane is detected while electric power should be disconnected when 1.5% methane is present. Details on mine air requirements are set forth in the Code of Federal Regulations (CFR) Part 30 Section 75. Concentrations are checked at different locations periodically by workers and/or foremen. Currently, for longwall operations, industry also relies on a single methane sensor located in the middle of the shearer. Note that methane is explosive in air between 5 and 15% by volume.

Though these hazards exist, longwall mining in underground coal mines is considered the safest and most productive mining method. However, due to its high productivity, the methane emissions from the large newly exposed coal face and from the gob area are often excessively high. As the longwall panels become wider (with the widest currently being 1,600 feet) and longer, the total amount of methane emitted from the longwall panel tends to increase proportionally with the area of the panel. To improve mine safety, Alpha Foundation has funded researchers at West Virginia University (WVU) to develop the innovative Methane Watchdog System (MWS).

Embodiment – Specific design executed by WVU researchers

[Although in the future tense, substantial portions of the system that is described below have already been built and verified. A multiple nodal system is currently installed in a test tunnel at the WVU Reedsville Farm.]

We are developing an innovative Methane Watchdog system, which will deploy a low-cost, multi-nodal methane measurement network to ultimately improve the health and safety of longwall coal mining operations. The system and its major components can be found in the schematics of Appendix C. The proposed system will employ a reliable and durable nodal methane-sensing network to monitor methane concentrations and velocity continuously along the full length of the longwall face. The system will measure, record, and report on discrete methane concentrations in nearly real time, along the front and rear ends of the canopy of the shields. The measured methane concentration distribution along the front tips of the shield canopy can be used as an algorithm input to decide whether the shearer should be de-energized before advancing into potentially

[1] Test Preparation Study Guide for Coal Mine Certification, https://laborcommission.utah.gov/media/pdfs/boilerelevatormine/pubs/Fire%20Boss.pdf

explosive methane-air pockets. The methane concentration distribution along the rear end of the shield canopy (the front edge of longwall gob) and its development trend over time will enable the development of an improved ventilation plan. In addition, historical data on methane emissions can be used as a new metric by which to develop mining operations for improved safety. The historical data can also be used to train a strategy or configure data management software to increase the reliability of prediction for a specific mine or longwall application. An example of the multi-nodal system is shown in Figure 1.

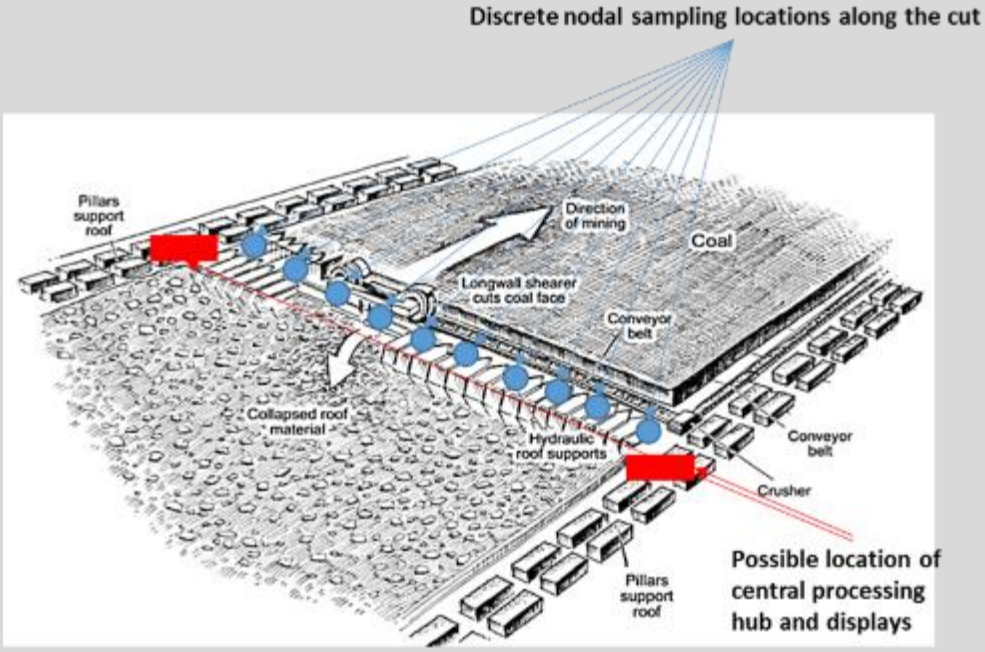

Figure 1: Example distribution of a multi-nodal sampling approach.

System Details

The current approach is to deploy a central processing hub (CPH) which has connectivity with each of the sampling units. The sampling units are distributed along the length of the longwall from the headgate to the tailgate. The current CPH is a robust industrial computer which can communicate with each node though ethernet cables. (Note: The longwall shields themselves have long been basic systems but are now becoming automated and include a variety of controls, electronics and proximity sensors).
The input signals are processed with necessary calibrations and parameters can be displayed on the user interface. The CPH is capable of outputting digital signals that can be used to control the sampler at each node and to de-energize mining equipment or else to activate intermittent ventilation or air handling equipment, or both. The CPH is also capable of storing historical data on internal or external solid-state devices for additional processing. The current CPH is a touch screen version that can be mounted through a NEMA approved enclosure. The CPH is currently used as the energy distribution system. The current system is powered with 24 VDC. Note the final system would likely use 12 VDC since all current mine shields have a common 12 VDC power network, our choice of 24 VDC was solely used to reduce current draw for testing. Figure 2 shows an example of the CPH and touch screen interface. Note that power and communication umbilical cords exit the enclosure for series distribution to the remote nodal samplers. (This mimics the shield to shield umbilicals used for hydraulic fluid, water, and power).

Figure 2: CPH for collection of nodal signals, conversion to engineering units, system control, and power supply.

The prototype system includes 10 sampling units, each capable of sampling from two discrete nodes. The number of sampling units (and nodes) could be expanded to suit an application. The goal of the sampling units is to provide discrete, fast response methane concentrations (not just detection at a threshold) at multiple planes along the long wall system. The sampling units can be easily integrated into new shield designs or retrofitted into current mine shields. Sampling units can be either evenly distributed or placed at specific locations of interest and correlated with shield identification number. Figure 1 shows an example of an equally space system. The goal of the multi-nodal approach is to enable continuous sampling at multiple locations to improve mine safety as opposed to current single point or intermittent measurement approaches. Information from each sampling unit may be considered singly or employed as input to a model or algorithm that determines the necessity for ceasing production or increasing ventilation.

There are numerous options to measure the methane concentrations at these discrete points. Some sensors and analyzers include catalytic bead sensors, metal oxide sensors (such as the MQ-4), infrared sensors (such as the Dynament), flame ionization detectors, and multiple spectroscopy systems including those using Fourier Transform IR, wavelength modulation, and off-axis cavity integration. Note that some sensors such as the MQ-4 and Dynament are impacted by higher hydrocarbon species (such as propane) but methane is the predominate species encountered in mining operations. Moreover, higher hydrocarbons contribute to overall flammability too, and often are more easily ignited than methane. The current system deploys both the MQ-4 and Dynament sensors. Each sampling unit is capable of sampling from multiple locations (discrete nodes) using an intermittent sampling strategy. The current approach enables the sample to be drawn in from a node near the front or rear of the shields. Therefore, the current system can provide methane concentration measurements from 20 locations (2 nodes per sampling unit).

Most methane sensors are passive devices that provide methane concentration at a single location, when the sample contacts the measurement elements. The Methane Watchdog System approach places the methane sensors in a sensor block housed within a NEMA enclosure (the sampling unit) at the mid span of the longwall shield. A method to draw in the sample is used to transport the sample from the node to the sampling unit and subsequently into the sensor block. Several methods exist to transport the sample. The original system was to

use an air powered ejector/eductor to induce a negative pressure within the sampling system. Such a method could be deployed if compressed air were available. Common to mining operations is the use of water for dust control, cooling, and other operations. We have designed a water powered ejector/eductor that can induce negative pressures to enable sampling. Due to laboratory limitations driving liquid pressures were limited to less than 100 PSIG. In discussion with industry the water distributed among the shield to shield network can be upwards of 400-1000 PSIG. Such high pressures could significantly improve ejector/eductor design enabling a more efficient design, reduced water flow, or further reduction in delay time (node filter entrance to sensor body). Other methods could include nodal pumps or a central pump (vacuum source) and manifold system.

Each sampling unit includes data acquisition capabilities to receive digital or analog sensor outputs. In addition, the DAQ systems can use "digital" analog outputs to control relays or valves. In the current design, the sampling unit controls a relay which then controls a three-way valve (or else two solenoid valves may be used). In the normally open position, the valve enables sampling from the face (shield tip), and in the closed position samples from the rear (gob area). Each sampling leg includes a filtration system at the node. A filtration system and its components ensure water droplets and coal dust are removed before entering the sampling tubes and sensor block where sensors are installed. Choice of filtration involves a competition between the desire for low dead volume (fast response), low pressure drop (best use of eductor) and efficacy of protective filtration.

While this active approach of delivering a sample to the central location from multiple locations has durability and simplicity benefits, it induces sampling delays and some sample diffusion effects. These impact the overall system response and can be modified in order to ensure acceptable frequencies. A sampling delay is induced based on the sampling flow rate (induced by eductor vacuum) and the equivalent lengths of tube, filtration system, and sensor block. Diffusion (mixing) can occur at both the filtration system and within the sensor block due to increases in equivalent volumes (decreases in velocity). Methods exist to create sharpened responses from signal inputs and two of the current inventors, Drs. Clark and Johnson, have deployed such methods in other systems. To reduce sampling delay times, the sample flowrate can be increased by modifying the ejector or pump system. The current system targets a sample flowrate of 1-2 standard liters per minute through a 1/8" nominal diameter sampling train. This facilitates delay times of only a few seconds. Combined with diffusion and sensor response, the total system response currently varies from around 30-60 seconds which when combined with multiple nodes, can still significantly improve mine safety. Embellishments and improvements (reducing the number of sources feeding a sensor, increasing flowrate with higher eductor energy, reducing pressure loss with larger diameter tubing) can reduce the delay to a few seconds.

Longwalls can now be well over 1000 ft and if a system included only 10 nodes the resolution would be 100 ft. The velocities of shearers range from 33-98 ft per minute (0.55-1.63 ft/s). Assuming an average of 1 ft/s, the system would still be capable of informing operators or systems ahead of entry into a high methane pocket. For this example, with a delay time of 60 seconds, the operator would still be 40 ft before the detected methane pocket.

Figure 3 shows a labeled cross section of the sensor block (see #17 in schematic) and Figure 4 shows the internals of a complete sampling unit (see #5 and #16-40 of schematic). In the current version, there is a single outlet (# 34) that would be connected to the ejector/eductor. The ejector/eductor would provide the motive power and negative pressure to draw samples to the sensor block. A three-way valve (#16) is controlled by a DC/DC relay (#37) and on/off output from the DAQ. The valve is either timer based or user selectable. There are two inlets (#32 and 33) that can be connected to sampling tubes/lines which run to the front and rear of the roofing support system (shields/canopy).

The sample first passes inside of a shielded dead volume to prevent entrainment of water droplets and large particles (in #6). It then passes through the filter media (in #6) to remove fine coal dust. The filters are oversized in order to ensure minimal pressure drop over continuous operation for 1 month. The sample then continues to the three-way valve (#16) and into the sensor block (#17). The metal sensor block is grounded to the NEMA enclosure (Note: An MSHA approved system would require additional safety such as sealed and explosion proof enclosure, check valve, etc.). The sample passes through the block and is first exposed to a thermocouple and

relative humidity sensor (#31 and 28). These sensor outputs are connected to the DAQ channels and read by the CPH which converts the analog signals to engineering units for subsequent determination of absolute humidity. The sample is then exposed to an absolute pressure sensor (#29). However, a differential pressure sensor could be deployed. In either case, the pressure sensor output voltage is measured with a DAQ channel and converted to engineering units within the CPH. The pressure sensor can be used in concentration corrections, absolute humidity calculations, and to either estimate flow rate and/or filter loading. In the current version, spare DAQ channels exist and could be used for additional pressure and flow sensors for monitoring flow conditions. (Note: We have recently obtained cost effective thermal mass flow meters for the 1-10 SLPM range and have already included their signal within the prototype system. The sensors are placed after the sensor block and prior to the eductor/ejector port).

The sample is then exposed to a sealed MQ-4 sensor (metal oxide sensor) (#30). The output voltage is measured with a DAQ channel and the output voltage is converted to a concentration of methane (by volume). Data can be presented as (parts per million – ppm) or on a volume basis (% which is common in the mining industry). This conversion is a multi-step process discussed below.
The sample is finally exposed to the Dynament IR sensor (#35) which also has a 0-5V analog output which is measured with a DAQ channel. It undergoes similar conversions to present methane concentration by volume. Each sensor can be calibrated individually. Depending on the primary methane sensor selected different corrections or calibrations are used as each sensor has its own unique responses to methane, other or interference gases, temperature, pressure, and humidity. An example of the calculation is shown in Equation 1, where each independent variable is presented as a K factor for adjustment.

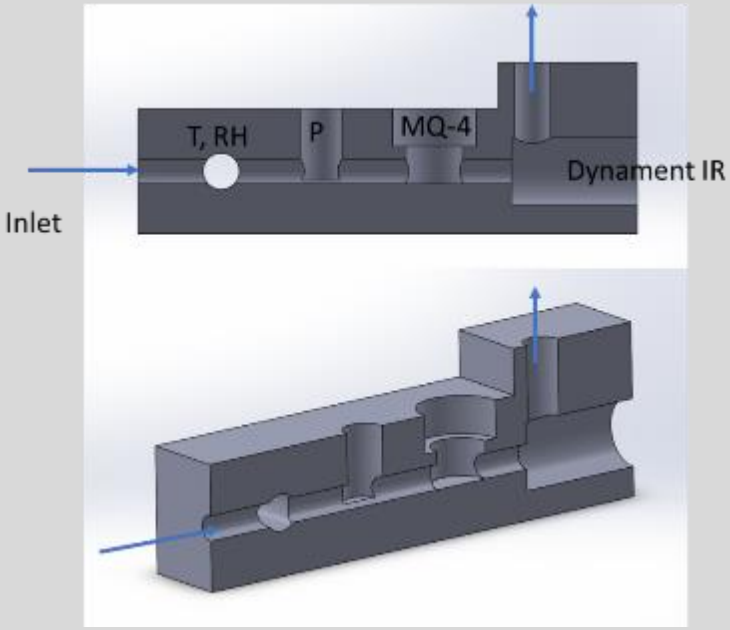

Figure 3: Sensor block for each sampling unit. The sample passes over key measurement sensors before being expelled from the unit.

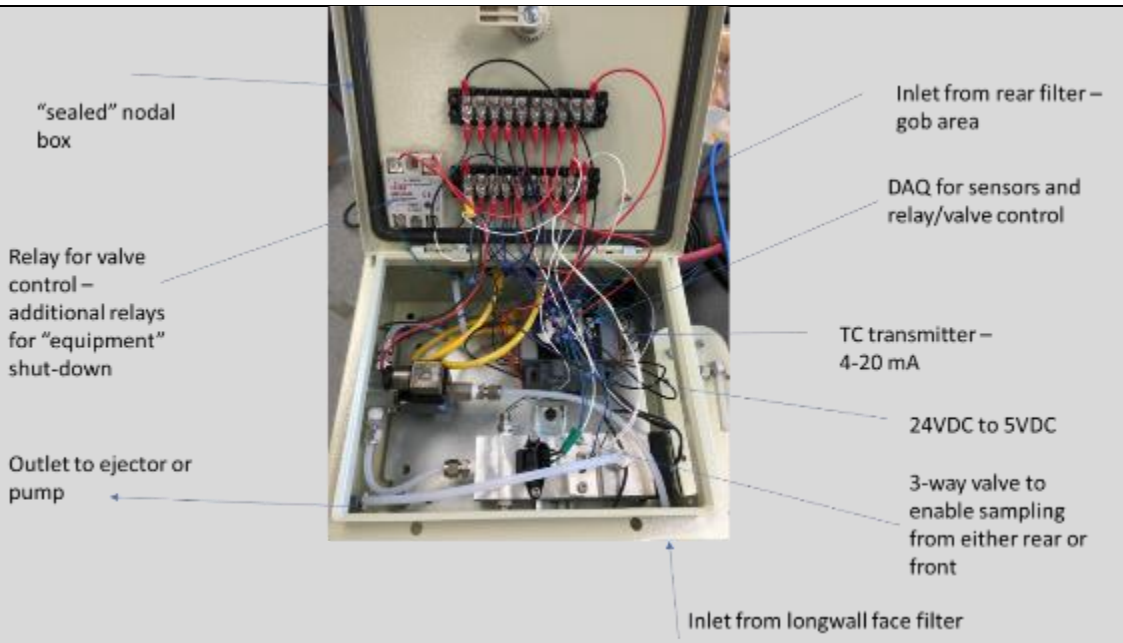

Figure 4: Sealed box of the sampling unit which includes all sensors and data acquisition equipment.

$$CH4\ (ppm) = V * Kcal * Ktemp * KH * K_P \qquad \text{Equation 1}$$

Capabilities/Benefits

- Enable continuous monitoring of methane concentrations
- Alert (visually/audibly) when methane exceeds 1.0% (1.5% for disconnection)
- Control relays to disable equipment, disconnect/isolate high voltage, operate fans or ventilators, sound alarms
- Enable remote monitoring of concentrations up to 1-5% for continued data collection after a methane event
- Only a single moving part per unit (if dual sampling point are used – else none)
- Includes anemometers to monitor ventilation air velocity at multiple points – continuously
- Estimate methane liberation rates and their trends for accurate prediction and modeling support
- Advanced model-based control could be used in addition to the "digital" on/off at 1.0 and 1.5%
- Records historical data on methane liberation rate, methane concentration and mine conditions
    - Used by industry for design
    - Used by regulators for guidance
    - Used by researchers
- Solid state main and backup drives
- Ability to communicate with other equipment, sensors, etc.
- Likely to develop into obligatory equipment through government rules or industry expectation

Comments on specification

The invention can be broadened in application to include a variety of industrial situations where an ignition source either potentially exists or is measured to exist at that point in time. As an example, monitors could exist to exclude mobile equipment such as forklifts from certain areas if those areas have elevated flammable gases present. It can also be broadened to include any style of pump rather than an eductor.

Straw Claims

1) A sampling and measurement method to quantify the concentration of hazardous or explosive gas in a deep mine atmosphere
wherein a sample is drawn from at least one first location by means of a tube or tubes
and wherein each sample is delivered by a tube or tubes to a volume within a sensor block at a second location
and wherein the sensor block incorporates at least one gas concentration sensor in communication with the volume
and wherein a vacuum is applied to the volume within the sensor block to facilitate flow of the sample to the second location

2) The method of claim 1 where the vacuum is derived from an eductor or ejector enabled by a supply of pressurized water or air

3) The method of claim 1 where the sensor block (#17) contains multiple similar sensors to assure functionality through redundancy

4) The method of claim 1 where the sensor block contains more than one type of gas concentration sensor, wherein each type is capable of measuring a different gas concentration range

5) The method of claim 1 where multiple tubes feed samples to the sensor block at the second location from multiple first locations

6) The method of claim 1 where a particulate trap or filter (within #6) is employed to prevent undesirable ingress of contaminants into the mouth of each tube at each first location

7) The method of claim 5 where one or more remotely controlled valves (#16) enable the selection of sampling tubes that feed sample gas to the sensor block at any point in time

8) The method of claim 7 where the valves are consolidated in a rotary valve body at the second location

9) The method of claims 2 and 5 where the quantitative vacuum, diameter of one or more tubes, diameter of one or more tubes and volume of the sensor block are selected to facilitate rapid transmission of the sample from the first location to the sensor at the second location

10) The method of claim 1 where at least one gas concentration sensor output is conveyed to a central processing hub (CPH, #10)

11) The method of claim 10 where the CPH communicates the gas concentration

12) The method of claim 10 where the CPH provides an input to the controller of a longwall mining system

13) The method of claim 12 where the CPH commands stoppage of the operation of the longwall mining system when one or more measured concentrations of gas exceed a threshold level.

14) The method of claim 10 where the CPH provides a command to a means for moving air at a location in the mine

15) The method of claims 5 and 10 where the processor employs an algorithm and at least one time-varying signal
representing gas concentrations from at least one first location to establish a command.

16) The method of claim 1 where one or more nodes, situated between the first and second locations, serve to gather sample flows from one or more first locations and transmit those sample flows selectively to the second location.

17) A sampling and measurement method to quantify the concentration of hazardous or explosive gas in a deep mine atmosphere
wherein a sample is transmitted from at least one first location by means of a tube or tubes to a sensor block at a second location
and wherein the sensor block incorporates at least one methane concentration sensor in communication with the volume
and wherein at least one pump establishes at least one sample flow from a first location to a second location
and wherein at least one signal from at least one methane concentration sensor is transmitted to a CPH at a third location
and wherein that CPH alerts workers to a hazard and controls devices that abate the hazard and records all or part of the data that the processor receives

18) The method of claim 1 and claim 17 where the first locations are points on the canopies (shield, #15) of longwall mining machines

19) The method of claim 1 and claim 17 where the first locations are points juxtaposed with cutters on machines used to mine coal

Figure 5: Sequence of methane monitors installed in tunnel at WVU Reedsville farm, connected and integrated with the CPH (central data logger/controller).

Figure 6: CPH in WVU Reedsville Farm tunnel gathering data from multiple samplers installed in a sequence of locations.

H. COMMERCIAL POTENTIAL

In your opinion, what is the commercial potential of the invention? What kind of product(s) would be sold? Into what market(s)? By what kind of company? How soon?

US 9,810,066 presents a longwall mining apparatus and discloses that "The present disclosure is based in part on the realization that methods for controlling a shearer in an underground mine require a considerable amount of operator assistance due to unavailability and incompleteness of automated control methods. As the underground mine is a tough and hazardous environment bearing a plurality of risks for operators such as methane gas explosions, it is desirable to reduce the required underground operator assistance." Insofar as the proposed system can automate safety improvements, it will encourage adoption. Successful demonstration of the proposed safety system to government agencies (MSHA, OSHA), to industrial management, and to workers' advocacy groups will encourage rulemaking or adoption of the technology. There is also potential in teaming with a mining equipment manufacturer to improve safety and hence competitiveness of that manufacturer's equipment.

I. MATERIALS

Detail the sources of critical materials (e.g. raw materials, chemicals, cell lines, antibodies, constructs, etc.) used to develop the invention:

Purchases of industrial equipment and components and purchase of supplies for 3D printing (funding from Alpha contract)

J. STATE OF DEVELOPMENT

1. Has the invention been tested, used experimentally, used routinely, offered for sale, or provided to another individual or laboratory?

Yes ☒ No ☐ *If yes, explain:*	A system is located in a test tunnel on the WVU Reedsville farm

2. Was a prototype created? Were materials synthesized or isolated?

Yes ☒ No ☐ *If yes, explain:*	Prototypes were created of nodes, the CHP and the eductor - advanced prototypes integrated as in J-1

K. PARTNERSHIP WITH NON-WVU AFFILIATES

1. Was the invention disclosed in an oral presentation or discussed with another individual, collaborator, or interested party?

Yes ☒ No ☐ *If yes, provide disclosure recipients:*	Discussion amongst the research group and with WVU employees for its tunnel deployment

2. Will the invention be disclosed in an oral or written presentation or with another individual, collaborator, or interested party within the next 6 months?

Yes ☒ No ☐ *If yes, provide disclosure recipients:*	Reports to Alpha foundation

3. Were any materials used in the invention's development under the terms of a material transfer agreement, a non-disclosure agreement, an inter-institutional agreement, or other contractual agreement?

Yes ☐ No ☒ *If yes, provide agreement details:*	

4. Was the invention conceived or reduced to practice under contract with an outside party?

Yes ☒ No ☐ *If yes, provide contract details:*	Alpha Foundation project

5. Are any inventors under contract with an outside party that may affect commercialization of the invention?

Yes ☐ No ☒ *If yes, provide contract details:*	Email from Alpha Foundation Director – "The Alpha Foundation does not have any intention to retain intellectual property in any way. You are free to proceed to protect your intellectual property as you see fit." – See Appendix D.

L. NAME OF WVU ADMINISTRATOR(S)

1. Print the name(s) of the WVU departmental chair(s). Signatures are not needed.

Jacky Prucz	Mechanical and Aerospace Engineering
Printed Name	*Department*

2. Print the name(s) of the WVU college/school dean(s). Signatures are not needed.

Earl Scime	Statler College of Engineering and Mineral Resources
Printed Name	*College/School*

M. SIGNATURE OF INVENTOR(S)

I hereby declare that the details furnished above are true and correct to the best of my knowledge. For WVU-affiliated inventors, the invention is submitted pursuant to the provisions of the WVU Intellectual Property Policy, available at https://policies.wvu.edu/finalized-bog-rules/bog-governance-rule-1-5-intellectual-property-rule-for-patent-copyright-and-trademark-rights. A wet signature is required from all inventors.

Derek Johnson	11/18/19	
Printed Name	*Date*	*Signature*
Nigel Clark	* 11/22/2019	*
Printed Name	*Date*	*Signature*
Amber Barr	11/18/19	
Printed Name	*Date*	*Signature*
Brian Cappellini	11/19/19	
Printed Name	*Date*	*Signature*

WEST VIRGINIA UNIVERSITY RESEARCH CORPORATION
OFFICE OF TECHNOLOGY TRANSFER
RECORD OF CONFIRMATORY ASSIGNMENT
TO
WEST VIRGINIA UNIVERSITY
BOARD OF GOVERNORS
ON BEHALF OF
WEST VIRGINIA UNIVERSITY

WHEREAS,

Printed Name(s) of Inventor(s) ("Assignor(s)")	Residential Address (No. P.O. Box)
1. Derek Johnson	313 Pentress Rd, Pentress, WV 26544
2. Nigel Clark	362 Old Lock 13 Rd, Morgantown, WV 26501
3. Amber Barr	418 Lloyd Rd, Summit Point, WV 25446
4. Brian Cappellini	1019 Deerwood Dr, Morgantown, WV 26508

Assignor(s) has/have invented/created certain new and useful intellectual property with a working title of:

TITLE OF INTELLECTUAL PROPERTY

Methane Watchdog System, A Cost-Effective Approach to Longwall Methane Monitoring and Control

which may become the subject of a United States or foreign patent application or any other type of intellectual property protection.

AND WHEREAS THE WEST VIRGINIA UNIVERSITY BOARD OF GOVERNORS ON BEHALF OF WEST VIRGINIA UNIVERSITY, a state institution of higher education existing under the laws of the State of West Virginia (hereinafter called "Assignee"), is desirous of acquiring the entire worldwide right, title, and interest in, to and under said invention/creation and in, to and under Letters Patent or similar legal protection including any intellectual property protections to be obtained therefore in the United States, its territorial possessions, and in any and all foreign countries.

NOW, THEREFORE, in consideration of the relationship between Assignor(s) and Assignee, the West Virginia University BOG Governance Rule 1.5, Intellectual Property Rule for Patent, Copyright, and Trademark Rights, and/or other good and valuable consideration, the receipt and sufficiency of all of which Assignor(s) hereby acknowledge(s), Assignor(s) has/have agreed to assign and do/does hereby assign, sell, transfer, and set over unto said Assignee, the entire right, title, interest in said intellectual property and improvements for the United States and its territorial possessions and all foreign countries and all divisions, reissues, continuations, continuations-in-part, renewals, and/or extensions thereof including all priority rights under the International Convention associated therewith for each country and the Union, said Assignee to have and to hold the interests herein assigned to the full ends of the terms of said Letters Patent and an and all divisions, reissues, continuations, continuations-in-part, substitutes, renewals, and/or extensions thereof, respectively, as fully and entirely as the same would have been held and enjoyed by Assignor(s) had this assignment not been made.

The Commissioner of Patents and Trademarks is requested to issue such Letters Patent in accordance herewith. Assignor(s) covenant that Assignor(s) is/are the lawful owner(s) of the inventions and improvements disclosed in said invention, that the same are unencumbered, that no license has been granted to make, use, offer for sale, sell or import said inventions or improvements of any of them, and that Assignor(s) has/have the full right to make this assignment.

Assignor(s) hereby covenant(s) with said Assignee, its successors, assigns and legal representatives that I/we have made to others no assignment, grant, mortgage, license, sale or agreement

affecting the rights and property conveyed and that we have the full right to convey the same as herein expressed.

And for the consideration aforesaid, Assignor(s) agree(s) jointly and individually that Assignor(s) will communicate to said Assignee or the representatives thereof any facts known to Assignor(s) respecting said inventions and improvements, and will, upon request, but without expense to Assignor(s), testify in any legal proceeding, sign all lawful papers, execute all divisional, reissue, continuation, continuations-in-part, substitutes, renewal, and/or all other patent applications, execute all rightful oaths, and generally do all other and further lawful acts, deemed necessary or expedient by said Assignee or by counsel for said Assignee, to assist or enable said Assignee to obtain and enforce full benefits from the rights and interests herein assigned. This assignment shall be binding upon Assignor(s) heirs, executors, administrators, successors, and/or assigns, and shall inure to the benefit of the heirs, executors, administrative successors and/or assigns, as the case may be, of said Assignee.

First Inventor

Date Executed 11/26/ , 2019 by

Derek Johnson

First Inventor (*printed name*)

First Inventor (*signature*)

State of WV County of Monongalia

The forgoing instrument was acknowledged before me this 11/26 , 2019 by

My commission expires 8/13 , 2024

Beth J. Corocran

Notary Public (*signature*)

OFFICIAL SEAL
NOTARY PUBLIC
STATE OF WEST VIRGINIA
SEAL / STAMP Beth J. Corocran
933 Ridgeway Avenue
Morgantown, WV 26505
My Commission Expires August 13, 2024

Second Inventor

Date Executed 11/22 12/3/19 , 2019 by

Nigel Clark

Second Inventor (*printed name*)

Second Inventor (*signature*)

State of WV County of Preston

The forgoing instrument was acknowledged before me this Dec. 3 , 2019 by

My commission expires December 26 , 2021

Patricia A. Goldie

Notary Public (*signature*)

Official Seal
Notary Public, State Of West Virginia
SEAL / STAMP Patricia A Goldie
526 Laurel Run Road
Bruceton Mills WV 26525
My commission expires December 26, 2021

Third Inventor

Date Executed 11/26 , 2019 by

Amber Barr

Third Inventor (*printed name*)

Third Inventor (*signature*)

State of WV County of Monongalia

The forgoing instrument was acknowledged before me this 11/26 , 2019 by

My commission expires 8/13 , 2024

Beth J. Corocran

Notary Public (*signature*)

OFFICIAL SEAL
NOTARY PUBLIC
STATE OF WEST VIRGINIA
Beth J. Corocran
933 Ridgeway Avenue
Morgantown, WV 26505
My Commission Expires August 13, 2024

OFFICIAL SEAL
NOTARY PUBLIC
STATE OF WEST VIRGINIA
Beth J. Corocran
933 Ridgeway Avenue
Morgantown, WV 26505
My Commission Expires August 13, 2024

Fourth Inventor			
Date Executed	11/26/19, 20___ by		
Brian Cappellini		Brian Cappellini	
Fourth Inventor (*printed name*)		Fourth Inventor (*signature*)	
State of WV	County of Monongalia		
The forgoing instrument was acknowledged before me this	11/26, 20 19 by		
My commission expires	8/12, 2024	OFFICIAL SEAL NOTARY PUBLIC STATE OF WEST VIRGINIA Beth J. Corcoran 933 Ridgeway Avenue Morgantown, WV 26505 My Commission Expires August 13, 2024	
Beth J. Corcoran			
Notary Public (*signature*)			